International Journal of Computational Engineering Research

Volume 4. Issue 10 October 2014

Open Access JOURNAL

International Journal of Computational Engineering Research is an international, peer-reviewed journal publishing an overview of IT research and algorithmic processes that create, describe and transform information to formulate suitable abstractions to model complex systems.

International Journal of Computational Engineering Research under Open Access category aims to provide advance in the study of the theoretical foundations of information and computation and of practical techniques.

International Journal of Computational Engineering Research explicates the complicated aspects of Information Technology & Software Engineering and focusing on research and experience that contributes to the improvement of software development practices. The Journal has a dual emphasis and contains articles that are of interest both to practicing information technology professionals and to university and industry researchers.

International Journal of Computational Engineering Research - Open Access uses online manuscript submission, review and tracking systems for quality and quick review processing. Submit your manuscript at

http://www.ijceronline.com/online-submission.html

Editors & Editorial Board

DR.Qais Faryadi
USIM (Islamic Science University of Malaysia)

Dr. Lingyan Cao
University of Maryland College Park,MD, US

Dr. A.V.L.N.S.H. Hariharan
Gitam University, Visakhapatnam, India

Dr. Md. Mustafizur Rahman
Universiti Kebangsaan Malaysia (UKM)

Dr. S. Morteza Bayareh
Islamic Azad University
Iran

Dr. Zahra Mekkioui
University of Tlemcen, Algeria

Dr. Yilun Shang
University of Texas at San Antonio, TX 78249

Lugen M.Zake Sheet
University of Mosul, Iraq

Mohamed Abdellatif
Graduate School of Natural Science and Technology

Meisam Mahdavi
University of Tehran
Iran

Dr. Ahmed Nabih Zaki Rashed
Menoufia University, Egypt

Dr. José M. Merigó Lindahl
University of Barcelona, Spain

Dr. Mohamed Shokry Nayle
Faculty of Engineering Tanta University Eygpt

Dr. Thanhtrung Dang
Hochiminh City University of Technical Education, Vietnam

Dr. Sudarson Jena
GITAM University, INDIA

Dr. S. Prakash
Professor, Sathyabama University. Chennai

Mr. J.Banuchandar
P.S.R Engineering College, Sivaksi, Tamilnadu

Dr. Vuda Sreenivasarao
Defence University College, Deberzeit, Ethiopia.

M.Chithik Raja
Salalah College of Technology, Oman

Md. Zakaria Mahbub
Islamic University Of Technoligy (IUT), Bangladesh

Dr. Mohana Sundaram Muthuvalu
Universiti Malaysia Sabah, Malaysia

Dr. Virajit A. Gundale
SITCOE, Yadrav, Kolhapur Maharashtra

Mohamed Abdellatif
Graduate School of Natural Science and Technology

CONTENTS:

Version II

ISSN (e): 2250 – 3005 || Vol, 04 || Issue, 10 || October – 2014 ||
International Journal of Computational Engineering Research (IJCER)

Furnish an Index Using the Works of Tree Structures

[1]Chiranjib Mukherjee [2]Dr.Gyan Mukherjee
[1]Research Scholar in Computer Science, Magadh University (INDIA)
[2]Department of Mathematics, S.P.S. College, B.R.A.B.University (INDIA)

ABSTRACT
We consider two tree-based indexing schemes that are widely used in practical systems as the basis for both primary and secondary key indexing. We define B-tree and its features, advantages, disadvantages of B-tree. The difference between B^+-tree and B-tree has also been discussed. We show the algorithm, examples and figures in the context of B^+-tree.

KEYWORDS: *Indexing Schemes, Primary key, Secondary key, B-tree, B^+-tree.*

I. INTRODUCTION

In a tree based indexing scheme the search generally starts at the root node. Depending on the conditions that are satisfied at the node under examination, a branch is made to one of several nodes, and the procedure is repeated until we find a match or encounter a leaf node.

Tree Schemes: Each node of the tree except the leaf nodes can be considered to consist of the following information:

$$[n, T_{i1}, k_{i1}, T_{i2}, k_{i2}, \ldots\ldots, T_{in}, k_{in}, T_{i(n+1)}]$$

Where the k_{ij}'s are key values and the T_{ij}'s are pointers. For an m-order tree the following conditions are true:

- $n < m$
- $k_{i1} \leq k_{i2} \leq \ldots. \leq k_{in}$
- each of the pointers, T_{ij}, $1 \leq j \leq (n+1)$, points to a sub tree containing values less than k_{ij} and greater than or equal to $k_{i(j-1)}$.

The leaf nodes of the B^+-tree are quite similar to the non leaf nodes, except that the pointers in the leaf nodes do not point to subtrees. The pointers T_{Lj}, $1 \leq j \leq n$, in the leaf nodes point to storage areas containing either records having a key value k_{ij}, or pointers to records, each of which has a key value k_{ij}. The number of key values in each leaf node is at least $[(m – 1)/2]$ and at most m-1.

The pointer $T_{L(n+1)}$ is used to chain the leaf nodes in a sequential order. This allows for sequential processing of the underlying file of records. The following conditions are satisfied by the nodes of a B^+-tree :-

- The height of the tree is ≥ 1.
- The root has at least two children.
- All nodes other than the root node and the leaf nodes have at least [m/2] children, where m is the order of the tree.
- All leaf nodes are at the same level.

Operations: All operations of B^+-tree require access to the leaf nodes.

Search: The number of nodes accessed is equal to the height of the tree. Once the required leaf node is reached, we can retrieve the pointer for the storage location containing the records; knowing the storage location, we can retrieve the required records.

Insertion: We assume that the records themselves would be inserted in the pertinent storage locations. Insertion and deletion that violates the conditions on the number of keys in a node requires the redistribution of keys among a node, its sibling and their parent. If after insertion of the key, the node has more than m-1 keys, the node is said to overflow. Overflow cam be handled by redistribution if the number of entries in the left or right sibling of the node is less than the maximum.

Deletion: The leaf node containing the key to be deleted is found and the key entry in the node deleted. If the resultant node is empty or has fewer than [(m-1)/2] keys,

- The data from the sibling nodes could be redistributed, i.e., the sibling has more than the minimum number of keys and one of these keys is enough to bring the number of keys in node TD to be equal to [(m-1)/2]
- The node TD is merged with the sibling to become a single node. This is possible if the sibling has only the minimum number of keys. The merger of the two nodes would still make the number of keys in the new nodes less than the maximum.

Capacity: The upper and lower limits of the capacity of a B^+-tree of order m may be calculated by considering each node of the tree to be maximally (m-1) keys or minimally full ([m/2]-1)keys. Let the height of the tree is h. As every key must occur in the leaf node and the leaf nodes may also contain a minimum of [(m-1)/2] and a maximum of (m-1) keys we have

$$2 * [(m-1)/2 * [m/2]^{h-2} < N < (m-1) * m^{h-1}$$

B-Tree : (Balanced Tree) The basic B-tree structure has growth to become one of the most popular techniques for organizing an index structure while accessing the records using such structure, several conditions of the tree must be true, to reduce disk access:

- The Height of the tree must be kept to a minimum.
- These must be no empty sub trees above the leaves of the tree.
- The leaves of the tree must be at the same level.
- All nodes except the leaves must have as few as two and as many as the maximum number of children.

The Features of a B-tree:-

- There is no redundant storage of search key values i.e., B-tree stores each search key value in only one node, which may contain other search key values.
- The B-tree is inherently balanced and is ordered by only one type of search key.
- The insertion and deletion operations are complex with the time complexity $O(\log_2 n)$.
- The number of keys in the nodes is not always the same. The storage management is only complicated if you choose to create more space for pointers keys otherwise the size of a node is fixed.
- The B-tree grows at the node as opposed to the Binary tree, BST and AVL trees.
- For a B-tree of order N with n nodes, the height is log n. The height of B-tree increases only because of a split at the root node.

Advantages of B-tree indexes:-

- There is no overflow problem inherent with the type of organization it is good for dynamic table- those that suffer a great deal of insert / update / delete activity.
- Because it is so large extent self-maintaining, it is good in supporting 24 hours operation.
- As data is retrieved by the index, it is always presented in order.
- 'Get next' queries are efficient because of the inherent ordering of rows within the index blocks.
- B-tree indexes are good for every large tables because they will need minimal reorganization.
- There is predictable access time for any retrieval because the B-tree structure keeps itself balanced, so that there is always the same number of index levels does increases both with the number of records and the length of the key value.

Disadvantages of B-tree indexes:-

- For static tables, there are better organizations that require fewer I/Os. ISAM indexes are preferable to B-tree in this type of environment.
- B-tree is not really appropriate for every small table because index look-up becomes a significant part of the overall access time.
- The index can use considerable disk space, especially in products which allow different users to create separate indexes on the same table/ column combinations.
- Because the indexed themselves are subject to modification when rows are updated, deleted or inserted, they are also subject to locking which can inhabit concurrency.

Difference between B^+-tree and B-tree:-

- Retrieval of the next record is relatively easy in the B^+-tree, this is not the case in the B-tree unless the internal nodes of the B-tree are linked in a sequential order.
- The deletions in a B^+-tree are always made in the leaf nodes. In a B-tree, a value can be deleted from any node, making deletions more complicated than in a B^+-tree.

- Insertions in a B^+-tree are always made in the leaf nodes. In the B-tree, insertions are made at the lowest non leaf node. Insertions (or deletions) may cause node splits and thereby affect the height of the tree in both cases.
- The capacity of the B-tree can be calculated in a manner similar to that used for the B^+-tree. That the order of the tree is dictated by physical storage availability, among other factors. For the same buffer size, the order of the B-tree would be less than that of the B^+-tree.

II. ALGORITHM – SEARCHING B^+-TREE

K_s, the search key
Found,(a Boolean value), and
A, the address of record if found
{nodes content : [n, T_1, k_1, T_2, k_2 ……, T_n , k_n, T_{n+1}]$k_{n+1} = \infty$ is assumed}
get root_node
while not leaf_node do
begin
i : = 1
while not (i > n or $K_s < k_i$) do
i : = i + 1
{T_i points to the subtree that may contain K_s}
get subtree T_i
end {while not leaf_node}
{search leaf node for key K_s}
{content of leaf node : [n, P_1, k_1, P_2, k_2 ……, P_n , k_n, P_{n+1}]}
i : = 1
found : = false
while not (found or i > n) do
begin
found : = $K_s = K_i$
if found then
A : = P_i
else i : = i + 1
end {while not (found or i > n)}

III. EXAMPLES AND FIGURES

Example1: Given a file containing the following records-

Books	Subject Area
2	Files
3	Database
4	Artificial intelligence
5	Files
7	Discrete structures
8	Software engineering
9	Programming methodology
.	.
.	.
.	.
40	Operating system
50	Graphics
51	Database
52	Data structures

Figure1: A B^+- tree of order 4 on Book- Each P_i is a pointer to the storage area containing records for the key Books = i; ⊥ represents a null pointer.

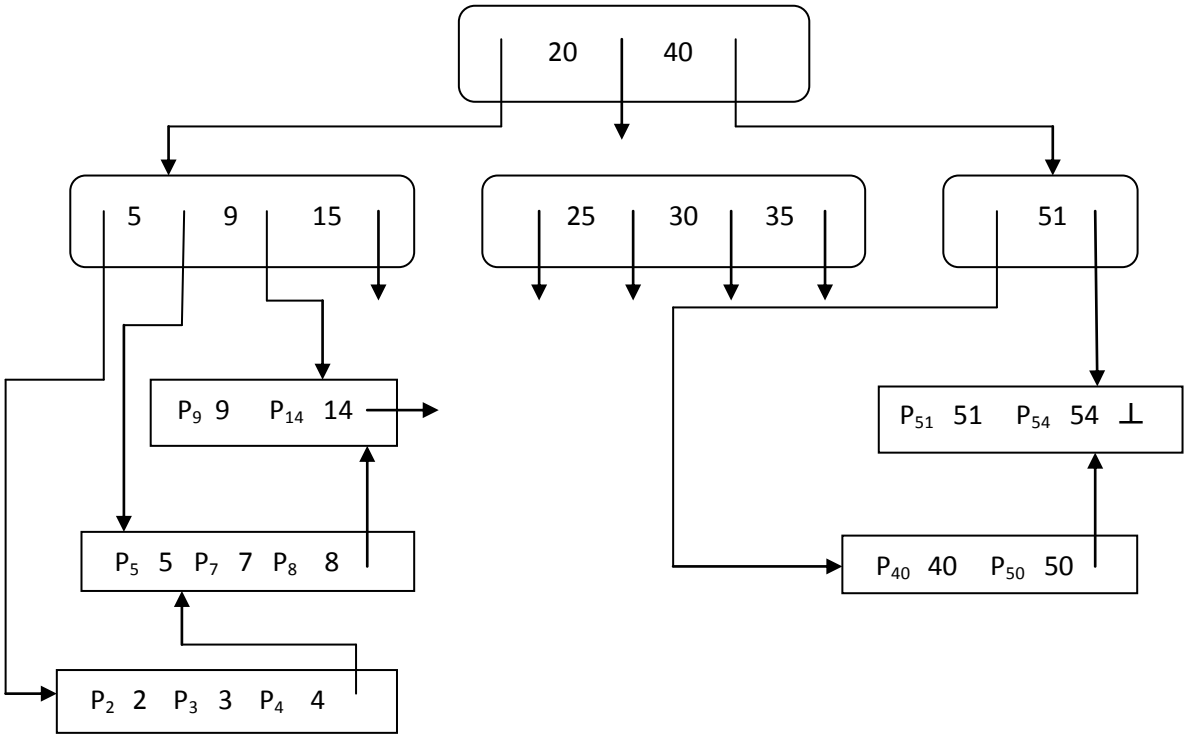

Example2: In the B^+-tree of example1, let us insert an entry for Books 1. The original contents of the leaf node (with the label PT_0) in which the key would be inserted are:

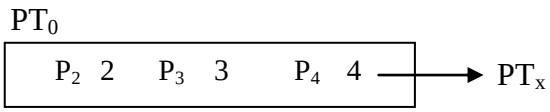

This nodes does not have a left sibling and the right sibling is already full. Hence, insertion of the key 1 would cause a split. Let the new node be PT_N. The contents of these nodes are below:

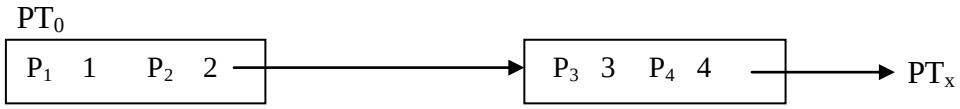

The pair < 3, PT_N > are passes to the parent node for insertion as indicated:

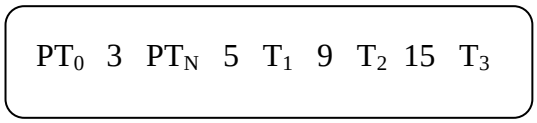

The insertion causes a split of this node into the following two nodes with the key value 5, along with a pointer passed to the parent of the node:

Let the address of the new node be P_Y . Then the pair < 5, P_Y > is passed to the parent node for insertion.
Figure2: The B^+- tree of example1 after insertion of the key for Books1.

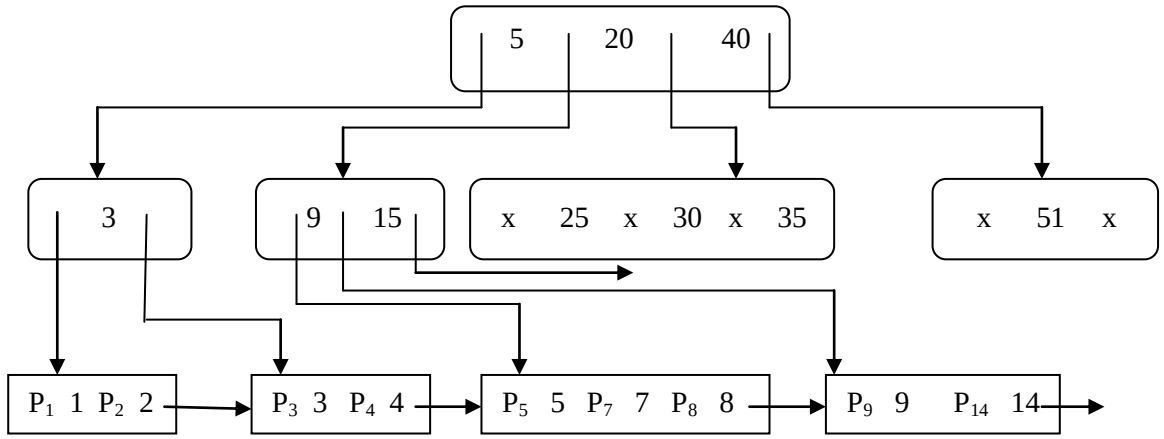

Example3: Let delete the entry for Books5 from the tree shown in example1. The resultant tree is shown in part (i) of fogure3.
Figure3: (i) The B^+-tree that results after the deletion of key 5 from the tree of example1.
(ii) The B^+-tree after the deletion of key 7.

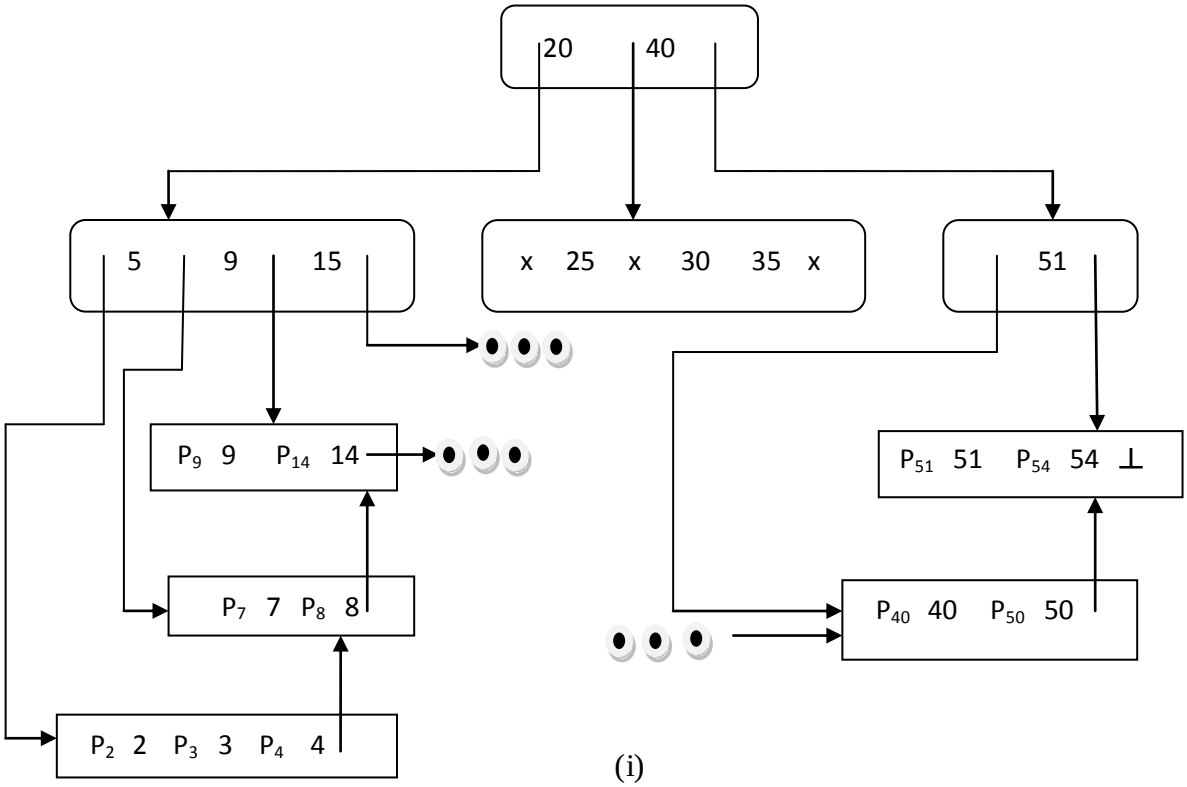

(i)

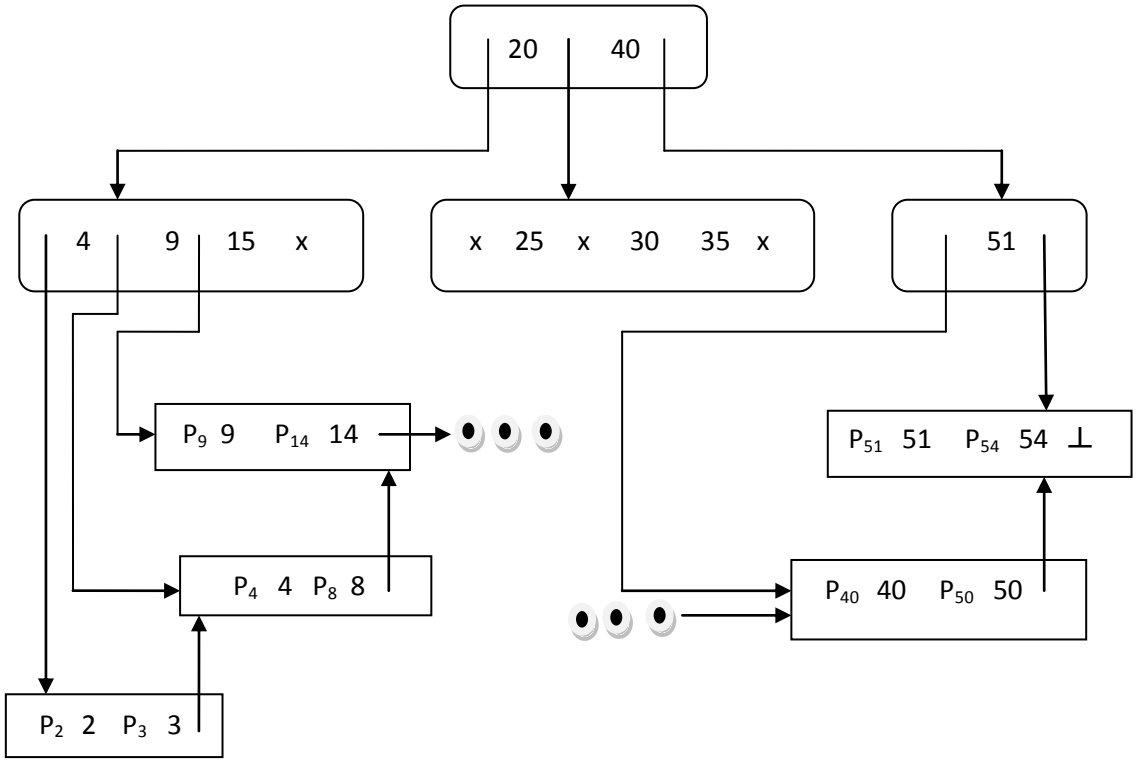

(ii)

Figure 4: Capacity of a B^+-tree.

Level	Number of nodes at level
1	1
2	m
.	.
.	.
.	.
h	m^{h-1}

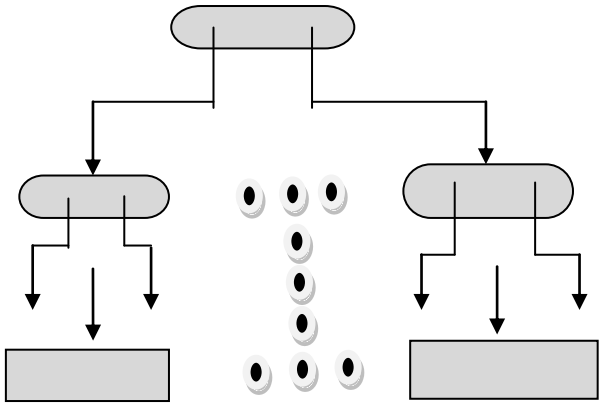

(a)

Level	Number of nodes at level
1	1
2	m
.	.
.	.
.	.
h	$2*[m/2]^{h-1}$

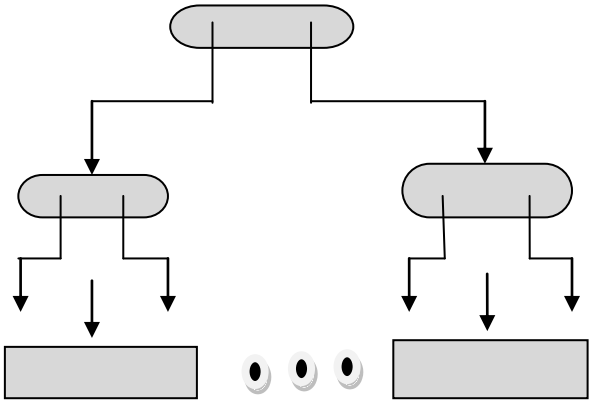

(b)

Example5: A B^+-tree for the following set of key values-(2,3,5,7,11,17,19,23,29,31).That the number of search key values that fit in one node is (a) 3 and (b) 7.
Figure: (a)

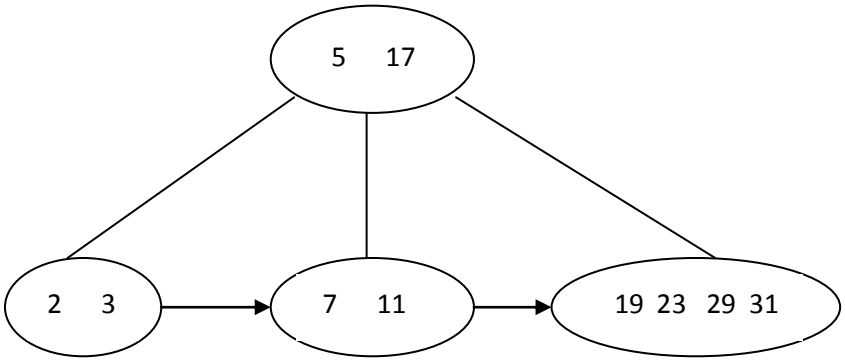

(b)

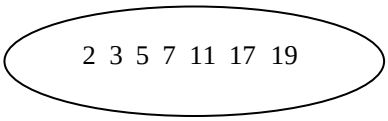

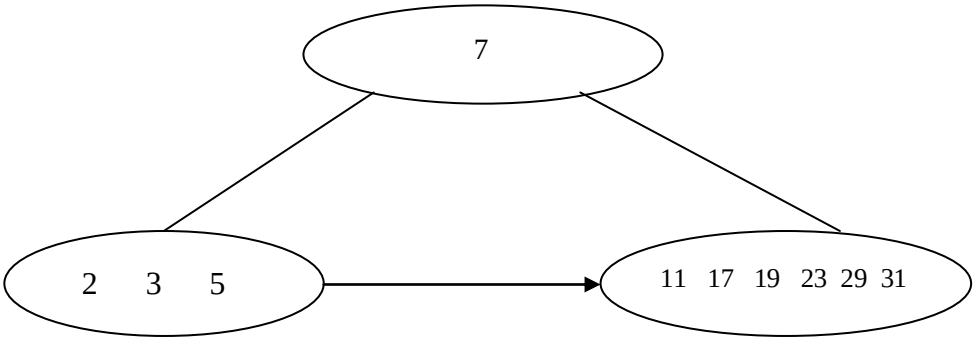

Example 6: Create a B-tree structure of the order 3 of the following relation.

Customer

C_No.	Name	Location
C1	N1	L1
C2	N2	L2
C9	N3	L2
C10	N4	L3
C11	N5	L3
C15	N6	L3
C19	N7	L4
C23	N8	L3
C25	N9	L4
C37	N10	L2
C32	N11	L2
C34	N12	L1

Figure 6:

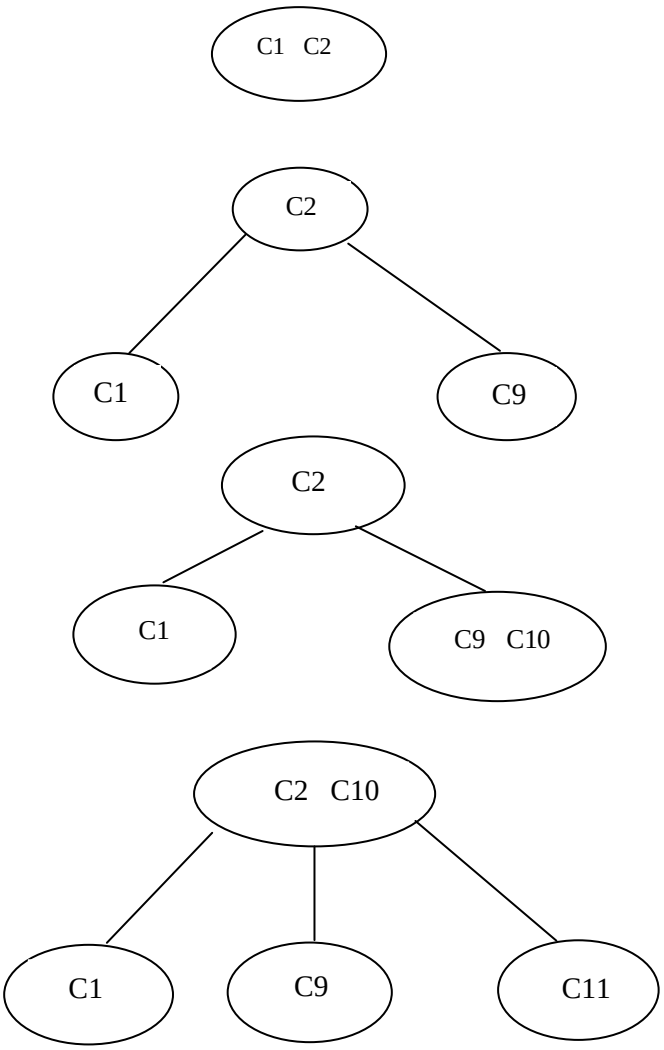

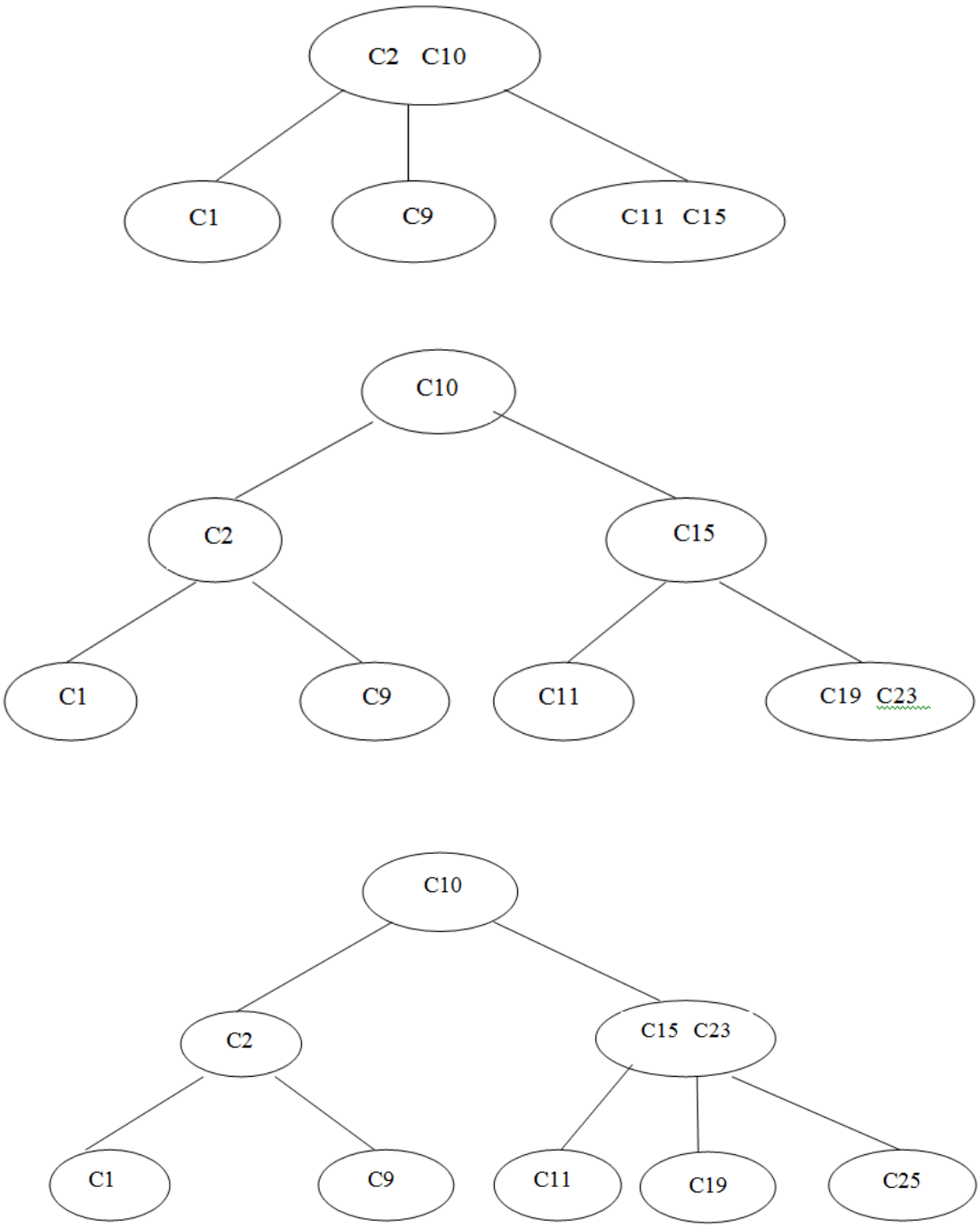
C2 C10
C1
C9
C11 C15
C10
C2
C15
C1
C9
C11
C19 C23
C10
C2
C15 C23
C1
C9
C11
C19
C25

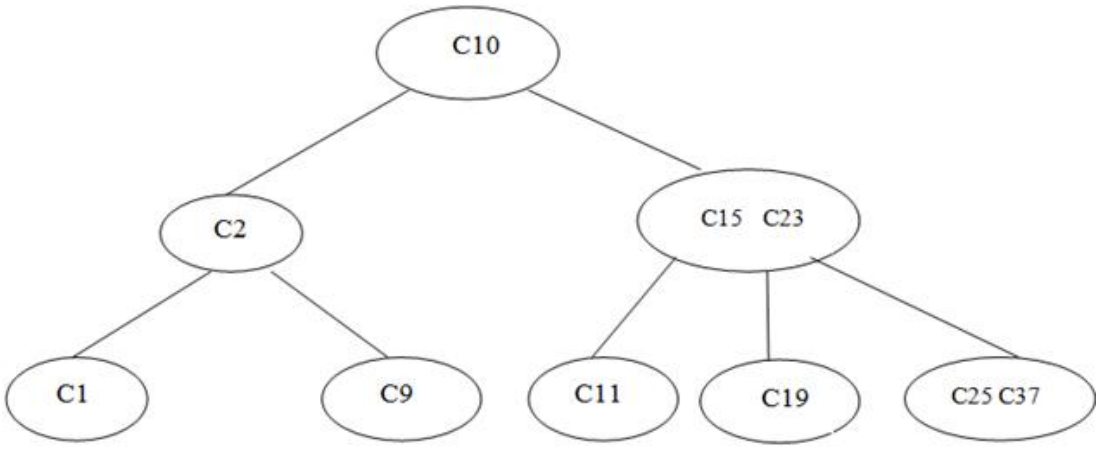
C10
C2
C15 C23
C1
C9
C11
C19
C25 C37

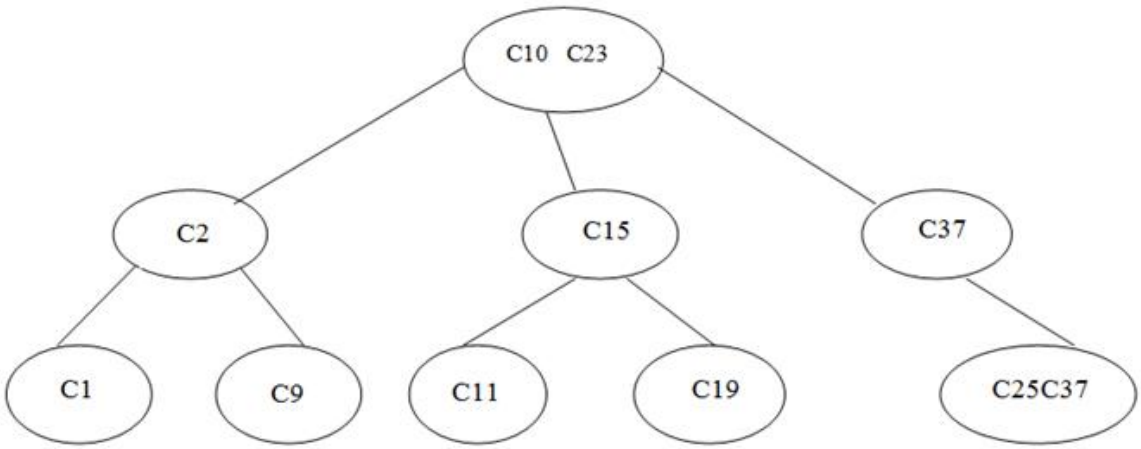
C10 C23
C2
C15
C37
C1
C9
C11
C19
C25C37

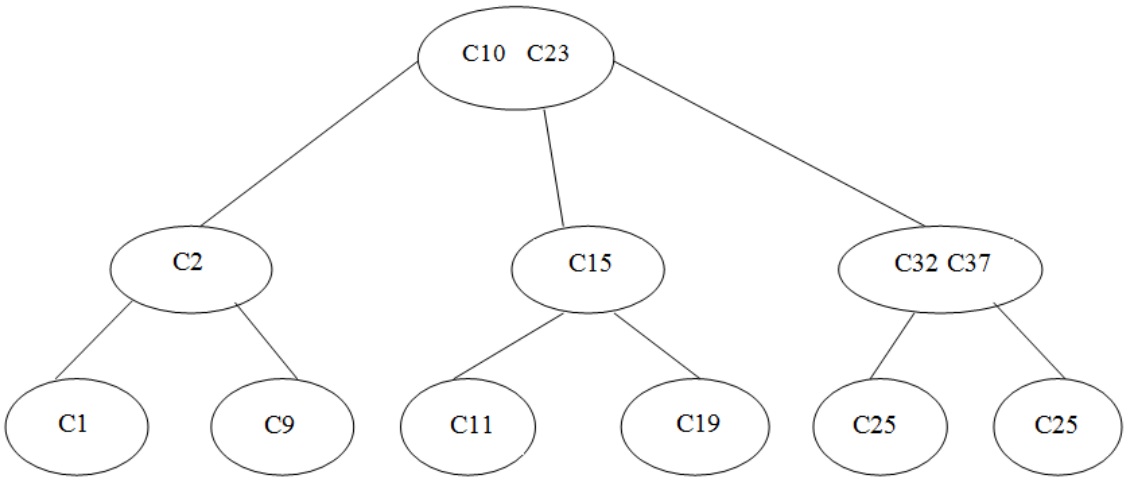
C10 C23
C2
C15
C32 C37
C1
C9
C11
C19
C25
C25

IV. CONCLUSION

Tree-based data organization schemes are used both for primary and secondary key retrieval. The B^+-tree scheme, each node of the tree except the leaf node contains a set of keys and pointers pointing to sub trees. The leaf nodes of the B^+-tree are similar to the non leaf or internal nodes except that the pointers in the leaf node point directly or indirectly to storage areas containing the required records. We also examined the method of performing the search and update operations using the B^+-tree and compared the B^+-tree with the B-tree.

REFERENCES

[1.] Avi Silberschatz, Henry F. Korth & S. Sudarshan; Database System Concept, 2010.
[2.] Alan L. Tharp; File Organization and Processing, John Wiley & Sons,2008.
[3.] Carolyn Begg , Thomas Connolly; Database System: A Practical Approach to Design, Implementation and Management, Addison-Wesley,2004.
[4.] Ramez Elmasri & Shamkant B. Navathe; Fundamental of Database Systen, Fourth Edition, Pearson Addison Wesley, NewYork,2003.
[5.] Hctor Garcia-Molina; Database System Implementation, Pearson Education,2000.
[6.] T. R. Harbon; File System Structures of Data Structures and Algorithms, Englewood Cliffs, NJ:Printice-Hall,1988.
[7.] P. Goyal; "File Organization" Computer Science report, Concordia University, Montreal,1987.
[8.] S. P. Ghosh; Database Organization for Data Management, Orlando, Academic Press, 1986.
[9.] E. Horowitz & S. Shani; Fundamentals of Data Structures, Rockville, Computer Science Press, 1982.

ISSN (e): 2250 – 3005 || Vol, 04 || Issue, 10 || October – 2014 ||
International Journal of Computational Engineering Research (IJCER)

Application of Microcontroller in Transmitter Section of Wireless System

Dr.M.J.Hedau
Department of Electronics, Shivaji Science College,Congressnagar, Nagpur, India

ABSTRACT:
The present paper describes how the microcontroller works in the transmitter section of wireless system. In last 40 years a silent but rapid revolution as far as electronics computing communication and control are concerned. Proof of this statement would be available in mobile handset, MP 3 player, automatic washing machine, microwave oven, portable digital blood pressure measurement and many more medical instruments, billing system in STD phone etc. This list is enomorous and growing exponteally. All these are possible because of usage of Microcontroller and having a PC which involves from microprocessor. Temperature is certainly among the most commonly measured parameters in industry, science, and academia. Recently, the growth of wireless instrumentation technology, along with some clever innovations, has provided new ways to apply temperature measurement sensors combined with personal computers to collect, tabulate, and analyze the data obtained.

Keywords: *Microcontroller, Temperature controller, CAN, flags, Buffer,ADC,Step response*

I. INTRODUCTION

Processor are 16-bit and 32-bit fixed- and floating-point processors include ARM based processors , ARM 9 family and Cortex-A8 processor-based microprocessors, video processors,[1] OMAP™ mobile applications processors, digital signal processors (DSP) and microcontrollers (MCUs).Microcontrollers have only been with us for a few decades but their impact (direct or indirect) on our lives is profound [2].Usually these are supposed to be just data processors performing exhaustive numeric operations. But their presence is unnoticed at most of the places like supermarkets, Weighing Scales, etc.

What inside them makes these machines smart? The answer is microcontroller. Creating applications for the microcontrollers is different than any other development job in electronics and computing [3].Before selecting a particular device for an application, it is important to understand what the different options and features are and what they can mean with regard to developing the application. It is to introduce the concept of microcontrollers, how it differs from microprocessors and different type of commercial microcontrollers available as well as their applications.

II. DESCRIPTION

Fig(1.1) is a Block diagram of wireless temperature monitoring system

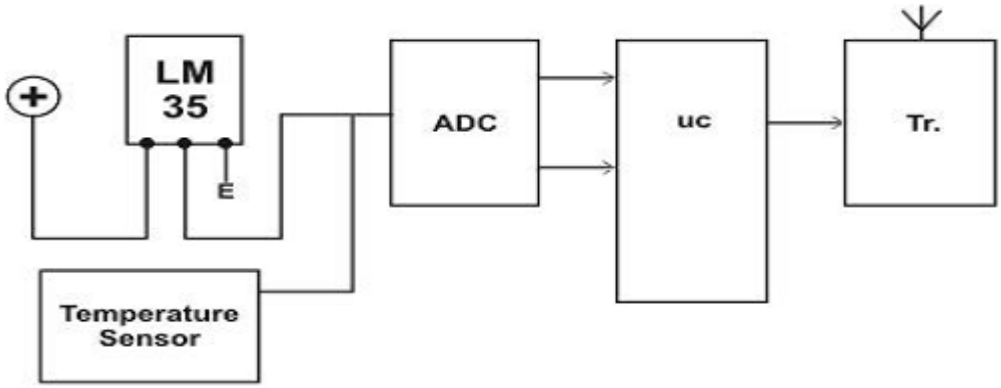

Fig(1.1) **:-** Block diagram of wireless temperature monitoring

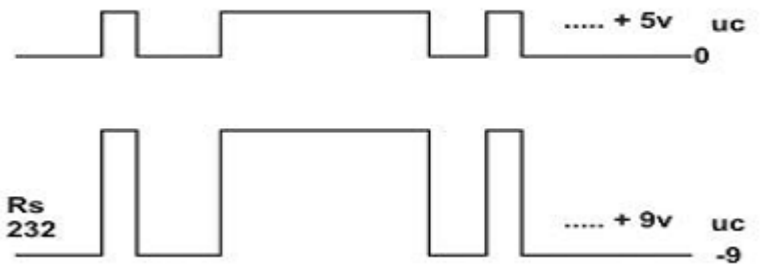

Fig(1.2) **:-** Clock cycle

This block diagram contains the wireless transmitter section. This section has microcontroller as a transmitter module, temperature sensor LM 35, ADC 0809.Each and every module in the transmitter section will be controlled by the Microcontroller. The Temperature sensor LM35 senses the temperature as analog signal, by the use of ADC 0809 these analog signals will be converted to digital and it will be transfer to the microcontroller. Microcontroller processes that digital signal and then transmits the digital signal through the Wireless Transmitter module as an analog signal [6].

ADC-809 has an inbuilt 8-channel multiplexer. It performs simultaneously A/D conversion of more than one analog signal. When the unknown analog input equals the reference voltage, the internal comparator output allows the digital output to become available at the output of the 8-bit latch. The characteristics of reference voltage is as shown in graph no.1 While the process of A/D conversion is initiated by positive pulse at the terminal marked 'START OF CONVERSION' the A/D converter produces the pulse at the terminal marked 'END OF THE CONVERSION'. This pulse is used to inform microcontroller that the cycle of A/D conversion has been completed.

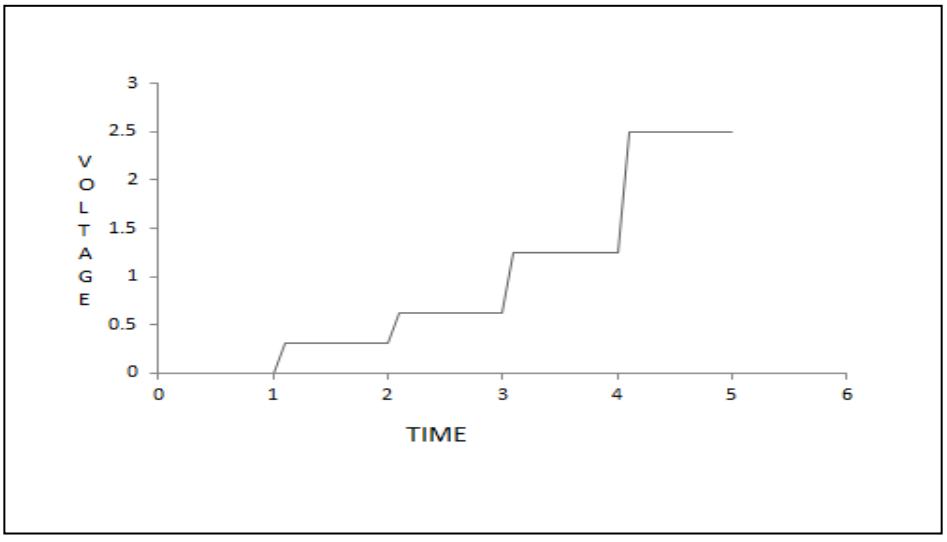

Graph No. 1: characteristics of reference voltage

This IC operates on a single DC supply of +5V.Thus +Vref ≤ +5V,- Vref is connected to ground. The input analog signal range is 0 to +5V.It is operates on the range of clock frequency from 10KHz to 12.80KHz.

The multiplexer address bits are operates as follows:

Output Enable	Logic Inputs			Channel Selected
	A	B	C	
1	0	0	0	CH 0
1	0	0	1	CH 1
1	0	1	0	CH 2
1	0	1	1	CH 3
1	1	0	0	CH 4
1	1	0	1	CH 5
1	1	1	0	CH 6
1	1	1	1	CH 7

Address logic input are controlled by programming the microcontroller system.

III. Transmitter Circuit

The transmitter module (TX433N) was interfaced to the microcontroller through the encoder IC HT12E.[3] It was used to modulate the digital data coming from the encoder IC into RF radio frequency signal by ASK modulation technique and transmitted via RF out antenna pin1, When a command was send from the µC, the encoder encodes the address and data bits upon getting transmission enable signal from the µC and send serially to the transmitter module Din pin2, the transmitter module converted the digital signal into RF signal and transmitted via wireless media.

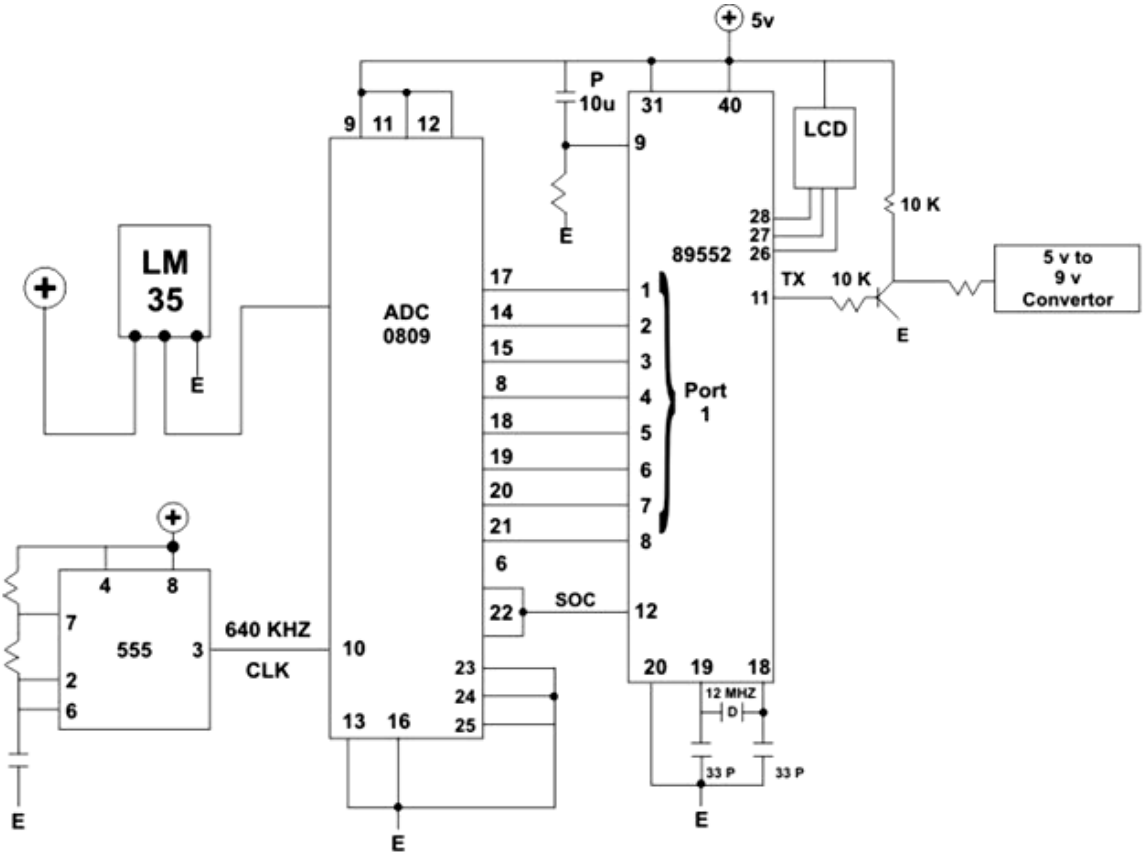

Fig(2.1) Transmitter Circuit using Microcontroller

The wireless transmitter module can be used to transmit data at up to 3 KHz from any standard CMOS/TTL source. The module had been made very simple to operate and offers low current consumption (typ. 11mA). Data can be supplied directly from a microprocessor or encoding device, thus keeping the component count down and ensuring a low hardware cost. TX1-433.92MHz was used in that module to transmit the data from the protected area. When the data had been received from the controller it then transmits the data at the frequency of 433.92MHz. The module was made very simple to operate, requiring only two connections. The module was also very efficient, used only 2.3mA which means that it may be driven directly from an encoder I/C or microcontroller. The output impedance had been designed to give optimum performance when coupled with a small antenna such as a tuned loop or short whip. The modules were compatible with the AM Receiver modules.

IV. CONCLUSION

In this system temperature sensor was used to detect a room temperature at a particular distance and transmit it through a wireless medium to a remote room. The output signal from the temperature sensor was digitized with ADC and fed to an embedded microcontroller 8051. The microcontroller was used to process the digital signal and the RF Transmitter module transmitted the data through a wireless medium at a frequency range of 433.92 MHz to a Receiver. A wireless temperature control based on embedded microcontroller had been demonstrated successfully. The performance of the wireless system was evaluated and compared with that of wired based temperature control. Its major advantage is that it does not require any physical wire to retrieve information from the sensor. This thesis can be extended further by adding more sensors and repeaters to make it possible to read temperatures from different locations. This is required in certain applications where temperatures from more rooms need to be monitored.

REFERENCES

[1]. ESPASA ROGER,VALERO,SMITH J.E ”Vector Architectures: Past, Present, and Future,” ICS ’98, Proceedings of the 1998 International Conference on Supercomputing, July 13-17, 1998, Melbourne, Australia. ACM, 1998.

[2]. WAWRYNEK J,ASANOVIC K,KINKSBBURY B. ”Spert-II: A vector Microprocessor System,” IEEE Computer, March 1996.

[3]. BAILEY, D.H., “Extra-High Speed Matrix Multiplication on the Cray-2”, SIAM Journal on Scientific and Statistical Computing, Vol. 9, No. 3, May 1988

[4]. BALSTER E.J., SCARPINO, F.A., and W.W SMARI, “Wavelet Transform for Real- Time Image Compression Using FPGAs,” 12th IASTED International Conference on Parallel and Distributed Computing and Systems, Las Vegas, Nevada, Nov. 6 – 9, 2000, pp. 232-238

[5]. CUCCIHA R., , “Exploiting Cache in Multimedia”, IEEE International Conference on Multimedia Computing and Systems, , pp. 345 – 350, June 7, 1999

[6]. M. J. Hedau, M. P. Dhore, P. B. Dahikar, “Application of Wireless Signal Simulation Via Cell-Phone “International Conference on circuit system and simulation, , pp. 92 – 95, Vol.7(2011) IACSIT Press, Singapore

[7]. M. J. Hedau, P. B. Dahikar, “Vector Architectures :The Multitasking , pp.55 – 62, Hislopia Journal 3 (1) 2010, ISSN-0976-2124

[8]. Schramm, W. (1954). How communication works. In W. Schramm (Ed.), The process and effects of communication (pp. 3-26). Urbana, Illinois: University of Illinois Press.

[9]. M. J. Hedau, M.P.Dhore, P. B. Dahikar, “Application of microcontroller in technical communication pp.191– 194, International journal of Emerging technology and application in engineeing, technology and science.Vol5

ISSN (e): 2250 – 3005 || Vol, 04 || Issue, 10 || October – 2014 ||
International Journal of Computational Engineering Research (IJCER)

Bi-objective Optimization Apply to Environmental and Economic Dispatch Problem Using the Method of Corridor Observations

Salomé Ndjakomo Essiane[1], Stève Perabi Ngoffe[2], Adolphe Moukengue Imano[3], Grégoire Abessolo Ondoa[4]

[1]*Lecturer, Electronic, Electrotechnic, Automatic and Telecommunications Laboratory, ERSEE, University of Douala - Cameroon*
[2] *Doctorate Student, Electronic, Electrotechnic, Automatic and Telecommunications Laboratory, ERSEE, University of Douala - Cameroon*
[3] *Associate Professor, Electronic, Electrotechnic, Automatic and Telecommunications Laboratory, ERSEE, University of Douala, BP. 8698 Douala - Cameroon*
[4] *Master of Sciences with thesis student, Electronic, Electrotechnic, Automatic and Telecommunications Laboratory, ERSEE , University of Douala - Cameroon*

ABSTRACT:
This paper presents a proposed and applicable optimization algorithm based on the evolutionary algorithm to solve an environmental and economic Dispatch (EED) problem. This problem is seen like a bi-objective optimization problem where fuel cost and gas emission are objectives .in this method, the optimal Pareto front is found using the concept of corridor observation and the best compromised solution is obtained by fuzzy logic. The feasibility of this method is demonstrated using power systems with three generation units, and it is compared with the other evolutionary methods of Optimization Toolbox of Matlab in terms of solution quality and CPU time. The simulated results showed that the proposed method is indeed capable of obtaining higher quality solutions in shorter computational time compared to other evolutionary methods. In addition the other advantage is that our approach solves in the same time a unit commitment problem and it can use with n-generation units.

KEYWORDS: *bi-objective, corridor observations, Evolutionary algorithm, fuel cost, gas emission, optimal PARETO front, optimization*

I. INTRODUCTION

The economic dispatching (ED) is one of the key problems in power system operation and planning. The basic objective of economic dispatch is to schedule the committed generating unit outputs so as to meet the load demand at minimum operating cost, while satisfying all equality and inequality constraints. This makes the ED problem a large – scale highly constrained non linear optimization problem. In addition, the increasing public awareness of the environmental protection and the passage of the Clean Air Act Amendments of 1990 have forced the utilities to modify their design or operational strategies to reduce pollution and atmospheric emissions of the thermal power plant. Several strategies to reduce the atmospheric emissions have been proposed and discussed. These include: installation of pollutant cleaning equipment, switching to low emission fuels, replacement of the aged fuel-burners with cleaner ones, and emission dispatching. The first three options require installation of new equipment and/or modification of the existing ones that involve considerable capital outlay and, hence, they can be considered as long-term options. The emission dispatching option is an attractive short-term alternative in which the emission in addition to the fuel cost objective is to be minimized. Thus, the ED problem can be handled as a multi-objective optimization problem with non-commensurable and contradictory objectives. In recent years, this option has received much attention [1–5] since it requires only small modification of the basic ED to include emissions.

In the literature concerning environmental/economic dispatch (EED) problem, different technics have been applied to solve EED problem. In [1, 2] the problem was reduced to a single objective problem by treating the emission as a constraint. This formulation, however, has a severe difficulty in getting the trade-off relations between cost and emission. Alternatively, minimizing the emission has been handled as another objective in addition to the cost [5]. However, many mathematical assumptions have to be given to simplify the problem. Furthermore, this approach does not give any information regarding the trade-offs involved. In other research direction, the multi-objective EED problem was converted to a single objective problem by linear combination of different objectives as a weighted sum [3], [6]. The important aspect of this weighted sum method is that a set of non-inferior (or Pareto-optimal) solutions can be obtained by varying the weights. Unfortunately, this requires multiple runs as many times as the number of desired Pareto-optimal solutions. Furthermore, this method cannot be used in problems having a non-convex Pareto optimal front. To overcome it, certain method optimizes the most preferred objective and considers the other objectives as constraints bounded by some allowable levels [5]. The most obvious weaknesses of this approach are that, then are time-consuming and tend to observed weakly non-dominated solutions [5].

The other direction is to consider both objectives simultaneously as competing objectives. The recent review to the Unit Commitment and Methods for Solving [7] showed that evolutionary algorithms are the most used in this case; certainly because they can efficiently eliminate most of the difficulties of classical methods [5]**.** The major problems of these algorithms, is to find the pareto optimal front and to conserve the non-dominated solutions during the search. In this paper we perform and apply one optimization method proposed in [9] to solve the EED problem. The particularity of this method is based to the fact that the search of front and optimal Pareto is found by the concept of corridor, and the archives is dynamic. This dynamism reduce the loses of the non-dominated solution during the different generations. In the second part of this paper, we present materials and methods to solve the problem, and the third part, present simulation and results obtained.

II. MATERIALS AND METHODS

In this part, we formulate the EED problem and present our approach to solve it.

2.1. Problem formulation

The EED problem is to minimize two competing objective functions, fuel cost and emission, while satisfying several equality and inequality constraints. Generally the problem is formulated as follows :

2.1.1. Problem objectives

- Minimization of fuel cost

The generator cost curves are represented generally by quadratic functions. The total fuel cost ($/h) in terms of period T, can be expressed as:

$$F\left(p_{i,t}\right) = \sum_{t=1}^{T} \sum_{i=1}^{Ng} c_{fi}\left(p_{i,t}\right) I_{i,t} + ST_{i,t}\left(1 - I_{i,t-1}\right) I_{i,t} \qquad (1)$$

Where

$$c_{fi}\left(p_{i,t}\right) = a_i + b_i p_{i,t} + c_i p_{i,t}^2 \qquad (2)$$

and $c_{fi}\left(p_{i,t}\right)$ is the generator fuel cost function; a_i, b_i and c_i are the cost coefficients of i^{th} generator; $P_{i,t}$, is the electrical output of i^{th} generator; Ng is the number of generators committed to the operating system ; $I_{i,t}$thestatut of differents generators ; ST_i the start-up cost .

- Minimization of gas emission

The atmospheric pollutants such as sulpher dioxides (SO_2) and nitrogen oxides (NO_X) caused by fossil-fueled thermal units can be modeled separately. However, for comparison purposes, the total emission (*ton/h)* in one period T of these pollutants can be expressed as:

$$E\left(p_{i,t}\right) = \sum_{t=1}^{T} \sum_{i=1}^{Ng} e_{fi}\left(p_{i,t}\right) I_{i,t} \qquad (3)$$

where

$$e_{fi}\left(P_{i,t}\right) = \left(\alpha_i + \beta_i p_{i,t} + \delta_i p_{i,t}^2\right) \qquad (4)$$

and α_i, β_i, δ_i are the emission coefficients of the i^{th} generator.

2.1.2. Objective constraints

- Power balance constraint

$$p_{load,t} - \sum_{i=1}^{Ng} p_{i,t} I_{i,t} = 0 \quad (5)$$

- Spinning reserve constraint :

$$p_{load,t} + R_t - \sum_{i=1}^{Ng} p_{\max,i} I_{i,t} \leq 0 \quad (6)$$

- Generation limit constraints :

$$p_{\min,i} I_{i,t} \leq p_{i,t} \leq p_{\max,i} I_{i,t} \quad , i = 1 \ldots\ldots Ng \quad (7)$$

- Minimum up and down time constraint :

$$I_{i,t} = \begin{cases} 1 \text{ if } T_i^{on} \prec T_i^{up} \\ 0 \text{ if } T_i^{off} \prec T_i^{down} \\ 0 \text{ or } 1 \text{ otherwise} \end{cases} \quad (8)$$

Where T_i^{up} represent the minimum up time of unit *i*; T_i^{down} the minimum down time of unit *i* T_i^{off} is the continuously off time of unit *i* and T_i^{on} the continuously on time of unit- *i* .

- Start-up cost

$$ST_i = \begin{cases} HST_i \text{ if } T_i^{down} \leq T_i^{off} \leq T_i^{down} + T_i^{cold} \\ CST_i \text{ if } T_i^{off} \succ T_i^{cold} + T_i^{down} \end{cases}$$

2.2. The proposed approach

2.2.1. Algorithm of corridors observations method

The different steps of the proposed approach to solve EED problem is summarize in the follow figure

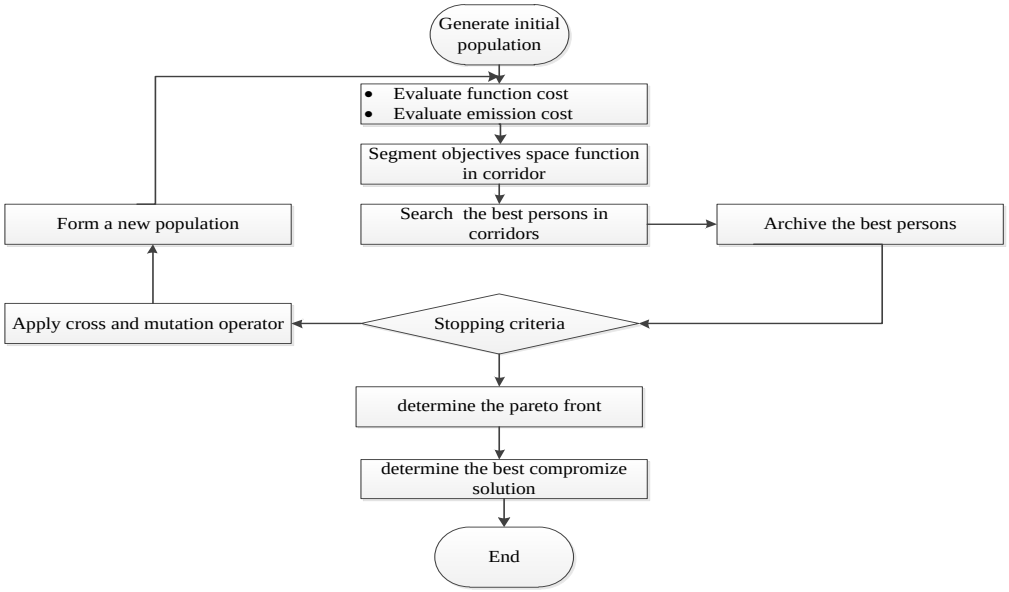

Figure 1: Different steps of the algorithms

- Step 1

In the first step, we start with to the status of different unit generation, were we create randomly the initial population. Each individual is a combination of each power generation unit

- Step 2

In the second, using equations (1) and (3) we evaluate the objective functions of this population

- Step 3

Using the minimum of the different objective functions of individuals who respect the constraints (5) to (8), we define the space solution and segment it to the corridors observation following the different axes which are specify by each function.

- Step 4

In each corridor, we search the best individual who have the minimum objectives functions, and the non feasible solutions are classified using the number and the rate of violation constraints. Those solutions will be used to increase the number of feasible solutions.

- Step 5

We keep in the archives those best individuals

- Step 6

We verify the stoping criteria define as [9] :

$$\xi = \ln(d) \tag{9}$$

where

$$d = \sum_{j=1}^{N_F} \left[\frac{1}{Cl} \sqrt{\sum_{i=1}^{cl} \left(\frac{F_{j,i}^{t} - F_{j,i}^{t-1}}{F_{\max} - F_{\min}} \right)} \right] \tag{10}$$

explain the metric progression of the best individuals in each corridor. N_F is the number of objectives functions ; Cl the number of corridor ; $F^{t}_{j,i}$, $F^{t-1}_{j,i}$ the j^{th} objective function of the best individual in i^{th} corridor ; F_{min} and F_{max} the minimum and maximum of the j function ; t is the present generation, t-1 the anterior generation. At times the maximum number of generation can be the alternative stopping criteria

- step 7

If the stopping criteria is not verified, we construct the new population using the selection ,cross and mutation operators apply to the archive population and we return to step 2.

- Step 8

If the stopping criteria is verified we find the best compromise solution among the individuals of the Pareto front. Due to imprecise nature of the decision maker's judgment, each objective function of the i-th solution is represented by a membership μ_i function defined as

$$\mu_i = \begin{cases} 1 & if \quad F_i \le F_i^{\min} \\ \dfrac{F_i^{\max} - F_i}{F_i^{\max} - F_i^{\min}} & F_i^{\min} \le F_i \le F_i^{\max} \\ 0 & if \quad F_i \ge F_i^{\max} \end{cases} \tag{11}$$

For each non-dominated solution, the normalized membership function is μ^k calculated as:

$$\mu^k = \frac{\sum_{i=1}^{N_F} \mu_i^k}{\sum_{k=1}^{M} \sum_{i=1}^{N_F} \mu_i^k} \tag{12}$$

where M is the number of non-dominated solutions. The best compromise solution is the one having the maximum of μ^k .

2.2.2. Implementation and strategy to search solution

To find the problem solution algorithm, we have to :

- Explore space solutions

During this step, the algorithm explore space solutions with using 0.9 percentage of random mutation operator and 0.1 percentage of uniform cross operator, it corresponding to the inequality $\varepsilon \ge -8$.

- Exploit space solutions

To exploit space solutions, the algorithm applied to the population random mutation a percentage of 0.9 and 0.1 percentage of arithmetic cross operator. it corresponding to the inequality $-18 \le \varepsilon \le -12$.

- Apply hybrid mode

It's a transition between exploration and exploitation which correspond to 0.5 percentage of cross probability and 0.5 percentage of mutation probability. The range of stopping criteria is: $-12 \le \varepsilon \le -8$

III. SIMULATION AND RESULTS

In order to validate the proposed procedure and to verify the feasibility of the corridor method to solve the EED, a 3-units generation system is tested [10] and extent to 6, 10 and 15 units génération. The proposed method is implemented with Matlab 2010.b on a core i3 2.1 GHz and the results are compared with other evolutionary algorithms (GA and GA multi-obj) of optimization tool. The data concerning the unit generation is given in table 1 to table 2 [10].

Table 1. The 3-units system data

Unit	P_i^{max} (MW)	P_i^{min} (MW)	a ($ /h)	b ($ /MWh)	c ($ /MW^{2}h)	R_i^{up} ($ /MW)	R_i^{down} ($ /MWh)
1	600	150	561	7.29	0.00156	100	100
2	400	100	310	7.85	0.00194	80	80
3	200	50	78	7.97	0.00482	50	50

Table 2. SO_2 and NOx coefficients emission gas data of 3-units

Units	α_{so_2} (tons/h)	α_{Nox} (tons/h)	β_{so_2} (tons/MWh)	β_{Nox} (tons/MWh)	δ_{so_2} (tons/MW^{2}h)	δ_{Nox} (tons/MW^{2}h)
1	0,5783298	0,04373254	0,00816466	-9,4868099 e^{-6}	1,6103e^{-6}	1,4721848 e^{-7}
2	0,3515338	0,055821713	0,00891174	-9,7252878 e^{-5}	5,4658 e^{-6}	3,0207577 e^{-7}
3	0,0884504	0,027731524	0,00903782	-3,5373734 e^{-4}	5,4658 e^{-6}	1,9338531 e^{-6}

In the implementation, we add the different coefficients of each gas per groups to have the coefficient of the whole gas.

3.1 Achievement of Pareto front

The Pareto front is obtained, keeping the best individuals (individuals who have the minimum fuel cost are conserved in relation to the emission axes and vice versa) that respect all the contraints in each corridor during the evolution. To simulate the evolution of pareto front we have initialize the population size at 300 , the maximum generation at 1000 ,the number of corridor at 50 and load demand is 1000MW.

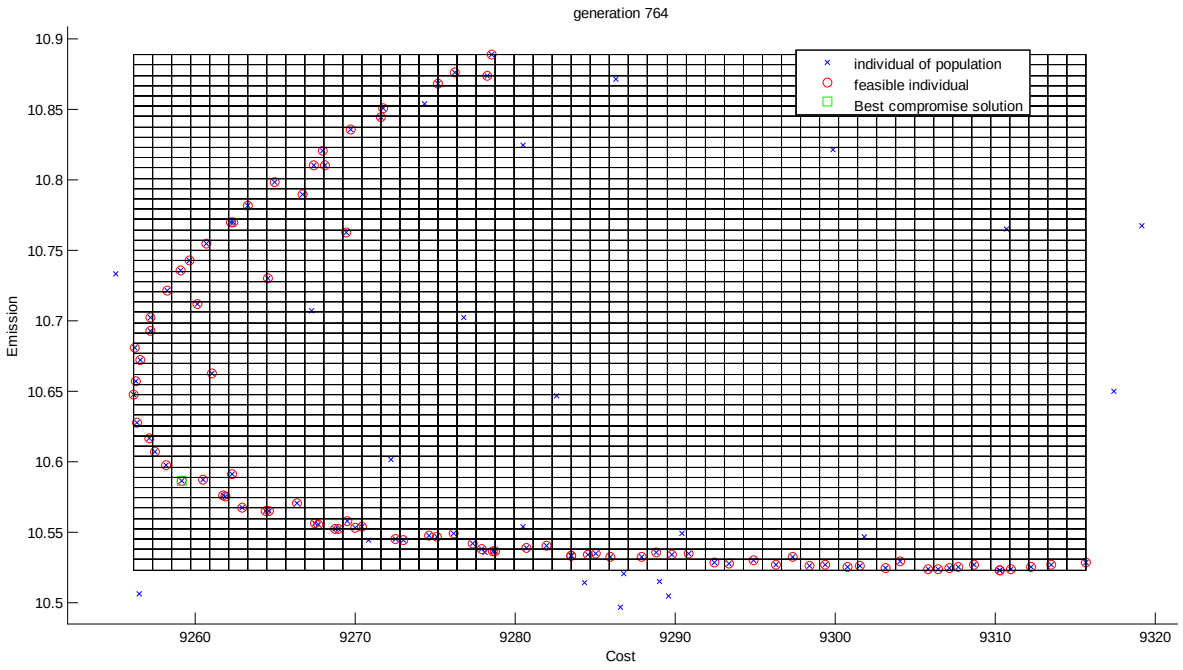

Figure 2 : Pareto optimal front at the end of process (1000MW load demand).

In the search of the best solution in each corridor, at the beginning the algorithm could not find the best feasible solutions but in the process of evolution the number of these solutions increases up to the Pareto optimal front.

3.1. Study of convergence

The curve convergence show that until one number of generations the algorithm finds the best solution, from this times gas emission and fuel cost is uniform. It expresses the performance of stopping criteria.

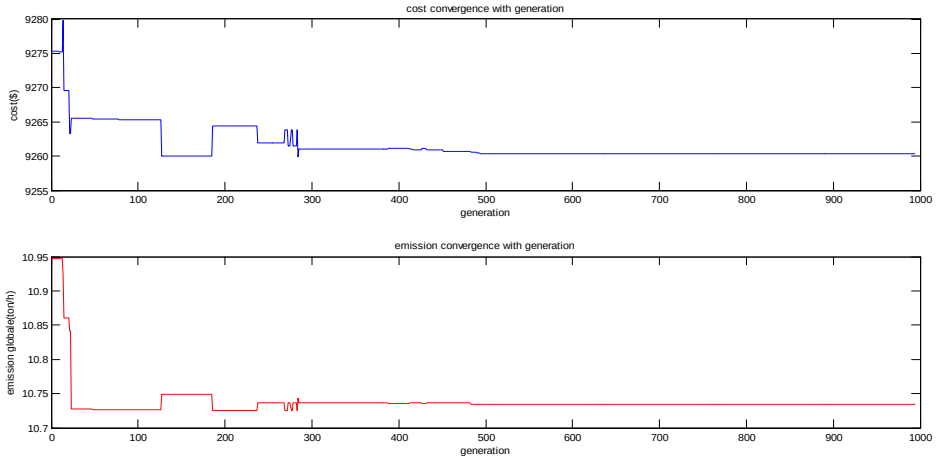

Figure 3: Convergence of fuel cost($) and gas emissions(ton/h) objective functions (1000MW).

3.2. Apply of method to 24 hours

To present the effectiveness of our approach to unit commitment and EED, we have apply it to plan the production of 3-units during 24 hours.

Table 3. Unit commitment and EED during 24 hours

Hours (H)	Demands (MW)	P1 (MW)	P2 (MW)	P3 (MW)	Fuel cost X10^3($)	Emission gas (ton/h)	Starting cost ($/MWh)	Total cost ($)
1	550	0	0	549.9	5.0415	5.6380		
2	600	0	0	599.9	5.4957	6.1468		
3	650	108.0382	0	541.8742	5.9646	6.6979	50	
4	700	114.5484	0	585.351	6.4169	7.2059		
5	750	150.228	0	599.67	6.8777	7.7323		
6	800	0	224.27	575.62	7.4424	8.5731	80	
7	850	0	250.314	599.58	7.8893	9.1188		
8	900	0	300.541	599.3621	8.3352	9.7188		
9	950	114.9563	239.4409	595.5072	8.8142	10.1626	50	
10	1000	128.8152	275.9956	595.0968	9.2607	10.7347		
11	1050	141.965	308.5501	599.3873	9.7144	11.3159		
12	900	0	300.03	599.8287	8.3342	9.7188		
13	850	0	250.0713	599.8287	7.8894	9.1184		
14	800	0	225.58	574.3207	7.4419	8.5747		
15	750	150.7585	0	599.1479	6.8779	7.7327	50	
16	700	114.5434	0	585.355	6.4116	7.2059		
17	650	108.0326	0	541.8732	5.9646	6.6979		
18	600	0	0	599.9	5.4957	6.1468		
19	730	130.2853	0	599.6148	6.6913	7.5171	50	
20	820	0	233.9595	585.9423	7.6209	8.7892	80	
21	860	0	260.1659	599.7343	7.9778	9.2361		
22	900	0	300.531	599.3721	8.3352	9.7188		
23	950	114.9553	239.4419	595.5072	8.8142	10.1626	50	
24	1000	128.8152	275.9956	595.0968	9.2607	10.7347		
Total					178.368		410	178778

In function of demand we see that some unit could be on and other off, to minimize the fuel cost and emission gas. The plan production of different units is represent in follow figure

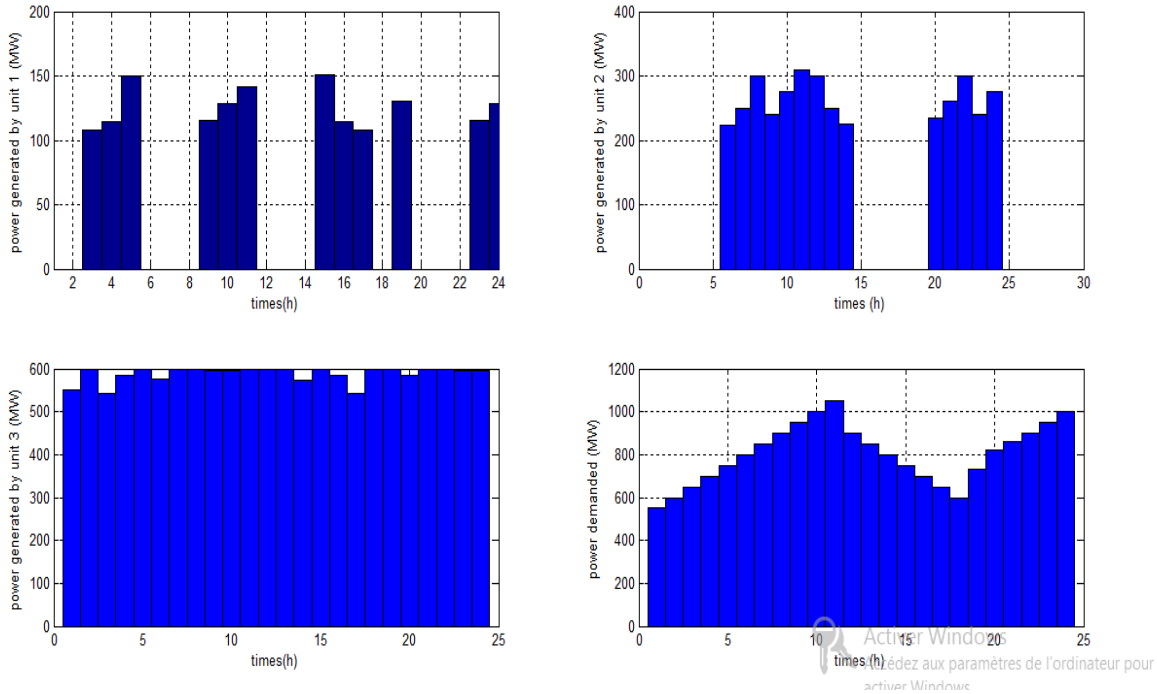

Figure 3: Production plan of different units

3.3. Comparison of results

To show the effectiveness of the proposed method, we have compared it with other evolutionary algorithm of optimization tool of matlab. The same parameter is considered and the criteria for comparisons are cost and average CPU times.

Tableau 4: Comparison methods with 1000MW of load demand

	GA	GA multi-obj.	corridor
P_1 (MW)	400.0587	399,999	598.4477
P_2 (MW)	399.9885	399,999	275.8265
P_3(MW)	199.9518	199,999	125.6293
Fuel Cost($ /h)	9879.2053	9878,988	9260,6
Emission ton/h	11.755	11,644	10.5768
Average CPU times	244.9135	261.9536	23.29854

This table show that our method is best in term of fuel cost and emission gas

3.4. Impact of numbers of units to fuel cost, gas emission and average CPU times

To show this impact, we have multiplied the number of units of our 3-units. The results are presented to follow table.

Tableau 5: Impact of numbers of units to fuel cost, gas emission and average CPU times

Number of units	3	6	10	15
Fuel cost($)	9.2606	9.1911	9.176	9.177
Gas emission(ton/h)	10.7347	10.2771	10.3679	10.3683
Average times(s)	23.29	31.92	49.40	104.61

This table show that when the number of units increases, the fuel cost, gas emission and average CPU decrease.

IV. CONCLUSION

In this paper, an approach based on the evolutionary algorithm has been presented and applied to environmental/economic power dispatch optimization problem. The problem has been formulated as a bi-objective optimization problem with competing fuel cost and environmental impact objectives. The proposed approach has a diversity-preserving mechanism to find Pareto-optimal solution. The optimal Pareto front is obtained from minimizing each objective function in each corridor and keeping the best individuals in dynamic achieves. Moreover, a fuzzy-based mechanism is employed to extract the best compromise solution over the trade-off curve. The results show that the proposed approach is efficient for solving bi-objective optimization

where multiple Pareto-optimal solutions can be found in one simulation run. In addition, the non-dominated solutions in the obtained Pareto-optimal set are well distributed and have satisfactory diversity characteristics. Comparatively to other approach, the most important aspect of the proposed approach is the reduce time to find optimal Pareto front, fuel cost, gas emission, the consideration of unit commitment problem and the possibility to manage system which have n-generation units and best compromise.

REFERENCES

[1] Brodesky S. F, Hahn R. W. Assessing the influence of power pools on emission constrained economic dispatch. IEEE Trans Power Syst 1986;1(1).pp:57–62.

[2] Granelli G. P, Montagna M, Pasini G. L, Marannino P. Emission constrained dynamic dispatch. Electr Power Syst Res 1992;24.pp: 56–64.

[3] Chang C. S, Wong K. P, Fan B. Security-constrained multiobjective generation dispatch using bicriterion global optimization. IEE Proc—GenerTransmDistrib 1995;142(4):406–14.

[4] R Manoj Kumar. Bavisetti, T.KranthiKiran. Optimization Of Combined Economic and Emission Dispatch Problem – A Comparative Study for 30 Bus Systems. IOSR Journal of Electrical and Electronics Engineering (IOSR-JEEE) 2012 ;Vol 2 : PP 37-43

[5] M. A. Abido. Environmental/Economic Power Dispatch Using Multiobjective Evolutionary Algorithms. IEEE Transactions On Power Systems ; 2003 VOL. 18, NO. 4. Pp :1529-1537

[6] Alkhalil Firas. «Supervision, économie et impact sur l'environnement d'un système d'énergie électrique associé à une centrale photovoltaïque »thèse de Doctorat Paris tech. 2011

[7] Samani.h, Razmezani.M and Naseh.M.R. (2013). Unit Commitment and Methods for Solving; a Review .J. Basic. Appl. Sci. Res., 3(2s) 358-364

[8] Lubing Xie, Songling Wang & Zhiquan Wu. Study on Economic, Rapid and Environmental Power Dispatch. Modern applied sciences vol.3 $N^0$6. 2009. pp :38-44

[9] Jean Dipama. « Optimisation Multi-Objectif Des Systèmes Énergétiques ».thèse soutenue à l'université de Montréal. 2010

[10] Farid Benhamida, Rachid Belhachem. Dynamic Constrained Economic/Emission Dispatch Scheduling Using Neural Network .Power Engineering And Electrical Engineering.Volume: 11 $N^0$1 .2013.pp :1-9

ISSN (e): 2250 – 3005 || Vol, 04 || Issue, 10 || October – 2014 ||
International Journal of Computational Engineering Research (IJCER)

On The Derivatives and Partial Derivatives of A Certain Generalized Hyper geometric Function

[1]Yashwant Singh, [2]Nandavasanthnadiger Kulkarni
[1]Department of Mathematics, Government College, Kaladera, Jaipur, Rajasthan, India
[2]Department of Mathematics, Dayananda Sagar college of arts, science and commerce, Kumaraswamy layout, Bangalore, Karnataka, India

ABSTRACT
In this paper, methods involving derivatives and the Mellin transformation are employed in obtaining finite summations for the $\overline{H}$ -function of two variables and certain special partial derivatives for the $\overline{H}$ -function of two variables with respect to parameters.

KEY WORDS: Derivatives, Partial derivatives, $\overline{H}$ -function of two variables, Mellin transformation.
(2000 Mathematics Subject Classification: 33C99)

I. INTRODUCTION

The $\overline{H}$ -function of two variables defined and represented by Singh and Mandia [12] in the following manner:

$$\overline{H}\left[x,y\right]=\overline{H}\begin{bmatrix}x\\y\end{bmatrix}=\overline{H}^{o,n_1:\ m_2,n_2:m_3,n_2}_{p_1,q_1:p_2,q_2;p_2,q_2}\left[\begin{matrix}x\\y\end{matrix}\middle|\begin{matrix}(a_j,\alpha_j;A_j)_{1,p_1},(c_j,\gamma_j;K_j)_{1,n_2},(c_j,\gamma_j)_{n_2+1,p_2},(e_j,E_j;R_j)_{1,n_3},(e_j,E_j)_{n_3+1,p_3}\\(b_j,\beta_j;B_j)_{1,q_1},(d_j,\delta_j)_{1,m_2},(d_j,\delta_j;L_j)_{m_2+1,q_2},(f_j,F_j)_{1,m_3},(f_j,F_j;S_j)_{m_3+1,q_3}\end{matrix}\right]$$

$$=-\frac{1}{4\pi^2}\int_{L_1}\int_{L_2}\phi_1(\xi,\eta)\,\phi_2(\xi)\phi_3(\eta)\,x^{\xi}y^{\eta}\,d\xi\,d\eta \qquad (1.1)$$

Where

$$\phi_1(\xi,\eta)=\frac{\prod_{j=1}^{n_1}\Gamma\left(1-a_j+\alpha_j\xi+A_j\eta\right)}{\prod_{j=n_1+1}^{p_1}\Gamma\left(a_j-\alpha_j\xi-A_j\eta\right)\prod_{j=1}^{q_1}\Gamma\left(1-b_j+\beta_j\xi+B_j\eta\right)} \qquad (1.2)$$

$$\phi_2(\xi)=\frac{\prod_{j=1}^{n_2}\left\{\Gamma\left(1-c_j+\gamma_j\xi\right)\right\}^{K_j}\prod_{j=1}^{m_2}\Gamma\left(d_j-\delta_j\xi\right)}{\prod_{j=n_2+1}^{p_2}\Gamma\left(c_j-\gamma_j\xi\right)\prod_{j=m_2+1}^{q_2}\left\{\Gamma\left(1-d_j+\delta_j\xi\right)\right\}^{L_j}} \qquad (1.3)$$

$$\phi_3(\eta)=\frac{\prod_{j=1}^{n_3}\left\{\Gamma\left(1-e_j+E_j\eta\right)\right\}^{R_j}\prod_{j=1}^{m_3}\Gamma\left(f_j-F_j\eta\right)}{\prod_{j=n_3+1}^{p_3}\Gamma\left(e_j-E_j\eta\right)\prod_{j=m_3+1}^{q_3}\left\{\Gamma\left(1-f_j+F_j\eta\right)\right\}^{S_j}} \qquad (1.4)$$

Where x and y are not equal to zero (real or complex), and an empty product is interpreted as unity p_i, q_i, n_i, m_j are non-negative integers such that $0 \le n_i \le p_i, o \le m_j \le q_j (i = 1,2,3;\ j = 2,3)$. All the $a_j (j = 1,2,\ldots, p_1), b_j (j = 1,2,\ldots, q_1), c_j (j = 1,2,\ldots, p_2), d_j (j = 1,2,\ldots, q_2),$

$e_j (j = 1,2,\ldots, p_3),\ f_j (j = 1,2,\ldots, q_3)$ are complex parameters. $\gamma_j \ge 0 (j = 1,2,\ldots, p_2), \delta_j \ge 0 (j = 1,2,\ldots, q_2)$ (not all zero simultaneously), similarly $E_j \ge 0 (j = 1,2,\ldots, p_3), F_j \ge 0 (j = 1,2,\ldots, q_3)$ (not all zero simultaneously). The exponents $K_j (j = 1,2,\ldots, n_3), L_j (j = m_2 + 1,\ldots, q_2), R_j (j = 1,2,\ldots, n_3), S_j (j = m_3 + 1,\ldots, q_3)$ can take on non-negative values.

The contour L_1 is in ξ -plane and runs from $-i\infty$ to $+i\infty$. The poles of $\Gamma\left(d_j - \delta_j \xi\right) (j = 1,2,\ldots, m_2)$ lie to the right and the poles of $\Gamma\left\{\left(1 - c_j + \gamma_j \xi\right)\right\}^{K_j} (j = 1,2,\ldots, n_2), \Gamma\left(1 - a_j + \alpha_j \xi + A_j \eta\right) (j = 1,2,\ldots, n_1)$ to the left of the contour. For $K_j (j = 1,2,\ldots, n_2)$ not an integer, the poles of gamma functions of the numerator in (1.3) are converted to the branch points.

The contour L_2 is in η -plane and runs from $-i\infty$ to $+i\infty$. The poles of $\Gamma\left(f_j - F_j \eta\right) (j = 1,2,\ldots, m_3)$ lie to the right and the poles of $\Gamma\left\{\left(1 - e_j + E_j \eta\right)\right\}^{R_j} (j = 1,2,\ldots, n_3), \Gamma\left(1 - a_j + \alpha_j \xi + A_j \eta\right) (j = 1,2,\ldots, n_1)$ to the left of the contour. For $R_j (j = 1,2,\ldots, n_3)$ not an integer, the poles of gamma functions of the numerator in (1.4) are converted to the branch points.

The functions defined in (1.1) is an analytic function of x and y , if

$$U = \sum_{j=1}^{p_1} \alpha_j + \sum_{j=1}^{p_2} \gamma_j - \sum_{j=1}^{q_1} \beta_j - \sum_{j=1}^{q_2} \delta_j < 0 \qquad (1.5)$$

$$V = \sum_{j=1}^{p_1} A_j + \sum_{j=1}^{p_3} E_j - \sum_{j=1}^{q_1} B_j - \sum_{j=1}^{q_3} F_j < 0 \qquad (1.6)$$

The integral in (1.1) converges under the following set of conditions:

$$\Omega = \sum_{j=1}^{n_1} \alpha_j - \sum_{j=n_1+1}^{p_1} \alpha_j + \sum_{j=1}^{m_2} \delta_j - \sum_{j=m_2+1}^{q_2} \delta_j L_j + \sum_{j=1}^{n_2} \gamma_j K_j - \sum_{j=n_2+1}^{p_2} \gamma_j - \sum_{j=1}^{q_1} \beta_j > 0 \qquad (1.7)$$

$$\Lambda = \sum_{j=1}^{n_1} A_j - \sum_{j=n_1+1}^{p_1} A_j + \sum_{j=1}^{m_2} F_j - \sum_{j=m_2+1}^{q_2} F_j S_j + \sum_{j=1}^{n_3} E_j R_j - \sum_{j=n_2+1}^{p_3} E_j - \sum_{j=1}^{q_1} B_j > 0 \qquad (1.8)$$

$$|\arg x| < \frac{1}{2}\Omega\pi, \ |\arg y| < \frac{1}{2}\Lambda\pi \qquad (1.9)$$

The behavior of the $\overline{H}$ -function of two variables for small values of $|z|$ follows as:

$$\overline{H}[x, y] = 0(|x|^{\alpha}|y|^{\beta}), \max\{|x|,|y|\} \to 0 \tag{1.10}$$

Where

$$\alpha = \min_{1\le j\le m_2}\left\lceil \left|\mathrm{Re}\left(\frac{d_j}{\delta_j}\right)\right|\right\rceil \qquad \beta = \min_{1\le j\le m_2}\left\lceil \left|\mathrm{Re}\left(\frac{f_j}{F_j}\right)\right|\right\rceil \tag{1.11}$$

For large value of $|z|$,

$$\overline{H}[x, y] = 0\left\{|x|^{\alpha'},|y|^{\beta'}\right\}, \min\{|x|,|y|\} \to 0 \tag{1.12}$$

Where

$$\alpha' = \max_{1\le j\le n_2}\mathrm{Re}\left(K_j\frac{c_j-1}{\gamma_j}\right),\ \beta' = \max_{1\le j\le n_3}\mathrm{Re}\left(R_j\frac{e_j-1}{E_j}\right) \tag{1.13}$$

Provided that $U < 0$ and $V < 0$.

If we take $K_j = 1(j = 1, 2, \ldots, n_2)$, $L_j = 1(j = m_2+1, \ldots, q_2)$, $R_j = 1(j = 1, 2, \ldots, n_3)$, $S_j = 1(j = m_3+1, \ldots, q_3)$ in (2.1), the $\overline{H}$-function of two variables reduces to H-function of two variables due to [9].

If we set $n_1 = p_1 = q_1 = 0$, the $\overline{H}$-function of two variables breaks up into a product of two $\overline{H}$-function of one variable namely

$$\overline{H}^{0,0:m_2,n_2:m_3,n_3}_{0,0:p_2,q_2:p_3,q_3}\left[\begin{matrix}x\\ y\end{matrix}\middle|\begin{matrix}--:(c_j,\gamma_j;K_j)_{1,n_2},(c_j,\gamma_j)_{n+1,p_2}:(e_j,E_j;R_j)_{1,n_3},(e_j,E_j)_{n_3+1,p_3}\\ --:(d_j,\delta_j)_{1,m_2},(d_j,\delta_j;L_j)_{m_2+1,q_2}:(f_j,F_j)_{1,m_3},(f_j,F_j;S_j)_{m_3+1,q_3}\end{matrix}\right]$$

$$= \overline{H}^{m_2,n_2}_{p_2,q_2}\left[x\middle|\begin{matrix}(c_j,\gamma_j;K_j)_{1,n_2},(c_j,\gamma_j)_{n_2+1,p_2}\\ (d_j,\delta_j)_{1,m_2},(d_j,\delta_j;L_j)_{m_2+1,q_2}\end{matrix}\right]\overline{H}^{m_3,n_3}_{p_3,q_3}\left[y\middle|\begin{matrix}(e_j,E_j;R_j)_{1,n_3},(e_j,E_j)_{n_3+1,p_3}\\ (f_j,F_j)_{1,m_3},(f_j,F_j;S_j)_{m_3+1,q_3}\end{matrix}\right] \tag{1.14}$$

If $\lambda > 0$, we then obtain

$$\lambda^2\overline{H}^{0,n_1:m_2,n_2:m_3,n_3}_{p_1,q_1:p_2,q_2:p_3,q_3}\left[\begin{matrix}x^{\lambda}\\ y^{\lambda}\end{matrix}\middle|\begin{matrix}(a_j,\lambda\alpha_j;A_j)_{1,p_1},(c_j,\lambda\gamma_j;K_j)_{1,n_2},(c_j,\lambda\gamma_j)_{n_2+1,p_2},(e_j,\lambda E_j;R_j)_{1,n_3},(e_j,\lambda E_j)_{n_3+1,p_3}\\ (b_j,\lambda\beta_j;B_j)_{1,q_1},(d_j,\lambda\delta_j)_{1,m_2},(d_j,\lambda\delta_j;L_j)_{m_2+1,q_2},(f_j,\lambda F_j)_{1,m_3},(f_j,\lambda F_j;S_j)_{m_3+1,q_3}\end{matrix}\right]$$

$$= \overline{H}^{0,n_1:m_2,n_2:m_3,n_3}_{p_1,q_1:p_2,q_2:p_3,q_3}\left[\begin{matrix}x\\ y\end{matrix}\middle|\begin{matrix}(a_j,\alpha_j;A_j)_{1,p_1},(c_j,\gamma_j;K_j)_{1,n_2},(c_j,\gamma_j)_{n_2+1,p_2},(e_j,E_j;R_j)_{1,n_3},(e_j,E_j)_{n_3+1,p_3}\\ (b_j,\beta_j;B_j)_{1,q_1},(d_j,\delta_j)_{1,m_2},(d_j,\delta_j;L_j)_{m_2+1,q_2},(f_j,F_j)_{1,m_3},(f_j,F_j;S_j)_{m_3+1,q_3}\end{matrix}\right] \tag{1.15}$$

$$\overline{H}^{0,n_1:m_2,n_2:m_3,n_3}_{p_1,q_1:p_2,q_2:p_3,q_3}\left[\begin{matrix}1/x\\ 1/y\end{matrix}\middle|\begin{matrix}(a_j,\alpha_j;A_j)_{1,p_1},(c_j,\gamma_j;K_j)_{1,n_2},(c_j,\gamma_j)_{n_2+1,p_2},(e_j,E_j;R_j)_{1,n_3},(e_j,E_j)_{n_3+1,p_3}\\ (b_j,\beta_j;B_j)_{1,q_1},(d_j,\delta_j)_{1,m_2},(d_j,\delta_j;L_j)_{m_2+1,q_2},(f_j,F_j)_{1,m_3},(f_j,F_j;S_j)_{m_3+1,q_3}\end{matrix}\right]$$

$$= \overline{H}^{0,n_1:m_2,n_2:m_3,n_3}_{p_1,q_1:p_2,q_2:p_3,q_3}\left[\begin{matrix}x\\ y\end{matrix}\middle|\begin{matrix}(1-b_j,\beta_j;B_j)_{1,q_1},(1-d_j,\delta_j)_{1,m_2},(1-d_j,\delta_j;L_j)_{m_2+1,q_2},(1-f_j,F_j)_{1,m_3},(1-f_j,F_j;S_j)_{m_3+1,q_3}\\ (1-a_j,\alpha_j;A_j)_{1,p_1},(1-c_j,\gamma_j;K_j)_{1,n_2},(1-c_j,\gamma_j)_{n_2+1,p_2},(1-e_j,E_j;R_j)_{1,n_3},(1-e_j,E_j)_{n_3+1,p_3}\end{matrix}\right] \tag{1.16}$$

II. MAIN RESULTS

If t be an arbitrary parameter and α', α'' be positive real numbers, then it can be verified that

$$D^{''}\left\{\overline{H}\left[z_1 t^{\alpha'}, z_2 t^{\alpha''}\right]\right\} = t^{e-3}\,\overline{H}^{o,n_1+1:\ m_2,n_2:m_3,n_2}_{p_1+1,q_1+1:p_2,q_2;p_2,q_2}$$

$$\left[\begin{matrix} z_1 t^{\alpha'} \\ z_2 t^{\alpha''} \end{matrix}\middle|\begin{matrix} (1-e+n;\alpha',\alpha''),\left(a_j,\alpha_j;A_j\right)_{1,p_1},\left(c_j,\gamma_j;K_j\right)_{1,n_2},\left(c_j,\gamma_j\right)_{n_2+1,p_2},\left(e_j,E_j;R_j\right)_{1,n_3},\left(e_j,E_j\right)_{n_3+1,p_3} \\ \left(b_j,\beta_j;B_j\right)_{1,q_1},(1-e;\alpha',\alpha''),\left(d_j,\delta_j\right)_{1,m_2},\left(d_j,\delta_j;L_j\right)_{m_2+1,q_2},\left(f_j,F_j\right)_{1,m_3},\left(f_j,F_j;S_j\right)_{m_3+1,q_3} \end{matrix}\right] \tag{2.1}$$

And

$$t^{e-1}\,\overline{H}^{0,0:m_2,n_2:m_3,n_3}_{0,0:p_2,q_2:p_3,q_3}\left[\begin{matrix} z_1 t^{\alpha'} \\ z_2 t^{\alpha''} \end{matrix}\middle|\begin{matrix} --:\left(c_j,\gamma_j;K_j\right)_{1,n_2},\left(c_j,\gamma_j\right)_{n+1,p_2}:\left(e_j,E_j;R_j\right)_{1,n_3},\left(e_j,E_j\right)_{n_3+1,p_3} \\ --:\left(d_j,\delta_j\right)_{1,m_2},\left(d_j,\delta_j;L_j\right)_{m_2+1,q_2}:\left(f_j,F_j\right)_{1,m_3},\left(f_j,F_j;S_j\right)_{m_3+1,q_3} \end{matrix}\right] =$$

$$t^{\frac{(e-1)}{2}}\,\overline{H}^{m_2,n_2}_{p_2,q_2}\left[\begin{matrix} z_1 t^{\alpha'} \end{matrix}\middle|\begin{matrix} \left(c_j,\gamma_j;K_j\right)_{1,n_2},\left(c_j,\gamma_j\right)_{n_2+1,p_2} \\ \left(d_j,\delta_j\right)_{1,m_2},\left(d_j,\delta_j;L_j\right)_{m_2+1,q_2} \end{matrix}\right] \times t^{\frac{(e-1)}{2}}\,\overline{H}^{m_3,n_3}_{p_3,q_3}\left[\begin{matrix} z_2 t^{\alpha''} \end{matrix}\middle|\begin{matrix} \left(e_j,E_j;R_j\right)_{1,n_3},\left(e_j,E_j\right)_{n_3+1,p_3} \\ \left(f_j,F_j\right)_{1,m_3},\left(f_j,F_j;S_j\right)_{m_3+1,q_3} \end{matrix}\right] \tag{2.2}$$

Differentiating (2.2) two times w.r.t. t and simplifying, it follows by induction that

$$\overline{H}^{0,1:m_2,n_2:m_3,n_3}_{1,1:p_2,q_2:p_3,q_3}\left[\begin{matrix} z_1 t^{\alpha'} \\ z_2 t^{\alpha''} \end{matrix}\middle|\begin{matrix} (1-e+n;\alpha',\alpha''):\left(c_j,\gamma_j;K_j\right)_{1,n_2},\left(c_j,\gamma_j\right)_{n+1,p_2}:\left(e_j,E_j;R_j\right)_{1,n_3},\left(e_j,E_j\right)_{n_3+1,p_3} \\ (1-e;\alpha',\alpha''):\left(d_j,\delta_j\right)_{1,m_2},\left(d_j,\delta_j;L_j\right)_{m_2+1,q_2}:\left(f_j,F_j\right)_{1,m_3},\left(f_j,F_j;S_j\right)_{m_3+1,q_3} \end{matrix}\right]$$

$$= \sum_{\substack{n_1,n_2=0 \\ n_1+n_2=n}}^{n} \frac{n!}{n_1!\,n_2!}\,\overline{H}^{0,0:m_2,n_2+1:m_3,n_3+1}_{0,0:p_2+1,q_2+1:p_3+1,q_3+1}$$

$$\left[\begin{matrix} z_1 t^{\alpha'} \\ z_2 t^{\alpha''} \end{matrix}\middle|\begin{matrix} --:\left(1+n_1-\frac{e+1}{2},\alpha';1\right)\left(c_j,\gamma_j;K_j\right)_{1,n_2},\left(c_j,\gamma_j\right)_{n+1,p_2}:\left(1+n_2-\frac{e+1}{2},\alpha'';1\right)\left(e_j,E_j;R_j\right)_{1,n_3},\left(e_j,E_j\right)_{n_3+1,p_3} \\ --:\left(d_j,\delta_j\right)_{1,m_2},\left(d_j,\delta_j;L_j\right)_{m_2+1,q_2},\left(1-\frac{e+1}{2},\alpha';1\right):\left(f_j,F_j\right)_{1,m_3},\left(f_j,F_j;S_j\right)_{m_3+1,q_3},\left(1-\frac{e+1}{2},\alpha'';1\right) \end{matrix}\right] \tag{2.3}$$

(2.3)readily admits an extension and we have

$$= \sum_{\substack{n_1,n_2=0 \\ n_1+n_2=n}}^{n} \frac{n!}{n_1!\,n_2!}\,\overline{H}^{o,n_1:\ m_2,n_2+1:\ m_3,n_2+1}_{p_1,q_1:p_2+1,q_2+1;p_2+1,q_2+1}$$

$$\left[\begin{matrix} z_1 t^{\alpha'} \\ z_2 t^{\alpha''} \end{matrix}\middle|\begin{matrix} \left(a_j,\alpha_j;A_j\right)_{1,p_1},\left(1+n_1-\frac{e+1}{2},\alpha';1\right),\left(c_j,\gamma_j;K_j\right)_{1,n_2},\left(c_j,\gamma_j\right)_{n_2+1,p_2},\left(1+n_2-\frac{e+1}{2},\alpha'';1\right),\left(e_j,E_j;R_j\right)_{1,n_3},\left(e_j,E_j\right)_{n_3+1,p_3} \\ \left(b_j,\beta_j;B_j\right)_{1,q_1},\left(d_j,\delta_j\right)_{1,m_2},\left(d_j,\delta_j;L_j\right)_{m_2+1,q_2},\left(1-\frac{e+1}{2},\alpha';1\right),\left(f_j,F_j\right)_{1,m_3},\left(f_j,F_j;S_j\right)_{m_3+1,q_3},\left(1-\frac{e+1}{2},\alpha'';1\right) \end{matrix}\right] \tag{2.4}$$

Considering various other forms that (2.1)admits, similar other results can be obtained.

In the next place, in view of (2.1) we note that the 2-dimensional Mellin-transformation ([6],11.2) $M^{''}$ of the $\overline{H}$ -function of two variables is given by

$$M^{''}(\overline{H}) = Q(-\xi,-\eta)$$

Provided

$$-\min_{1\le j\le m_2}\mathrm{Re}\left(\frac{d_j}{\delta_j}\right) < \xi < \max_{1\le j\le n_2}\mathrm{Re}\left(K_j\frac{c_j-1}{\gamma_j}\right)$$

$$-\min_{1\le j\le m_3}\operatorname{Re}\left(\frac{f_j}{F_j}\right)<\eta<\max_{1\le j\le n_3}\operatorname{Re}\left(R_j\frac{e_j-1}{E_j}\right)$$

We also note that, since (1.7 (30) of Erdelyi [7]) for a positive integer N ,

$$\psi(a+N)-\psi(a)=\sum_{k=1}^{N}\frac{(-1)^{k-1}N!}{k(N-k)!}\frac{\psi(a)}{\psi(a+k)};\psi(a)=\frac{\Gamma'(a)}{\Gamma(a)},$$

Partial differentiation of the gamma product $\Gamma\left(1-\frac{e}{2}+\alpha'\xi+\alpha''\eta\right)\Gamma\left(1+\frac{e}{2}+\alpha'\xi+\alpha''\eta\right)$ w.r.t. the arbitrary parameter e at $e=N$ can be expressed as a finite sum

$$\frac{\partial}{\partial e}\left\{\Gamma\left(1-\frac{e}{2}+\alpha'\xi+\alpha''\eta\right)\Gamma\left(1+\frac{e}{2}+\alpha'\xi+\alpha''\eta\right)\right\}\Bigg|_{e=N}$$

$$=\frac{1}{2}\Gamma\left(1-\frac{N}{2}+\alpha'\xi+\alpha''\eta\right)\sum_{k=1}^{N}\frac{(-1)^{k-1}N!}{k(N-k)!}\frac{\Gamma\left(1+\frac{N}{2}+\alpha'\xi+\alpha''\eta\right)}{\Gamma\left(1+\frac{N}{2}-k+\alpha'\xi+\alpha''\eta\right)},$$

Where α',α'' are positive real numbers.

Thus for $n>0, N>0$, we have

$$M''\left\{\overline{H}_{p_1+2,q_1:p_2,q_2;p_2,q_2}^{o,n_1+2:\ m_2,n_2:m_3,n_2}\left[\begin{matrix}z_1\\z_2\end{matrix}\right.\right.$$

$$\left.\left.\begin{matrix}\left(-\frac{e}{2};\alpha',\alpha''\right),\left(\frac{e}{2};\alpha',\alpha''\right),(a_j,\alpha_j;A_j)_{1,p_1},(c_j,\gamma_j;K_j)_{1,n_2},(c_j,\gamma_j)_{n_2+1,p_2},\left(1+n_2-\frac{e+1}{2},\alpha'';1\right),(e_j,E_j;R_j)_{1,n_3},(e_j,E_j)_{n_3+1,p_3}\\(b_j,\beta_j;B_j)_{1,q_1},(d_j,\delta_j)_{1,m_2},(d_j,\delta_j;L_j)_{m_2+1,q_2},\left(1-\frac{e+1}{2},\alpha';1\right),(f_j,F_j)_{1,m_3},(f_j,F_j;S_j)_{m_3+1,q_3},\left(1-\frac{e+1}{2},\alpha'';1\right)\end{matrix}\right]_{e=N}\right\}$$

$$=\frac{N!}{2}\sum_{k=1}^{N}\frac{(-1)^{k-1}N!}{k(N-k)!}\frac{\Gamma\left(1+\frac{N}{2}-\alpha'\xi-\alpha''\eta\right)\Gamma\left(1-\frac{N}{2}-\alpha'\xi-\alpha''\eta\right)}{\Gamma\left(1+\frac{N}{2}-k-\alpha'\xi-\alpha''\eta\right)}$$

$$\times Q(-\xi,-\eta)$$

$$M''\left\{\frac{N!}{2}\sum_{k=1}^{N}\frac{(-1)^{k-1}}{k(N-k)!}\overline{H}_{p_1+3,q_1+1:p_2,q_2;p_2,q_2}^{o,n_1+3:\ m_2,n_2:m_3,n_2}\left[\begin{matrix}z_1\\z_2\end{matrix}\right.\right.$$

$$\left.\left.\begin{matrix}\left(-\frac{N}{2};\alpha',\alpha''\right),\left(-\frac{N}{2};\alpha',\alpha''\right),\left(\frac{N}{2};\alpha',\alpha''\right),(a_j,\alpha_j;A_j)_{1,p_1},(c_j,\gamma_j;K_j)_{1,n_2},(c_j,\gamma_j)_{n_2+1,p_2},(e_j,E_j;R_j)_{1,n_3},(e_j,E_j)_{n_3+1,p_3}\\(b_j,\beta_j;B_j)_{1,q_1},\left(-\frac{N}{2}+k;\alpha',\alpha''\right),(d_j,\delta_j)_{1,m_2},(d_j,\delta_j;L_j)_{m_2+1,q_2},(f_j,F_j)_{1,m_3},(f_j,F_j;S_j)_{m_3+1,q_3}\end{matrix}\right]\right\} \quad (2.5)$$

But for $z^{(i)}=u^{-\alpha^{(i)}}, i=1,2$, (2.5) can be written as

$$\frac{\partial}{\partial e}\left\{ \overline{H}^{o,n_1+2:\ m_2,n_2:m_3,n_2}_{p_1+2,q_1:p_2,q_2;p_2,q_2}\left[\begin{matrix} z_1 \\ z_2 \end{matrix}\right.\right.$$

$$\left.\left.\left|\begin{matrix} \left(-\frac{e}{2};\alpha',\alpha''\right),\left(\frac{e}{2};\alpha',\alpha''\right),(a_j,\alpha_j;A_j)_{1,p_1},,(c_j,\gamma_j;K_j)_{1,n_2},(c_j,\gamma_j)_{n_2+1,p_2},(e_j,E_j;R_j)_{1,n_3},(e_j,E_j)_{n_3+1,p_3} \\ (b_j,\beta_j;B_j)_{1,q_1},(d_j,\delta_j)_{1,m_2},(d_j,\delta_j;L_j)_{m_2+1,q_2},(f_j,F_j)_{1,m_3},(f_j,F_j;S_j)_{m_3+1,q_3} \end{matrix}\right|_{e=N}\right\}$$

$$= \frac{N!}{2}\sum_{k=1}^{N}\frac{(-1)^N u^{\frac{N}{2}}}{k\,(N-k)!}$$

$$D_u^{N-k}\left\{ u^{\frac{N}{2}-k}\,\overline{H}^{o,n_1+2:\ m_2,n_2:m_3,n_2}_{p_1+2,q_1:p_2,q_2;p_2,q_2}\left[\begin{matrix} z_1 \\ z_2 \end{matrix}\right.\right.$$

$$\left.\left.\left|\begin{matrix} \left(-\frac{N}{2};\alpha',\alpha''\right),\left(\frac{N}{2};\alpha',\alpha''\right),(a_j,\alpha_j;A_j)_{1,p_1},,(c_j,\gamma_j;K_j)_{1,n_2},(c_j,\gamma_j)_{n_2+1,p_2},(e_j,E_j;R_j)_{1,n_3},(e_j,E_j)_{n_3+1,p_3} \\ (b_j,\beta_j;B_j)_{1,q_1},(d_j,\delta_j)_{1,m_2},(d_j,\delta_j;L_j)_{m_2+1,q_2},(f_j,F_j)_{1,m_3},(f_j,F_j;S_j)_{m_3+1,q_3} \end{matrix}\right|\right\} \qquad (2.6)$$

If we express the derivative into a sum, carry out the differentiations, interchange the order of summation and simplify, we obtain

$$\frac{\partial}{\partial e}\left\{ \overline{H}^{o,n_1+2:\ m_2,n_2:m_3,n_2}_{p_1+2,q_1:p_2,q_2;p_2,q_2}\left[\begin{matrix} z_1 \\ z_2 \end{matrix}\right.\right.$$

$$\left.\left.\left|\begin{matrix} \left(-\frac{e}{2};\alpha',\alpha''\right),\left(\frac{e}{2};\alpha',\alpha''\right),(a_j,\alpha_j;A_j)_{1,p_1},,(c_j,\gamma_j;K_j)_{1,n_2},(c_j,\gamma_j)_{n_2+1,p_2},(e_j,E_j;R_j)_{1,n_3},(e_j,E_j)_{n_3+1,p_3} \\ (b_j,\beta_j;B_j)_{1,q_1},(d_j,\delta_j)_{1,m_2},(d_j,\delta_j;L_j)_{m_2+1,q_2},(f_j,F_j)_{1,m_3},(f_j,F_j;S_j)_{m_3+1,q_3} \end{matrix}\right|_{e=N}\right\}$$

$$= \frac{N!}{2}\sum_{p=0}^{N-1}\frac{(-1)}{p!(N-p)!}\overline{H}^{o,n_1+2:\ m_2,n_2:m_3,n_2}_{p_1+2,q_1:p_2,q_2;p_2,q_2}$$

$$\left[\begin{matrix} z_1 \\ z_2 \end{matrix}\right.\left|\begin{matrix} \left(-\frac{N}{2};\alpha',\alpha''\right),\left(\frac{N}{2}+p;\alpha',\alpha''\right),(a_j,\alpha_j;A_j)_{1,p_1},,(c_j,\gamma_j;K_j)_{1,n_2},(c_j,\gamma_j)_{n_2+1,p_2},(e_j,E_j;R_j)_{1,n_3},(e_j,E_j)_{n_3+1,p_3} \\ (b_j,\beta_j;B_j)_{1,q_1},(d_j,\delta_j)_{1,m_2},(d_j,\delta_j;L_j)_{m_2+1,q_2},(f_j,F_j)_{1,m_3},(f_j,F_j;S_j)_{m_3+1,q_3} \end{matrix}\right| \qquad (2.7)$$

Similar other results can be obtained by considering products or quotients of such gamma functions whose partial derivatives w.r.t. the arbitrary parameter involved can be expressed as a finite sum.

For example, for the quotient

$$\frac{\Gamma(1-e-N+\alpha'\xi+\alpha''\eta)}{\Gamma(1-e+\alpha'\xi+\alpha''\eta)},$$

We have

$$\frac{\partial}{\partial e}\left\{ \overline{H}^{o,n_1+1:\ \ m_2,n_2:m_3,n_2}_{p_1+1,q_1+1:p_2,q_2;p_2,q_2}\left[\begin{matrix} z_1 \\ z_2 \end{matrix}\right.\right.$$

$$\left.\left.\left|\begin{matrix} (e+N;\alpha',\alpha''),\left(\frac{e}{2};\alpha',\alpha''\right),(a_j,\alpha_j;A_j)_{1,p_1},,(c_j,\gamma_j;K_j)_{1,n_2},(c_j,\gamma_j)_{n_2+1,p_2},(e_j,E_j;R_j)_{1,n_3},(e_j,E_j)_{n_3+1,p_3} \\ (b_j,\beta_j;B_j)_{1,q_1},(e;\alpha',\alpha''),(d_j,\delta_j)_{1,m_2},(d_j,\delta_j;L_j)_{m_2+1,q_2},(f_j,F_j)_{1,m_3},(f_j,F_j;S_j)_{m_3+1,q_3} \end{matrix}\right|\right\}$$

$$= N\,!\sum_{k=0}^{N}\frac{(-1)^{k-1}}{p\,(N-k)\,!}\overline{H}^{o,n_1+1:\quad m_2,n_2:m_3,n_2}_{p_1+1,q_1+1:p_2,q_2;p_2,q_2}$$

$$\left[\begin{matrix} z_1 \\ z_2 \end{matrix}\left|\begin{matrix} (e+N;\alpha',\alpha''),\left(a_j,\alpha_j;A_j\right)_{1,p_1},\left(c_j,\gamma_j;K_j\right)_{1,n_2},\left(c_j,\gamma_j\right)_{n_2+1,p_2},\left(e_j,E_j;R_j\right)_{1,n_3},\left(e_j,E_j\right)_{n_3+1,p_3} \\ \left(b_j,\beta_j;B_j\right)_{1,q_1},(e+k;\alpha',\alpha''),\left(d_j,\delta_j\right)_{1,m_2},\left(d_j,\delta_j;L_j\right)_{m_2+1,q_2},\left(f_j,F_j\right)_{1,m_3},\left(f_j,F_j;S_j\right)_{m_3+1,q_3} \end{matrix}\right.\right\} \qquad (2.8)$$

REFERENCES

[1]. Buschman, R.G.; Contigous relations and related formulas for the H-function of Fox, Jnanabha, A2, (1972)39-47.

[2]. Buschman, R.G.; Partial derivatives of the H-function with respect to parameters expressed as finite sums and as integrals, Univ. Nac. Tucuman Rev. Ser., A24, (1974),149-155.

[3]. Buschman, R.G. and Gupta, K.C.; Contigous relations for the H-function of two variables, Indian J. Pure Appl. Math.,6(1975),1416-1421.

[4]. Deshpande, V.L.; On the derivatives of G-function of two variables and their applications, Proc. Nat. Acad. Sci. India, 41A, (1971), 60-68.

[5]. Deshpande, V.L.; Finite sum representations of the H-function of two and more variables with respect to parameters, Indian J. Pure Appl. Math., 10, (1979), 1514-1524.

[6]. Doetsch, Gustav; Handbuch der Laplace-transformation, Vol. I, Verlag Birkhauser, Basel (1950).

[7]. Erdelyi, A. et. al.; Higher Transcendental Functions, vol. I, McGraw-Hill Book Co., Inc., New York (1953).

[8]. Mathai, A.M.; Products and ratios of generalized gamma variables, Skand. Akt., 55(1972), 193-198.

[9]. Mittal, P.K. & Gupta, K.C.; An integral involving generalized function of two variables. *Proc. Indian Acad. Sci. Sect. A*(75)☹1961), 67-73.

[10]. Reed, I.S.; The Mellin type of double integral, Duke Math. J., 17(1971), 565-572.

[11]. Saxena, R.K.; On the H-function of n-variables, Kyungpook Math. J., 17(1977), 221-226.

[12]. Singh,Y. and Mandia, H.; A study of *H* -function of two variables, International Journal of Innovative research in science,engineering and technology,Vol.2,(9)(2013),4914-4921.

[13]. Srivastava, H.M. and Daoust, M.C.; Certain generalized Neumann expansions associated with the Kampe de Feriet function, Nederl. Akad. Wetensch. Proc. Ser. A, 72=Indag. Math., 31(1969),449-457.

[14]. Srivastava, H.M. and Panda, R.; Some bilateral generating functions for a class of generalized hypergeometric polynomials, J. Reine Angew. Math., 283/284 (1976a), 265-274.

[15]. Srivastava, H.M. and Panda, R.; Expansion theorems for the H-function of several complex variables, J. Reine Angew. Math., 228(1976b), 129-145.

[16]. Srivastava, H.M. and Singhal, J.P.; On a class of generalized hypergeometric distributions, Jnanabha, A2(1972), 1-9.

[17]. Tandon, O.P.; Contigous relations for the H-function of n-variables, Indian J. Pure Appl. Math., 11(1980), 321-325.

ISSN (e): 2250 – 3005 || Vol, 04 || Issue, 10 || October – 2014 ||
International Journal of Computational Engineering Research (IJCER)

Design and Optimization of Axial Flow Compressor

Koduru. Srinivas[1], Kandula. Deepthi[2], K.N.D.Malleswara Rao[3]
[1] PG student, Department of Mechanical Engineering, Vikas College of Engineering & Technology, Nunna
[2] Guide (Asst.prof), Department of Mechanical Engineering, Vikas College of Engineering & Technology, Nunna
[3]Asst.prof, Department of Mechanical Engineering, P.C.C, Vijayawada, AP, INDIA

ABSTRACT
An axial flow compressor is one in which the flow enters the compressor in an axial direction (parallel with the axis of rotation), and exits from the gas turbine, also in an axial direction. The axial-flow compressor compresses its working fluid by first accelerating the fluid and then diffusing it to obtain a pressure increase. In an axial flow compressor, air passes from one stage to the next, each stage raising the pressure slightly. The energy level of air or gas flowing through it is increased by the action of the rotor blades which exert a torque on the fluid which is supplied by an electric motor or a steam or a gas turbine. In this thesis, an axial flow compressor is designed and modeled in 3D modeling software Pro/Engineer. The present design has 30 blades, in this thesis it is replaced with 20 blades and 12 blades. The present used material is Chromium Steel; it is replaced with Titanium alloy and Nickel alloy. Structural analysis is done on the compressor models to verify the strength of the compressor. CFD analysis is done to verify the flow of air.

KEYWORDS : *Axial Flow, Ansys, Compressor, CFD, Gas Turbine, PRO-E*

I. INTRODUCTION

Axial Compressor

An **axial compressor** is a machine that can continuously pressurize gases. It is a rotating, airfoil-based compressor in which the gas or working fluid principally flows parallel to the axis of rotation. This differs from other rotating compressors such as centrifugal compressors, axi-centrifugal compressors and mixed-flow compressors where the fluid flow will include a "radial component" through the compressor.

Transonic Axial Compressor : Transonic axial flow compressors are today widely used in aircraft engines to obtain maximum pressure ratios per single-stage. High stage pressure ratios are important because they make it possible to reduce the engine weight and size and, therefore, investment and operational costs.

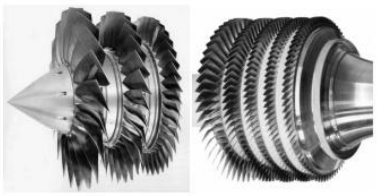

Fig 1 Transonic lpc (left) and hpc (right) eurofighter typhoon engine EJ200

Three-dimensional shaped blades : The preceding paragraph has shown that a certain maturity in transonic compressors has been reached regarding the general airfoil aerodesign. But the flow field in a compressor is not only influenced by the two-dimensional airfoil geometry. The three-dimensional shape of the blade is also of great importance, especially in transonic compressor rotors where an optimization of shock structure and its interference with secondary flows is required. Many experimental and numerical works can be found in the literature on the design and analysis of three-dimensional shaped transonic bladings.

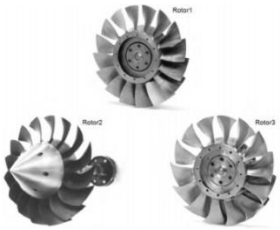

Fig 2 Transonic Compressor Test Rotors

III. THEORETICAL CALCULATIONS

Pressure = 0.904N/mm^2 ; Temperature = 288K

Absolute Velocity

$$C_1 = \frac{C_{a_1}}{\cos \alpha_1} = \frac{150}{\cos(12)} = 177.75 \text{m/s}$$

C_{a_1}= Constant axial velocity

α_1 = Radius between blade to blade

IV. MODELING IN PRO-E

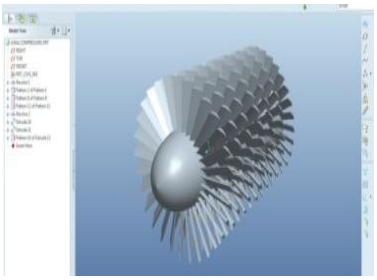

Fig 3: 30 blades

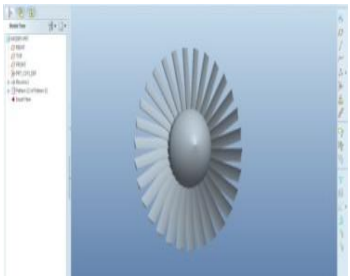

Fig 4:20 blades

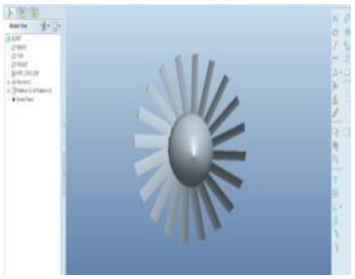

Fig 5: 12 blades

V. RESULTS & DISCUSSION

Analysis of Compressor 30 Blades
Nickel Alloy

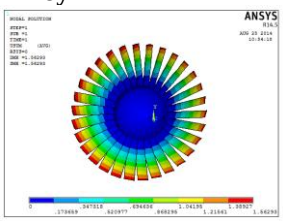

Fig 6: Displacement vector

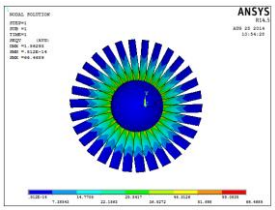

Fig 7: Stress vonmises vector

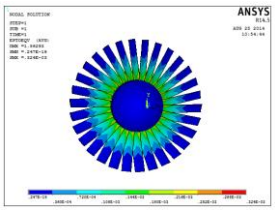

Fig 8: Strain vonmises vector

5.1.2 Titanium

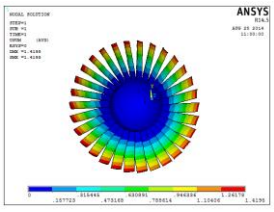

Fig 9: Displacement vector vector

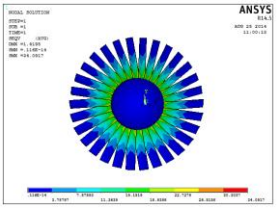

Fig 10: Stress vonmises vector

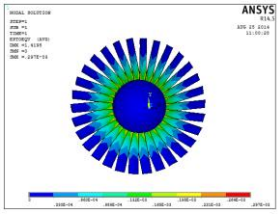

Fig 11: Strain vonmises

5.1.4 Steel

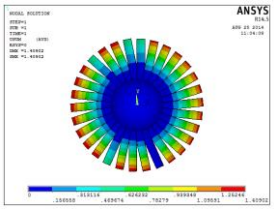

Fig 12: Displacement vector vector

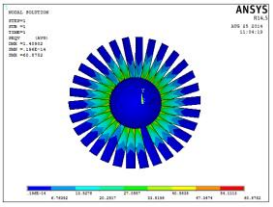

Fig 13: Stress vonmises vector

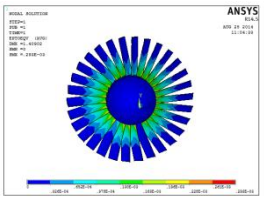

Fig 14: Strain vonmises

5.2 Analysis of Compressor 20 blades

5.2.1 Nickel alloy

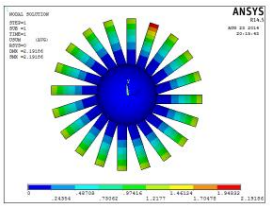

Fig 15: Displacement vector vector

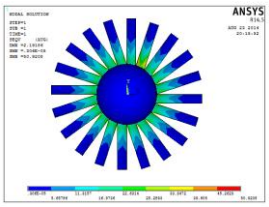

Fig 16: Stress vonmises vector

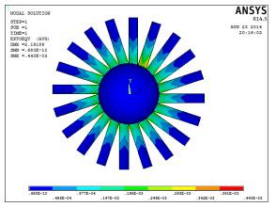

Fig 17: Strain vonmises

5.2.2 Titanium

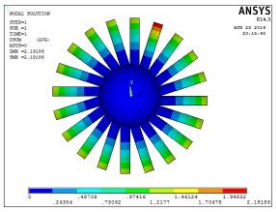

Fig 18: Displacement vector vector

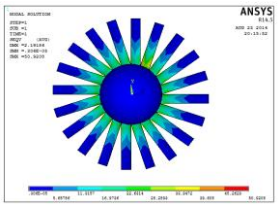

Fig 19: Stress vonmises vector

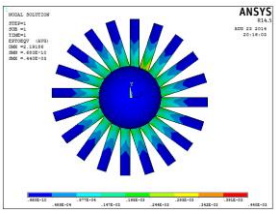

Fig 20: : Strain vonmises

5.2.3 Steel

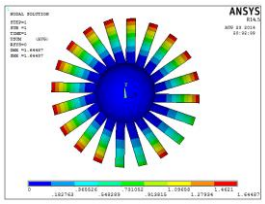

Fig 21: Displacement vector

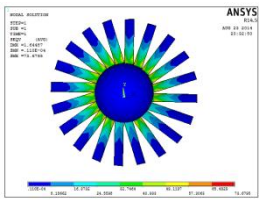

Fig 22: Stress vonmises vector

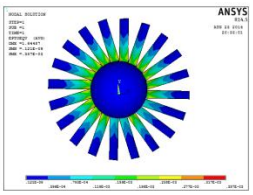

Fig 23: Strain vonmises vector

5.3 12 Blades

5.3.1 Nickel alloy

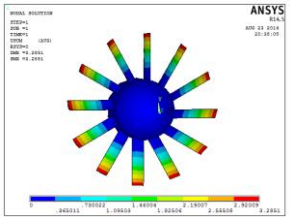

Fig 24:Displacement vector

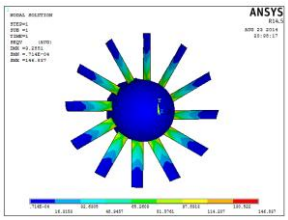

Fig 25: Stress vonmises vector

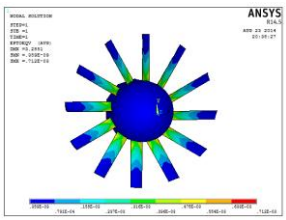

Fig 26: Strain vonmises vector

5.3.2 Titanium

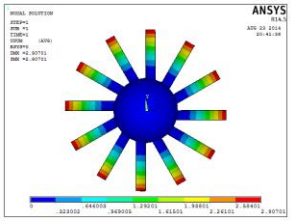

Fig 27: Displacement vector

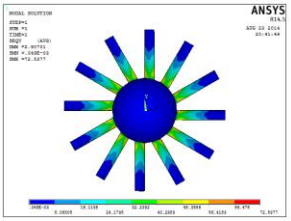

Fig 28: Stress vonmises vector

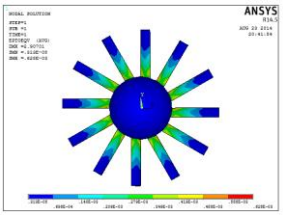

Fig 29: Strain vonmises vecto

5.3.3 Steel

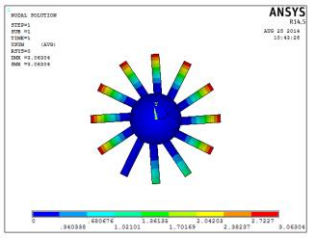

Fig 30: Displacement vector

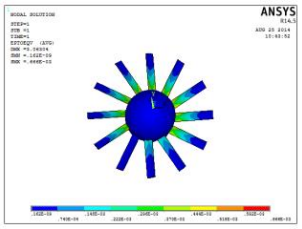

Fig 31: Stress vonmises vector

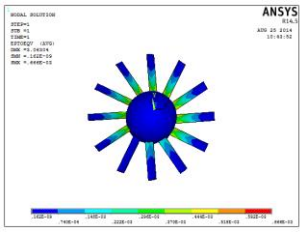

Fig 32:Strain vonmises vector

6. CFD Analysis

6.1 30Blades

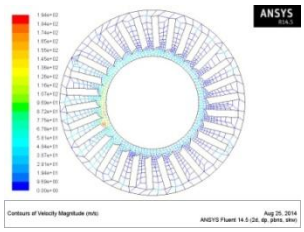

Fig 33: Velocity magnitude

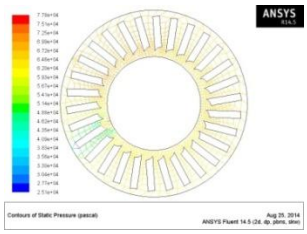

Fig 34: Static pressure

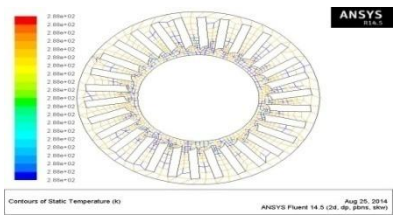

Fig 35: Temperature

6.2 20 Blades

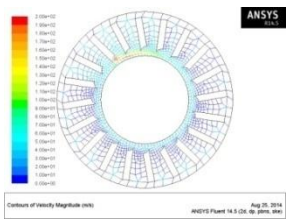

Fig 36:magnitude

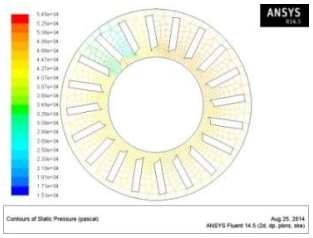

Fig 37: Static pressure

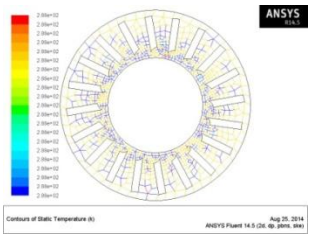

Fig 38: Temperature

6.3 12 Blades

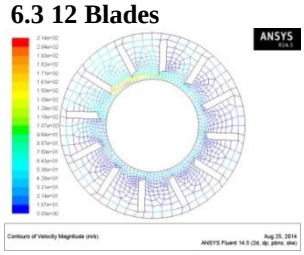

Fig 39: magnitude

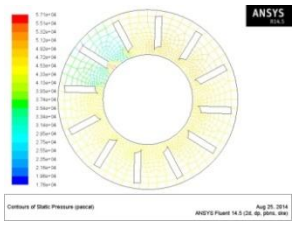

Fig 40:Static pressure

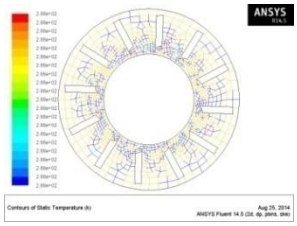

Fig 41:Temperature

VI. RESULTS TABLE

7.1 At 30 blades

	Displacement(mm)	Stress(N/mm^2)	Strain
Nickel alloy	1.56293	66.4689	0.324e-03
Titanium	1.4195	34.0917	0.29e-03
Steel	1.40902	60.8752	0.29e-03

Table 1: Result of 30 blades

7.2 At 20 blades

	Displacement(mm)	Stress(N/mm2)	Strain
Nickel alloy	2.06664	99.2341	0.485e-03
Titanium	2.19186	50.920	0.440e-03
Steel	1.64487	73.6795	0.357e-03

Table no 2 Result of 20 blades

7.3 At 12 blades

	Displacement(mm)	**Stress(N/mm^2)**	**Strain**
Nickel alloy	3.2851	146.837	0.712e-03
Titanium	2.90701	72.5377	0.628e-03
Steel	3.06304	138.669	0.666e-03

Table no 3 Result of 12 blades

7.4 CFD Results

	30 blades	**20 blades**	**12 blades**
Velocity (m/s)	$1.94e^{+02}$	$2.00e^{+02}$	$2.14e^{+02}$
Pressure(N/mm^2)	$7.78e^{+04}$	$5.45e^{+04}$	$5.71e^{+04}$
Temperature(k)	$2.88e^{+02}$	$2.88e^{+02}$	$2.88e^{+02}$
Mass flow rate (kg/s)	0.081484798	0.1520251	0.23096226

Table no 4 CFD Result

VII. CONCLUSION

In this thesis, an axial flow compressor is designed and modeled in 3D modeling software Pro/Engineer. The present design has 30 blades, in this thesis it is replaced with 20 blades and 12 blades. The present used material is Chromium Steel, it is replaced with Titanium alloy and Nickel alloy. Titanium alloy and Nickel alloy are high strength materials than Chromium Steel. The density of Titanium alloy is less than that of Chromium Steel and Nickel alloy. So using Titanium alloy for compressor blade decreases the weight of the compressor Structural analysis is done on the compressor models to verify the strength of the compressor. The stress values for less than the respective yield stress values for Titanium alloy and Nickel alloy. The stress value is less for titanium alloy than Nickel alloy, so using Titanium alloy is better. By using 12 blades the stresses are increasing, but are within the limits. CFD analysis is done to verify the flow of air. The outlet velocity is increasing for 12 blades, pressure is more for 30 blades and mass flow rate is more for 12 blades.
So it concluded that using Titanium alloy and 12 blades is better for compressor blade.

REFERENCES

[1] Design Methodology of a Two Stage Axial Compressor by Gaddam Srikanth Ȧ, S.Srinivas Prasad Ȧ, V.Mahesh Kumar Ȧ and B.Mounica Reddy
[2] Numerical Investigation of Flow In An Axial Flow Compressor Cascade by T. Suthakar, Akash, National Institute of Technology, Tiruchirappalli
[3] Effect of Variations in Aspect Ratio on Single Stage Axial Flow Compressor Using Numerical Analysis by Kumbhar Anil H., Aashish Agarwal, PG Student, Asso. Professor, Technocrats Institute of Technology, Bhopal, M.P, India.
[4] Numerical Simulation of an Axial Compressor with Non Axisymmetric Casing Treatment by N.Gourdain, M.Montagnac, J.F.Boussuge CERFACS, Computational Fluid Dynamics Team 31057 Toulouse, France
[5] Stall Inception in Axial Flow Compressors by I. J. Day
[6] Modeling of the double leakage and leakage spillage flows in axial flow compressors by Hui Du, Xianjun Yu, Baojie Liu
[7] Frank Sieverding, Beat Ribi, Michael Casey, Michael Meyer (2004) Design of Industrial Axial Compressor Blade Sections for Optimal Range and Performance .
[8] S M Yahya (2003) Fundamentals of Compressible flow, 81-224-1468-0, Tata Mc-Graw Hill.
[9] Philip G. Hill, Carl R. Peterson (2010), Mechanics and Thermodynamics of Propulsion, 0201146592, Addison-Wesley
[10] Jack D. Mattingly (1996), Elements of Gas turbine Propulsion, 0-07-912196-9, Tata Mc-Graw Hill.

ISSN (e): 2250 – 3005 || Vol, 04 || Issue, 10 || October – 2014 ||
International Journal of Computational Engineering Research (IJCER)

Design & Optimization of a Rim Using Finite Element Analysis

[1,]Turaka.venkateswara Rao , [2,]Kandula. Deepthi , [3,]K.N.D.Malleswara Rao
[1] *PG student, Department of Mechanical Engineering, Vikas College of Engineering & Technology, Nunna*
[2] *Guide (Assit.Prof), Department of Mechanical Engineering, Vikas College of Engineering & Technology, Nunna*
[3]*Asst.prof, Department of Mechanical Engineering, P.C.C, Vijayawada, AP, INDIA*

ABSTRACT
Rims are critical components of your vehicle wheel. The wheel is a device that enables efficient movement of an object across a surface where there is a force pressing the object to the surface. There are so many kinds of wheels are created from the ancient age for the today's world there are two kinds of wheels mostly used. In the present every vehicle was designed with alloy wheels which are more efficient than spokes wheels.
In this project we designed the rim from the existing dimensions by modeling software. There are the models are prepared in this project one is actual one which is used in normal/regular vehicles, second one is modified one which is used in latest vehicles and the last one is the modification of latest rim. The three rims are analyzed in Ansys by using 4 different materials which are Al alloy which is a regular material and another three are Mg alloy, Zn alloy & Steel alloy. The results were compared and the best material with best model was proposed to the company.

KEYWORDS: ***Ansys****, Al alloy, Steel alloy, Spokes wheels.*

I. INTRODUCTION

The alloy used in the finest road wheels today is a blend of aluminum and other elements. The term "magnesium wheel" is sometimes incorrectly used to describe alloy wheels. Magnesium is generally considered to be an unsuitable alloy for road usage due to its brittle nature and susceptibility to corrosion. In market, mostly aluminum alloy wheel is used. Pure aluminum is soft, ductile, and corrosion resistant and has a high electrical conductivity. In consequence it is widely used for foil and conductor cables, but alloying with other elements is necessary to provide the higher strengths needed for other applications. Aluminum alloy wheels are cast into a mold in a hot liquid state and cooled, which makes them more accurate in both the heavier and lighter areas. The end result is a balance that has less weight on the wheel and less stress on the tire. Aluminum alloy wheels also provide a lighter weight for the racing enthusiast, and can be machined for a brilliant appearance. Steel wheels are a great way to provide basic transportation for a basic car, but for those who want to extend the life of their tires and have a smoother ride, alloy wheels are the way to go. Alloy metals provide superior strength and dramatic weight reductions over ferrous metals such as steel, and as such they represent the ideal material from which to create a high performance wheel. In fact, today it is hard to imagine a world class racing car or high performance road vehicle that doesn't utilize the benefits of alloy wheels.

II. MODELING BY USING PRO-E

III.

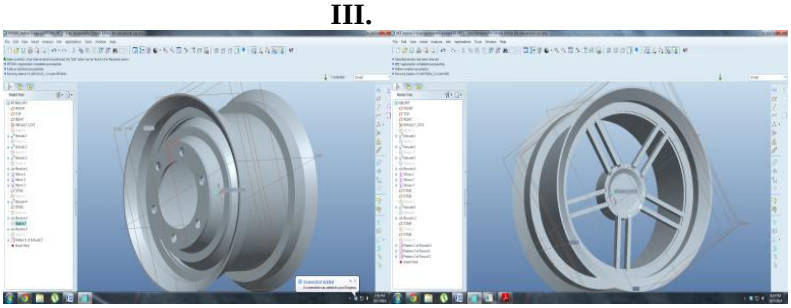

Fig no.1 Actual model Fig no.2 Modified 5 spokes model

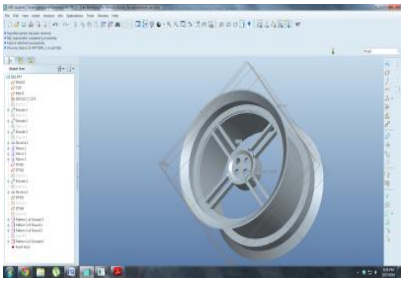

Fig no.3 Optimized 4 spokes model

III. RESULTS & DISCUSSION

Actual rim model results:

Al alloy:

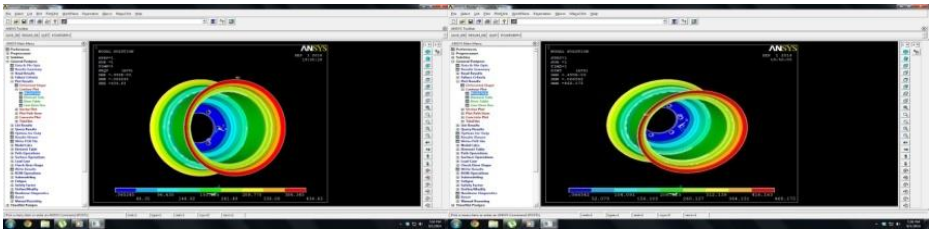

Fig no.4 Stress **Fig no.5 Displacement**

3.1.2 Steel alloy:

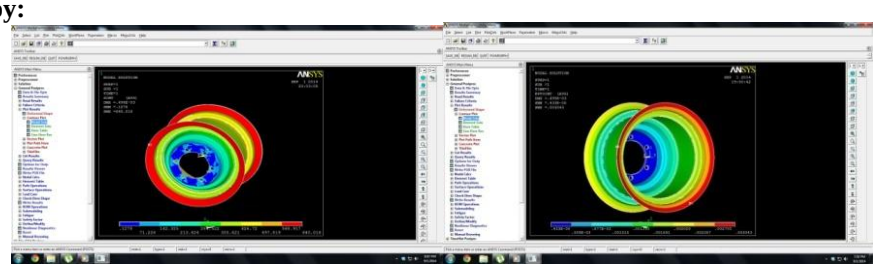

Fig no.6 Stress **Fig no.7 Displacement**

3.1.3 Mg alloy:

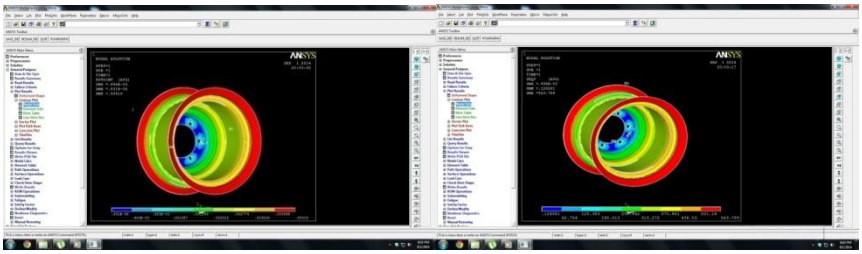

Fig no.8 Stress **Fig no.9 Displacement**

3.1.4 Zn alloy:

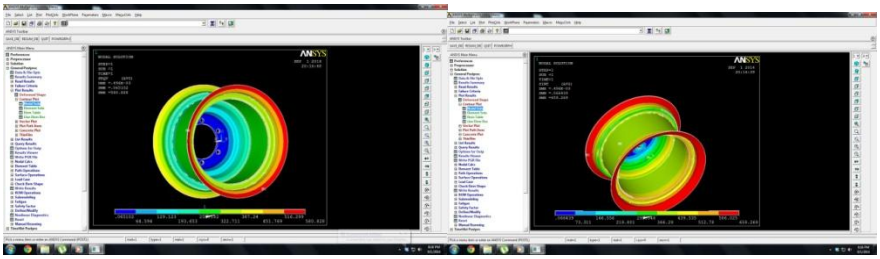

Fig no.10 Stress **Fig no.11 Displacement**

3.2 Modified 5 spokes model results:

3.2.1 Al alloy:

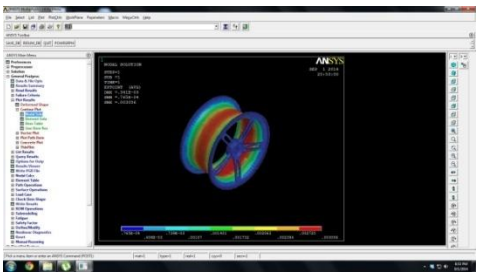

Fig no.12 Stress

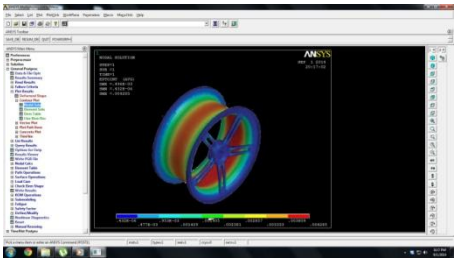

Fig no.13 Displacement

3.2.2 Steel alloy:

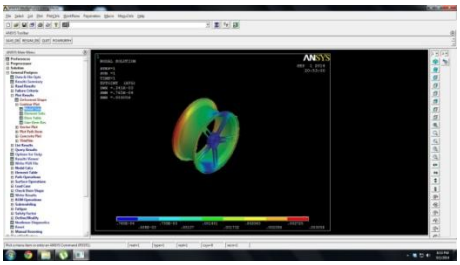

Fig no.14 Stress

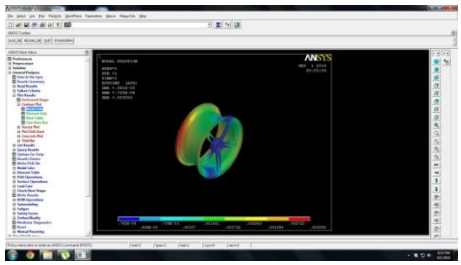

Fig no.15 Displacement

3.2.3 Mg alloy:

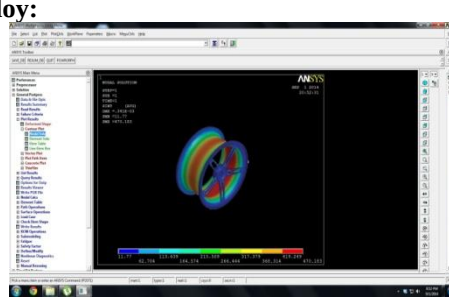

Fig no.16 Stress

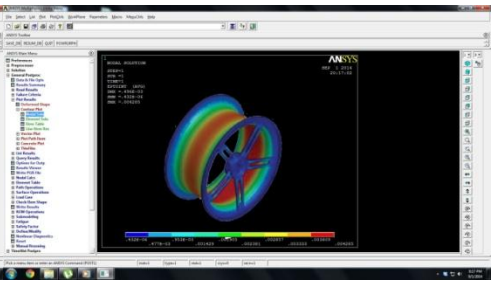

Fig no.17 Displacement

3.2.4 Zn alloy:

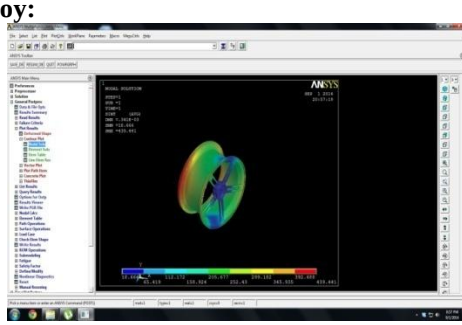

Fig no.18 Stress

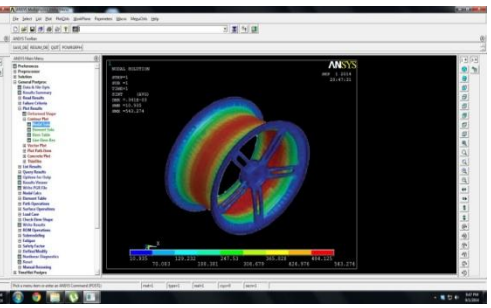

Fig no.19 Displacement

3.3 Optimized 4 spokes model results:

3.3.1 Al alloy:

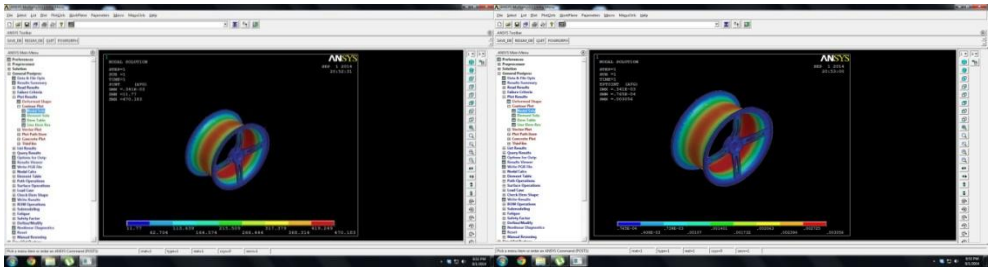

Fig no.20 Stress **Fig no.21 Displacement**

3.3.2 Steel alloy:

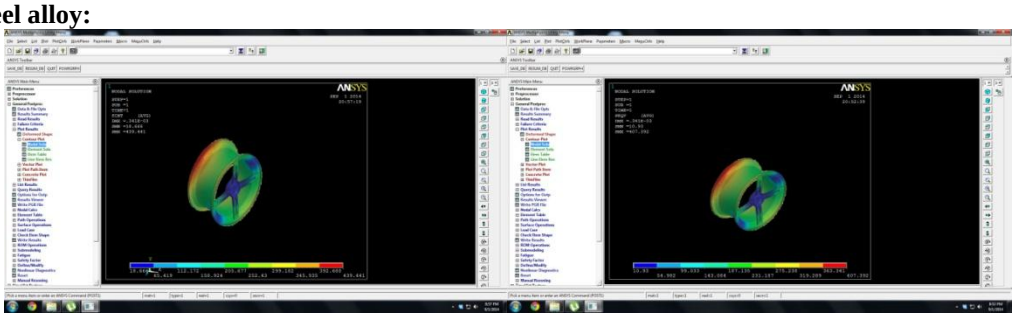

Fig no.22 Stress **Fig no.23 Displacement**

3.3.3Mg alloy:

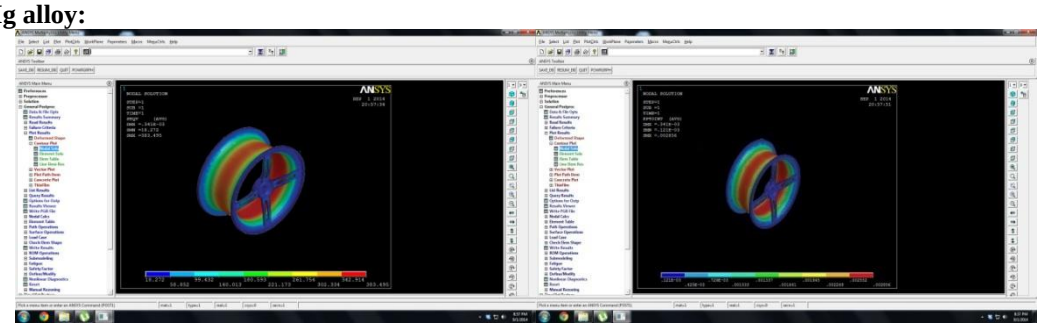

Fig no.24 Stress **Fig no.25 Displacement**

3.3.4 Zn alloy:

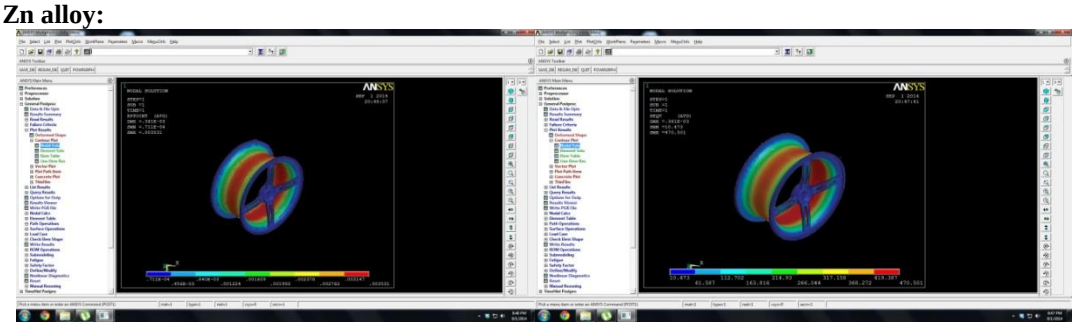

Fig no.26 Stress **Fig no.27 Displacement**

IV. RESULTS SUMMARY

Model		Material used			
		Al alloy	Steel alloy	Mg Alloy	Zn alloy
Actual model	Stress	46.5326	139.7056	31.929	56.931
	Displacement	0.208	0.1363	0.2613	0.1932
Modified 5 spokes model	Stress	45.386	133.267	29.374	59.654
	Displacement	0.231	0.1269	0.2938	0.1892
optimized 4 spokes model	Stress	39.486	126.254	34.894	54.326
	Displacement	0.197	0.2012	0.2943	0.1802

Table no.1 results

V. CONCLUSION

The modeling is done in pro-e and the model was saved in the IGES format and imported into Ansys. In the ansys software the analysis of 3 models done by changing the materials. The results were tabulated and compared in the investigation we came to know that For actual rim the stress values are low for Mg alloy compared to all other alloys which are used in this project. The al Alloy and Zn alloy values are nearer to the Mg alloy so these alloys may use in the shortage of Mg alloy. For the modified 5 spokes model stress values are low for Mg alloy compared to other alloys and the results are nearly same for Al & Zn alloy and the situation is continues as actual rim model. In the optimized 4 spokes model also Mg alloy performs very good compared to all other alloy here also the situation is same. Form this we conclude that steel alloy not to recommend for any type of rims manufacturing and the Mg alloy is good for all types of rims manufacturing in the second place Al alloy may be used. In the consideration of models the new optimized 4 spokes can be used by changing the ribs thickness form this rims weight also reduces.

[1] **Future scope:**
Further we can do optimization of material thickness to reduce the material consumption.
[2] Further we can improve life of component by using advanced fatigue strain life approach.

REFERENCES:

[1] google.com
[2] youtube.com
[3] ntpl
[4] machine design by RS KURMI
[5] SAE J175 Reaffirmed SEP2003
[6] www.nafems.com
[7] HyperWorks help, topology optimization
[8] K.J. Bathe, "Finite Element Procedures in Engineering Analysis", Prentice-Hall, Inc.
[9] Design Guide and Procedures, Hyundai Motor Corporation.
[10] Nitin S. Gokhale, "Practical Finite Element Analysis", Finite To Infinite
[11] K. Mahadevan and Balaveera Reddy, "Design Data Hand Book".
[12] "Finite Element Analysis", Chandra Pautla.
[13] "Strength Of Materials", Ramambrutham.
[14] "Ansys User Manual",
[15] "Metal Fatigue" , Ralfh Stefunson, Ali Fatemi & A.O. Cuph.
[16] "MSC Fatigue User Manual",
[17] Metal_fatigue_in_engineering by Stefan.
[18] Fatigue Life Analysis of Aluminum Wheels by Simulation of Rotary Fatigue Test Liangmo Wang* - Yufa Chen - Chenzhi Wang - Qingzheng Wang School of Mechanical Engineering, Nanjing University of Science & Technology, China
[19] Fatigue properties of a cast aluminium alloy for rims of car wheels. .Bosi,G.L.Garagnani
[20] Modeling and Fatigue Analysis of Automotive Wheel Rim by subbarao

ISSN (e): 2250 – 3005 || Vol, 04 || Issue, 10 || October– 2014 ||
International Journal of Computational Engineering Research (IJCER)

Scale Invariant Feature Transform Based Face Recognition from a Single Sample per Person

R.Pavithra[1], Prof. A. Usha Ruby [2], Dr. J. George Chellin Chandran[3]
Dept of PG CSE, CSI College of Engineering, Ketti, The Nilgiris, India[1]
Research scholar, Bharath University, Chennai, India[2]

ABSTRACT

The technological growth has a serious impact on security which has its own significance. The core objective of this project is to extract the facial features using the local appearance based method for the accurate face identification with single sample per class .The face biometric based person identification plays a major role in wide range of applications such as Airport security, Driver's license, Passport, Voting System, Surveillance. This project presents face recognition based on granular computing and robust feature extraction using Scale Invariant Feature Transform (SIFT) approach. The Median filter is used to extract the hybrid features and the pyramids are generated after the face granulation. Then, DoG pyramid will be formed from successive iterations of Gaussian images. By this granulation, facial features are segregated at different resolutions to provide edge information, noise, smoothness and blurriness present in a face image. In feature extraction stage, SIFT descriptor utilized to assign the intersecting points which are invariant to natural distortions. This feature is useful to distinguish the maximum number of samples accurately and it is matched with already stored original face samples for identification. The simulated results will be shown used granulation and feature descriptors has better discriminatory power and recognition accuracy in the process of recognizing different facial appearance.

INDEX TERMS: *Single sample per class, Median Filter, Dog pyramid, Scale Invariant Feature Transform*

I. INTRODUCTION

"Biometrics" means "life measurement" but the term is usually associated with the use of unique physiological characteristics to identify an individual. The application which most people associate with biometrics is security. However, biometric identification has eventually a much broader relevance as computer interface becomes more natural. Knowing the person with whom you are conversing is an important part of human interaction and one expects computers of the future to have the same capabilities. A number of biometric traits have been developed and are used to authenticate the person's identity. The idea is to use the special characteristics of a person to identify him. By using special characteristics we mean the using the features such as face, iris, fingerprint, signature etc, this method of identification based on biometric characteristics is preferred over traditional passwords and PIN based methods for various reasons such as: The person to be identified is required to be physically present at the time-of-identification. Identification based on biometric techniques obviates the need to remember a password or carry a token.

A biometric system is essentially a pattern recognition system which makes a personal identification by determining the authenticity of a specific physiological or behavioral characteristic possessed by the user. Biometric technologies are thus defined as the "automated methods of identifying or authenticating the identity of a living person based on a physiological or behavioral characteristic".
A biometric system can be either an 'identification' system or a 'verification' (authentication) system, which are defined below.

Identification - One to Many: Biometrics can be used to determine a person's identity even without his knowledge or consent. For example, scanning a crowd with a camera and using face recognition technology, one can determine matches against a known database.

Verification : One to One: Biometrics can also be used to verify a person's identity. For example, one can grant physical access to a secure area in a building by using finger scans or can grant access to a bank account at an ATM by using retinal scan. The process of receiving and analyzing visual information by the human species is referred to as sight, perception or understanding. Similarly, the process of receiving and analyzing visual information by digital computer is called as digital image processing and scene analysis. Processing of an image includes improvement in its appearance and efficient representation. So the field consists of not only feature extraction, analysis and recognition of images, but also coding, filtering, enhancement and restoration. The entire process of image processing and analysis starts from the receiving of the visual information and ends in giving out of description of the scene. The major components of the image processing system are image sensor, digitizer, processor, display unit and storage unit.

Face Recognition-A Survey : A facial recognition system is a computer application for automatically identifying or verifying a person from a digital image or a video frame from a video source. One of the ways to do this is by comparing selected facial features from the image and a facial database. It is typically used in security systems and can be compared to other biometrics such as fingerprint or eye iris recognition systems. Face recognition technology is used to extract information from facial images with the help of a face recognition device, without any human interaction. Unlike face detection technology, face recognition technology uses image processing algorithms to recognize, and then compare human facial images with the ones that are stored in the database of face recognition device. Face recognition technology enabled device analyzes the characteristics of overall structure of human face, including width of nose, shape of cheekbones, width between nose and jaw edges, and distance between eyes. For example, an algorithm may analyze the relative position, size, and/or shape of the eyes, nose, cheekbones, and jaw. These features are then used to search for other images with matching features. Other algorithms normalize a gallery of face images and then compress the face data, only saving the data in the image that is useful for face recognition. A probe image is then compared with the face data. One of the earliest successful systems is based on template matching techniques applied to a set of salient facial features, providing a sort of compressed face representation. Recognition algorithms [1, 3,5, 10, 12] can be divided into two main approaches, geometric, which look at distinguishing features, or photometric, which is a statistical approach that distills an image into values and compares the values with templates to eliminate variances. Popular recognition algorithms include Principal Component Analysis using Eigen faces [1, 3], Linear Discriminate Analysis [5], Elastic Bunch Graph Matching using the Fisher face algorithm, the Hidden Markov model, the Multi linear Subspace Learning using tensor representation.

II. EXISTING SYSTEM

Discriminant analysis methods are tools for face recognition. But this is not be used for the single sample per person scenario because of "with- in subject variability". This variability is established using images in the generic training set for which more than one sample per person is available. When images are under drastic facial expression variation, the discriminant analysis method can't be used. LDA (Linear Discriminant Analysis) [5] is one of the discriminant analysis methods. It fails to improve the performance, because the complex distribution of the data set is caused by large intrapersonal variations, which still exist in each cluster of that method. LDA uses a Fisher face [1,5] algorithm. It uses the dataset to store multiple images (with- in variability) of a same person. PCA (Principal Component Analysis) [2] is also not suitable for the single sample per class problem. LBP (Local Binary Pattern) [12] is not only used for face detection but also for face recognition. But LBP is not a robust face finder. To digitally process an image, it is first necessary to reduce the image to a series of numbers that can be manipulated by the computer. Each number representing the brightness value of the image at a particular location is called a picture element, or pixel.

A typical digitized image may have 512 × 512 or roughly 250,000 pixels, although much larger images are becoming common. Once the image has been digitized, there are three basic operations that can be performed on it in the computer. For a point operation, a pixel value in the output image depends on a single pixel value in the input image. For local operations, several neighboring pixels in the input image determine the value of an output image pixel. In a global operation, all of the input image pixels contribute to an output image pixel value. An image is enhanced when it is modified so that the information it contains is more clearly evident, but enhancement can also include making the image more visually appealing. There are two popular approaches to face recognition. One approach transforms face images into specific transformation domains. Among the works that appear in the literature are Eigen face, Gabor filters, Fourier Transform, and wavelets. Another approach is to extract principal lines and creases from the face. However, this method is not easy because it is sometimes difficult to extract the line structures that can discriminate every individual well.
From the literature survey, it had been inferred that local matching method will be more efficient comparing to holistic matching method. Hence we can eliminate the high dimensionality problem. It had been found that

multiple samples per class lead to increase space complexity. In order avoid this space complexity problem, single sample per class is considered. In this single sample per class single image of a person is used for matching the face image.

III. PROPOSED SYSTEM

The proposed system use a robust face finder called SIFT(Scale Invariant Feature Transform). By using this feature the face can be fluently detected and recognized. Although only one classifier is trained, and using that frontal, occluded and profile faces are detected.

The proposed system includes Four modules: (1) Image Preprocessing, (2) Feature extraction, (3) face granulation, (4)Face recognition or face identification.

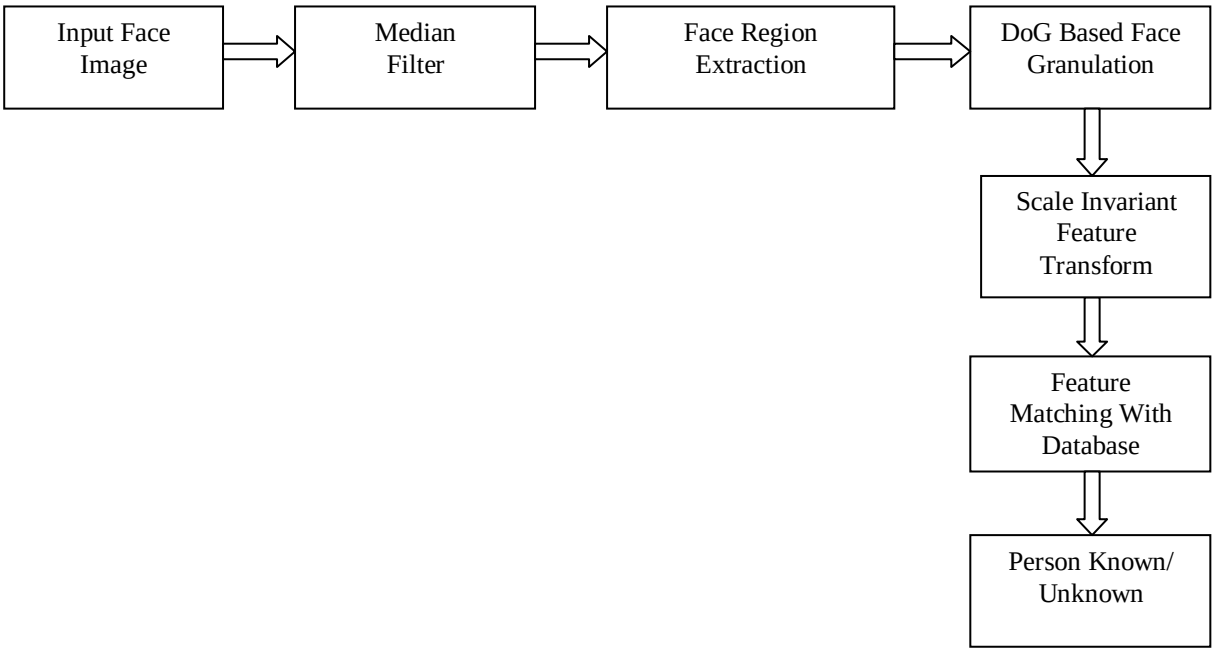

Fig 1 Detailed Diagram for Proposed System

The first stage of recognition starts with face detection module will be used to obtain face images, which have normalized intensity, are uniform in size and shape and depict only the face region. Here granular computing and face features will be presented to match face images in various illumination changes. The Gaussian operator generates a sequence of low pass filtered images by iteratively convolving each of the constituent images with a 2-D Gaussian kernel. Then, DOG pyramid will be formed from successive iterations of Gaussian images. By this granulation, facial features are segregated at different resolutions to provide edge information, noise, smoothness and blurriness present in a face image. In feature extraction stage, SIFT descriptor utilized to assign the intersecting points which are invariant to natural distortions. This feature is useful to distinguish the maximum number of samples accurately and it is matched with already stored original face samples for identification.

Granular Computing & DoG : After digital image has been obtained, the next step deals with preprocessing that image. The key function of preprocessing is to improve the image in ways that increase the chances for success of the other processes. Typically preprocessing deals with techniques for segregating at different resolutions to provide edge information, noise, smoothness and blurriness present in a face image. Subsequently the face granulation is done to generate the Difference of Gaussian (DoG) pyramids to recognize the face by using the granular computing and face features will be presented to match face images in various illumination changes. The Gaussian operator generates a sequence of low pass filtered images by iteratively convolving each of the constituent images with a 2-D Gaussian kernel. Then, DOG pyramid will be formed from successive iterations of Gaussian images.

Face Recognition : Recognition is the process that assigns a mark to an object depends on the information provided by its descriptors. Having extracted the hybrid features in the feature extraction step, the Face granulation is done to produce out the Difference of Gaussian (DoG) pyramid formation. The DoG pyramids are produced to analyze the Euclidean distance to discern the face images valiantly

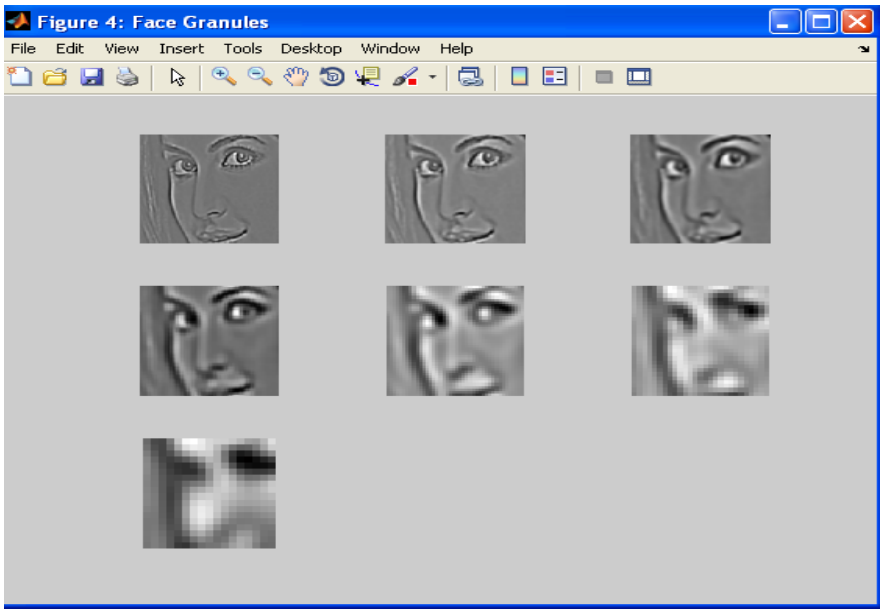

Fig 2 Face Granulation Values

The above Fig 2 gives us the clearest idea of getting out the output values based upon the identification of face vector values along with the different usage of granules computed and taken as successive outcomes. The performance is to be measured based on the comparison with the normal input image and the classified granules computed image.

IV ALGORITHMS

4.1 Algorithm for Difference of Gaussian (DoG)

Difference of Gaussians is a feature enhancement algorithm that involves the subtraction of one blurred version of an original image from another, less blurred version of the original. In the simple case of grayscale images, the blurred images are obtained by convolving the original grayscale images with Gaussian kernels having differing standard deviations. Blurring an image using a Gaussian kernel suppresses only high-frequency spatial information. Subtracting one image from the other preserves spatial information that lies between the ranges of frequencies that are preserved in the two blurred images. Thus, the difference of Gaussians is a band-pass filter that discards all but a handful of spatial frequencies that are present in the original gray scale image.

i)MATHEMATICS OF DIFFERENCE OF GAUSSIANS

Given a m-channels, n-dimensional image

$$I : \{\mathbb{X} \subseteq \mathbb{R}^n\} \rightarrow \{\mathbb{Y} \subseteq \mathbb{R}^m\} \quad \text{----------(1)}$$

The difference of Gaussians (DoG) of the image I is the function

$$\Gamma_{\sigma 1,\sigma 2} : \{\mathbb{X} \subseteq \mathbb{R}^n\} \rightarrow \{\mathbb{Z} \subseteq \mathbb{R}\} \text{--------(2)}$$

Obtained by subtracting the image I convolved with the Gaussian of variance σ_2^2 from the image I convolved with a Gaussian of narrower variance σ_1^2, with $\sigma_2 > \sigma_1$. In one dimension, Γ is defined as:

$$\Gamma_{\sigma 1,\sigma 2}(x) = I * \frac{1}{\sigma_1\sqrt{2\pi}} e^{-(x^2)/(2\sigma_1^2)} - I * \frac{1}{\sigma_2\sqrt{2\pi}} e^{-(x^2)/(2\sigma_2^2)} \quad \text{---------- (3)}$$

and for the centered two-dimensional case :

$$\Gamma_{\sigma,K\sigma}(x,y) = I * \frac{1}{2\pi\sigma^2} e^{-(x^2+y^2)/(2\sigma^2)} - I * \frac{1}{2\pi K^2\sigma^2} e^{-(x^2+y^2)/(2K^2\sigma^2)} \quad \text{---------- (4)}$$

Which is formally equivalent to:

$$\Gamma_{\sigma,K\sigma}(x,y)= I * \frac{1}{2\pi\sigma^2} e^{-(x^2+y^2)/(2\sigma^2)} - \frac{1}{2\pi K^2\sigma^2} e^{-(x^2+y^2)/(2K^2\sigma^2)} \text{ ---------- (5)}$$

Which represents an image convoluted to the difference of two Gaussians, which approximates a Mexican Hat function. As a feature enhancement algorithm, the difference of Gaussians can be utilized to increase the visibility of edges and other detail present in a digital image. The difference of Gaussians algorithm removes high frequency detail that often includes random noise, rendering this approach one of the most suitable for processing images with a high degree of noise. Differences of Gaussians have also been used for blob detection in the scale-invariant feature transform.

In fact, the DoG [11] as the difference of two Multivariate normal distribution has always a total null sum and convolving it with a uniform signal generates no response. It approximates well a second derivate of Gaussian (Laplacian of Gaussian) with K~1.6 and the receptive fields of ganglion cells in the retina with K~5. It may easily be used in recursive schemes and is used as an operator in real-time algorithms for blob detection and automatic scale selection.

4.2 Scale Invariant Feature Transform(SIFT) : It generates image features, "key points invariant to image scaling and rotation partially invariant to change in illumination [14].For any object there are many features, interesting points on the object that can be extracted to provide a "feature" description of the object. SIFT image features provide a set of features of an object that are not affected by many of the complications experienced in other methods, such as object scaling and rotation. While allowing for an object to be recognized in a larger image SIFT image features also allow for objects in multiple images of the same location, taken from different positions within the environment, to be recognized. SIFT features are also very resilient to the effects of "noise" in the image.

To aid the extraction of these features the SIFT algorithm applies a 4 stage filtering approach:

i)Scale-Space Extreme Detection : This stage of the filtering attempts to identify those locations and scales that is identifiable from different views of the same object. This can be efficiently achieved using a "scale space" function. Further it has been shown under reasonable assumptions it must be based on the Gaussian function.
The scale space is defined by the function:
$L(x, y, \sigma) = G(x, y, \sigma) * I(x, y)$
Where * is the convolution operator, $G(x, y, \sigma)$ is a variable-scale Gaussian and $I(x, y)$ is the input image.
Difference of Gaussians is one such technique, locating scale-space extreme, $D(x, y, \sigma)$ by computing the difference between two images, one with scale k times the other. $D(x, y, \sigma)$ is then given by:
$D(x, y, \sigma) = L(x, y, k\sigma) - L(x, y, \sigma)$
To detect the local maxima and minima of $D(x, y, \sigma)$ each point is compared with its 8 neighbors at the same scale, and its 9 neighbors up and down one scale. If this value is the minimum or maximum of all these points then this point is an extreme.

ii) Key point Localization : This stage attempts to eliminate more points from the list of key points by finding those that have low contrast or are poorly localized on an edge.

It involves three main steps. They are

a) Interpolation of nearby data for accurate position : First, for each candidate key point, interpolation of nearby data is used to accurately determine its position. The initial approach was to just locate each key point at the location and scale of the candidate key point. The new approach calculates the interpolated location of the extreme, which substantially improves matching and stability.

b) Discarding low-contrast key points : To discard the key points with low contrast, the value of the second-order Taylor expansion D(x) is computed at the offset x. If this value is less than 0.03, the candidate key point is discarded.

c) Eliminating edge responses : The DoG function will have strong responses along edges, even if the candidate key point is not robust to small amounts of noise.

For poorly defined peaks in the DoG function, the principal curvature across the edge would be much larger than the principal curvature along it. Finding these principal curvatures amounts to solving for the eigenvalues of the second-order Hessian matrix, H:

$$H = \begin{pmatrix} D_{xx} & D_{xy} \\ D_{xy} & D_{yy} \end{pmatrix}$$

iii)ORIENTATION ASSIGNMENT

This step aims to assign a consistent orientation to the key points based on local image properties. The key point descriptor can then be represented relative to this orientation, achieving invariance to rotation.

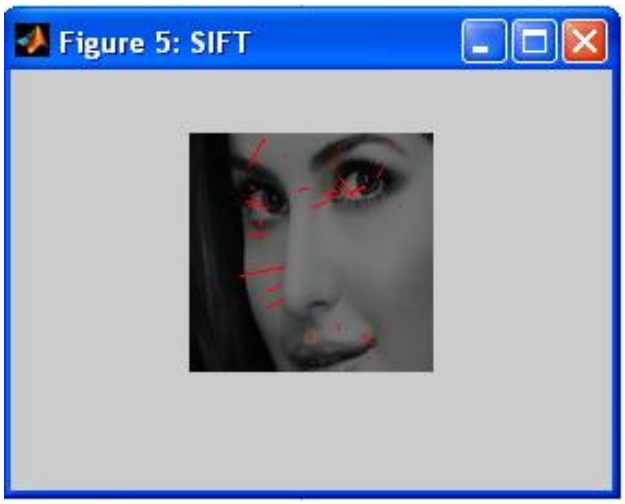

Fig 3 SIFT Calculating Values

iv)Key point Descriptor : The local gradient data, used above, is also used to create key point descriptors. The gradient information is rotated to line up with the orientation of the key point and then weighted by a Gaussian with variance of 1.5 * key point scale. This data is then used to create a set of histograms over a window centered on the key point. Key point descriptors typically uses a set of 16 histograms, aligned in a 4x4 grid, each with 8 orientation bins, one for each of the main compass directions and one for each of the mid-points of these directions. This result in a feature vector containing 128 elements. These resulting vectors are known as SIFT keys and are used in a nearest-neighbors approach to identify possible objects in an image.

V EXPERIMENTAL RESULTS

In this section we have evaluated the performance of Difference of Gaussian and feature extraction based on Scale Invariant Feature Transform. Here we test the proposed approach using FERET dataset for face recognition. The image is cropped and made into 64X64 from middle of location of eyes. Here we have considered the local features such as eyes, nose, mouth and chin and also detects properties of relations (e.g. areas, distances, angles) between the features are used as descriptors for face recognition. We have considered 1sample per person for each individual person. Here we will store each person's image in the FERET database and later which can be used for matching. FERET database is a standard database which is used for storing images. And the resolution of image is 128X128.The results shows that the combined features are useful to distinguish the maximum number of samples accurately and it is matched with already stored original face samples for identification. The results produced by using this method provide better discriminatory power for recognizing different facial appearance with accurate results.

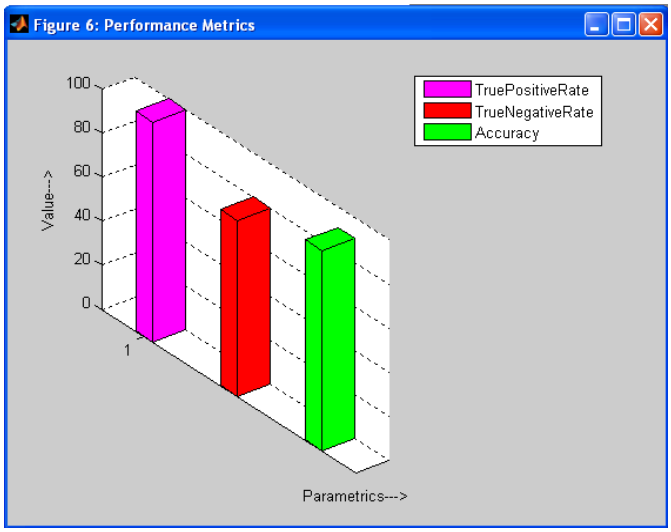

Fig 4 Performance of the Proposed System

VI CONCLUSION AND FUTURE ENHANCEMENT

In this paper, we used local matching method for Face recognition using Difference of Gaussian, Scale Invariant Feature Transform .Here first the facial features are features are segregated at different resolutions to provide edge information, noise, smoothness and blurriness present in a face image using Difference of Gaussian. SIFT descriptor utilized to assign the intersecting points which are invariant to natural distortions .This feature is useful to distinguish the maximum number of samples accurately and it is matched with already stored original face samples for identification. Since we are using single sample, the space and time complexity is reduced and performance has improved. In future, the face recognition system will be enhanced by applying Robust Local Ternary Pattern.

REFERENCES

[1] M. Turk and A.Pentland,"Eigenfaces for recognition",Journal of Cognitive Neuroscience, *vol. 3, no. 1, pp. 71-86,1991.*

[2] Gunjan Dashore, Dr. V.Cyril Raj Dr.MGR Educational and Research Institute Chennai, Tamilnadu, INDIA," An Efficient Method For Face Recognition Using Principal Component Analysis (PCA)"

[3] Yang, D. Zhang, A. Frangi and J. Yang,"Two dimensional PCA: a new approach to appearance-based face representation and recognition" IEEE Transactions on Pattern Analysis and Machine Intelligence, *vol. 26, pp. 131-137, 2004.*

[4] J. Wu and Z. Zhou, "Face recognition with one training image per person", Pattern Recognition Letters, *vol. 23, no. 14, pp. 1711-1719, 2002.*

[5] Li-Fen Chen!, Hong-Yuan Mark Liao",Ming-Tat Ko", Ja-Chen Lin!, Gwo-Jong Yu," A new LDA-based face recognition system which can solve the small sample size problem."

[6]. Turk M, Pentland A, Neurosci J (1991) Eigenfaces for recognition. J CognNeurosci *3(1):71–86*

[7] Lawrence S, Lee Giles C, Tsoi A, Back A (1997 Face recognition:a convolutional neural-network approach.IEEE Trans Neural Netw *8(1):98–113*

[8] A.Martinez, "Recognizing imprecisely localized, partially occluded, and expression variant faces from a single sample per class", *IEEE Transactions on Pattern Analysis and Machine Intelligence, vol. 24, no. 6, pp. 748-763, 2002.*

[9] X. Tan, S. Chen, Z. Zhou and F. Zhang, "Face recognition from a single image per person: A survey", *Pattern Recognition, vol. 39, pp. 1725-1745, 2006.*

[10] C. Liu and H. Wechsler, "Gabor feature based classification using the enhanced fisher linear discriminant model for face recognition", *IEEE Transactions on Image Processing, vol. 11, no. 4, pp. 467-476, 2002.*

[11]. Jie Chen, Member, IEEE, Shiguang Shan, Member, IEEE, Chu He, Guoying Zhao, Matti Pietika¨inen, Senior Member, IEEE, Xilin Chen, Senior Member, IEEE, and Wen Gao, Fellow, IEEE,(2010)WLD: A Robust Local Image Descriptor. *IEEE transactions on pattern analysis and machine intelligence, vol. 32, no. 9.*

[12] S. Li, W. Liu, D. Lin and X. Tang, "Nonparametric subspace analysis for face recognition", *Proceedings of the IEEE International Conference on Computer Vision and Pattern Recognition, vol. 2, pp. 961-966, 2005.*

[13] R. Brunelli and T. Poggio, "Face recognition: feature versus templates", *IEEE Transactions on Pattern Analysis and Machine Intelligence, vol. 15, no. 10, pp. 1042-1052, 1993.*

[14] Yu-Yao Wang, Zheng-Ming Li, Long Wang, Min Wang, Harbin Institute of Technology Shenzhen Graduate School," A Scale Invariant Feature Transform Based Method"*Journal of Information Hiding and Multimedia Signal Processing* ©2013 *ISSN 2073-4212* Ubiquitous International *Volume 4, Number 2, April 2013.*

ISSN (e): 2250 – 3005 || Vol, 04 || Issue, 10 || October – 2014 ||
International Journal of Computational Engineering Research (IJCER)

Modeling Sediment Accumulation at Kenyir Reservoir Using GSTARS3

Manal M.A. Albayati
Department of Civil Engineering, Faculty of Engineering and Technology Infrastructure
Infrastructure University Kuala Lumpur (IUKL)
Malaysia

ABSTRACT
An attempt was made in this study to predict the Kenyir reservoir sedimentation deposition processes at Terengganu, Malaysia. The purpose of this study is to determine the amount and location of sediment accumulated since the start of the Kenyir dam operation. The assessment was undertaken using GSTARS3 sediment transport model, which was integrated with GIS to display the output as sequences of grids. ArcView was used to convert the GSTARS3 model output to Arc View GIS grid format. The study successfully integrated GSTARS3 and ArcView models. The study demonstrates the ability of the adopted methodology to visualize the accumulated sedimentation during the operation period of the Kenyir dam.

KEYWORDS: *Modeling, Sediment deposition, Reservoir, GSTARS3, ArcView.*

I. INTRODUCTION

Reservoir sedimentation can be a serious problem with many disadvantages. The control of reservoir sedimentation needs good instrumentations, trained man power and financial support (Simons and Sentürk, 1992). Sedimentation in a reservoir may affect hydropower generation due to the abrasion of turbines and other dam components (Morris and Fan, 1998). The efficiency of a turbine is largely depends upon the hydraulic properties of its blades. The erosion and cracking of the tips of turbine blades by water-borne sand and silt can reduces their generating efficiency and causing expensive repairs. Reservoir sedimentation also affects the benefits of navigation, water supply, and flood mitigation (Patrick, 1996).

Predicting the amount of sediment coming into a reservoir, its deposition, and its accumulation throughout the years are important for hydraulic engineering. Despite the advances made in understanding factors involved in reservoir sedimentation, predicting the accumulation of sediment in a reservoir is still a complex problem. Empirical models, based on surveys and field observations, have been developed and applied to estimate annual reservoir sedimentation load, accumulated reservoir sedimentation load, and accumulated reservoir sedimentation volume after a given number of years of reservoir operation (Morris and Fan 1998). Several mathematical models for predicting reservoir sedimentation have been developed based on the equations of motion and continuity for water and sediment such as those proposed by Thomas and Prashum (1977), Chang (1984), Molinas and Yang (1986), Hamrick (2001), Toniolo and Parker (2003), Andualem and Yonas (2008). Some of these 1D models have additional specific features such as the GSTARS which is developed Molinas and Yang (1986) based on the theory of minimum stream power (Yang and Song, 1986). GSTARS and it's modified and further improved GSTARS3 (Yang and Simöes, 2002) and GSTARS4 (Yang and Ahn, 2011) can be applied for the determination of optimum channel width and geometry for a given set of hydraulic and sediment conditions.

GSTARS3 sediment transport model was used in this study to predict sediment load from the watershed discharged to a reservoir. GSTARS3 and its modified versions were developed as generalized water and sediment-routing computer models for solving complicated river and reservoir engineering problems.GSTARS3 was applied by Yang and Simöes (2001) to simulate delta formation in a laboratory channel. GSTARS3 was also used to simulate sedimentation processes in the Rio Grand Reservoir, New Mexico, USA. The results for both applications show good agreements between simulated and measured results. Yang and Simöes (2002) also successfully applied the GSTARS3 model to simulate sedimentation and delta movement in the Terbela Reservoir in Pakistan. However, GSTARS3 has never been applied to simulate sediment movement in a reservoir located in tropical region.

Geographical information system (GIS) applications in water resources modeling have been increased in recent year to take advantage of the spatial data representation capabilities, (Molnar and Julien 1997), (Millward and Mersey 1999, (Baigorria and Consuelo 2006), (Fu. et al. 2004) and (Chen et al. 2005). In this study, GSTARS3 sediment transport model is integrated with Arc View to predict and visualize the pattern of sedimentation accumulation in the Kenyir Reservoir, Terengganu, Malaysia.

The Study Area

Kenyir Reservoir is the largest man-made lake in Southeast Asia. Kenyir dam and reservoir are designed for hydroelectric power generation and flood mitigation purposes. The dam is located at 50 km south west of Kuala Terengganu Malaysia, on the Terengganu River. The dam construction started in 1978 and completed in 1986. The dam operation started in 1987. One operational problem is the increase of sedimentation accomulation in front of the intake structure. This can be observed during extremely low water level. Murky water has been discharged from the turbines during the rainy seasons. At the same time, inflow of river waters from the Berang and Kenyir Rivers were observed to be high sediment load. There is a concern that in a few years sediments will start flowing into the turbines causing damages and outages which may be require expensive dredging (TNB Research, Malaysia, 2006).

II. METHODOLOGY

This study includes data collection, data preprocessing and model selection. The model selected for the catchment is calibrated and verified before any flow and sediment transport simulation is carried out.
The study demonstrates that GSTARS3 can be used to estimate sediment transport in rivers and inflow to the Kenyir Reservoir.

GSTARS3 model (Generalized Sediment Transport model for Alluvial River Simulation) has been used to address several specific issues in reservoir sedimentation. GSTARS has the ability to simulate and predict the hydraulic and sediment variation in both the longitudinal and transverse directions. GSTARS3 also has the ability to simulate and predict the change of alluvial channel profile and cross sectional geometry, regardless whether the channel width is variable or fixed.

III. DATA REQUIRED

Application of GSTARS3 computer model requires the use of appropriate data. The data has to be processed into ASCII data files so they can be recognized by GSTARS3. Figure 1 shows a flow chart for the application of GSTARS3 sediment model and its integration with ArcView.

3-1 Channel Geometry

The first step to model a river system using GSTARS3 involves the approximation of channels bed and geometry in a semi-two-dimensional manner. Channel cross sections are described by X-Y coordinate pairs, i.e., by pairs with lateral location (X) and bed elevation (Y). In this study, 18 cross sections were used to represent the Berang reach above the Kenyir Reservoir and 16 cross sections were used to represent the Kenyir reach above the Kenyir reservoir.

3-2 Hydrologic Data

The second step in GSTARS3 simulation is to incorporate hydrology data which are mainly the river reach and water stage. The hydrograph and rating curve can be used for this purpose. In this study, the model was run to simulate the progress of sediment accumulation in the Kenyir reservoir for 16 years (1991-2006). Sediment discharge from the Berang River and Kenyir River are included in the simulation. The selected period of simulation was divided into four 4- year intervals. Figures 2 and 3 show the hydrographs for Berang and Kenyir Rivers, respectively.

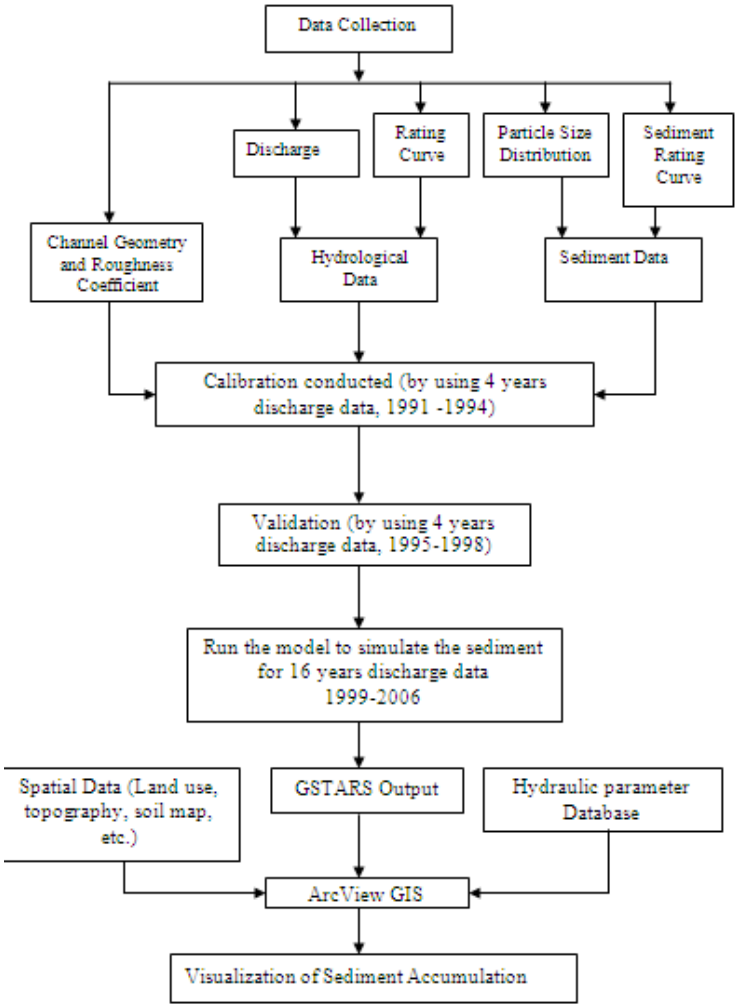

Figure 1: Flow chart for GSTARS3 sediment transport model integrating with ArcView

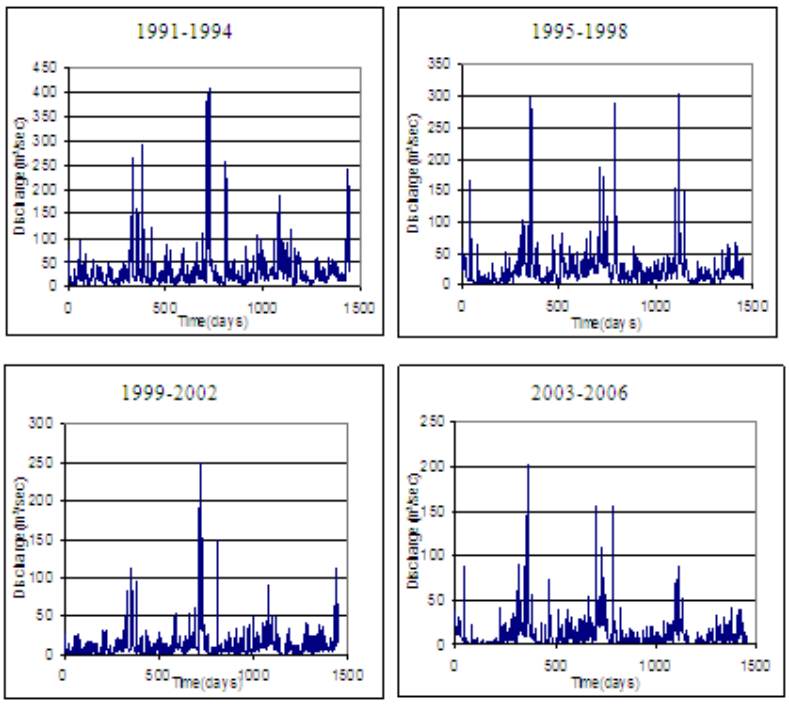

Figure 2: Discharge data of the Berang River for different periods

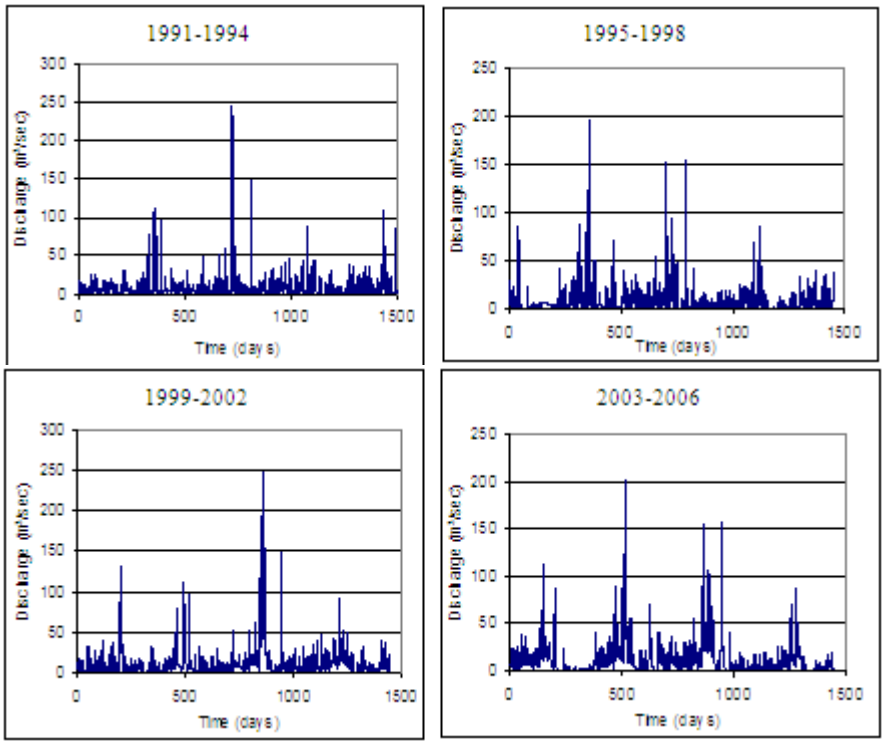

Figure 3: Discharge data of the Kenyir River for different periods

3-3 Sediment Data and Laboratory Work

Sediment data includes bed material size distribution for the reach of study and the sediment inflow hydrograph entering the reach. Sediment mixtures are characterized by gradation curves. Usually, bed graduation curve is used to define the nature of bed material. In this study, samples of sediment were collected from both Kenyir river and Berang river and the samples were taken to the laboratory in order to conduct grain size analysis.

Procedure for standard sieve analyses was followed in order to get the particle graduation. The retained sample fraction in each sieve is taken and weighted. The weighted fractions can be represented by a cumulative frequency curve that is made by plotting the sieve opening (grain size) versus a cumulative percent finer or coarser. Figures 4 and 5 show the grain size distributions for Berang and Kenyir basins, respectively.

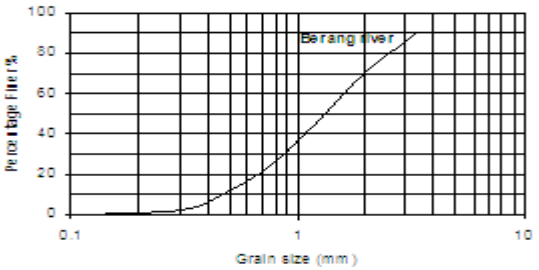

Figure 4: Grain size Distribution Curve for Berang basin

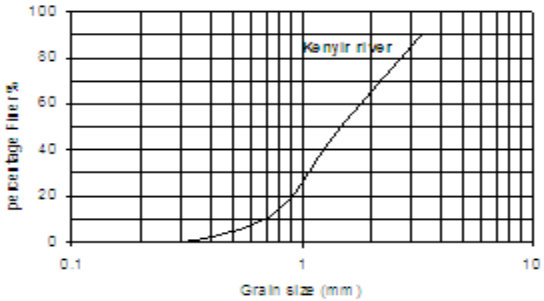

Figure 5: Grain size Distribution Curve for Kenyir basin

The incoming sediment discharge of Berang river and Kenyir river is specified as a function of water discharge described by the following relationship:

$Q_s = 0.648\ Q$ for Berang river (1)

$Qs = 0.4104\ Q$ for Kenyir river (2)

Sediment transport is computed using the Yang's sand (1973) and gravel (1984) transport Equations, respectively.

3- Calibration and Validation

GSTARS3 model was calibrated by employing the bathymetry data for the period from 1991 to 1994. For model calibration, a reasonable value for the Manning's roughness coefficient was selected. Figures 6 and 7 show the calibration for the Berang River thalweg profile and Kenyir River thalweg profile, respectively. The model was validated to evaluate its performance. This was achieved by using the parameters that were adjusted during the calibration. The bathymetry data from 1995 to 1998 was used for validation. Figures 8 and 9 show the validation for the Berang River and Kenyir River, respectively.

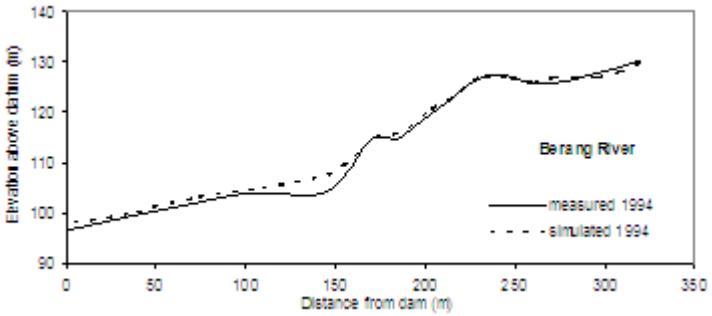

Figure 6: Calibration of the Thalweg for Berang River

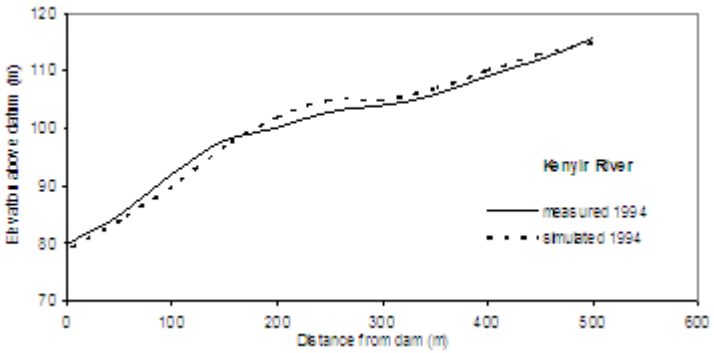

Figure 7: Calibration of the Thalweg for Kenyir River

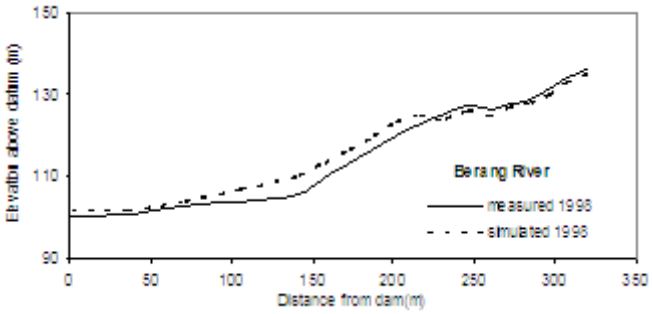

Figure 8: Validation of the Thalweg for Berang River

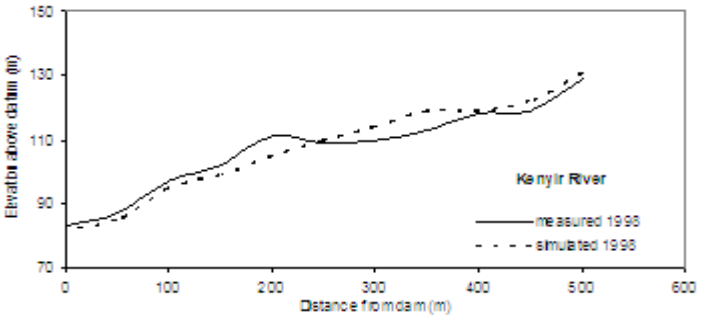

Figure 9: Validation of the Thalweg for Kenyir River

IV. STATISTICAL ANALYSES

Performance of the GSTARS sediment transport model was statistically assessed. The assessment includes the computation of the coefficient of determination (R^2), the mean square error (MSE) and the mean absolute percentage error (MAPE). Mood et al. (1974) proposed the use of MSE and MAPE for model assessment. MSE was used to measure the error in the model prediction while MAPE was used to measure the error in percentage. MSE and MAPE are defined as:

$$MSE = \frac{1}{N}\sum_{i=1}^{N}\left(Eli_{measured} - Eli_{simulated}\right)^2 \quad (3)$$

$$MAPE = \frac{1}{N}\sum_{i=1}^{N}\left|Eli_{measured} - Eli_{simulated}\right|100 \quad (4)$$

where $Eli_{measured}$ is the measured bed elevation (m) obtained from the survey, $Eli_{simulated}$ is the simulated bed elevation (m) obtained from the model output, and N is number of data sets used.

V. RESULTS AND DISCUSSION

5-1 GSTARS Results

The performance of GSTARS3 sediment model was tested using MSE, MAPE, and R^2 for the Berang River and Kenyir River. For Berang river, the results show that the GSTARS3 sediment model gave a better fit and the same results were obtained for the Kenyir river. Tests for Berang river simulation results show that the value of the MSE is 0.51 m, MAPE is 5.5 %, and coefficient of determination (R^2) is 0.97. Also tests for the Kenyir River simulation results show that the values of the MSE is 0.55 m, MAPE is 6.2 % and coefficient of determination (R^2) is 0.96, as shown in Table 1. GSTARS3 simulation results show good agreement with the historical records of thalweg profile for both Berang and Kenyir rivers. The error between predicted and recorded thalweg was found to be less than 10 %. Error less than 20 % was acceptable by Yang (2000) when he compared the simulation results with historical record of Terbela reservoir in Pakistan. The simulations of bed elevation in both locations are shown in Figure 10 and Figure 11. The simulated and measured results were found in agreement.

Table 1: Statistical Analysis for the GSTARS3 Model

Location	MSE (m)	MAPE (%)	R^2
Berang River	0.51	5.5	0.97
Kenyir River	0.55	6.2	0.96

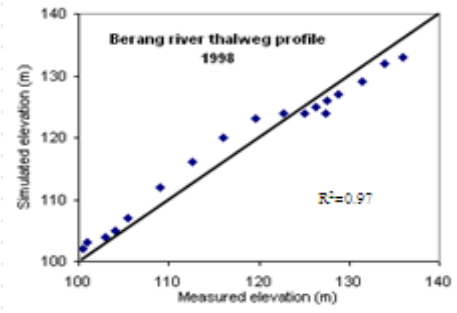

Figure 10: Comparison between the GSTARS3 model simulated and measured results along the Berang River thalweg

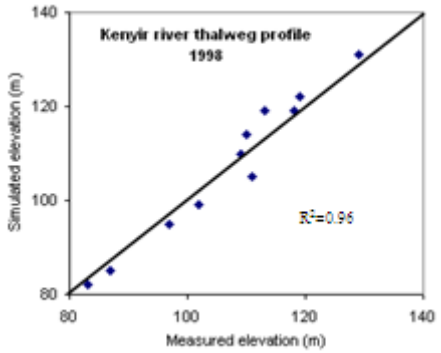

Figure 11: Comparison between the GSTARS3 model simulated and measured results along the Kenyir River thalweg

GSTARS3 program has the ability to determine the amount of sediment that exit the river reach and also to determine the sediment accumulation by size fraction. Based on GSTARS3 capabilities, amounts of sediment were simulated for every four years as shown in Figure 12. The sediment accumulation by particle size fraction for each reach was determined and shown in Table 2. It is noted that the amount of sediment exit from Berang river is greater than that exit from Kenyir river. The simulation results show that sediment rate was increased 62 % for Berang river and 38 % for kenyir river during sixteen years. However it is reasonable to compare it with Terbela reservoir in Pakistan, the sediment amounts that enter Terbela reservoir from 1976 until 1994 were equal to 1.01 $\times 10^{10}$ tons but Tapu reservoir in Thailand received 2.3×10^{6} tons of sediment from 1987 to 1990. Notably, these two reservoirs (Terbela in Pakistan and Tapu in Thailand) were modeled using GSTARS3 program

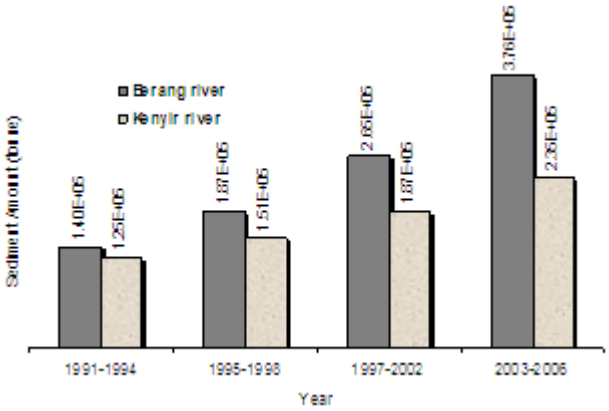

Figure 12: Sediment amount enter the reservoir from two rivers (Tonne)
Table 2: Sediment accumulation exit the reach by size fraction

Location	Year	Accumulative sediment exit the reach by size fraction (Ton)				
		Fine –Medium sand (0.12-0.24) mm	**Coarse sand (0.42-0.85) mm**	**Very coarse sand (0.85-2.0)mm**	**Very fine gravel (2.0-3.35) mm**	**Total**
Berang	1994	2.1×10^{4}	4.9×10^{4}	8.78×10^{4}	4.2×10^{3}	1.4×10^{5}
	1998	2.8×10^{4}	6.55×10^{4}	8.78×10^{4}	5.6×10^{3}	1.87×10^{5}
	2002	3.8×10^{4}	9.27×10^{4}	1.24×10^{5}	7.8×10^{3}	2.65×10^{5}
	2006	6.54×10^{4}	1.28×10^{5}	1.76×10^{5}	1.1×10^{4}	3.76×10^{5}
					Total	9.68×10^{5}
Kenyir	1994	8.75×10^{3}	5.0×10^{4}	4.0×10^{4}	2.6×10^{4}	1.25×10^{5}
	1998	1.06×10^{4}	6.04×10^{4}	4.83×10^{4}	3.17×10^{4}	1.51×10^{5}
	2002	1.3×10^{4}	7.48×10^{4}	6.0×10^{4}	4.0×10^{4}	1.87×10^{5}
	2006	1.64×10^{4}	9.4×10^{4}	7.52×10^{4}	4.93×10^{4}	2.35×10^{5}
					Total	6.98×10^{5}

4-2 Results of Integrating GSTARS with ArcView GIS

The important step in modeling process is to source out computed sediment and cross section geometry output generated from GSTARS3 model. Once the parameters shown in Figure 13 are imported into ArcView database format, various relationships can be established. Figure 13 shows the relationship between the control point in each cross section and the ArcView parameter table. Each point in the cross section has its coordinate (X-Y), distance from the dam location (Dis) and elevation (Ele).

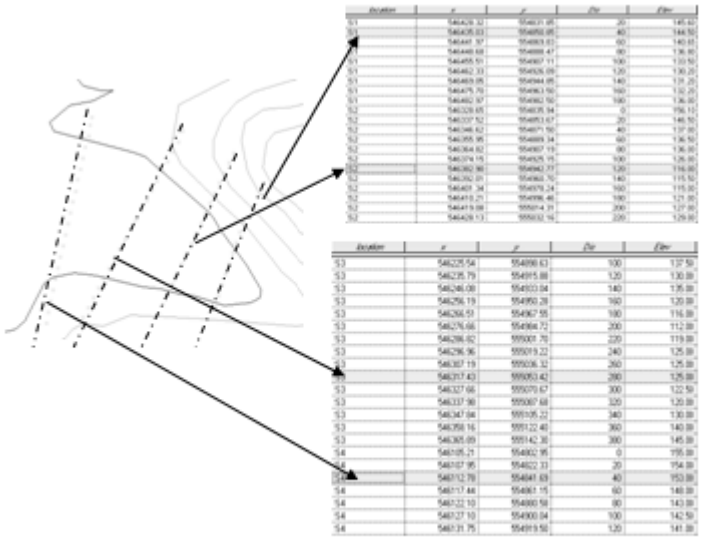

a- Actual location of reference

b- ArcView parameter table

Figure 13: Relationship between map and imported parameter from GSTARS3 model at Kenyir Reservoir intersection with Berang River

An Integrated Triangular Irregular Network (ITIN) model was created by combining geometry information from GSTARS3 program with the extended contour line from outside modeling area. Figure 14 and Figure 15 show the changes in elevation with time for both Berang river and Kenyir river respectively. The elevation was made up of square cells which contain 250 rows and 350 columns and 54,518 cells and each cell represent an area of 14.45 m^2.

Figures 14 and 15 show that most of the sediment from Berang river was found deposited at the distance between 350 m to 210 m from the dam and that from Kenyir river was found at the distance between 500 m to 380 m from the dam. This may be related to the large amount of un-submerged and submerged vegetation that are exist at these two locations.

Figure 14 for Berang river show that the elevations of points at section (1) in the year 1991 range between 112 m to 146 m, this elevation started to increase to be range between 122 m to 146 m in the year of 2006, while the elevation of points at cross section (6) started to increase from the range between 112 m to 146 m in the year 1991 to be range between 132 m to 146 m in the year of 2006. The Figure also shows the change in the shape of cross sections according to the change of elevations. This will help in making the decision about the locations that are needed to be dredged.

Figure 15 shows that the elevation of points at cross section (1), Kenyir river, ranged between 109 m to 130 m in the year of 1991, then increased to be rang between 131 m to 146 m in the year of 2006. Cross section (8) has the same changes of elevation range. The Figure also shows the movement of sediment towards the dam starting from 1991 until 2006, this movement led to change the depth and shape of all section within the study area. It is also shown that the simulation of sediment deposition can be improved using Geographic Information System, and the sediment movement was successfully visualized within the channel boundary.

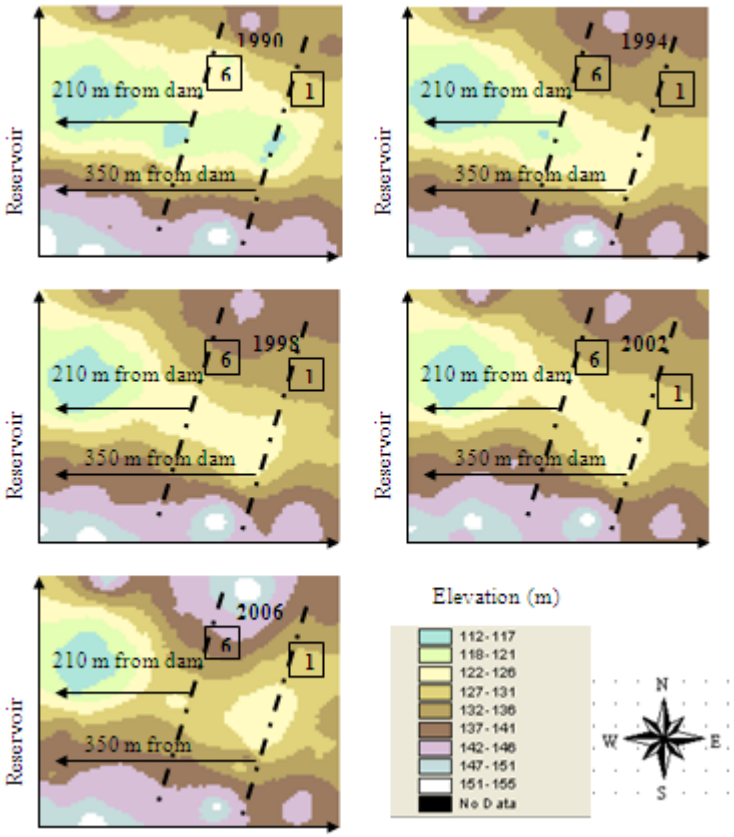

Figure 14: Elevation for Berang River at confluence point with Kenyir reservoir

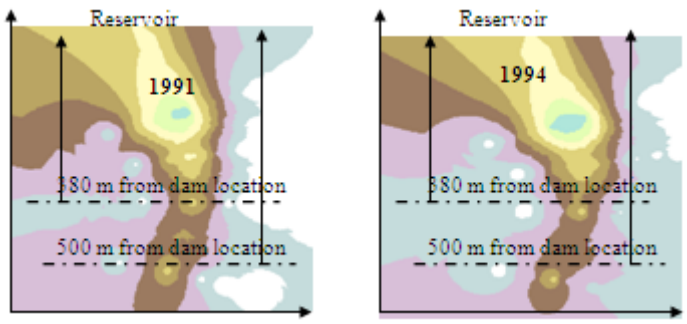

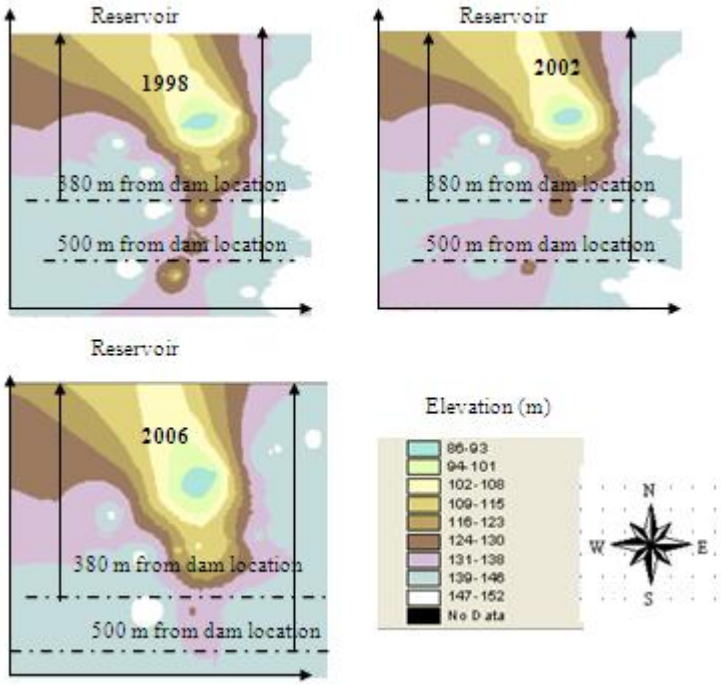

Figure 15: Elevation for Kenyir River at confluence point with Kenyir reservoir

VI. CONCLUSIONS

The main purposes of this study are:

(1) To simulate sediment inflow to the Kenyir Reservoir from Berang River and Kenyir River using GSTARS3 sediment transport model. Various statistical parameters (MSE, MAPE and R^2) were used to test the performance of GSTARS3 in simulating the amount of sediment accumulation. The results show that the simulation using GSTARS3 model were in agreements and the computed error was found to be 5.5 % for the case of Berang River and 6.2 % for the case of Kenyir River.

(2) To visualize the sediment accumulation in the Kenyir Reservoir and to identify the amount and location of sediment accumulation since the operation of Kenyir dam. GSTARS3 model was integrated with ArcView. It shows that the simulation of sediment accumulation can be improved using Geographic Information System. The sediment movement was successfully visualized within the channel boundary. Integrating GSTARS3 model with ArcView is a new technique for the management of reservoir sedimentation processes.

Two locations in Kenyir Reservoir were selected to demonstrate the success of integrating the GSTARS3 model with ArcView. These locations are at the confluences of Berang river and Kenyir river with Kenyir reservoir. GSTARS3 model was carried out separately to simulate the sediment deposition in Kenyir reservoir for the period from 1991 to 2006. The sedimentation rates from the two rivers are shown in Table 2.

REFERENCES

[1]. Andualem, G., & Yonas, M. (2008). Prediction of sediment inflow to Legedadi reservoir using SWAT watershed and CCHEID sediment transport models. Nile Basin water Engineering Scientific magazine, 1, 65-74.

[2]. Baigorria, G. A., & Romero, C. C. (2006). Assessment of erosion hotspots in a watershed: Integrating the WEPP model and GIS in a case study in the Peruvian Andes. Environmental Modelling & Software, 22, 1175-1183.

[3]. Chang, H. H. (1984). Mathematical Model of Erodible Channels. Journal of Hydraulic Engineering, 110(2), 157-172.

[4]. Fu, G., Chen, S., & McCool, D. (2004). Modeling the impact of no till practice on soil erosion and sediment yield with RUSLE, SEDD, and ArcView. Soil and Tillgage Research, 85, 38-49.

[5]. Hamrick, J. M. (n.d.). EFDC1D - A one dimensional hydrodynamic and sediment transport model for river and stream networks: model theory and users guide. www.epa.gov/athens/publications/Pub2001.html. Retrieved September 1, 2001, from www.epa.gov.athens/publications/reports/EPA_600_R_01_037.pdf

[6]. Millward, A. A., & Mersey, J. E. (1999). Adapting the RUSLE to model soil erosion potential in a moumtainous tropical watershed. CATENA, 38, 109-129.

[7]. Molinas, A., & Yang, C. (1986). Computer Program User Manual for GSTARS, Generalised Stream Tube for Alluvial River Simulation. Denver, Colorado, USA.: U.S. Bureau of Reclamation Technical Service Center.

[8]. Molnar, D., & Julien, P. (1997). Estimation of upland erosion using GIs. Computers and Geosciences, 24(2), 183-192.

[9]. Mood, A., Graybill, F., & Boes, D. (1974). Introduction to the Theory of Statistic. NewYork: McGrawHill.

[10]. Morris, G., & Fan, J. (1998). Reservoir Sedimentation Handbook, Design and Management of Dams, Reservoir, and Watershed for Sustaiable Use. NewYork: McGraw Hill.

[11]. Patrick, M. G. (1996.). Sedimentation Problems with Dams . International Rivers. http://www.internationalrivers.org/en/node/1476

[12]. Simons, D.B.and Sentürk, F. (1992). Sediment transport technology: water and sediment dynamics. Littleton (Colo.): Water resources publication.

[13]. Thomas, W., & Prashum, A. (1977). Cited by Hong Lee and Hui Ming. Numerical simulation of scour and deposition in a channel network. International Journal of Sediment Research, 18(1), 32-49.
[14]. Toniolo, H., & Parker, G. (2003). 1D Numerical modeling of reservoir sedimentation. Coastal and Estuarine Morphodynamics, 1, 457-468.
[15]. Yang, C. (1973). Incipient motion and sediment transport. Journal of Hydraulic division, 99(10), 1679-1704.
[16]. Yang, C. (1984). Unit stream power equation for gravel. Journal of Hydraulic Engineering, 110(12), 1783-1797.
[17]. Yang, C., & Song, C. (1986). Theory of minimum energy and energy dissipation rate. Encyclospedia of Fluid Mechanics, 1, 353-399.
[18]. Yang, C., & Simöes, F. (2001 and 2002). Users Manual for GTARS3(Generalized Sediment Transport model for alluvial River Simulation version 3.0). Denver, Colorado, USA.: Technical Service Center..U.S. Bureau of Reclamation .
[19]. Yang, C., Simöes, F. J., Huang, J., & Greimann, B. (2005). Generalized SedimentTransport Models for Alluvial Rivers and Reservoir. US-China Workshop on advanced Computational modeling in Hydroscience & Engineering, Sep, 19-21.
[20]. Yang, C., & Ahn, J. (2011). Users Manual for GTARS4 (Generalized Sediment Transport model for Alluvial River Simulation version 4.0). Fort Collins, Colorado, USA.: Hydroscience and Training Center, Colorado State University.

ISSN (e): 2250 – 3005 || Vol, 04 || Issue, 10 || October– 2014 ||
International Journal of Computational Engineering Research (IJCER)

Impact of Misalignments on Root Stresses of Hypoid Gear Sets

Avutu. Madhusudhana reddy[1], Gowthamtham reddy. Vudumula[2]

[1] PG student, Department of Mechanical Engineering, Vikas College of Engineering & Technology, Nunna
[2] Guide (Asst.prof), Department of Mechanical Engineering, Vikas College of Engineering & Technology, Nunna, Vijayawada, AP, INDIA

ABSTRACT

The hypoid gears are a subtype of bevel gears. Hypoid gears are similar in appearance to spiral bevel gears. They differ from spiral-bevel gears in that the axis of the pinion is offset from the axis of the gear. On observation the hypoid gear seems to be similar in appearance to the helical bevel gears. The main difference being that the planes of the input and the output gears are different . This allows for more efficient intermeshing of the pinion and driven gear. Since the contact of the teeth is gradual, the hypoid gear is silent in operation as compared to the spur gears.These gears are usually used in industrial and automotive application and hence the material used is a metal like stainless steel. A major application of hypoid gears is in car differentials where the axes of engine and crown wheel are in different planes.In this thesis, the impact of misalignments on root stresses of hypoid gear sets is investigated theoretically with FEA. An experimental set-up designed to allow operation of a hypoid gear pair under loaded quasi-static conditions with various types of tightly controlled misalignments is introduced. These experimental data is collected from journal paper. Structural analysis is done to verify the strength of the hypoid gear for alignment and misalignment.Software for modeling is Pro/Engineer and for analysis is Cosmos.

KEYWORDS : *Cosmos, FEA , Hypoid gears , PRO-E, Structural Analysis*

I. INTRODUCTION TO GEARS

A gear is a rotating machine part having cut teeth, or cogs, which mesh with another toothed part in order to transmit torque. Two or more gears working in tandem are called a transmission and can produce a mechanical advantage through a gear ratio and thus may be considered a simple machine. Geared devices can change the speed, magnitude, and direction of a power source. The most common situation is for a gear to mesh with another gear, however a gear can also mesh a non-rotating toothed part, called a rack, thereby producing translation instead of rotation.

The gears in a transmission are analogous to the wheels in a pulley. An advantage of gears is that the teeth of a gear prevent slipping.

II. NOMENCLATURE

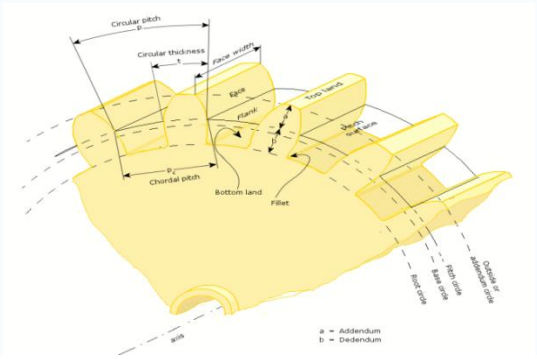

Fig.1 Nomenclature

III. INTRODUCTION TO HYPOID GEARS

The hypoid bevel gears, mostly used at the main transmission of motor vehicles, are non-concurrent gears. Hypoid bevel gearings are spiral and are manufactured on the same machines as the concurrent spiral bevel gearings. The research on concurrent bevel gears lead to the development of an international standard ISO/DIN on bevel gear strength calculus. In the case of hypoid bevel gears there are less references and a gear strength standard is not yet developed. Even if the relative slippery between the tooth profiles is relatively high, binding is not the main gear failure, because the gears are made of cemented steels, with high hardness, tooth profile has good finishing and good quality lubrication

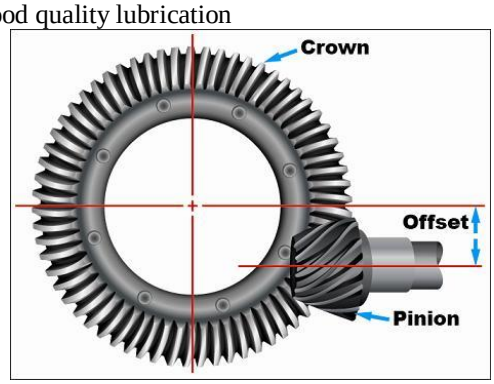

Fig.2 Hypoid gear

4.1 Hypoid Gear Materials

Gear composition is determined by application, including the gear's service, rotation speed, accuracy and more.

- **Cast iron** provides durability and ease of manufacture.
- **Alloy steel** provides superior durability and corrosion resistance. Minerals may be added to the alloy to further harden the gear.
- **Cast steel** provides easier fabrication, strong working loads and vibration resistance.
- **Carbon steels** are inexpensive and strong, but are susceptible to corrosion.
- **Aluminum** is used when low gear inertia with some resiliency is required.
- **Brass** is inexpensive, easy to mold and corrosion resistant.
- **Copper** is easily shaped, conductive and corrosion resistant. The gear's strength would increase if bronzed.
- **Plastic** is inexpensive, corrosion resistant, quiet operationally and can overcome missing teeth or misalignment. Plastic is less robust than metal and is vulnerable to temperature changes and chemical corrosion. Acetyl, delrin, nylon, and polycarbonate plastics are common.
- **Other** material types like wood may be suitable for individual applications.

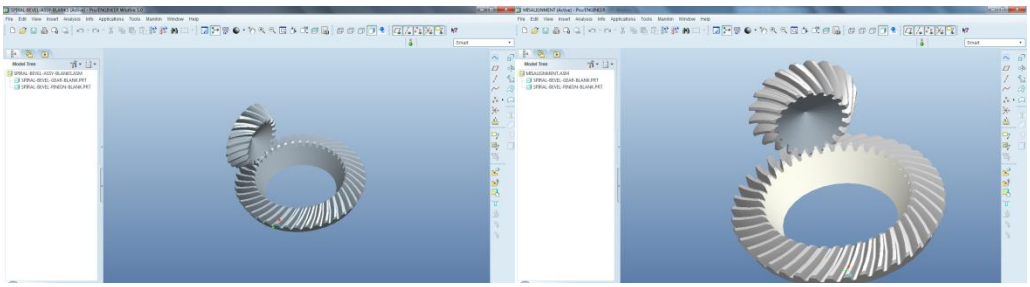

Fig.3 Assembly **Fig.4 Misalignment**

IV. INTRODUCTION TO FEA

Finite element analysis (FEA) is a fairly recent discipline crossing the boundaries of mathematics, physics, engineerin and computer science. The method has wide application and enjoys extensive utilization in the structural, thermal and fluid analysis areas. The finite element method is comprised of three major phases: (1) **pre-processing**, in which the analyst develops a finite element mesh to divide the subject geometry into subdomains for mathematical analysis, and applies material properties and boundary conditions, (2) **solution**, during which the program derives the governing matrix equations from the model and solves for the primary quantities, and (3) **post-processing**, in which the analyst checks the validity of the solution, examines the values of primary quantities (such as displacements and stresses), and derives and examines additional quantities (such as specialized stresses and error indicators).

V. ANALYSIS FOR HYPOID BEVEL GEAR – PERFECT MISALIGNMENT

5.1 STEEL

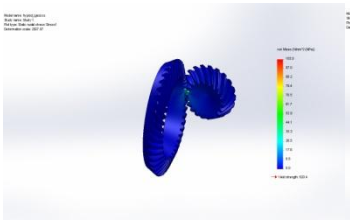

Fig.5 Hpiod igess – study 1 –stress

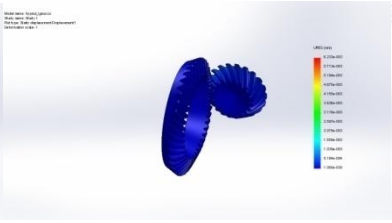

Fig.6 Hypiod igesss study 1 - 1- displacement

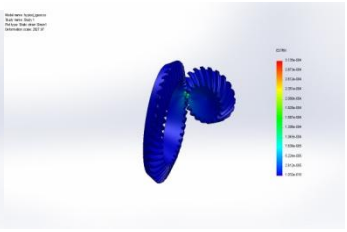

Fig.7 Hpiod igesss – study strain

5.2 ALUMINUM ALLOY

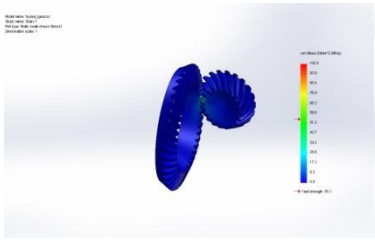

Fig .8 Hypoid igesss –study 1 –stress-stress

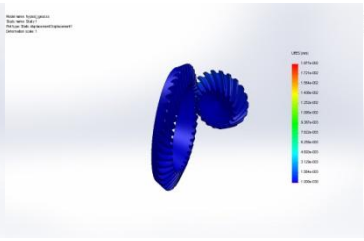

Fig.9 Hypoid igesss -study 1- Displacement

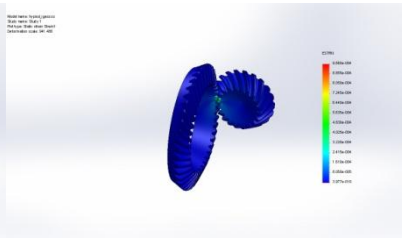

Fig.10 Hypoid igesss - -study 1- strain –strain

VI. PERFECT ALIGNMENT OF HYPOID BEVEL GEARS

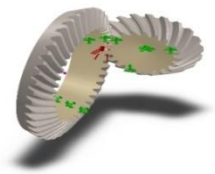

Fig.11 Assembly 2

6.1-STEEL

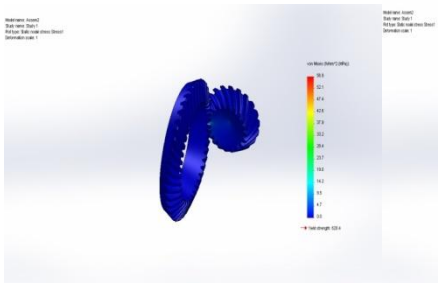

Fig.12 Assem2-Study 1-Stress-Stress1

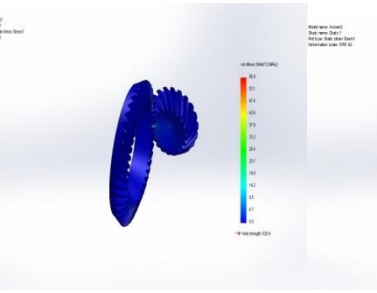

Fig.13 Assem2-Study1-Displacement

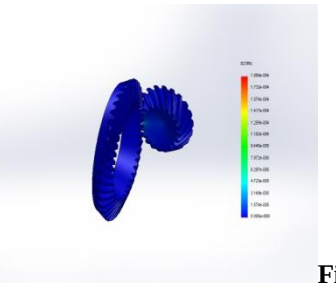

Fig.14 Assem2-Study 1-Strain

6.2 ALUMINUM ALLOY

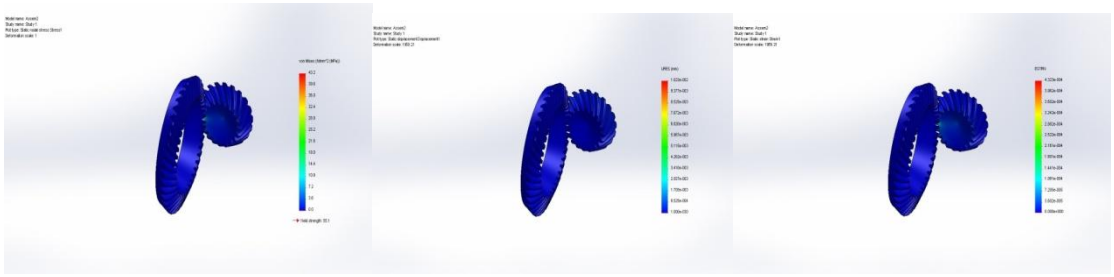

Fig.15 Assem2-Study 1-Stress-Stress1 Fig.16 Assem2-Study 1-Displacement- Fig.17 Assem2-Study1-Strain-

Displacement1 **Strain1**

VII. RESULTS TABLE

TYPE	MATERIAL	RESULTS		
		DISPLACEMENT(mm)	STRESS(N/mm^2)	STRAIN
MISALIGNMENT	STEEL	6.233E-003	105.8	3.135e-002
	ALUMINUM ALLOY	1.877E-002	102.5	9.660e-004
ALIGNMENT	STEEL	3.411E-003	56.9	1.889e-004
	ALUMINUM ALLOY	1.023E-002	43.2	4.323e-004

Table.1 results

VIII. CONCLUSION

In this thesis, the impact of misalignments on root stresses of hypoid gears is investigated. 3D modeling is done in Pro/Engineer. Two models with perfect alignment and misalignment are designed.

The forces acting on the hypoid gear are calculated theoretically. Structural analysis and Modal analysis are done on the designed models to verify the stresses developed. The materials used are Steel and Aluminum Alloy. Analysis is done Solidworks.

By observing the analysis results, the stresses are increased almost by double when the gears are misaligned. So it can be concluded the deviation angle of contact defined as a major contributor of increasing of stress on the tooth root thereby probably could lead to a fatigue initiation at the maximum stress region and finally leads to breakage of the gear.

By comparing the results between two materials, the stress values are less when Aluminum alloy (6061) is used compared with that of steel and also its density is less, thereby reducing the weight of the gears. By reducing the weight, mechanical losses will be reduced. The gear will perform more efficiently and the life time of the gear also increased.

REFERENCES

[1]. PAPER 1 - The Stress Distribution of Gear Tooth Due to Axial Misalignment Condition by M.R. Lias, T.V.V.L.N. Rao, M. Awang and M.A. Khan

[2]. Experimental and numerical analysis of the effect of gear center distance variation and misalignment error on the dynamic behavior of narrow-faced spur gear drives by Mohamed Ben Amara, Mohamed Maatara and Aref Maaleja

[3]. An analytical method to calculate misalignment in the journal bearing of a planetary gear system by Pralay Kumar Das, Shiam Sunder Gupta

[4]. Design and simulation of meshing of new type of worm-gear drive with localized contacts by Inhwan Seol, Soonbae Chung

[5]. DETECTION OF A GEAR COUPLING MISALIGNMENT IN A GEAR TESTING DEVICE by François Combet, Nadine Martin, Pierre Jaussaud, François Léonard

[6]. Al-Hussain, K.M. and I. Redmond, 2002. Dynamic response of two rotors connected by rigid mechanical coupling with parallel misalignment. J. Sound Vibr.,

[7]. Ali , S.M.J. and O.D. Mohammad, 2008. Load sharing on spur gear teeth and stress analysis when contact ratio changed. Eng. Tech. J.

[8]. Ameen, H.A., 2010. Effect of shaft misalignment on the stresses distribution of spur gears. Eng. Tech. J.

[9]. Ariatedja, J.B. and O. Mamat, 2011. A semi-elliptical crack modeling and fracture constraint on failure diagram. J. Applied Sci.

[10]. Atanasovska, I. and V. Nikolic, 2000. The analysis of the factor of load distribution over tooth pairs in mesh in respect of contact stress of tooth flanks. J. Tech. Mech. Eng.,

ISSN (e): 2250 – 3005 || Vol, 04 || Issue, 10 || October– 2014 ||
International Journal of Computational Engineering Research (IJCER)

Analysis of Serial Pinned Joints in Composite Materials

Kodali. Vikas[1], Kandula. Deepthi[2]
[1] PG student, Department of Mechanical Engineering, Vikas College of Engineering & Technology, Nunna
[2] Guide (Asst.prof), Department of Mechanical Engineering, Vikas College of Engineering & Technology, Nunna, Vijayawada, AP, INDIA

ABSTRACT

Pin jointed structures are more regularly used because they are simple to design, relatively inexpensive to make, easy to construct, and easy to modify. A pin joint is a solid cylinder-shaped device, similar to a bolt, which is used to connect objects at the joint area. The pin can only transmit a force and has no ability to resist rotation. They can be 'fixed' structures such as frames, or they can be structures that move, more normally referred to as mechanisms.

In practice pin jointed structures often use bolts which are tightened and therefore they can resist rotation to a certain extent. This type of joint connection allows each object to rotate at the point of joint connection. Most mechanical devices that require bending or opening typically use a pin joint. These joints can be welded solid or allow movement between the two connected objects.

In this thesis, analysis is done on the E Glass and S2 Glass epoxy composite plate with two serial holes by varying distance from the free edge of the plate to the diameter of the first hole and width of the specimen to the diameter of the holes and also and the distance between center of two holes-to-hole diameter. Structural and Fatigue analysis are done using Cosmos.

KEYWORDS: *Cosmos, Fatigue, PRO-E,Structural Analysis, Pin joints.*

I. INTRODUCTION

1.1 Mechanical joints

A mechanical joint is a part of a machine which is used to connect another mechanical part or mechanism. Mechanical joints may be temporary or permanent.

1. Knuckle joint
2. Turnbuckle
3. Pin joint
4. Cotter joint
5. Bolted joint
6. Screw joint
7. Welded joint

2.2 About pinned joints

In mechanical engineering, there are multiple methods for fastening objects together. A pin joint is a solid cylinder-shaped device, similar to a bolt, which is used to connect objects at the joint area. This type of joint connection allows each object to rotate at the point of joint connection. Most mechanical devices that require bending or opening typically use a pin joint.

II. OVER VIEW OF COSMOS WORKS

Cosmos works is a useful software for design analysis in mechanical engineering. That's an introduction for you who would like to learn more about COSMOS Works. COSMOS Works is a design analysis automation application fully integrated with Solid Works.

This software uses the Finite Element Method (FEM) to simulate the working conditions of your designs and predict their behavior. FEM requires the solution of large systems of equations. Powered by fast solvers, COSMOS Works makes it possible for designers to quickly check the integrity of their designs and search for the optimum solution.

III. ANALYSIS OF PINNED JOINT

3.1 Original model

3.1.1 S2 glass fiber Structural analysis

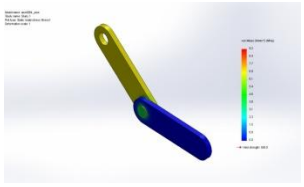

Fig1:Study 1-stress –stress1

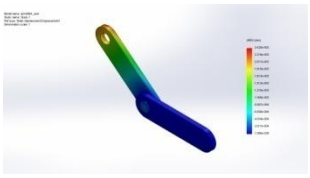

Fig2: Study 1-Displacement –displacement1

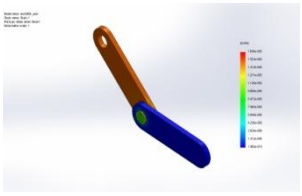

Fig3:Study 1- strain strain 1

3.1.2 Fatigue analysis

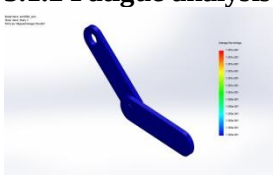

Fig4 :Study2-results-results1

Fig5:Study 2-results-results2

Fig 6: Study 2 –results-results3

3.2E glass epoxy

3.2.1Structural analysis

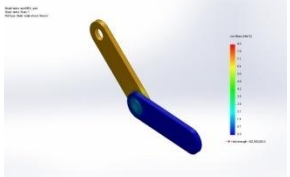

Fig7: Study 1 – stress – stress1

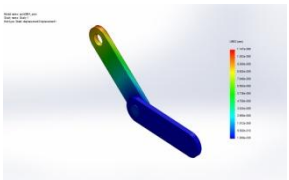

Fig8: Study 1 displacement – displacement1

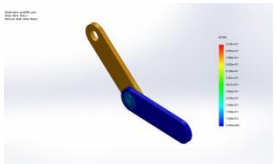

Fig9: Study 1-strain –strain 1

3.2.2 Fatigue analysis

Fig10: Study 2- results –results 1

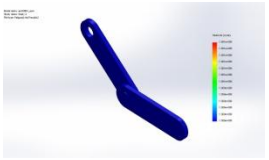

Fig11: Study 2 – results –results

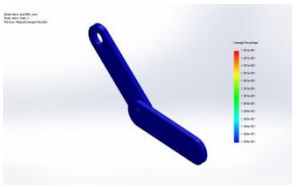

Fig12: Study 2-results –results3

3.3Changing hole distance

3.3.1 S_2 Glass structural analysis

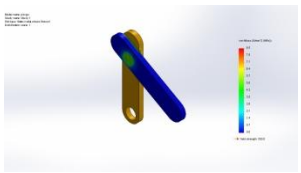

Fig13: Study 1- stress –stress1

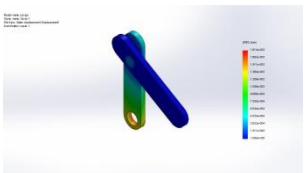

Fig14: Study 1-Displacement – displacement 1

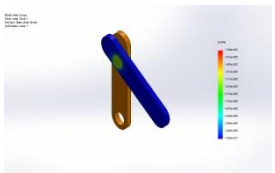

Fig15: Study 1-Strain –strain 1

3.3.2 Fatigue analysis

Fig16: Study 2-Results- results1

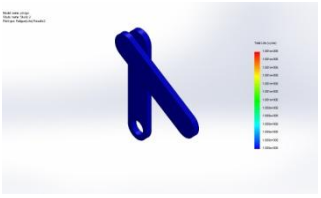

Fig17: Study 2 –Results –result 3

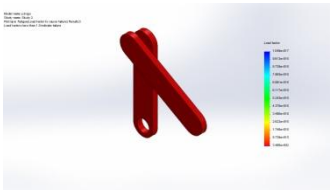

Fig18: STUDY 2 –Results –results

3.4E GLASS

3.3.1 Structural analysis

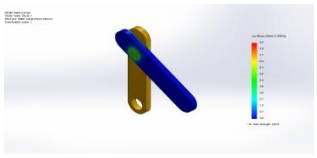

Fig19: Study 1-Stress-Stress1

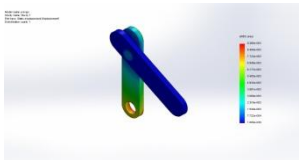

Fig20: Study 1-Displacement-Displacement1

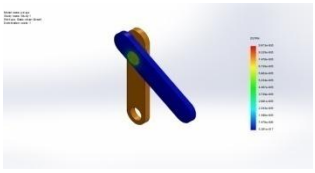

Fig21 : Study 1-Strain-Strain1

3.3.2 Fatigue analysis

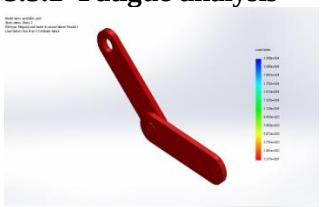

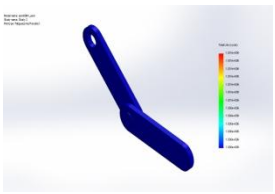

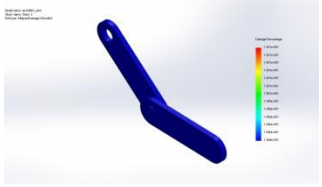

Fig22: Study 2-Results-Results1

Fig23: Study 2-Results-Results2

Fig24: Study 2-Results-Results3

3.5 Changing link position

3.5.1 S2 glass fatigue analysis

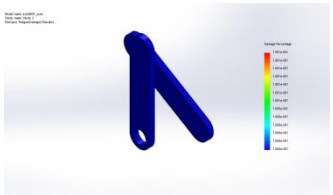

Fig25: Study 2-Results-Results1

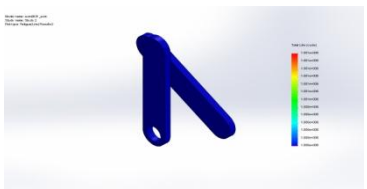

Fig26: Study 2-Results-Results

Fig27: Study 2-Results-Results3

3.5.2 E glass fatigue analysis

Fig28: Study 2-Results-Results1

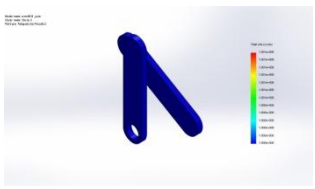

Fig29: Study 2-Results-Results2

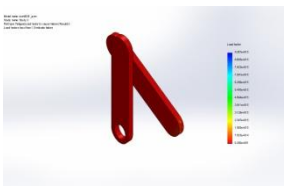

Fig30 :Study 2-Results-Results

3.6 Changing fixed area

3.6.1 S2 glass fatigue analysis

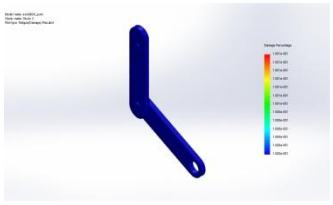

Fig31:Study 2-Results-Results1

Fig32:Study 2-Results-Results2

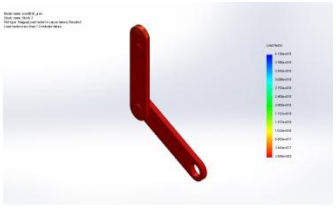

Fig33: Study 2-Results-Results3

3.6.2 Fatigue analysis

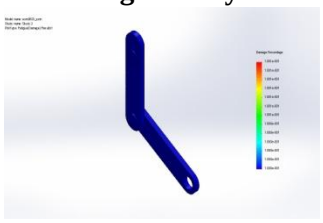

Fig34: Study 2-Results-Results1

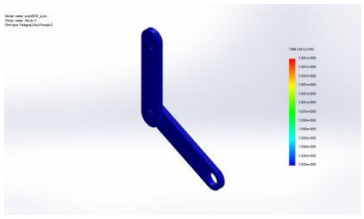

Fig35: Study 2-Results-Results2

Fig36: Study 2-Results-Results3

IV. RESULTS TABLE

4.1 Original model

Static	Stress (N/mm^2)	Displacement (mm)	Strain
S2 Glass	9.2	2.420e-003	1.694e-006
E Glass	8.5	1.147e-008	9.234e-011

Table no.1 Static results

Fatigue	Damage	Load factor	Life
S2 Glass	1.001e-001	2.771e+019	1.001e+006
E Glass	1.001e-001	2.269e+024	1.001e+006

Table no.2 Fatigue results

4.2 Changing hole distance

Static	Stress (N/mm^2)	Displacement (mm)	Strain
S2 Glass	8.5	1.813e-003	1.756e-006
E Glass	8.5	9.266e-003	8.973e-006

Table no.3 Static results

Fatigue	Damage	Load factor	Life
S2 Glass	1.001e-001	1.049e+017	1.001e+006
E Glass	1.001e+001	2.055e+016	1.001e+006

Table no.4 Fatigue results

4.3 Changing link

Static	Stress (N/mm^2)	Displacement (mm)	Strain
S2 Glass	8.8	4.113e-004	1.619e-006
E Glass	8.7	8.962e-003	8.960e-006

Table no.5 Static results

Fatigue	Damage	Load factor	Life
S2 Glass	1.001e-001	3.442e+017	1.001e+006
E Glass	1.001e-001	9.387e+015	1.001e+006

Table no.6 Fatigue results

4.4 Changing fixed area

Static	Stress (N/mm^2)	Displacement (mm)	Strain
S2 Glass	9.6	2.200e-003	1.810e-006
E Glass	9.6	1.124e-002	9.251e-006

Table no.7 Static results

Table no.8 Fatigue results

Fatigue	Damage	Load factor	Life
S2 Glass	1.001e-001	4.130e+018	1.001e+006
E Glass	1.001e-001	1.642e+018	1.001e+006

V. CONCLUSIONS

In this thesis, analysis is done on the E Glass and S2 Glass epoxy composite pinned joints with two serial holes by varying distance from the free edge of the plate to the diameter of the first hole and width of the specimen to the diameter of the holes and also and the distance between center of two holes-to-hole diameter. Structural and Fatigue analysis are done using Cosmos.

By observing the structural analysis results, the stress and displacement values are less than their respective strength values. So using composite materials is safe for serial pinned joints. By observing fatigue analysis results, damage factor is very less for both materials, life is about $1e^6$ cycles.

REFERENCES

[1]. Experimental and numerical analysis of pinned-joints composite laminates: Effects of stacking sequences by UA Khashaba, Mechanical Engineering Department, Faculty of Engineering, King Abdulaziz University, Jeddah, Saudi Arabia
[2]. A Numerical and Experimental Study of Woven Composite Pin-Joints by F. Pierron, Department of Mechanical and Materials Engineering, France
[3]. Computation Method in Failure Analysis of mechanically Fastened Joints at Layered Composites by iIvana Ilić – Zlatko Petrovic – Mirko Maksimović – Slobodan Stupar – Dragi Stamenković, Serbia
[4]. Influence of Filler Materials on Pinned Joints of Woven Glass Fiber Reinforced Epoxy Composites by H.M. Harsha, M.C. Murugesh and K.N. Bharath
[5]. Department of Mechanical Engineering, GM Institute of Technology, Davangere, Karnataka, India
[6]. Two-Dimensional Modeling of Composite Pinned-Joint Failure by Larry B. Lessard, Mahmood M. Shokrieh, Department of Mechanical Engineering, McGill University, Montreal, Quebec

ISSN (e): 2250 – 3005 || Vol, 04 || Issue, 10 || October– 2014 ||
International Journal of Computational Engineering Research (IJCER)

Reversible Data Hiding in Encrypted color images by Reserving Room before Encryption with LSB Method

[1] Sabeena O.M, [2] Rosna P. Haroon
[1]*Dept. of CSE Ilahia College Of Engineering and Technology, Kerala,India*
[2]*Assistant Professor Dept. of CSE Ilahia College Of Engineering and Technology, Kerala, India*

ABSTRACT
Reversible data hiding is the technique in which data in the cover image reversibly can retrieve after the extraction of hidden data in it. The technique provides the secrecy for a data, and also for its cover image. Ancestor methods of reversible data hiding were vacates room for data hiding after encryption, which leads to some errors at the time of data extraction and image recovery. Here describes a novel method of reversible data hiding in which, Reserving room before encryption in images, so that image extraction is subjected to free of errors. Here we are proposing an LSB plane method for the data hiding, which will result more space for embedded secret data. Moreover the usage of colour images as cover images will helps to store more data in different channels.

KEY WORDS*— reversible data hiding, LSB plane method*

I. INTRODUCTION

In most cases of data hiding, the cover images will experience some distortion due to data hiding and cannot be inverted back to the original form. That is, some permanent distortion has occurred to the cover image even after the hidden data have been extracted out. In a wide range of applications like medical, military and law forensic fields, distortion of cover images does not allowed. So reversible data hiding is essential for these cases. In this technique the cover image can losslessly recover after the extraction of hidden data. So many RDH techniques have introduced in recent years. One of a general framework for RDH is first extracting compressible features of original cover and then compressing them losslessly, more space can be saved for embedding auxiliary data. Another popular method is based on difference expansion (DE), in which the difference of each pixel group is expanded like multiplication by even numbers. Then the least significant bits (LSBs) of the difference are all-zero and can be used for embedding messages. Another considerable strategy for RDH is histogram shift (HS), in which space is surplus for data embedding by shifting the highest possible value of histogram of gray values. Encryption is an effective and popular means of privacy protection. A content owner can encrypt his message before sending to another person as it converts the original and meaningful content to abstruse one. In some applications a block. This process is performing with the help of spatial correlation in decrypted image. In another method, at the decoder side by further exploiting the spatial correlation using a different estimation equation and side match technique, which provides much lower error rate. These two methods mentioned above rely on spatial correlation of original image to extract data. Implies that, decryption must be done in the encrypted before data extraction. All the above methods try to vacate room from the encrypted images directly. Because of the entropy of encrypted images has been maximized, these techniques can only obtain small payloads or generate marked image with poor quality for large payload and all of them are subject to some error rates on data extraction and/or image restoration. Some methods can use error correcting codes, also pure payload can consume. In this paper, we proposes a novel method for RDH in encrypted color images, for which we do not "vacate room after encryption", but "reserve room before encryption" [1]. We can first empty out spaces by embedding LSBs of some pixels into other pixels with a LSB plane method and then encrypt the image, so the place of these LSBs in the encrypted image can be used to hide data bits. This method separate data extraction from image decryption and data extraction and image recovery are free of any error.

II. RELATED WORKS

Reversible data hiding was first established as a technique of attaining the cover image after the extraction of hidden data. Here utilizes the zero or the minimum points of the histogram of an image and slightly modifies the pixel gray scale values to embed data into the image [2]. The computational complexity for technique is low, but it is only applicable at gray scale images. Then the Reversible Data Hiding with Optimal Value Transfer emerges to find the optimal rule of value modification under a payload-distortion criterion.

An optimal value transfer matrix can be obtained by maximizing a target function using iterative algorithm, for a practical reversible data hiding scheme [3]. The technique undergoes the prediction so Computation complexity will be higher. Encryption is an effective and popular means of privacy protection. Through the work Reversible Data Hiding in Encrypted Image proposes a reversible data hiding scheme for encrypted image. Then the additional data can be embedded into the image by modifying a small portion of encrypted data, after encrypting the entire data of a gray image [5]. The received image provides original image through decryption using encryption key and data using data hiding key. For encrypted images, the compression efficiency can be improved as how the source dependency is exploited. So a work developed as Efficient Compression of Encrypted Gray scale Images. The paper proposes a resolution progressive compression scheme which compresses the encrypted image progressively in resolution, such that the decoder can attain low-resolution version of the image [4]. The statistics can be used to analyze next resolution level. An Improved method of Reversible Data Hiding in Encrypted Images is Using Side Match. Here proposes an improved data extraction and image recovery method over Zhang's work. The Zhang's work partitions an encrypted image into blocks, and each block carries one bit by flipping three LSBs of a set of pre-defined pixels [6]. Thus leads to estimation of new algorithm for better calculation of smoothness of image blocks. According to the descending order of the absolute smoothness difference between two candidate blocks, the extraction and recovery of blocks are performed. Also side match technique reduces the error rate.

In the first phase, a content owner encrypts the original image using a key. Then, a data-hider may vacates some spare space by performing compression on least significant bits using a data-hiding key to accommodate some additional data. Using Separable Reversible Data Hiding in Encrypted Image, with an encrypted image containing additional data, even receiver does not know the image content he can extract the additional data using data hiding key [7]. Also receiver can decrypt the received data to obtain an image similar to the original one using encryption key, but cannot extract the additional data. Receiver can recover the original content and extract additional data without any error using the encryption key and data-hiding key. Watermarking embeds information into a digital signal. After the hidden data is extracted, receiver can restorethe original image without any distortion. Reversible Image Watermarking is a scheme using an interpolation technique, which can embed a large amount of data into images with unknowable modification [8]. Here assigns the interpolation-error. Due to lesser modification of pixels, quality of image will be higher. Reversible Watermarking Algorithm Using Sorting and Prediction is another algorithm without using a location map is used for reversible watermarking. This algorithm employs prediction errors to hide data into an image. To record the prophesy errors based on magnitude of its local variances a sorting technique is used [9]. Using sorted prophesies errors and a reduced size location map allows us to hide more data in the image with less distortion.

Then improved a Reversible Data Hiding Scheme Via Optimal Codes for Binary Covers. It improves the recursive construction to approach the rate–distortion bound. Also they generalize the method using a decompression algorithm as the coding scheme to hide data and prove that the generalized codes can reach the rate–distortion bound [10]. Also proves the compression algorithm reaches entropy. By the proposed binary codes, they improve three RDH schemes that use binary feature sequence as covers. Reversible Data Embedding Using Difference Expansion is a novel reversible data embedding method for digital images. They explore the redundancy in digital images to achieve very high overwhelming capacity, and keep the distortion low. Here needs to access location map and also can be performed at gray image only.

III. PROPOSED SYSTEM

The proposed architecture consists of a Reserving Room Before Encryption (RRBE) method for the data hiding in color images and also allows the reversible extraction of cover image. The architecture shown below in figure 1 is architecture of RRBE. VRAE images are sometimes inefficient and difficult to extract data, we like to reverse the order of encryption and vacating room, i.e., reserving room before image encryption at content owner side, becomes a novel framework "reserving room before encryption (RRBE)" which leads to the more natural and much easier Reversible data hiding tasks in encrypted images. Here the content owner first reserves enough space on original image and then converts the image into its encrypted version with the encryption key. Now, the data hiding process in encrypted images is inherently reversible for the data hider only needs to accommodate data into the spare space previously reserved. The data extraction and image recovery are identical to VRAE. Using color images as the cover images, more data can become hidden. We can reserve more space from three channels of colour image.

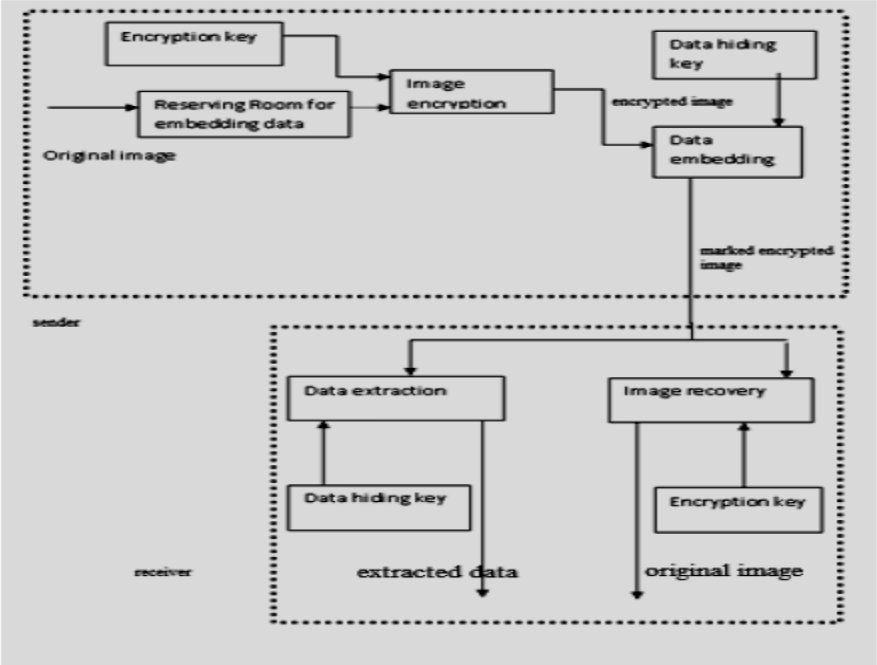

Figure 1. Architecture of RRBE

IV. SOLUTION METHODOLOGY

Here in the proposed architecture a practical framework based on "RRBE" method in color image, which primarily consists of following stages: reserving room in image, encryption of image, data hiding, data extraction and image recovery.

A. Reserving Room in Image

Actually the first stage can divide into two parts, image partition and self reversible embedding.

1.*Image partition*:

Here we uses the LSB planes for the reserving room operation, so the goal of image partition is to construct a smoother area [1], on which standard RDH algorithms can achieve better performance. To do that, without loss of ordinarily, take the 3 channels of original image as 8 bits gray-scale images with its size is M X N and pixels Ci,j belongs to [0,255]. 1<=i<=M, 1<=j<=N. so we have to perform every operation to the three channels of the image. First, the content owner extracts from the original image, along the rows, Discrete overlapping blocks whose number is determined by the size of to-be-embedded messages, denoted by *l*[1]. In detail, every block consists of *m* rows, where *m = [l/N]* and the number of blocks can be computed through *n=M-m+1[1]*. An important thing is that each block is overlapped by pervious or sub sequential blocks along the rows. The content owner, selects the particular block with the highest smoothness to be A, and puts it to the front of the image concatenated by the rest part B with fewer textured areas as shown below.To find smoother area we can use histogram of the cover image [1].

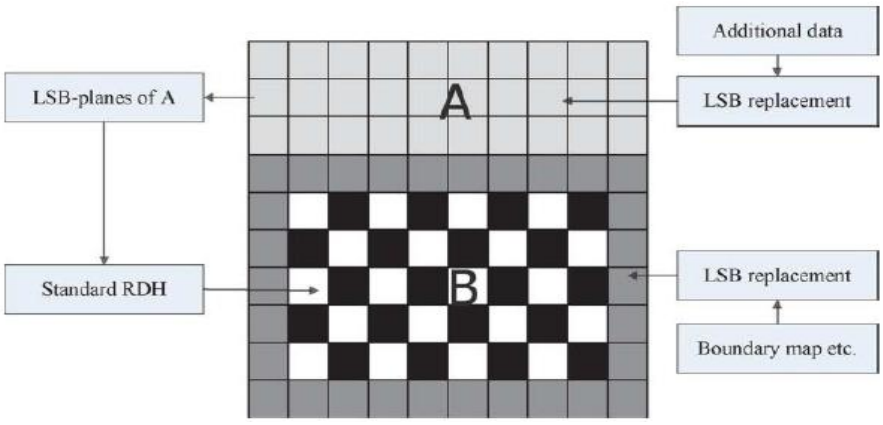

Fig. 2. Illustration of image partition and embedding process[1].

2..Self-Reversible Embedding:

The goal of self-reversible embedding is to embed the LSB-planes of A into B. Pixels in the rest of image B are first categorized into two sets: white pixels with its indices i and j satisfying (i+j)mod2 = 0 and black pixels whose indices meet (i+j)mod2 = 1, as shown in Fig. 2 Then, each white pixel, Bi,j is estimated by the interpolation value[1] obtained with the four black pixels surrounding it as follows

$$B'_{i,j} = w_1 B_{i-1,j} + w_2 B_{i+1,j} + w_3 B_{i,j-1} + w_4 B_{,j+1}$$

Where the weight *w*i, 1<= i<=4. The estimating error is calculated via ei,j = Bi,j - B'i,j and then some data can be embedded into the estimating error sequence. Also the same steps have to do for the black pixels and find ei,j.

B. Encryption of image

We can create encrypted image E by performing the encryption on rearranged self-embedded image, denoted by X. Encryption of X can easily obtain using a stream cipher. For a color image, we take the three channels as three grayscale images. For example, a gray value Xi,j ranging from 0 to 255 can be represented by 8 bits, Xi,j(0), Xi,j(1),…… Xi,j(7) [1], such that

$X_{i,j}(k)=[X_{i,j}/2^k]\bmod 2$, k=0,1,….7

Exclusive- or operation can be used for obtaining encrypted bits

$$E_{i,j}(k)= X_{i,j}(k) \oplus r_{i,j}(k)$$

Where ri,j(k) is generated by a standard stream cipher determined by the encryption key. At last, we embed 10 bits information into LSBs of first 10 pixels in encrypted version of A to tell data hider the number of rows and the number of bit-planes [1] he can embed information into After image encryption to provide the privacy of the content owner being protected, any third party cannot see the content without using encryption key.

C. Data hiding

Data hider will not be provided with the original image. He can embed data to the encrypted image. The embedding process can start at AE which is encrypted version of A. The data hider read 10 bits information in LSBs of first 10 encrypted pixels, as it is arranged at the top of encrypted image. After knowing how many bit-planes and rows of pixels he can modify, he can simply adopt LSB replacement to substitute the available bit-planes with additional data m. The data hider analyzes additional data and the hiding process proceeds with that information. Every pixel values will be converted to binary form and binaries of data bits appended to last bit of pixel values. So a new image will be generated. Anyone who does not having the data hiding key could not extract the additional data.

D. Data extraction and image recovery

Data extraction can do completely independent from image decryption. So the order of them implies two different practical applications.

1) Case 1*: Extracting Data From Encrypted Images [1]:* To manage and update personal information of images which are encrypted for protecting clients' privacy, a poor database manager may only get access to the data hiding key and have to manipulate data in encrypted domain. The feasibility of work is when following the order of data extraction before image decryption.

The database manager gets the data hiding key for decrypting the LSB-planes of AE and extract the additional data m by directly reading the decrypted version. Leakage of original content avoids because the whole process is entirely operated on encrypted domain.

2) Case 2: *Extracting Data From Decrypted Images:* we can proceed with the following scenarios,

a) Generating the Marked Decrypted Image: To form the marked decrypted image X'' which is made up of A'' and B'', the content owner should do following two steps [1].

• Step 1. With the encryption key, the content owner decrypts the image except the LSB-planes of AE[1]. The decrypted version of E' containing the embedded data can be calculated by

$$X''_{i,j}(k)= E'_{i,j}(k) \oplus r_{i,j}(k)[1]$$

And

$$X''_{i,j}= \mathrm{Sum}(X''_{i,j}(k) \oplus r_{i,j}(k) \times 2^k)[1]$$

 Step 2. Extract SR and ER in marginal area of B''. By rearranging A''[1] and B'' to its original state, the plain image containing embedded data is obtained.

b) Data Extraction and Image Restoration* [1]*: After generating the marked decrypted image, the content owner can further extract the data and recover original image[1].

V.CONCLUSION AND FUTURE WORK

Reverse data hiding for colored images are proposed here in this paper. Previous methods have implemented several techniques for data hiding for Gray scale images only. For encrypted images, RDH is done by reserving room before encryption, by using LSB Plane Method as opposed to the one which have proposed Histogram Shifting. Thus the data hider can benefit from the extra space in each channel of the color image. Time delay may arise for color images when reserving room before encryption. By resizing the image we can remedied it out but we have to compensate for the extra space utilization.

VI.ACKNOWLEDGMENT

The authors wish to thank the Management and Principal and Head of the Department(CSE) of Ilahia College of Engineering and Technology for the support and help in completing this work.

REFERENCES

[1]. Kede Ma, Weiming Zhang, Xianfeng Zhao,, "Reversible Data Hiding in Encrypted Images by Reserving Room Before Encryption," IEEE TRANSACTIONS ON INFORMATION FORENSICS AND SECURITY, VOL:8 NO:3 YEAR March 2013

[2]. Z. Ni, Y. Shi, N. Ansari, and S. Wei, "Reversible data hiding," *IEEE Trans. Circuits Syst. Video Technol.*, vol. 16, no. 3, pp. 354–362, Mar.2006.

[3]. T. Kalker and F.M.Willems, "Capacity bounds and code constructions for reversible data-hiding," in *Proc. 14th Int. Conf. Digital Signal Processing (DSP2002)*, 2002, pp. 71–76.

[4]. W. Liu, W. Zeng, L. Dong, and Q. Yao, "Efficient compression of encrypted grayscale images," *IEEE Trans. Image Process.*, vol. 19, no. 4, pp. 1097–1102, Apr. 2010.

[5]. X. Zhang, "Reversible data hiding in encrypted images," *IEEE Signal Process. Lett.*, vol. 18, no. 4, pp. 255–258, Apr. 2011.

[6]. W. Hong, T. Chen, and H.Wu, "An improved reversible data hiding in encrypted images using side match," *IEEE Signal Process. Lett.*, vol.

[7]. X. Zhang, "Separable reversible data hiding in encrypted image," *IEEE Trans. Inf. Forensics Security*, vol. 7, no. 2, pp. 826–832, Apr. 2012.

[8]. L. Luo *et al*., "Reversible image watermarking using interpolation technique," *IEEE Trans. Inf. Forensics Security*, vol. 5, no. 1, pp. 187–193, Mar. 2010.

[9]. W. Zhang, B. Chen, and N. Yu, "Improving various reversible data hiding schemes via optimal codes for binary covers," *IEEE Trans. Image Process.*, vol. 21, no. 6, pp. 2991–3003, Jun. 2012.

[10]. V. Sachnev, H. J. Kim, J. Nam, S. Suresh, and Y.-Q. Shi, "Reversible watermarking algorithm using sorting and prediction," *IEEE Trans. Circuits Syst. Video Technol.*, vol. 19, no. 7, pp. 989–999, Jul. 2009.

[11]. J. Tian, "Reversible data embedding using a difference expansion," *IEEE Trans. Circuits Syst. Video Technol.*, vol. 13, no. 8, pp. 890–896, Aug. 2003.

ISSN (e): 2250 – 3005 || Vol, 04 || Issue, 10 || October– 2014 ||
International Journal of Computational Engineering Research (IJCER)

New Flavone from the Aerial Parts of Bougainvillea Glabra

Dr. Amal Hussein Ahmed
Pharmacognosy Department, Faculty of Pharmacy, Al- Azhar University, Cairo, Egypt

ABSTRACT

New flavone was isolated for the first time from the methanolic extract of the aerial part of Bougainvillea glabra (Nyctaginaceae) & identified as luteolin-7-O-[2''-O-(5'''-O-feruloyl)- b-D-apiofuranosyl]- b-D-glucopyranoside in addition to five flavonoids isolated& identified after comparing their spectra with reported ones as vitexin, isovitexin, chrysoeriol, apigenin& luteolin .

Key Words: *Bougainvillea Glabra, Nyctaginaceae, flavones, luteolin-7-O-[2''-O-(5'''-O-feruloyl)- b-D-apiofuranosyl]- b-D-glucopyranoside& flavonoids.*

I. INTRODUCTION

Bougainvillea (family: *Nyctaginaceae*) is a very common ornamental plant grown almost all over the world in tropical and subtropical gardens [1]. It is grown as a shrub as well as a climber [2] . *Bougainvillea* was named after the world traveler, Louis de Bougainville, who discovered it in Brazil in 18th century and brought it to Europe where it became both widespread and popular [3] .Genus *Bougainvillea* (Four-o'clock) includes eighteen species native of tropical and subtropical regions of south America from Brazil west to Peru and south to southern Argentina [4] .The most horticulturally important three species of Bougainvillea are *B. spectabilis* Willdenow, *B. glabra* Choisy, and *B. peruviana* [5] . The leaves are alternate, simple ovate acuminate, 4-13 cm long [3] . The actual flower of the plant is small and generally white but each cluster of three flowers are surrounded of three or six bracts with the bright colors associated with plant, including pink, magenta, purple, red orange, white or yellow [4-6] . *Bougainvillea glabra* 'choicy' was first identified by Swiss botanist Jacques Denys Choisy in 1850. *B.glabra* which is also known as Lesser Bougainville, Snow White & Paper flower , has been used in a variety of disorders including diarrohea, acidity ,cough and sore throat. Decoction of dried flowers used for leucorrhoea and decoction of the stem used in hepatitis[7&8]. The main used part of the plant is leaves [8] . The reported constituents in leaf of *Bougainvillea glabra* 'Choicy' are alkaloids, flavonoids, tannins, saponins and proteins [7] . The leaves of *Bougainvillea glabra* are reported to have anti-inflammatory activities [8] , anti-hyperglycemic activity [9] , insecticidal activity , anti hyperglycemic activity ,anti ulcer , antimicrobial and antidiarrhoeal activity [10-14] . Hydroalcoholic extract of *Bougainvillea glabra* leaves showed inhibitory effect against all gram positive and gram negative bacteria except *Bacillus subtilis* and *Micrococcus leuteus* [15&16] .

Experimental Section

Plant Material

The plant materials (leaves) were collected during Feb.-March 2009 from Al- Orman garden, Giza, Egypt. The botanical identity of plant was kindly authenticated by Engineer Tereesa, Herbal specialist in Al-Orman garden, Egypt.

General experimental procedures

Ultraviolet spectrophotometric analysis

Chromatographically pure materials 1 mg each were dissolved in analytically pure methanol then subjected to UV spectroscopic investigation in 4 ml capacity quartz cells 1 cm thick using a Carl Zeiss spectrophotometer PMQ II. AlCl3, AlCl3/HCl, fused NaOAc / H3BO3 and NaOMe reagents were separately added to the methanolic solution of investigated material and UV measurements were then carried out.

Nuclear magnetic resonance spectroscopic analysis

The NMR spectra were recorded on a Varian Mercury VX-300 NMR spectrometer. 1H- spectra run at 300 MHz and 13C- spectra were run at 75.46 MHz in deutrated dimethylsulphoxide (DMSO-d6). Chemical shifts are quoted in γ and were related to that of the solvents.

GC-MS

The mass spectra were recorded on a Shimadzu GCMS-QP-1000 EX mass spectrometer at 70 eV. Identification and determination of the absolute configuration of monosaccharide units were performed on a Shimadzu 5050A quadrupol mass spectrometer .

Preparation of Plant Extract

The dried leaves of *Bougainvillea glabra* (1Kg) were powdered and extracted successively with Methanol. The methanolic extract (5.0 g) was subjected to column chromatography& eluted with gradient mixtures of methanol: water giving 3 fractions; fraction eluted with 7:3 methanol: water mixture (1.7 g), fr. 3:1 (0.81 g) and fr. Eluted with pure MeOH (0.5 g), respectively. The fr. Eluted with Methanol: H2O 3:1 ,was chromatographed on Sephadex LH-20 with H_2O:MeOH (1:1) as eluent. Fractions (each 5 mL) were collected and checked by TLC [Silica gel plates, $CHCl_3$:MeOH:PrOH:H_2O (5:6:1:4), organic phase]. Same fractions collected together, giving 413 fractions. Five flavonoids were isolated from fractions no. 52-59, 60-63, 156-160, 234-256 and 284-301& were identified as vitexin (15 mg), isovitexin (28 mg), chrysoeriol (8 mg), apigenin (8 mg) and luteolin (5 mg), respectively. Fraction 74-82 (60 mg) was further purified by semi-preparative HPLC leading to the isolation of a pure new compound named compound I.

RESULTS& DISCUSSION

Five flavonoids were isolated from the methanolic extract of the aerial part of Bougainvillea glabra& identified after comparing their spectra with reported ones as vitexin, isovitexin, chrysoeriol, apigenin& luteolin in addition to a pure compound (**I**).

Vitexin

Light yellow powder, melting point: 203-204 °C : UV : 335, 271 nm (MeOH).
1H-NMR : δ 3.53 (1H, m, H-5″), 3.54 (1H, m, H-3″), 3.57 (1H, m, H-4″), 3.74 (1H, dd, J = 12.3, 5.5 Hz, H-6a″), 3.77 (1H, dd, J = 12.3, 2.0 Hz, H-6b″), 4.11 (1H, t, J = 9.0 Hz, H-2″), 4.85 (1H, d, J = 9.9 Hz, H-1″) 6.44 (1H, s, H-8), 6.60 (1H, s, H-3), 6.95 (2H, d, J = 8.6 Hz, H-3′, 5′), 7.85 (2H, d, J = 8.6 Hz, H-2′, 6′).

13C-NMR (125 MHz, CD3COCD3 + D2O): δ 61.7 (C-6″), 70.6 (C-4″), 72.0 (C-2″), 74.5 (C-1″), 79.2 (C-3″), 81.6 (C-5″), 95.3 (C-8), 103.4 (C-3), 104.3 (C-10), 108.7 (C-6), 116.7 (C-3′, 5′), 122.4 (C-1′), 129.0 (C-2′, 6′), 157.7 (C-9), 161.0 (C-5), 162.0(C- 4′), 164.5 (C-7), 165.0 (C-2), 183.1 (C-4)

ESI-MS $[M+H]^+$ m/z 433.1

Comparing the above mentioned data with the published literature [17-21], it was concluded that this compound is vitexin.

Isovitexin

Yellow powder, mp 231-232. UV λ max (nm): 267, 332 (MeOH).

1H NMR (300MHz, DMSO-*d*6) *δ*: 6.78 (1H, s, 8-H), 6.51 (1H, s, 3-H), 6.93 (2H, d, *J*=8.8Hz, 3', 5'-H), 7.93 (2H, d, *J*=8.8Hz, 2', 6'-H), 4.82 (1H, m, glu 1-H), 3.15~4.84 (10H, m).

ESI MS (*m/z*): 431$[M-H]^-$. All data were identical to those of isovitexin [17, 22-25].

Luteolin

Yellow powder, mp 327-328. **IR (KBr) *ν*max**: 3402, 2629, 1653, 1618, 1510, 1356, 1301, 1259, 1165, 1031, 999, 947, 860, 829, 793, 739cm-1. **UV λ max** (nm): 261, 307 (MeOH); 265, 364 (NaOMe); 267, 412 (AlCl3); 265, 352 (AlCl3/HCl).
1H-NMR *δ*: 6.25 (1H, d, *J*=2.1Hz, 6-H), 6.54 (1H, d, *J*=2.1Hz, 8-H), 6.57 (1H, s, 3-H), 7.00 (1H, d, *J*=8.4Hz, 5'-H), 7.46 (1H, dd, *J*=2.1,8.4Hz, 6'-H), 7.52 (1H, d, *J*=2.1Hz, 2'-H), 13.01 (1H, s, 5-OH).
ESI-MS (*m/z*): 285 [M-H]-, 284,256.
All data were identical to those of luteolin [17, 20-22].

Chrysoeriol
Yellow powder, mp 327-328 . **IR (KBr) *ν*max**: 3352, 1651, 1624, 1564,1510, 1435, 1350, 1300, 1209, 1171, 1032, 993, 867, 835, 793, 764 cm-1. UV λ max (nm): 264, 341 (MeOH); 261, 402 (NaOMe); 274, 349, 387 (AlCl3); 272, 349, 385 (AlCl3/HCl).
1H-NMR : 6.25 (1H, d, *J*=2.1Hz, 6-H), 6.55 (1H, d, *J*=2.1Hz, 8-H), 6.69 (1H, s, 3-H), 7.00 (1H, d, *J*=8.3Hz, 5'-H), 7.60 (1H, dd, *J*=2.1,8.3Hz, 6'-H), 7.63 (1H, d, *J*=2.1Hz, 2'-H), 4.00 (1H, s, 4'-OCH3), 13.01 (1H, s, 5-OH).
ESI-MS (*m/z*): 299 [M-H]-, 284, 256. All data were identical to those of chrysoeriol [17, 24-25].

Apigenin
1H NMR : *γ*7.83 (2H, *d*, *J* = 8.8 Hz, H-2*0* and H-6*0*), 6.92 (2H,
d, *J* = 8.8 Hz, H-3*0* and H-5*0*), 6.83 (1H, *d*, *J* = 2.1 Hz, H-6), 6.71 (1H, *d*, *J* = 2.1 Hz, H-8), 6.58 (1H, *s*, H-3).
13C NMR: *γ* 180.45 (*s*, C-4), 164.94 (*s*, C-5), 164.41 (*s*, C-2), 162.60 (*s*, C-4*0*), 160.72 (*s*, C-9), 160.16 (*s*, C-7), 129.30 (*d*, C 2*0* and C-6*0*), 123.14 (*s*, C-1*0*), 117.06 (*d*, C-3*0* and C-5*0*), 109.39 (*s*, C-10), 106.57 (*d*, C-3), 104.83 (*d*, C-6), 99.34 (*d*, C-8). Comparing these data with the published ones [17-20] revealed that the product is Apigenin.

Compound (I) was isolated as a yellow amorphous solid (mp 252-254 ºC). The UV spectral data showed absorption bands at 248 nm and 334 nm. The IR spectrum presented bands at 3433 cm^{-1} (OH), at 1655 cm^{-1} (C=O) and 1605 cm^{-1} (C=C).

The molecular formula of compound (**I**) was calculated as $C_{36}H_{36}O_{18}$, showed a [M-H] at *m/z* 755 (calculated for $C_{36}H_{36}O_{18}$-H). Key fragmentation ions occurred at *m/z* 579 [M-*E*-feruloyl-H]$^-$, *m/z* 561 [M-*E*-feruloyl-H_2O-H]$^-$, *m/z* 447 [M-*E*-feruloyl-apiose-H]$^-$ and *m/z* 285 [M-*E*-feruloyl-apiose-glucose-H]$^-$.

The ^{1}H NMR spectrum (Table 1) showed signals at d 7.34 (1H, d, *J* 8.0 Hz), d 7.35 (1H, brs) and at d 6.88 (1H, d, *J* 8.0 Hz) assigned to H-6', H-2' and H-5' respectively, two doublets at d 6.68 (1H, d, *J* 2.0 Hz) and d 6.36 (1H, d, *J* 2.0 Hz), attributed to H-8 and H-6 of the A-ring, and one singlet at d 6.54 (1H, s) attributed to H-3 typical of a luteolin derivative. Signals at d 6.17 (1H, d, *J* 16 Hz, H-a), d 7.30 (1H, d, *J* 16 Hz, H-b), d 7.07 (1H, d, *J* 1.5 Hz, H-2""), d 6.69 (1H, d, *J* 8.0 Hz, H-5"") and d 6.87 (1H, d, *J* 8.0 and 1.5 Hz, H-6"") suggested the presence of an *E*-feruloyl unit.[26] A signal at d 3.74 (3H, s) indicates the presence of a methoxyl group.[27] NOESY experiment showed correlation between signal at d 3.74 (OMe) and at d 7.07, thus establishing the methoxyl group at position 3"" of the *E*-feruloyl unit.

A doublet at d 5.20 (1H, d, *J* 7.5 Hz, H-1") and a singlet at d 5.38 (1H, s) in the ^{1}H NMR spectrum revealed the presence of two anomeric hydrogen from two sugar units. The TOCSY experiment with irradiation at d 5.20 displayed the spin system of the b-D-glucopyranoside unit, whereas irradiation at d 5.38 resulted only in the singlet at d 3.75 (1H, s) suggesting an apiofuranosyl unit. The coupling constant of the anomeric proton at d 5.20 (1H, d, *J* 7.5 Hz) indicated that the present glucose unit has a b-configuration.[27]

The ^{13}C NMR experiment presented 35 signals, from which 15 were attributed to the aglycone, 9 to the *E*-feruloyl unit, 6 to the b-D-glucopyranosyl unit, and with 5 was possible determined a apiofuranosyl unit.[28]

The apiose unit was characterized through ^{1}H and ^{13}C NMR experiments compared to the literature data. In the ^{1}H NMR spectrum, apiose unit with OH linked to C-1''' and OH linked to C-2''' in *trans* configuration presents constant coupling $J_{1,2}$ 0-1 Hz, whereas *cis* configuration is characterized by $J_{1,2}$ 3-4 Hz.[16,17] The chemical shift of C-1 in ^{13}C NMR experiments in pyridine-d_5 to the a-D-apiofuranoside is d 105 and d 112 to b-D-apiofuranoside,[18] whereas in DMSO-d_6 these isomers produce signals at d 108 and d 109, respectively.[29-31] Thus, the apiose unit in (**1**) was identified as being a b-D-apiofuranoside.

The structure and bonds of these units on compound I was established from *g*HMQC and *g*HMBC experiments. *g*HMQC experiment showed direct correlations between carbons and the respective hydrogens (Table 1). *g*HMBC experiments showed long-range correlations between the hydrogen signal at d 5.20 (H-1" glucose) and the carbon signal at d 162.4 (C-7 aglycone), and between the hydrogen signal at d 3.52 (H-2" glucose) and the carbon signal at d 108.2 (C-1''' apiose). Besides, the chemical shift of the C-2" of the glucose (d 75.8) unit was clearly dishielded (+3) compared to the chemical shift of the analogous carbon resonance of a non-substituted glucose unit (d 72.9), supporting the glucose (1→2) apiose linkage.[28,29] The *g*HMBC experiment also showed correlation between the hydrogen signal at d 4.06 (H-5''' apiose) and the carbon signal at d 166.3 (*E*-feruloyl, C=O) thus evidencing the esterification at this position. The foregoing evidences in combination

with the downfield shift of the C-5''' apiofuranosyl (d 66.6) when compared to a non-acylated analogue (d 62.4) also supported this conclusion. Therefore, compound I was identified as luteolin-7-*O*-[2''-*O*-(5'''-*O*-feruloyl)- b-D-apiofuranosyl]- b-D-glucopyranoside (Figure 1).

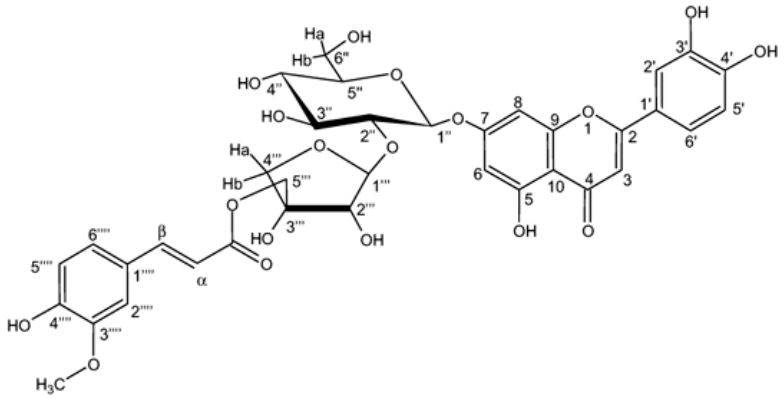

Figure 1. Structure of compound (**1**).

REFERENCES

[1]. N.A.SAHU& D. J. SAXENA, "*Int J Pharm Bio Sci. July; 3(3): (P) 247 – 250,* (2012) ".
[2]. A.Elumalai; M.C. Eswaraiah; K.M.Lahai& H.A.Shaik A, " *Asian J. Res. Pharm. Sci.; vol. 2; Issue 3. Page 85-87* (2012)*"*.
[3]. INTERNATIONAL JOURNAL OF DRUG DISCOVERY AND HERBAL RESEARCH (IJDDHR), " 2(1): January –March; 272 -274), (2012)**".**
[4]. J.M. JANCY RANI ;D.G.CHANDRAMOHAN& R.R. RENGANATHAN ,*" Int. J. Pharm Pharm Sci, Vol 4, Suppl 2, 12-16,* (2000) " .
[5]. V. I. Gupta; M.L.Georg;, L.M. Joseph; M.L. Singhal& H. P. Singh ,*" Journal of Chemical and Pharmaceutical Research,1(1): 233-237(*2009).
[6]. Research Journal of Pharmaceutical, Biological and Chemical Sciences, July – September, RJPBCS Volume 3 Issue 3 Page No. 605 (2012).
[7]. E.E. Sheeja ; E S. Edwin; A. R. Amal; V.B. Gupta& A.C. Rana *"Planta Indica. 1; 33-36*(2005) *"*.
[8]. S.N. Giri; A.K. Biswas; B.P. Saha& S.P. Pal.(1998): "*d. J. Pharm Sci. 50, 42-49, 1998*" .
[9]. Bolognesi A, Polito L, Olivieri F, Valbonesi P, Barbieri L, Battelli MG , "*Planta ,203: 422-429,1997* ".
[10]. Y. Schlein, R.L. Jacobson and G.C. Muller "*Am J Trop Med Hyg. ;65:300-303*"(2001).
[11]. E.S. Edwin, E.E. Sheeja, E. Toppo, V. Tiwari and K.R. Dutt. *"Ars pharm.;48(2):135-144*"(2007).
[12]. E.S. Edwin , E.E. Sheeja, A.Amalraj , R. Soni, G .Smita and V.B. Gupta, "*Planta Indica;2(3):25-26*, (2006) ".
[13]. Adebayo, OT Alabi, BV Owoyele, AO Soladoye. *"Nat. Prod.;3(4): 187-192*, (2009)*"* .
[14]. GI 14. H. Saikia & A. Lama: "*International Journal of Pharmaceutical Sciences and Drug Research; 3(2): 141-145,* (2011) *"* .
[15]. Mosmann, T: *"Journal of Immunological Methods, 65, 55-63,* (1983) *"* .
[16]. N. Anwer, S. Salik& D.Ahmed : "*Int. J. Agric. Biol.;11(5): 647-650* , (2009) *"* .
[17]. Agrawal PK,: *"Elsevier Science Publishing Co. Inc.: New York, pp. 283-364*, (1989) *"*.
[18]. Agrawal PK,: "*Phytochemistry 31(10): 3307- 3330,* (1992) *"* .
[19]. Francis A; Chul S; Masami T; Masahiro I& Michio H . *"Biochem. 64(2): 443-446*, (2000) *"* .
[20]. Fanshawe DB: " *East Afr. Agric.J. 32 :108*, (1966) *"* .
[21]. SU Ya-lun, Wang Yu-lan, YANG Jun-shan"*Chin Tradit Herb Drugs, 24(7): 343-344,* (1993) *"* .
[22]. Singab A. "*Natural medicines, 49(1): 96*, (1995) *"* .
[23]. LING Yun; ZHANG Yong-lin; CAI Shen. "*China J Chin Mater Med, 23 (4): 233-256,* (1998) *"* .
[24]. Lin, L.; Xie, N.; Chen, Z.H.; Wei, M.; Liu, X.F.; Liu, Y.P. *"J. Guangzhou Univ. Tradit. Chin. Med*. *16*, 46–51, (1999) *"*.
[25]. Horowitz, R.M " *B. Chem. Ind. (UK), 21, 498–498,* (1964) *"* .
[26]. Tronchet, J. M. J.; Tronchet, J. *"Carbohydr. Res. 34*, 263, (1974) *"* .
[27]. Kitagawa, I.; Sakagami, M.; Hashiuchi, F.; Zhou, J. L.; Yoshikawa, M.; Ren, J. *"Chem. Pharm. Bull., 37, 551,* **(**1989) *"*.
[28]. Jung, M. J.; Kang, S. S.; Jung, Y. J.; Choi, J. S. *"Chem. Pharm. Bull., 52, 1501, (2004) "*.
[29]. Mathias, L.; Vieira, I. J. C.; Braz-Filho, R.; Rodrigues-Filho, E. A. " *J. Nat. Prod., 61,* 1158, (1998) *"* .
[30]. Bashir, A.; Hamburger, M.; Gupta, M. P.; Solis, P. N.; Hostettmann, K. "*Phytochemistry, 30, 3781,* (1991) *"* .
[31]. Daniel Rinaldo; Clenilson M. Rodrigues; Juliana Rodrigues; Miriam Sannomiya; Lourdes C. dos Santos; Wagner Vilegas *J. Braz. Chem. Soc. vol.18 no.6*, (2007)" .

Table 1: NMR Spectral Data of Compound (I)

Position	1HNMR	13CNMR	gHMBC
2		164.5	H-3
3	6.52s	103	
4		181.5	
5	12.93	161.2	H-6
6	6.36 d	99.1	H-8
7		162.3	H-1"; H-6; H-8
8	6.69 d	94.5	H-6
9		156.9	H-8
10		105.4	H-6; H-3; H-8
1'		122.1	
2'	7.35 brs	113.6	H-6'
3'		149.4	H-5'
4'		145.1	H-2' ; H-6'
5'			
6'	7.34 d	119.2	
Glucose			
1"	5.2 d	97.8	H-2"
2"	3.52 t	75.8	
3"	3.43 t	76.7	H-2"
4"	3.21 t	69.8	H-2"
5"	3.48 m	77.1	H-4" ; H-3"
6"	a)3.5 m b)3.71 d	60.6	
Apiose			
1"'	5.38 s	108.3	H-2", H-2"'
2"'	3.77 s	76.5	
3"'		77.5	H-2"'; H-4"'
4"'	a)3.78 b)4.4	73.9	H-5"' ; H-2"
5"'	4.07 brs	66.7	H-2"'; H-4"'
E-Feruloyl			
α	6.16 d	113.7	H- β
β	7.30 d	144.9	H-6"" ; H-2""
1""		125.3	H-α ; H-5""
2""	7.06 d	110.7	H-6""; H- β
3""		147.7	-OCH3
4""		149.3	H-6""; H-2""
5""	6.68 d	115.4	H-6""
6""	6.87 dd	122.8	H-2"" ; H- β
-OCH3	3.74 s	55.5	
C=O		166.3	H-5""; H- β

Chemical shifts (γ) are in ppm

ISSN (e): 2250 – 3005 || Vol, 04 || Issue, 10 || October– 2014 ||
International Journal of Computational Engineering Research (IJCER)

Survey on Existing Text Mining Frameworks and A Proposed Idealistic Framework for Text Mining by Integrating IE and KDD

Prakhyath Rai[1], Vijaya Murari T[2]
1 PG Scholar, Dept. of Computer Science & Engineering, NMAM Institute of Technology, Nitte, India
2 Asst. Professor, Dept. of Computer Science & Engineering, NMAM Institute of Technology, Nitte, India

Abstract:
Text Mining can be defined as a technique which is used to extract interesting information or knowledge from text documents which are usually in unstructured form. Information Extraction (IE) and Knowledge Discovery from Databases (KDD) are both useful approaches for discovering information in textual corpora. Information Extraction concerns locating of specific terms in natural-language documents. Knowledge Discovery in Databases is the process of discovering useful knowledge from a collection of data. This paper provides an analysis on various emerging text mining framework and methodologies. This paper examines text mining frameworks such as DiscoTEX (Discovery from Text Extraction), RAPIER (Robust Automatic Production of Information Extraction Rules), EPD (Effective Pattern Discovery) and BWI (Boosted Wrapper Induction. This paper provides an analysis of various text mining frameworks and defines their benefits and deficiencies which are then taken into consideration for proposing a novel framework for text mining referred as RDIET. The proposed framework uses an automatically learned IE system to extract a structured database from unstructured textual corpus, and then mines the database for deducing interesting relationships using KDD tools. The proposed technique concentrates in achieving mutual benefits of IE and KDD. IE enables the application of KDD to unstructured textual corpora and KDD can discover predictive rules useful for enhancing IE performance.

Keywords: *BWI, Categorization, Clustering, DiscoTEX, Effective Pattern Discovery, Information Extraction, Knowledge Discovery from Databases, Text Mining, Knowledge Discovery from Text, RAPIER, Standard Rule Induction.*

I. INTRODUCTION

Modern information system allows firms to capture vast amounts of data. Much of this data is structured data that can be analyzed using traditional database software. Increasingly, however, large amounts of data such as textual data are unstructured. Manual analysis of this unstructured textual data is increasingly impractical, and as a result, text mining methods are developed to automate the process of analyzing textual data. Text mining is used to extract the relevant information or knowledge or patterns from different sources that are in unstructured form. It typically consists of (i) information retrieval (IR), which gathers and filters documents, (ii) information extraction (IE), and (iii) data mining for discovering unexpected associations between known facts. IE and KDD have some deficiencies. Information extraction can identify relevant sub-sequences of text, but is usually unaware of emerging, previously unknown knowledge and regularities in a text and thus cannot form new facts or new hypothesis. Knowledge Discovery in Databases limits to deduce explicit relationships from the collection of data. Complementary to information extraction, emerging text mining methods and techniques promise to overcome the deficiencies of information extraction. Developing a knowledge-based or a machine learned IE systems is time and labour intensive. The challenge in this iterative engineering process is that extraction rules must be (i) sufficient background knowledge to extract the full extent of available information and (ii) accuracy in extraction of relevant according to a giving specification. Additional deficiencies of IE approaches are that they (i) extract only explicit knowledge but not new, previously unknown knowledge, such as new relationships between entities, (ii) are better at simple extraction tasks than complex relation or event extraction, and (iii) do not offer information on novelty, reliability, and level of interest of extracted information. Common approaches no longer seem to be appropriate for handling the large amounts of existing information and do not meet the demands of an effective and accurate IE system. Emerging methods and techniques of text and data mining promise to overcome the shortcomings of IE and

concentrate in improving the quality of IE. In summary, the open issues in state-of-the-art IE approaches make further developments necessary. There has been much discussion about combining IE and data mining [1] [2] [3], and these first initiatives have been successful, although they address relatively small problems.

II. LITERATURE SURVEY

Text mining is used to extract the relevant information or knowledge or patterns from different sources that are in unstructured form. Text mining mainly concentrates on text refinement and knowledge distillation. Text refinement is an approach of transforming free-form text or document to intermediate form and knowledge distillation is used to deduce patterns or knowledge from intermediate form. Several techniques have been proposed for text mining including conceptual structure, association rule mining, episode rule mining, decision trees, and rule induction methods. In addition, Information Retrieval (IR) techniques have widely used the "bag-of-words" model [1] for tasks such as document matching, ranking, and clustering. Information extraction (IE) and knowledge discovery from databases (KDD) are both useful approaches for discovering information in textual corpora, but they have some deficiencies. Information extraction can identify relevant sub-sequences of text, but is usually unaware of emerging, previously unknown knowledge and regularities in a text and thus cannot form new facts or new hypothesis. Complementary to information extraction, emerging text mining methods and techniques promise to overcome the deficiencies of information extraction. KDD limits itself to deducing relationships implicitly from collection of data. Text mining approaches and applications use IE as a pre-processing task in the text mining process and implement IE and data mining tasks sequentially, making integration of the two techniques impossible. Mooney discussed two approaches: the first one extracts general knowledge directly from a text, and the second one first extracts structured data from text documents or web pages and then applies traditional data mining techniques to discover new knowledge from extracted data. The DiscoTEX system [2] is an example of the second approach, which uses the previously discovered rules to predict information overlooked in the extraction step. In summary, due to the many open issues of state-of-art IE approaches further development is necessary. Many text mining techniques have been proposed in the last decade. However, using these discovered knowledge (or patterns) in the field of text mining is difficult and ineffective. The reason is that some useful long patterns with high specificity lack in support (i.e., the low-frequency problem). Even not all frequent short patterns are useful. Hence, misinterpretations of patterns derived from data mining techniques lead to the ineffective performance. Effective pattern discovery technique overcome the low-frequency and misinterpretation problems of text mining, the technique uses two processes, pattern deploying and pattern evolving, to refine the discovered patterns in text documents [4].The (unheralded) preliminary step in most of the applications of automated text analysis involves keywords to choose documents from large corpus of text data. Some of the computer-assisted statistical approach suggests keywords from available text, without needing any structured data as inputs. The framework suggested by Gary King, Patrick Lam and Margaret E Roberts poses the statistical problem in a new way, which leads to a widely applicable algorithm. This approach is based on training classifiers, extracting information from their mistakes, and then summarizing results with Boolean search strings [6].

III. ANALYSIS OF TEXT MINING FRAMEWORKS

DiscoTEX Framework: DiscoTEX (Discovery from Text Extraction) uses a learned information extraction system to transform text into more structured data which is then mined for interesting relationships. The initial version of DiscoTEX integrates an IE module acquired by an IE learning system, and a standard rule induction module. In addition rules mined from a database extracted from a corpus of texts are used to predict additional information to extract from future documents. DiscoTEX concentrates in improving recall factor of extraction mechanism, thereby enhancing F-measure by a moderate amount. DiscoTEX has a shortcoming in obtaining the precision of underlying documents to the expected mark [2].

RAPIER Framework: RAPIER (Robust Automated Production of Information Extraction Rules) uses relational learning to construct unbounded pattern-match rules for information extraction given a database of texts and filled templates. The learned patterns employ limited syntactic and semantic information to identify potential slot fillers and their surrounding context. RAPIER is bottom-up learning algorithm that incorporates techniques from several inductive logic programming systems and allows patterns to have constraints on the words, parts-of-speech tags, and semantic classes present in the filler and the surrounding text. RAPIER can achieve a good extraction precision. RAPIER lacks itself in achieving effective recall on underlying documents [3].

EPD Framework: EPD (Effective Pattern Discovery) is an innovative approach which includes the processes of pattern deploying and pattern evolving, to improve the effectiveness of using and updating discovered patterns for finding relevant and interesting information. This approach overcomes the low-frequency and misinterpretation problems which are frequent obstacles in text mining. Effective Pattern Discovery by employing pattern deploying and pattern evolving processes refines the discovered patterns in text

documents, thereby enhancing the future mining process. Effective Pattern Discovery approach overcomes major shortcomings found in text mining approaches but involves huge complexities in its approaches [4].

BWI Framework: BWI (Boosted Wrapper Induction) is an approach to build a trainable information extraction system. Like wrapper induction techniques BWI learns relatively simple contextual patterns identifying the beginning and end of relevant text fields. BWI uses AdaBoost algorithm in repeated fashion for learning boundaries. BWI concentrates in repeated execution so that patterns missed by previous rules can be extracted. BWI provides high precision on underling documents. BWI limits itself in acquiring effective recall [5].

IV. PROPOSED TEXT MINING FRAMEWORK

The amount of textual data that is available for researchers and business to analyze is increasing at a dramatic rate. Information extraction (IE) and knowledge discovery from databases (KDD) are both useful approaches for discovering information in textual corpora, but they have some deficiencies. Information extraction can identify relevant sub-sequences of text, but is usually unaware of emerging, previously unknown knowledge and regularities in a text and thus cannot form new facts or new hypothesis. Complementary to information extraction, emerging text mining methods and techniques promise to overcome the deficiencies of information extraction. This paper proposes a framework for text mining that combines the benefits of both the approaches by integrating information extraction and knowledge discovery from databases using an information extraction system for transforming natural-language documents into structured data which can be then used for discovering relevant information and interesting relationships. For Example, suppose we discovered that computer-science jobs requiring "MySQL" skills are "database" jobs in many cases. If Information Extraction system manages to locate "MySQL" in language slot but failed to extract "database" in the area slot, in such cases relationships can be derived. The framework proposed in this paper aims to develop software that allows extracting specific information from unstructured data such as html-tagged text, text documents or documents with .pdf, .doc or .docx extensions and create text databases. The proposed framework in designing a new IE methodology, is referred as RDIET (Recognition and Discovery of Information from Extracted Text), which is based on various statistical and machine learning techniques. Integration of IE and KDD must concentrate on following areas:

Requirement Specification and Analysis: At the preliminary stage all the requirements of each phase have to be specified and analyzed sensibly.

Selection of Techniques: Suitable IE and KDD methodology have to be chosen to meet the strategized solution.

Interface Design: A suitable interface between IE and KDD has to be designed. The interface must facilitate bi-directional communication, so that IE produces accurate and significant hypothesis for the subsequent mining process.

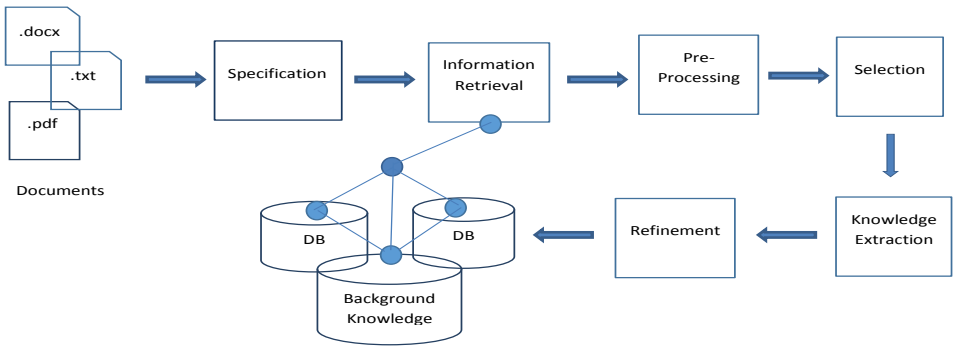

Figure 1: Architecture of RDIET

Figure 1 depicts individual phases of RDIET methodology. The phases are outlined in the following sub-section:

Specification: Specification concentrates in providing information regarding the purpose of text mining analysis and provides description on specification of templates.

Information Retrieval: Information Retrieval aims to collect/Fetch documents either online or offline and also defines certain crawling techniques to be used in functioning of this phase.

Pre-Processing: Several method exist that exploit the syntactic structure and their semantics, using different representations (such as characters, words, terms or concepts) of the documents. Tokenization and text-processing methods such as filtering are applied in RDIET to reduce the size of the data set.

Selection: Functioning of this phase is being strategized into either categorization or clustering based on the requirement, Categorization is a supervised technique based upon the set of input and output, In order to classify the document the set of input and output examples are used to train the classifier on the basis of known examples then unknown examples are categorized automatically. Clustering is a technique used to group similar documents but it differs from categorization, in this documents are clustered on the fly instead of through the use of predefined topics, this is unsupervised technique in which no inputs or patterns are predefined, it is based on the concept of dividing similar text into same cluster with each of it consisting certain number of documents.

Knowledge Extraction: For efficient and easy integration of IE and KDD, it is necessary to evaluate the methods and techniques of data mining in terms of the requirements of the novel IE methodology. The predictive relationships between different slot fillers discovered by data mining methods are the basis for integrating IE and KDD. These provide additional evidence of what information should be extracted from text resources. For example, suppose that the rule "VoiceXML ∈ language" → "Mobile ∈ area". If the IE system extracted "VoiceXML ∈ language" but failed to extract "Mobile ∈ area", we may want to assume there was an extraction error and add "Mobile" to the area slot, potentially improving recall. Therefore, after applying extraction rules to a document, RDIET applies its mined rules to the resulting initial data to predict additional potential extractions. This phase is quiet useful in validation, to mine missing data in order to complete specified templates, to identify inconsistent information, or to de-duplicate information.

Refinement: Because text mining can result in a huge number of templates and slots, which cannot be fixed in the specification phase, the performance measures recall, precision and F-measure are generally more informative than an analysis of the accuracy of extracted novel facts. Measures are used to discard uninteresting extracted information and patterns in the mining process, hence improving mining efficiency. They rank patterns and extracted information to enable a kind of filtering in the early phase of IE. Moreover, measures are applied in the refinement phase to select and present interesting patterns to the user.

Background Knowledge: Semantic and reasoning aspects are used in various points of RDIET methodology. Background knowledge enriches knowledge discovery operations on processed documents and is able to enhance concept extraction and validation. Consequently, background knowledge is important in text mining and IE because it allows pattern abundance to be limited, and is used in pre-processing to provide a consistent lexical representation of documents.

V. CHALLENGES IN PROPOSED FRAMEWORK

Some emerging challenges have been identified for future research:

Choice of appropriate IE and KDD methods: The selection of appropriate variables, data mining algorithms, model assessment and refinement are key components of this project. Automatic feature selection and extraction should support this process.

Performance: Integrating IE and KDD promises to increase performance (in terms of recall and precision). For instance, integrated KDD methods enable more precise feature selection for IE, which in turn reduces the feature space to the most significant information for mining new knowledge.

Extending information extraction measures: Identifying interesting relationships in textual documents is becoming a resource-intensive task because there are many weak links between various entities. A user cannot decide which are really interesting ones – in the volume of information – which is a critical aspect to be taken into consideration. KDD techniques and their measures reduce the amount of information, which in turn increases system performance.

Validating the applicability of Framework: In order to validate the proposed framework, RDIET suitable performance metrics have to be selected. The evaluation of RDIET will be effected by (i) measuring the performance of a current IE process, which will be compared to (ii) an IE process resulting from RDIET, which additionally enables a general benchmark of the interest level of mined Information.

VI. CONCLUSION

Text mining is the discovery, which discovers the previously unknown information by extracting it automatically from different written sources. Text Mining is a new research area which draws on information retrieval, data mining, machine learning, and natural language processing. By appropriately integrating techniques from each of these disciplines, useful new methods for discovering knowledge from large text corpora can be developed. The problem of Knowledge Discovery from Text (KDT) is to extract explicit and implicit concepts and semantic relations between concepts using Natural Language Processing (NLP) techniques. Text mining is similar to data mining expect that data mining approaches are designed for handling the structured data but text mining can work with the unstructured or semi structured data sets such as e-mails,

full text documents, HTML files etc. Various applications of text mining are spam filtering, monitoring public opinions, automatic labelling of documents in business libraries, analysis of junk mails etc.
Merits of Text Mining:

- Databases can store less amount of information and this problem has been resolved through text mining as it can extract relevant useful information from large text and put them in appropriate slots of databases.
- IE and KDD approaches support extraction of information from textual corpora accurately and efficiently.

Demerits of Text Mining:

- No programs can be made in order to analyze the unstructured text directly, to mine the text for information or knowledge.
- The information which is initially needed is nowhere written.

Based on the analysis made on various text mining frameworks in the initial sections of the paper the following inferences can be noted;

RAPIER framework and BWI framework provide high precision on underlying documents whereas these frameworks limit themselves in achieving required recall. DiscoTEX framework provides high recall but limits itself to moderate precision on underlying documents. Effective Pattern Discovery framework overcomes the shortcomings of various text mining approaches but involves complex computations.

The benefits and deficiencies of the analyzed frameworks are taken into consideration for proposing a novel framework for text mining referred as RDIET. The proposed framework, RDIET is expected to overcome the deficiencies of the text mining approaches as its deigned in an order to grab the benefits of IE and KDD by taking into account all the various limitations of analyzed frameworks. The proposed framework uses an automatically learned IE system to extract a structured database from unstructured textual corpus, and then mines the database for deducing interesting relationships using KDD tools. IE enables the application of KDD to unstructured textual corpora and KDD can discover predictive rules useful for enhancing IE performance.

REFERENCES

[1] R Baeza-Yates and B Ribeiro-Neto. "Modern Information Retrieval", ACM Press, New York, 1999.
[2] Raymond J Mooney and Un Yong Nahm, " Text Mining with Information Extraction", Proceedings of the 4th International MIDP Colloquium, pages 141-160, Van Schaik Pub., South Africa, 2005.
[3] M E Califf and R J Mooney, "Relational Learning of Pattern-Match Rules for Information Extraction", Proceedings of the 16th National Conference on Artificial Intelligence (AAAI-99), pages 328-334, Orlando, FL, July 1999.
[4] Ning Zhong, Yuefeng Li and T. Grance, "Effective Pattern Discovery for Text Mining," IEEE Transactions on Knowledge and Data Engineering, Vol. 24, No. 1, January 2012.
[5] D Freitag and N Kushmerick, "Boosted Wrapper Induction", Proceedings of the 17th National Conference on Artificial Intelligence (AAAI-2000), pages 577-583, Austin, TX, July 2000.
[6] Gary King, Patrick Lam and Margaret E Aroberts, "Computer-Assisted Keyword and Documents from Unstructured Text", 2014.

ISSN (e): 2250 – 3005 || Vol, 04 || Issue, 10 || October– 2014 ||
International Journal of Computational Engineering Research (IJCER)

Finding the Stresses and Deflection of a Snag Crane Sun Spur Gear Using Fea Package

Surendra Babu. Koganti[1], T.Mastanaiah[2]
[1] PG student, Department of Mechanical Engineering, Vikas College of Engineering & Technology, Nunna
[2] Guide (Assoc.prof), Department of Mechanical Engineering, Vikas College of Engineering & Technology, Nunna

ABSTRACT

Gears are machine elements that transmit motion by means of successively engaging teeth. The stresses are developed when two gears are mated. Two spur gear teeth in action are generally subjected to two types of stresses. One is bending stresses which are developed by fatigue bending another one is contact stress causing contact fatigue. These two types of stresses may not get their maximum values at the same point of contact fatigue. These types of failures can be minimized by careful analysis of the problem during the design stage and creating proper tooth surface profile with proper manufacturing methods.

This project investigates the various stresses and deflection developed in sun gear tooth of sun gearbox which is used in Snag Crane. In this study, perform the calculation for sun gear tooth to calculate bending, shear, wear & deflection using theoretical method.The model was created using modeling software and the analysis is done using ansys. Here the analysis is performed on the root fillet of the spur gear tooth. The analysis is done two conditions as circular root fillet and actual root fillet of a gear tooth. The results of the analyses from ANSYS are compared with the theoretical values. Comparison of ANSYS results in circular root fillet & actual root fillet also carry out. In addition to the project we are changing the material of the sun gear and comparing the results. In the addition of this project we are finding the contact stresses of the mating gears. The theoretical values which are formed from the Hertz equation are compared with the Fea values which are generate from ansys. For the analysis, steel and grey cast iron are used as the materials of spur gear. The results show that the difference between maximum contact stresses obtained from Hertz equation and Finite Element Analysis is very less and it is acceptable. The deformation patterns of steel and grey cast iron gears depict that the difference in their deformation is negligible.

Keywords: Ansys, Planetary gear, Pro-e, Sun gear, Snag Crane.

1. INTRODUCTION

The main purpose of gear mechanisms is to transmit rotation and torque between axes. The gear wheel is a machine element that has intrigued many engineers because of numerous technological problems arises in a complete mesh cycle. In order to achieve the need for high load carrying capacity with reduced weight of gear drives but with increased strength in gear transmission, design, gear tooth stress analysis, tooth modifications and optimum design of gear drives are becoming major research area. Gears with involute teeth have widely been used in industry because of the low cost of manufacturing. Transmission error occurs when a traditional non-modified gear drive is operated under assembly errors. Transmission error is the rotation delay between driving and driven gear caused by the disturbances of inevitable random noise factors such as elastic deformation, manufacturing error, alignment error in assembly. It leads to very serious tooth impact at the tooth replacing point, which causes a high level of gear vibration and noise. At the same time, edge contact often happens, which induces a significant concentration of stress at the tooth edge and reduces the life time of a gear drive.

Many researchers have proposed modified shapes for traditional gears to localize the bearing contact thereby avoiding edge contact. In the present work, involute spur gear teeth for the selected module, gear ratio, centre distance and number of teeth is taken for analysis. Two more sets of differently crowned involute spur gear teeth are also considered for stress and tooth contact analysis. The procedure followed to create the 3D models of teeth in mesh is described. Proportions of contact ellipses are determined. Their performance behavior is studied by assuming loading at pitch point under static load and frictionless hypothesis. In order to handle critical profile variations, the analyses are done in three dimensions with face contact model. surface Contact Stress (SCS), Root Bending Stress (RBS), and Tooth Deflection (TD) calculations of the pair of spur gears with and without lead crowning are carried out through FEM.

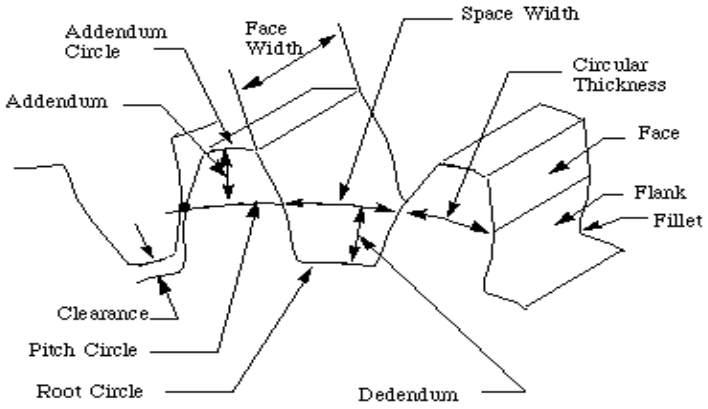

Fig 1. Spur Gear nomenclature

II. MODELING BY USING PRO-E

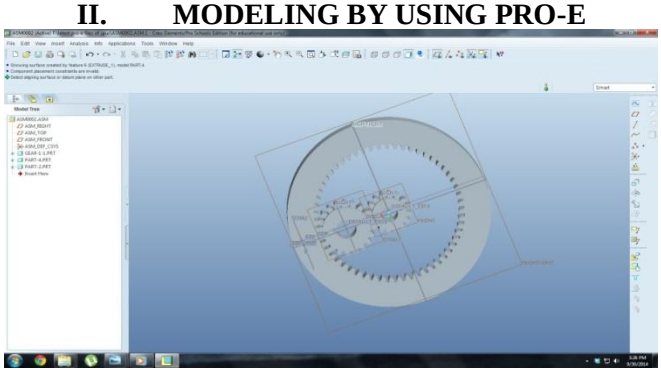

Fig 2. Assembly model in pro-e

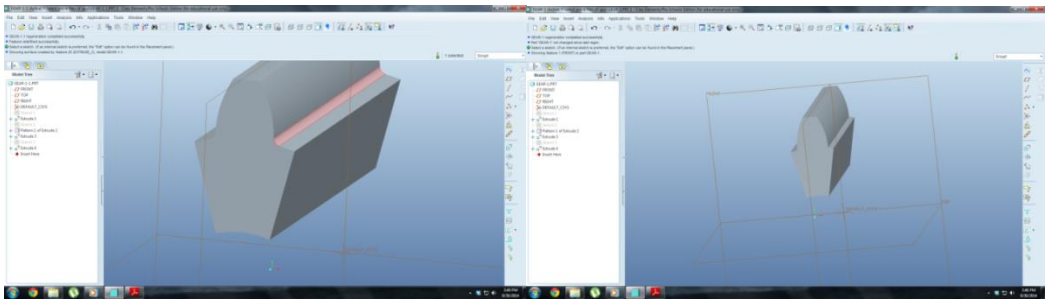

Fig 3. Circular fillet tooth profile **Fig 4. Actual fillet tooth profile**

III. RESULTS & DISCUSSION

3.1. Shear stress

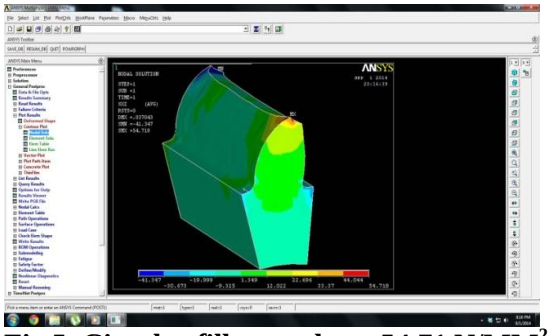

Fig 5. Circular fillet result σ_s =54.71 N/MM^2

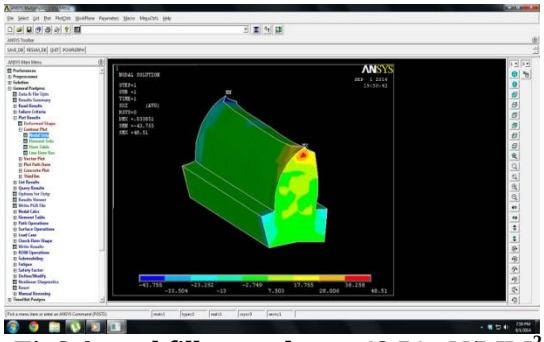

Fig6.Actual fillet result σ_s =48.51 N/MM^2

1.2. Bending Stress

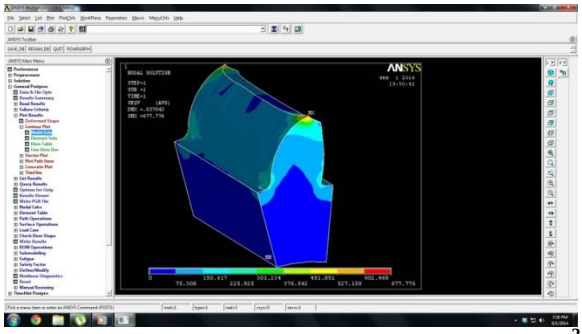

Fig 7.Circular fillet result σ_b =677.776 N/MM^2

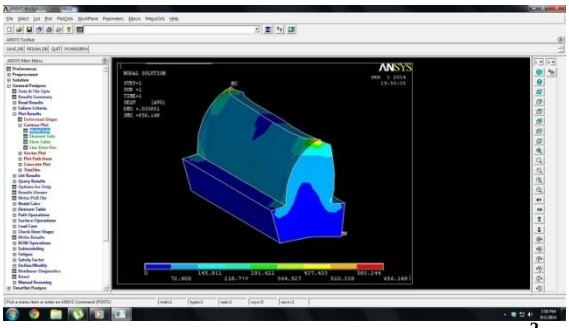

Fig 8.Actual fillet result σ_b =6561.49N/MM^2

1.3. Deflection

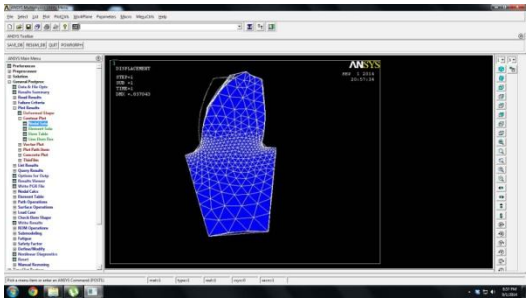

Fig 9.Circular fillet deflection = 0.037043 mm

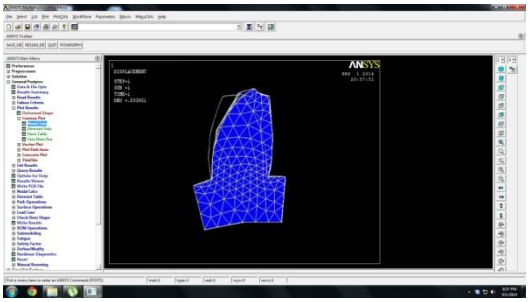

Fig 10. Actual fillet deflection = 0.033851 mm

3.4. Wear stress

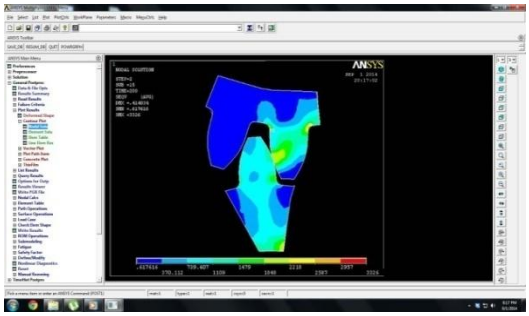

Fig 11.circular fillet result σ_c = 1848 N/MM^2

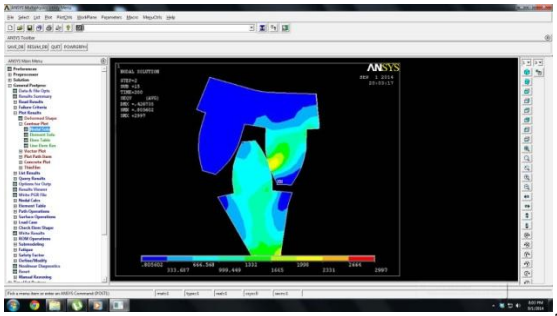

Fig 12. actual fillet result σ_c = 1998 N/MM^2

3.5. Calculation of Contact Stresses by Ansys

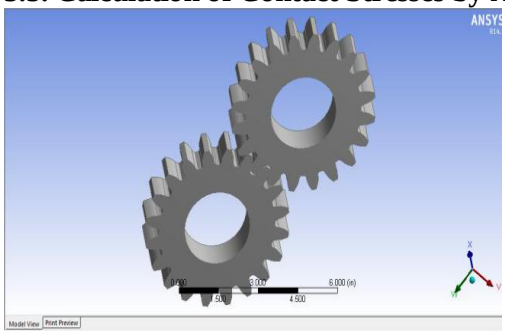

Fig 13. Assembly of Spur Gears

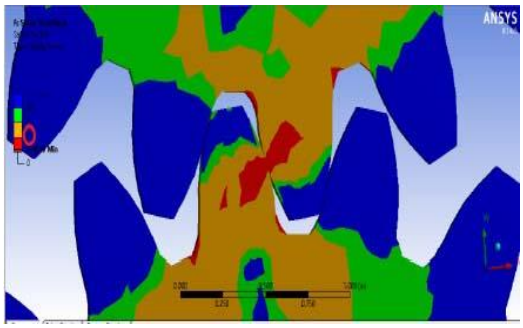

Fig 14. Safety Factor for Grey Cast Iron

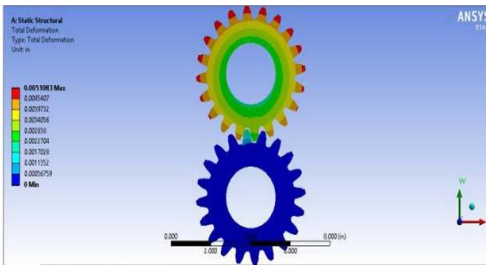

Fig 15. Deformation pattern for Steel gear

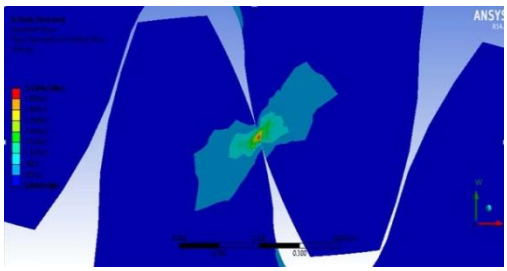

Fig 16. Stress distribution Grey Cast Iron gear

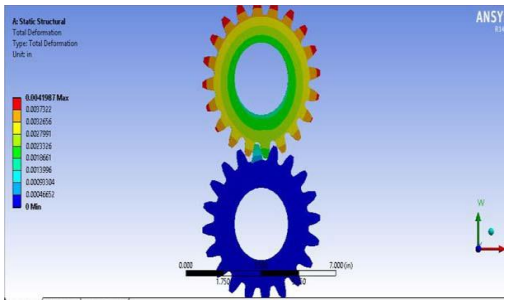

Fig 17.Deformation pattern for Grey Cast Iron gear

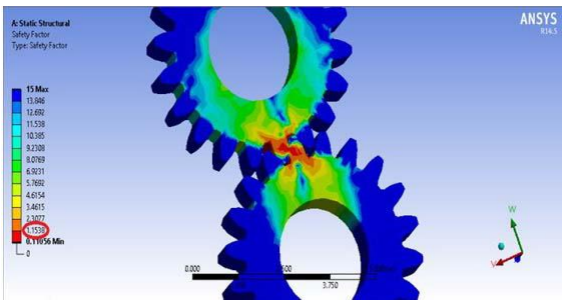

Fig 18. Safety Factor for Steel Gear

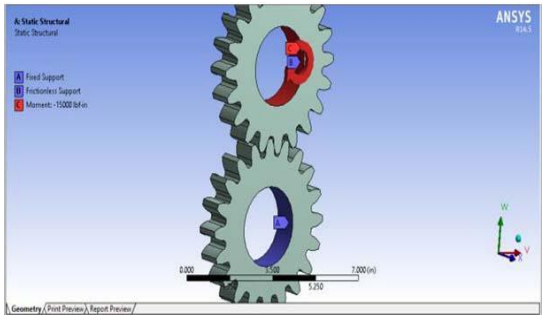

Fig 19.Boundary Condition

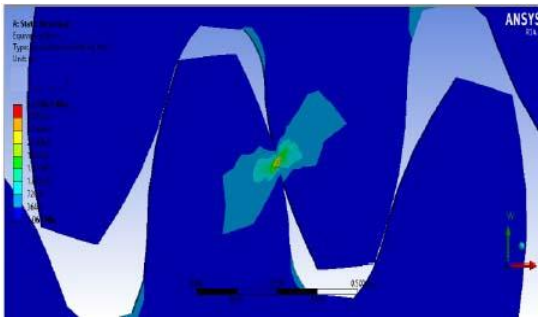

Fig 20.Stress distribution in Steel gear

ANALYSIS	THEORETICAL VALUES	FOR ACTUAL FILLET RADIUS	FOR CIRCULAR FILLET RADIUS
Bending stress(N/mm^2)	532.94	656.149	677.776
Shear stress(N/mm^2)	33.24	48.51	54.71
Wear stress (N/mm^2)	2509.1546	1998	1848
Deflection(mm)	0.0368090	0.033851	0.037043

Table no 1: bending, shear &wear stresses & deflection result

Gear	(Hertz) (MPa)	(ANSYS) (MPa)	Difference (%)
Steel	2254.9821	2261.2052	0.28
Grey CI	2334.6414	2365.1782	1.29

Table no 2: Comparison of maximum contact stress obtained from Hertz equation and ANSYS

IV. CONCLUSION

The analysis process on the sun gear there are three types of stresses are found bending stress, shear stress and wear stress. And also deflection values are found. ANSYS results for various stresses and deflections are nearer to theoretical values for sun gear of planetary gear system of snag crane. The values of bending & shear stress value for actual root fillet design in comparison to that of stresses values in circular root fillet design are reduced. Also there is increase in wear stress value for actual root fillet design in comparison to that of stresses values in circular root fillet design. And also it is observed that the deflection in actual root fillet is also less comparing to the circular root fillet gear tooth.

Therefore from the analysis it is also found that the circular fillet design is more optimum for lesser number of teeth in pinion & actual fillet design is more suitable for higher number of teeth in gear and whatever may be the pinion speed. In addition to that the ANSYS results indicates that the gears with actual root fillet design will result in better strength, reduced bending stress & also improve the fatigue life of gear material.
Finally we conclude that circular fillet design is more optimum compared to actual fillet design.

The theoretical maximum contact stress is calculated by Hertz equation. Also the finite element analysis of spur gear is done to determine the maximum contact stress by ANSYS. It was found that the results from both Hertz equation and Finite Element Analysis are comparable. From the deformation pattern of steel and grey cast iron, it could be concluded that difference between the maximum values of steel and grey CI gear deformation is very less.

REFERENCES

[1]. Machine design by S.Md.Jalaludeen, Anuradha agencies.
[2]. Machine design by R.K. Jain
[3]. Machine design by 'R.S. Kurmi'
[4]. Design of machine elements by 'Bandri'
[5]. Machine design by R.K. Rajput
[6]. Design data book by Md.jalaludeen
[7]. Design data book by P.S.G. College
[8]. www.cs.cmu.edu/People/rapidproto/mechanisms/references.html
[9]. Mechanical Engg design – Joseph E. Shigley.
[10]. Design data book – P.S.G. College of technology.
[11]. Design data book – K.Mahadevan & K.Balaveera Reddy.
[12]. Analysis and approximation of contact problem By Mircea Sofonia
[13]. Elastic contact analysis by boundary elements By Susumu Takahashi
[14]. "A comprehensive analysis of fillet and contact stresses in straight spur gears" By M.A. Alfares
[15]. Y. A. Tesfahunegn and F. Rosa, "The Effects of the Shape of Tooth Profile Modif ication on the Transmission Error Bending and Contact Stress of Spur Gears," Jour- nal of Mechanical Engineering Science, Vol. 224, No. 8, 2010, pp. 1749-1758.
[16]. C.-F. Tsai, T.-L. Liang and S.-C. Yang, "Mathematical Model of the Planeta ry Gear Mechanism with Double Circular-Arc Teeth," Transactions of the CSME Ide la SCGM, Vol. 32, No. 2, 2008, pp. 267-282
[17]. R. Patchigolla and Y. P. Singh, "Finite Element Analysis of Large Spur Gear Tooth and Rim with and without Web Effects-Part I and II," The 2006 ASEE Gulf-Southwest Annual Conference, Southern University and A & M Col- lege.
[18]. Modern Mechanical Engineering, 2011, 1, 56-68 doi:10.4236/mme.2011.12008 Published Online November 2011 (http://www.SciRP.org/journal/mme)

ISSN (e): 2250 – 3005 || Vol, 04 || Issue, 10 || October– 2014 ||
International Journal of Computational Engineering Research (IJCER)

Effect of orientation angle of elliptical hole in thermoplastic composite plate at different loads

[1]Sadinenh Asha Rani, [2]S.C.Sireesha
[1] PG student, Department of Mechanical Engineering, Qis college of engineering & technology, Ongole
[2] Guide (Asst.prof), Department of Mechanical Engineering, Qis college of engineering & technology, Ongole

ABSTRACT:

Fiber-reinforced thermoplastic polymers are the primary reasons for their use in many structural components in the aircraft, automotive, marine, and other industries due to their low density, high strength, high stiffness to weight ratio, excellent durability and design flexibility. They are now used in applications ranging from space craft frames to ladder rails, from aircraft wings to automobile doors, from rocket motor cases to oxygen tanks, and from printed circuit boards to tennis rackets. Their use is increasing at such a rapid rate that they are no longer considered advanced materials. Residual stresses in the composite plates are particularly important. They can lead to premature failure. Therefore, the characterization of the elasto-plastic response of thermoplastic composite must be carried out along the credible design processes for composite structures involving plasticity effects in the nonlinear behavior.

In this thesis, residual stresses developed on Flouoro polymer laminated thermoplastic composite plates with central elliptical hole which is subjected to in-plane loading is determined by applying different loads. The effects of orientation angle of elliptical hole in the composite laminated plate under various in-plane loads, elliptical hole is rotated from 0° to 90° by 15° increments counterclockwise. Analysis is done in Ansys.

I. INTRODUCTION

A composite material is made by combining two or more materials – often ones that have very different properties. The two materials work together to give the composite unique properties. However, within the composite you can easily tell the different materials apart as they do not dissolve or blend into each other.

- Natural composites
- Early composites
- Making composites

II. STRUCUTRAL ANALYSIS BYANSYS

2.1 Strucutral analysis of plate with different orientation angles of elliptical hole

2.1.1 Flouropolymer At Pressure – 5.5 (Orientation angle - 90^0)

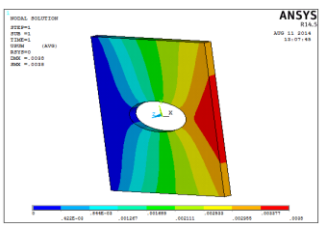

Figure 1.Displacement

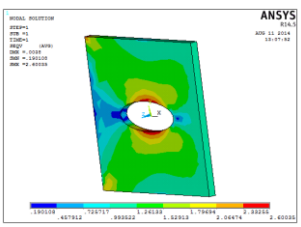

Figure 2.Stress

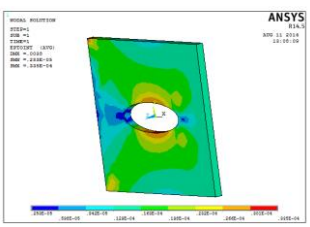

Figure 3.Strain

2.1.2 Orientation angle -45^0

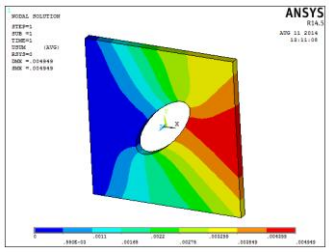

Figure 4.Displacement

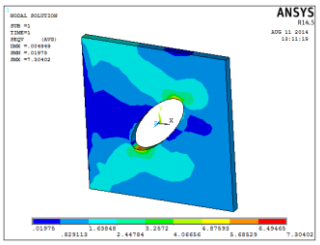

Figure 5.Stress

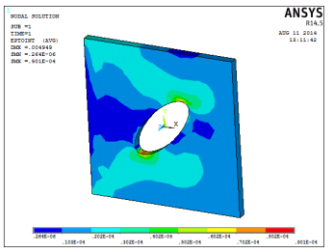

Figure 6.Strain

2.1.3 Orientation angle -30^0

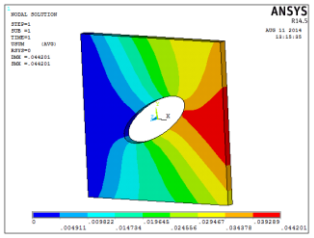

Figure 7.Displacement

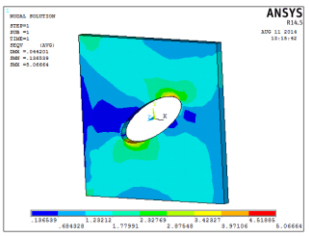

Figure 8.Stress

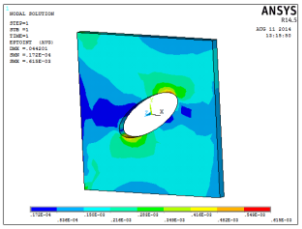

Figure 9.Strain

2.1.4 Orientation angle – (-45^0)

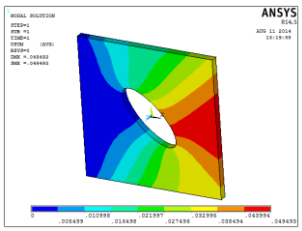

Figure 10.Displacement

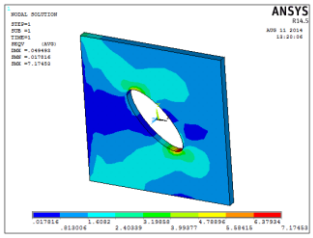

Figure 11.Stress

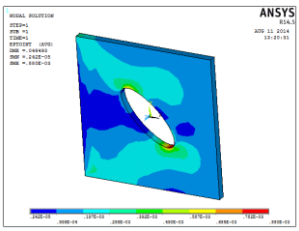

Figure 12.Strain

2.1.5 Orientation angle –(-30^0)

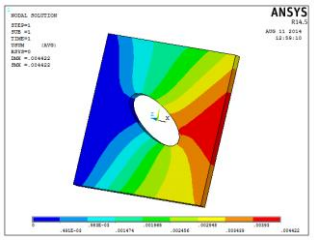

Figure 13.Displacement

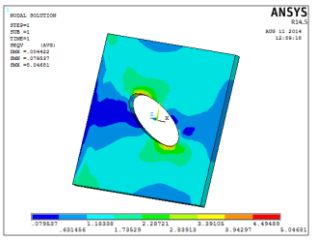

Figure 14.Stress

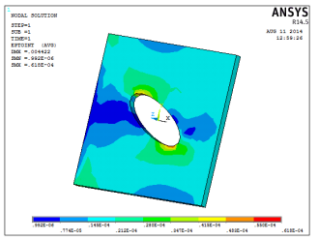

Figure 15.Strain

2.2 Pressure-6n/mm^2

2.2.1 Orientation angle - 90^0

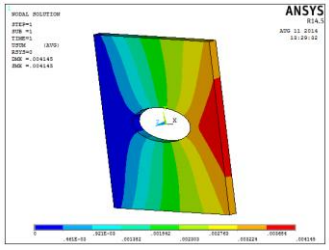

Figure 16.Displacement

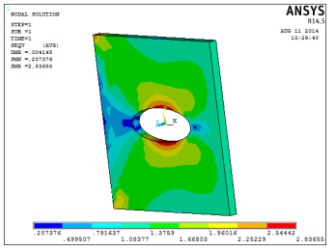

Figure 17.Stress

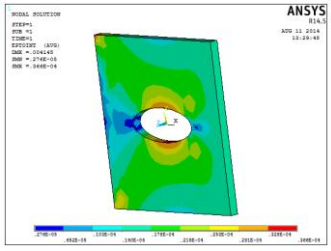

Figure 18.Strain

2.2.2 Orientation angle -45^0

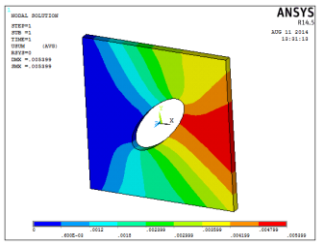

Figure 19.Displacement

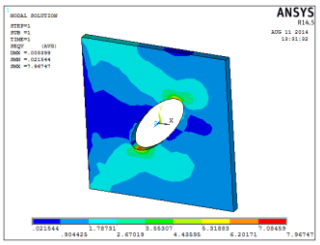

Figure 20.Stress

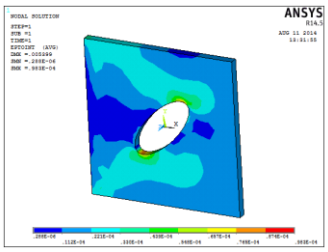

Figure 21.Strain

2.2.3 Orientation angle -30^0

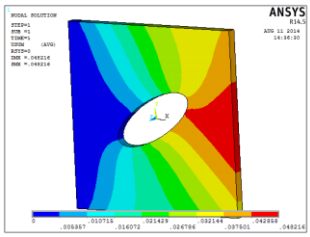

Figure 22.Displacement

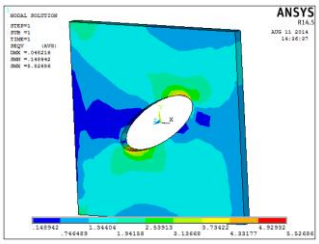

Figure 23.Stress

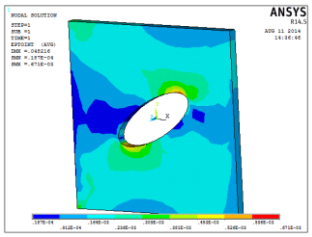

Figure 24.Strain

2.2.4 Orientation angle – (-45^0)

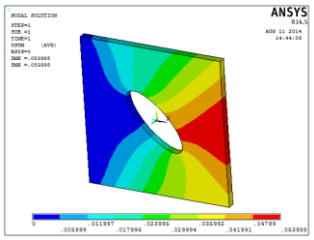

Figure 25.Displacement

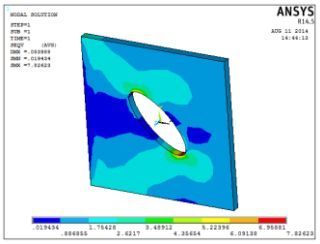

Figure 26.Stress

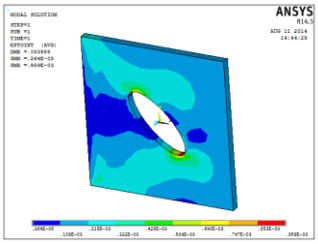

Figure 27.Strain

2.2.5 Orientation angle –(-30^0)

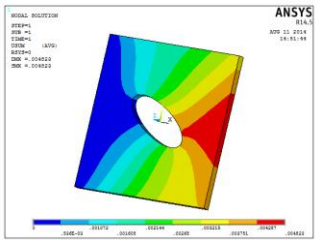

Figure 28.Displacement

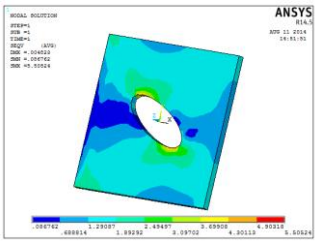

Figure 29.Stress

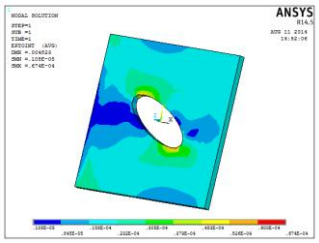

Figure 30.Strain

2.3 Pressure – 6.5n/mm^2

2.3.1 Orientation angle – 90^0

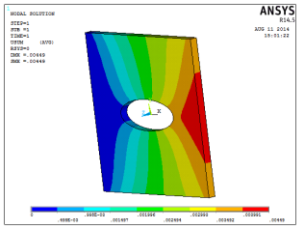

Figure 31.Displacement

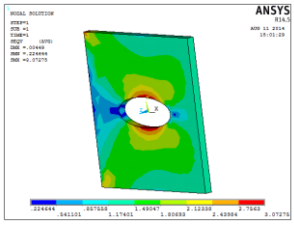

Figure 32.Stress

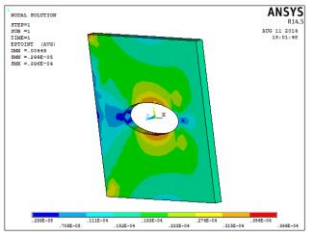

Figure 33.Strain

2.3.2 Orientation angle – 45^0

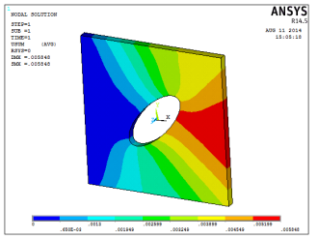

Figure 34.Displacement

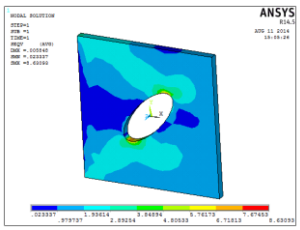

Figure 35.Stress

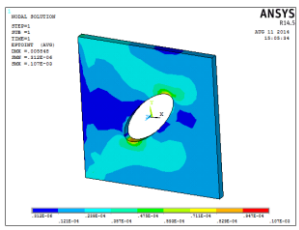

Figure 36.Strain

2.3.3 Orientation angle – 30^0

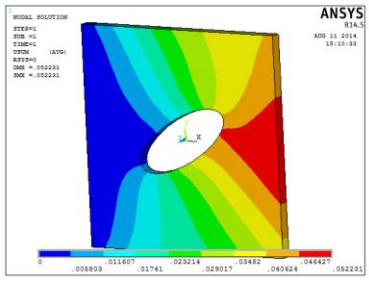

Figure 37.Displacement

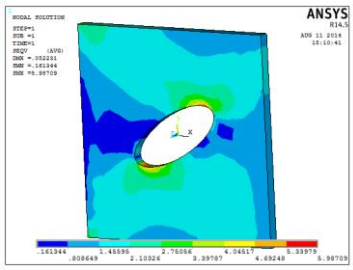

Figure 38.Stress

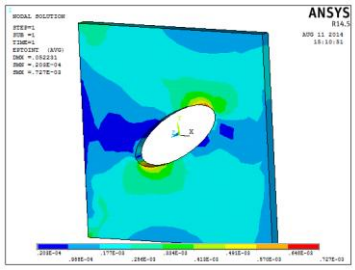

Figure 39.Strain

2.3.4 Orientation angle – (-45^0)

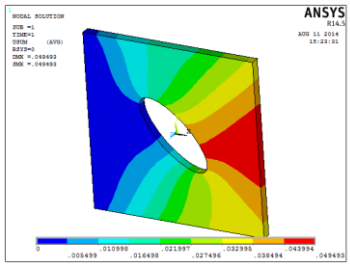

Figure 40.Displacement

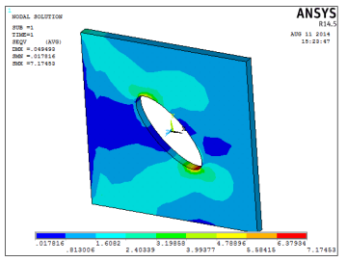

Figure 41.Stress

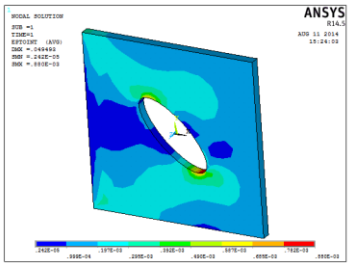

Figure 42.Strain

2.3.5 Orientation angle – (-30^0)

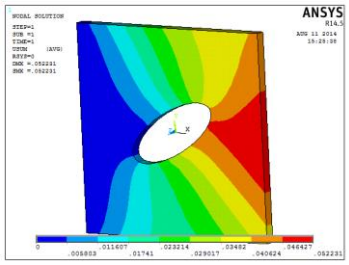

Figure 43.Displacement

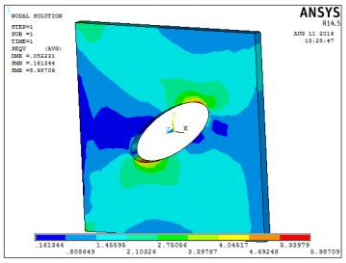

Figure 44.Stress

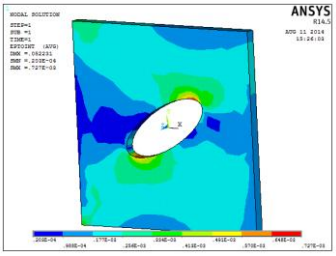

Figure 45.Strain

III. RESULTS TABLE

3.1 Pressure -5.5n/mm^2

	Angle 90	**Angle 45**	**Angle 30**	**Angle -45**	**Angle -30**
Displacement (mm)	0.0038	0.00949	0.44201	0.049493	0.004422
Stress (N/mm^2)	2.60035	7.30402	5.06664	7.17453	5.04681
Strain	$0.335E^{-04}$	$0.901E^{-04}$	$0.615E^{-03}$	$0.880E^{-03}$	$0.618E^{-04}$

3.2 Pressure - 6n/mm^2

	Angle 90	**Angle 45**	**Angle 30**	**Angle -45**	**Angle -30**
Displacement (mm)	0.004145	0.005399	0.048216	0.053988	0.004823
Stress (N/mm^2)	2.83655	7.96747	5.52686	7.82623	5.50524
Strain	0.366E^{-04}	0.983E^{-04}	0.671E^{-03}	0.959E^{-03}	0.674E^{-04}

3.3 Pressure – 6.5n/mm^2

	Angle 90	**Angle 45**	**Angle 30**	**Angle -45**	**Angle -30**
Displacement (mm)	0.00449	0.005848	0.052231	0.049493	0.52231
Stress (N/mm^2)	3.07275	8.63093	5.98709	7.17453	5.98709
Strain	0.396E^{-04}	0.107E^{-03}	0.727E^{-03}	0.880E^{-03}	0.727E^{-03}

IV. CONCLUSION

In this thesis, stresses developed on Flouoro polymer laminated thermoplastic composite plates with central elliptical hole which is subjected to in-plane loading is determined by applying different loads. The effects of orientation angle of elliptical hole in the composite laminated plate under various in-plane loads, elliptical hole is rotated from 0° to 90° by 15° increments counterclockwise. The orientation angles are 90^0, 45^0, 30^0, -45^0 and -30^0. Analysis is done in Ansys.By observing the analysis results, the stress concentration is more at the hole and is reducing towards the end of the plate. The stresses are increasing from 90^0 orientation angle to the 45^0 orientation angle and then reducing to 30^0 orientation angles.

When the hole is oriented at counter clockwise directions, the stress values are less with respective to the positive angles. The stress concentration is more when the hole is oriented at 45^0. The better orientation angle of hole is 90^0 since the stresses are less when compared with other orientation angles.

1. References

[1]. Buckling analysis of Composite Plate with Central Elliptical Cut out by Sa'el Saleh Al-Jameel Dr. Rafi K. Albazzaz

[2]. Stress Concentration around Circular/Elliptical/Triangular Cutouts in Infinite Composite Plate by Dharmendra S Sharma

[3]. Assessment of the Buckling Behavior of Square Composite Plates with Circular Cutout Subjected to In-Plane Shear by Husam Al Qablan, Hasan Katkhuda and Hazim Dwairi

[4]. Finite element analysis of stress concentrations and failure criteria in composite plates with circular holes by Abdelhak Khechai, Abdelouahab Tati, Abdelhamid Guettala

[5]. Vibration Analysis of Laminated Composite Plates with Holes Syed Altaf by Hussain, V. Pandurangadu, K. Palani Kumar

[6]. Akbulut, H. and Sayman, O. 2001. An investigation on buckling of laminated plates with central square hole.

[7]. Baba, B. 2007. Buckling behavior of laminated composite plates.

[8]. Baba, B. and Baltaci, A. 2007. Buckling characteristics of symmetrically and antisymmetrically laminated composite plates with central cutout.

[9]. Baltaci, A., Sarikanat, M. and Yildiz, H. 2006. Buckling analysis of laminated composite circular plates with holes.

[10]. Ghannadpour, S., Najafi, A., and Mohammadi, B. 2006. On the buckling behavior of cross-ply laminated composite plates due to circular/elliptical cutouts

ISSN (e): 2250 – 3005 || Vol, 04 || Issue, 10 || October– 2014 ||
International Journal of Computational Engineering Research (IJCER)

Structural and vibration analysis of delaminated composite beams

[1]Narra.Sowjanya, [2]Mulluri.Haritha
[1] PG student, Department of Mechanical Engineering, Qis College of engineering & technology
[2] Guide (Asst.prof), Department of Mechanical Engineering, Qis College of engineering & technology, Ongole

ABSTRACT:

Delamination is a mode of failure for composite materials. Modes of failure are also known as 'failure mechanisms'. In laminated materials, repeated cyclic stresses, impact, and so on can cause layers to separate, forming a mica-like structure of separate layers, with significant loss of mechanical toughness. Some manufacturers of carbon composite bike frames suggest to dispose of the expensive frame after a particularly bad crash, because the impact could develop defects inside the material. Due to increasing use of composite materials in aviation, delamination is increasingly an air safety concern, especially in the tail sections of the airplanes.

In this thesis, the effects of delamination length on the stresses and natural frequency of symmetric composite beams are analyzed using Ansys software. The composite material considered is carbon fiber. Structural and Frequency analysis are done on the composite beam by varying the delamination lengths.

I. INTRODUCTION

- **Introduction to beam**

A beam is a structural element that is capable of withstanding load primarily by resisting bending. The bending force induced into the material of the beam as a result of the external loads, own weight, span and external reactions to these loads is called a bending moment.

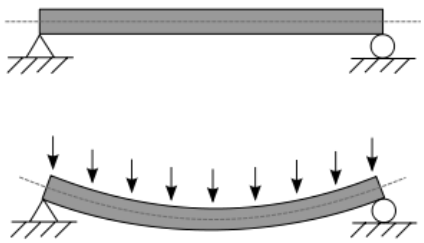

Figure 1. Beam figure

A statically determinate beam, bending (sagging) under an evenly distributed load

- **Overview**

Historically beams were squared timbers but are also metal, stone, or combinations of wood and metal such as a flitch beam. Beams generally carry vertical gravitational forces but can also be used to carry horizontal loads (e.g., loads due to an earthquake or wind or in tension to resist rafter thrust as a tie beam or (usually) compression as a collar beam). The loads carried by a beam are transferred to columns, walls, or girders, which then transfer the force to adjacent structural compression members. In light frame construction joists may rest on beams.

In carpentry a beam is called a plate as in a sill plate or wall plate, beam as in a summer beam or dragon beam.

- **Delamination**

Delamination is a mode of failure for composite materials. Modes of failure are also known as 'failure mechanisms'. In laminated materials, repeated cyclic stresses, impact, and so on can cause layers to separate, forming a mica-like structure of separate layers, with significant loss of mechanical toughness. Delamination also occurs in reinforced concrete structures subject to reinforcement corrosion, in which case the oxidized metal of the reinforcement is greater in volume than the original metal. The oxidized metal therefore requires greater space than the original reinforcing bars, which causes a wedge-like stress on the concrete. This force eventually overcomes the relatively weak tensile strength of concrete, resulting in a separation (or delamination) of the concrete above and below the reinforcing bars.

II. DELAMINATION LENGHTS

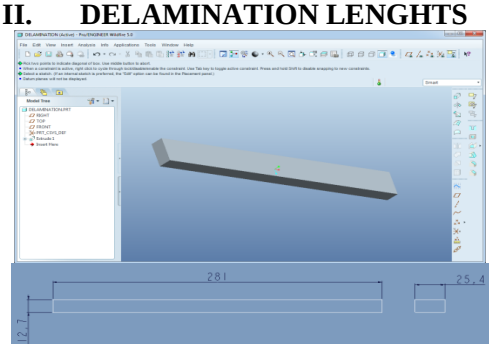

Fig.2 Delamination lengths

1.1 Structural analysis of delaminated beam

2.1.1 Carbon fiber

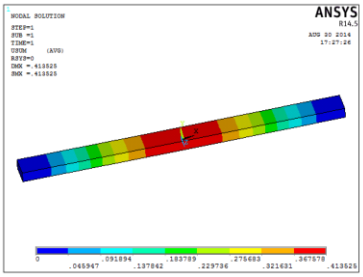

Figure 2.Displacement

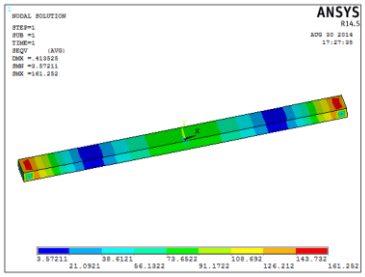

Figure 3.Stress

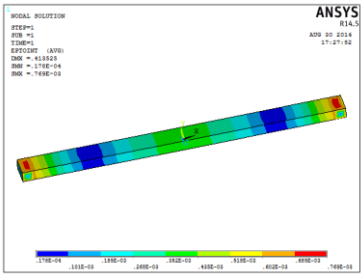

Figure 4.Strain

2.1.2 Kevlar

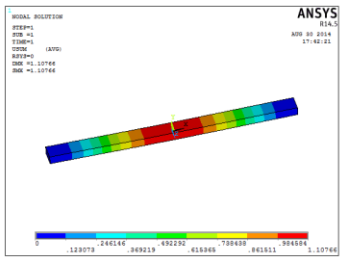

Figure 5.Displacement

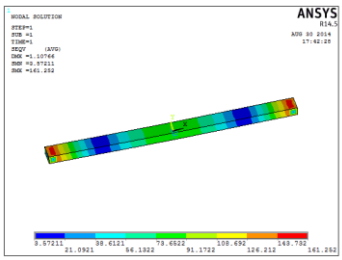

Figure 6.Stress

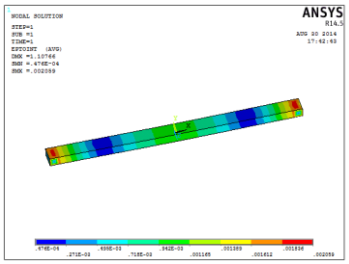

Figure 7.Strain

2.1.3 Floura polymer

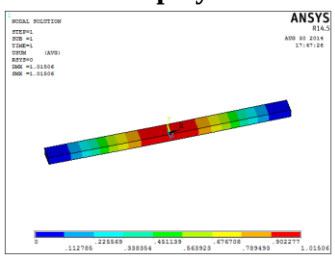

Figure 8.Displacement

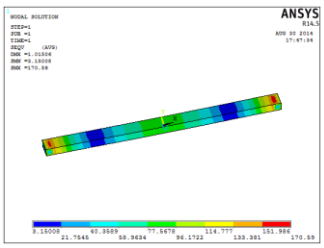

Figure 9.Stress

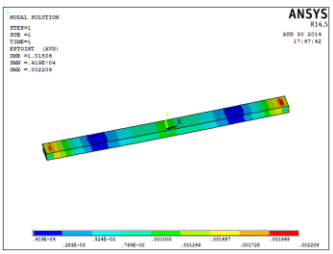

Figure 10.Strain

1.2 Structural analysis of changed delaminated beam

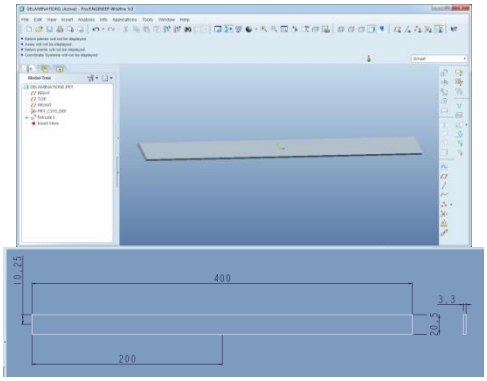

Figure 11. Change delamination lenths

2.2 Structural analysis – solid element

2.2.1 Carbon fiber

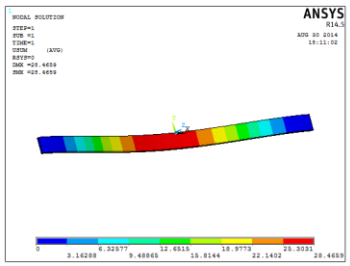

Figure 12.Displacement

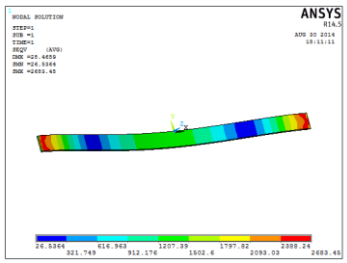

Figure 13.Stress

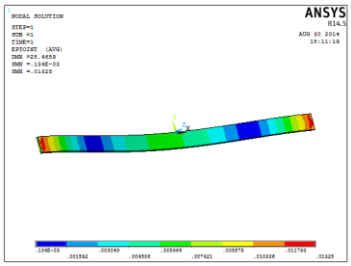

Figure 14.Strain

2.2.2 Kevlar

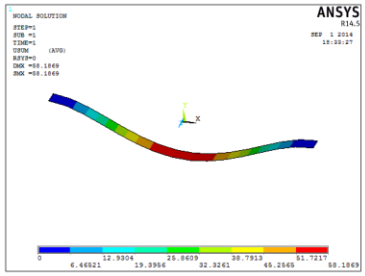

Figure 15.Displacement

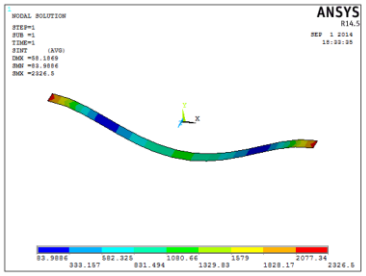

Figure 16.Stress

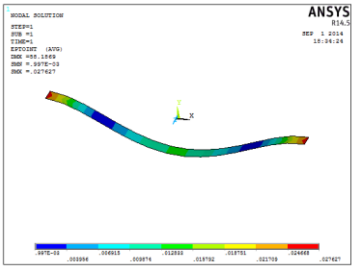

Figure 17.Strain

2.2.3 Floura polymer

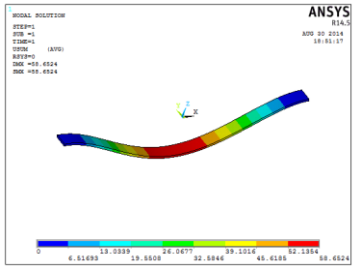

Figure 18.Displacement

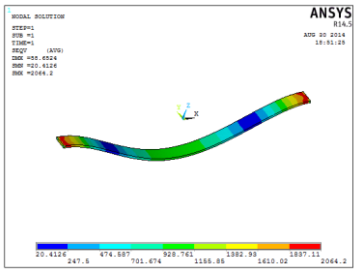

Figure 19.Stress

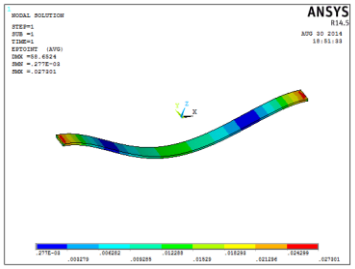

Figure 20.Strain

2.3 Shell element – 5layers

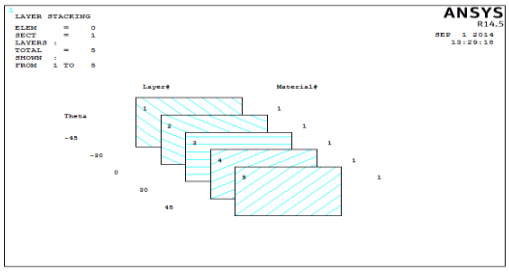

Figure 21. Layer stacking

2.3.1 Carbon fiber

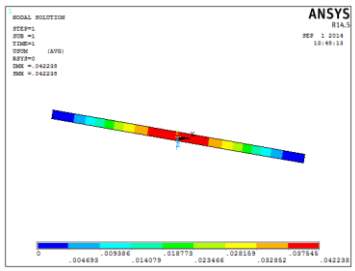

Figure 21.Displacement

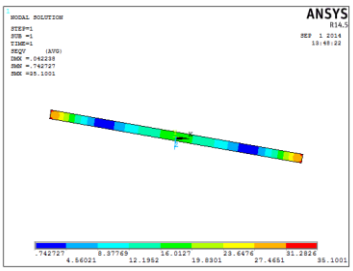

Figure 22.Stress

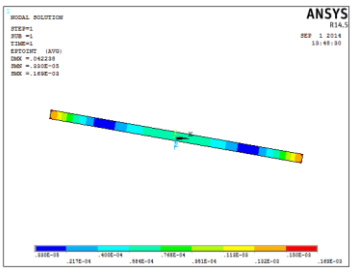

Figure 23.Strain

2.3.2 Kevlar

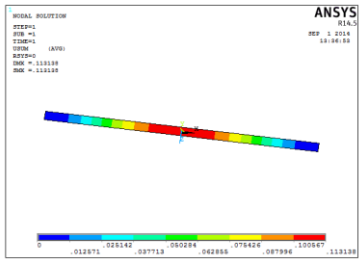

Figure 24.Displacement

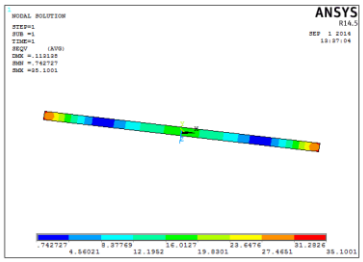

Figure 25.Stress

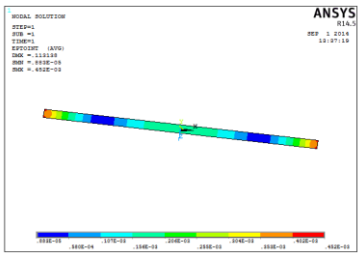

Figure 26.Strain

2.3.3 Floura polymer

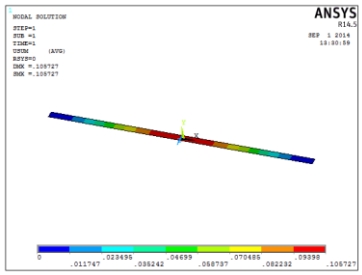

Figure 27.Displacement

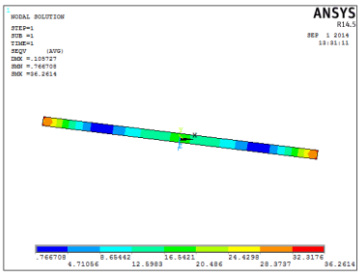

Figure 28.Stress

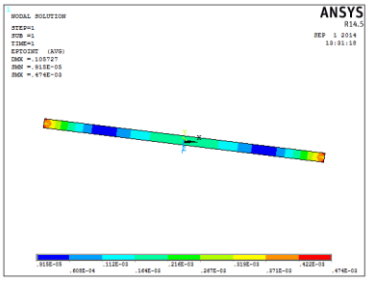

Figure 29.Strain

2.4 Changing lengths

2.4.1 Carbon fiber

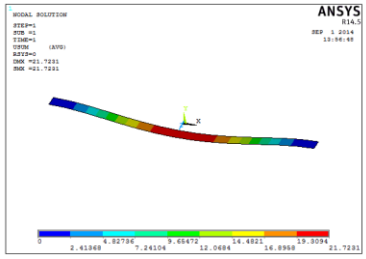

Figure 30.Displacement

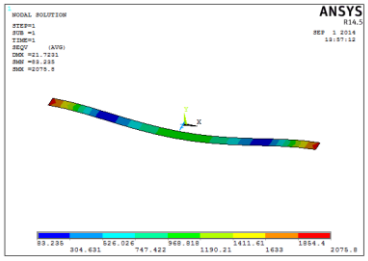

Figure 31.Stress

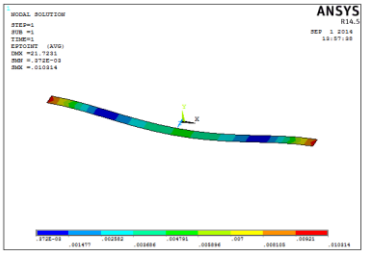

Figure 32.Strain

2.4.2 Kevlar

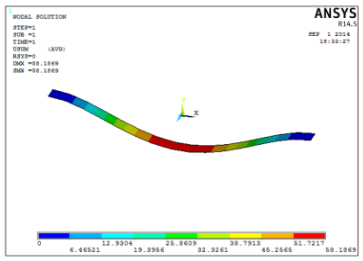

Figure 33.Displacement

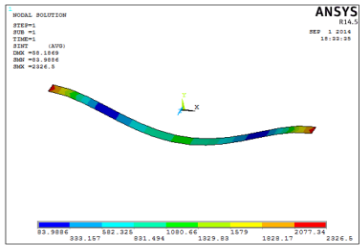

Figure 34.Stress

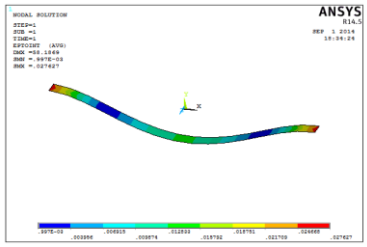

Figure 35.Strain

2.4.3 Floura polymer

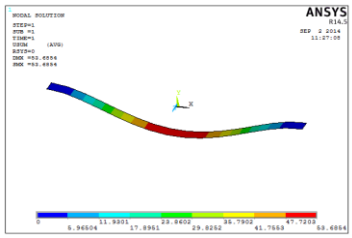

Figure 36.Displacement

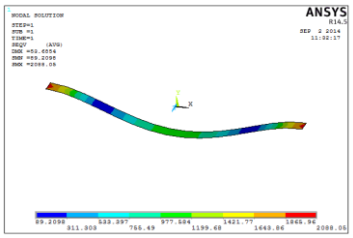

Figure 37.Stress

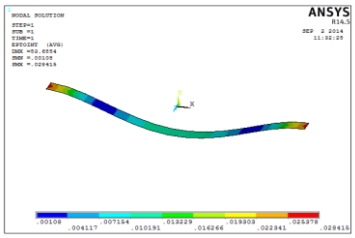

Figure 38.Strain

III. RESULTS TABLE

3.1 Delamination length – 381mm

	Carbon fiber	Kevlar	Floura polymer
Displacement (mm)	0.413526	1.10766	1.01506
Stress (N/mm^2)	161.252	161.252	170.69
Strain	0.769	0.002059	0.0002209

Table 1. Results of Displacement –Stress-Strain

	Carbon fiber	Kevlar	Floura polymer
Displacement (mm)	0.0422	0.113	0.105
Stress (N/mm^2)	35.1001	35.101	36.2614
Strain	0.000169	0.000452	0.000474

Table 2. Results of Shell element

3.2 Delamination length – 400mm

	Carbon fiber	Kevlar	Floura polymer
Displacement (mm)	28.4659	58.1869	58.6524
Stress (N/mm^2)	2683.45	2326.5	2064.2
Strain	0.01329	0.027	0.027301

Table 3. Results of Displacement –Stress-Strain

	Carbon fiber	Kevlar	Floura polymer
Displacement (mm)	21.7231	58.1869	53.6854
Stress (N/mm^2)	2075.8	2326.5	2088.05
Strain	0.01	0.027	0.28418

Table 4. Results of Shell element

IV. CONCLUSION

In this thesis, structural analysis and modal analysis is done to determine the stresses and the natural frequency of simply supported composite beam with single-edge delamination. The analysis is done by taking two delamination lengths.The delamination lengths considered are 381mm and 400mm. The analysis is done for 3 composite materials to determine the effect of delamination using solid element. Finite element analysis is done in AnsysBy observing the structural analysis results, the displacements and stresses are increased by increasing the delamination length. So the composite materials fail when the delamination increases.Modal analysis is done to determine the natural frequencies. By observing the analysis results, the natural frequencies decrease when length of delamination on the beam increase.

Analysis is also done by taking shell element by considering 5 layers. By observing the analysis results, the displacements and stresses are increased by increasing the delamination length.

REFERENCES

[1]. A Dynamic Stiffness Element for Free Vibration Analysis of Delaminated Layered Beams by Nicholas H. Erdelyi and Seyed M. Hashemi

[2]. Frequency response analysis of a delaminated smart composite plate by Bin Huang, Heung Soo Kim

[3]. Vibration Analysis of Delaminated Composite Laminates in Prebuckled States Based on a New Constrained Model by Hsin-Piao Chen, John J. Tracy, Ramon Nonato

[4]. Analytical solution for the dynamic analysis of a delaminated composite beam traversed by a moving constant force by Mohammad H Kargarnovin, Mohammad T Ahmadian, Ramazan-Ali Jafari-Talookolaei

[5]. Free vibration analysis of delaminated composite beams by Jaehong Lee

[6]. E. F. Crawley, The natural modes of graphite/epoxy cantilever plates and shells, *Composite Materials*, 13 (1979) 195–205.

[7]. J. T. S. Wang, D. Shaw and O. Mahrenholtz, Vibration of rotating rectangular plates, *J. Sound and Vibration*, 112(3) (1987) 455–468.

[8]. D. Shaw, K. Y. Shen and J. T. S. Wang, Flexural vibration of rotating rectangular plates of variable thickness, *J. Sound and Vibration*, 126(3) (1988) 373–385. C

[9]. M. S. Qatu and A. W. Leissa, Vibration studies for laminated composite twisted cantilever plates, *I. J. Mechanical Sciences*, 33 (1991) 927–940.

[10]. K. M. Liew, C. M. Lim and L. S. Ong, Vibration of pret-wisted cantilever shallow conical shells, *I. J. Solids Structures*, 31 (1994) 2463–74.

ISSN (e): 2250 – 3005 || Vol, 04 || Issue, 10 || October– 2014 ||
International Journal of Computational Engineering Research (IJCER)

Design & Analysis of a Disc Brake using Fea

Velveeta Lakshmikanth Chowdary[1], N. Amara Nageswara Rao[2]
[1]PG student, Department of mechanical engineering, Nimra institute of science & technology, Ibrahimpattanam
[2]Guide (Assoc.Prof), Department of mechanical engineering, Nimra institute of science & technology, Ibrahimpattanam

ABSTRACT:

Disc brake consists of a cast iron disc bolted to the wheel hub and a stationary housing called caliper. The caliper is connected to some stationary part of the vehicle like the axle casing or the stub axle as is cast in two parts each part containing a piston. In between each piston and the disc there is a friction pad held in position by retaining pins, spring plates. The passages are so connected to another one for bleeding. Each cylinder contains rubber sealing ring between the cylinder and piston Due to the application of brakes on the disc brake rotor, heat generation takes place due to friction and this temperature so generated has to be conducted and dispersed across the disc rotor cross section. The aim of this paper was to investigate the temperature fields and also structural fields of the solid disc brake during short and emergency braking with four different materials. The distribution of the temperature depends on the various factors such as friction, surface roughness and speed. The effect of the angular velocity and the contact pressure induces the temperature rise of disc brake. The finite element simulation for two-dimensional model was preferred due to the heat flux ratio constantly distributed in circumferential direction. We will take down the value of temperature, friction contact power, nodal displacement and deformation for different pressure condition using analysis software with four materials namely cast iron, cast steel, aluminum and carbon fiber reinforced plastic. Presently the Disc brakes are made up of cast iron and cast steel. With the value at the hand we can determine the best suitable material for the brake drum with higher life span. The detailed drawings of all parts are to be furnished.

Keywords: *Ansys, Brake Drum, Disc Brake, Friction Pad, Wheel Hub, Pro-e.*

I. INTRODUCTION

- **CLASSIFICATION OF BRAKES**

The mechanical brakes according to the direction of acting force may be divided into the following two groups:

a) Radial brakes:

In these brakes the force acting on the brakes drum is in radial direction. The radial brakes may be subdivided into external brakes and internal brakes.

b) **Axial Brakes**:

In these brakes the force acting on the brake drum is only in the axial direction. i.e. Disk brakes, Cone brakes.

c) Disc brake

A disk brake consists of a cast iron disk bolted to the wheel hub and a stationary housing called caliper. The caliper is connected to some stationary part of the vehicle like the axle casing or the stub axle as is cast in two parts each part containing a piston. In between each piston and the disk there is a friction pad held in position by retaining pins, spring plates etc. passages are drilled in the caliper for the fluid to enter or leave each housing. The passages are also connected to another one for bleeding. Each cylinder contains rubber-sealing ring between the cylinder and piston.

- **Disc brake working:**

The disc brake is a wheel brake which slows rotation of the wheel by the friction caused by pushing brake pads against a brake disc with a set of calipers. The brake disc (or rotor in American English) is usually made of cast iron, but may in some cases be made of composites such as reinforced carbon–carbon or ceramic matrix composites. This is connected to the wheel and/or the axle. To stop the wheel, friction material in the form of brake pads, mounted on a device called a brake caliper, is forced mechanically, hydraulically, pneumatically or electromagnetically against both sides of the disc. Friction causes the disc and attached wheel to slow or stop. Brakes convert motion to heat, and if the brakes get too hot, they become less effective, a phenomenon known as brake fade. Disc-style brakes development and use began in England in the 1890s. The first caliper-type automobile disc brake was patented by Frederick William Lanchester in his Birmingham, UK factory in 1902 and used successfully on Lanchester cars. Compared to drum brakes, disc brakes offer better stopping performance, because the disc is more readily cooled. As a consequence discs are less prone to the "brake fade"; and disc brakes recover more quickly from immersion (wet brakes are less effective). Most drum brake designs have at least one leading shoe, which gives a servo-effect. By contrast, a disc brake has no self-servo effect and its braking force is always proportional to the pressure placed on the brake pad by the braking system via any brake servo, braking pedal or lever, this tends to give the driver better "feel" to avoid impending lockup. Drums are also prone to "bell mouthing", and trap worn lining material within the assembly, both causes of various braking problems.

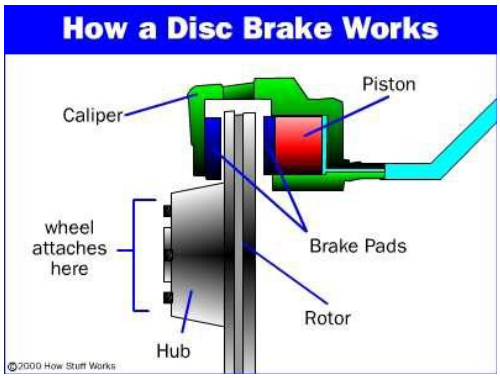

Fig. 1 Disk Brake

II. MODELING BY USING PRO-E

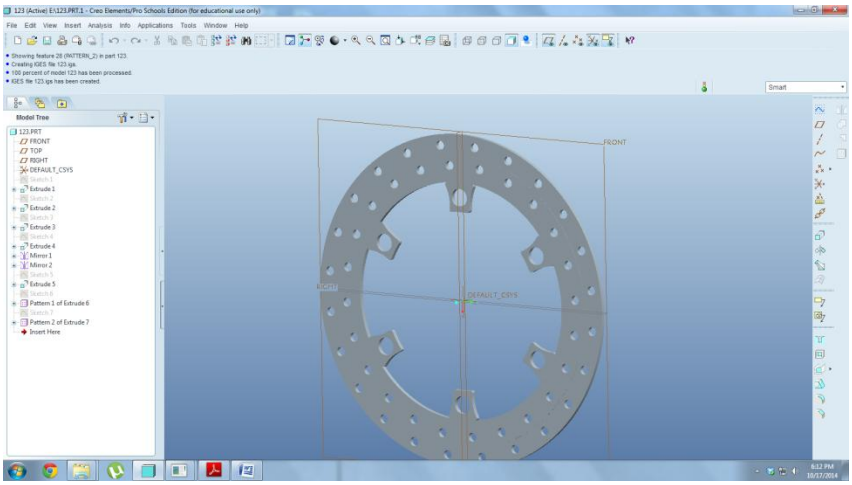

Fig.2 Disc brake model in Pro-e

III. RESULTS & DISCUSSION:

- **Thermal Analysis- Nickel Chrome Steel**

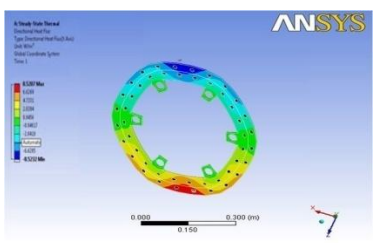

Fig.3 Temperature

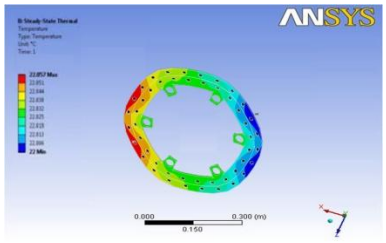

Fig.4 Directional heat Flux

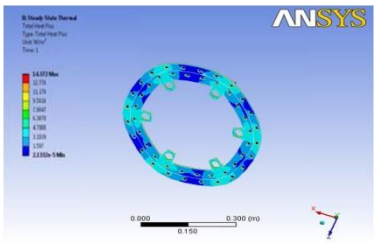

Fig.5 Total Heat Flux

- **Thermal Analysis- Aluminium Alloy**

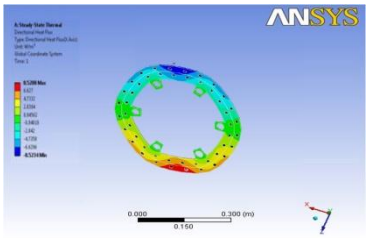

Fig.6 Temperature

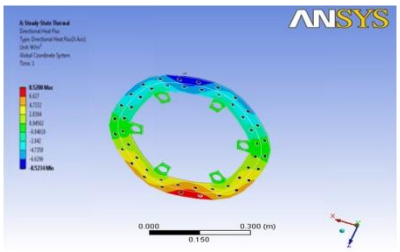

Fig.7 Directional heat Flux

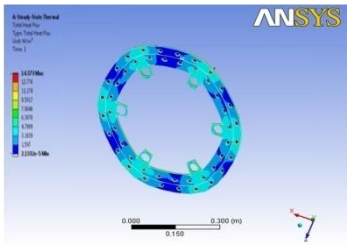

Fig.8 Total Heat Flux

- **Thermal Analysis- Cast Iron**

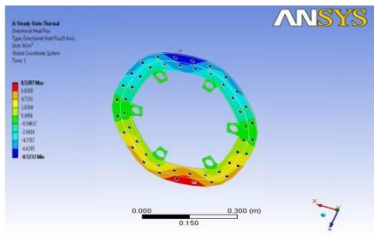

Fig.9 Temperature

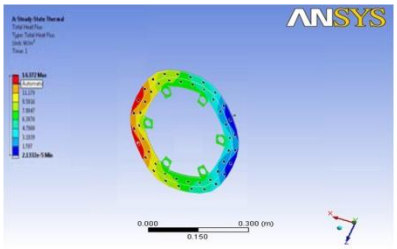

Fig.10 Directional heat Flux

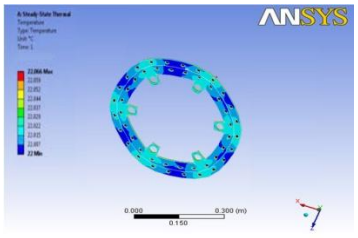

Fig.11 Total Heat Flux

- **Thermal Analysis- Carbon Reinforced Polymer**

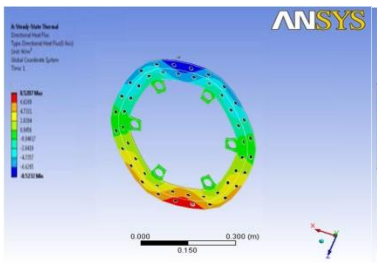

Fig.12 Temperature

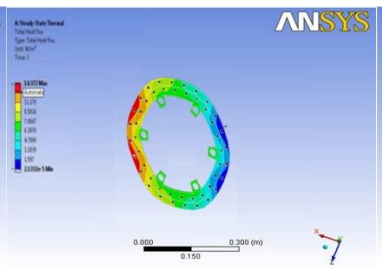

Fig.13 Directional heat Flux

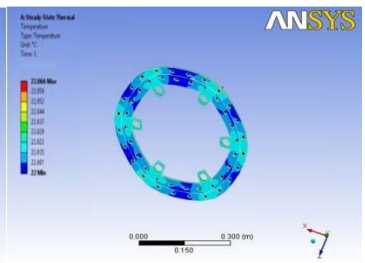

Fig.14 Total Heat Flux

- **Structural Analysis- Nickel Chrome Steel**

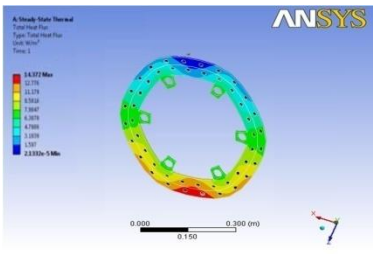

Fig.15 Equivalent Stress

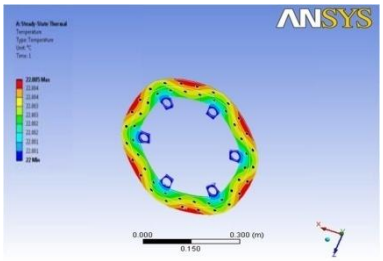

Fig.16 Total Deformation

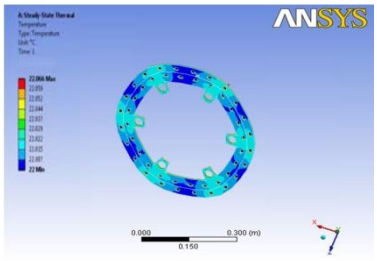

Fig.17 Strain Energy

- **Structural Analysis- Aluminium Alloy**

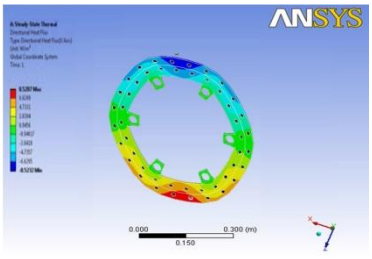

Fig.18 Equivalent Stress

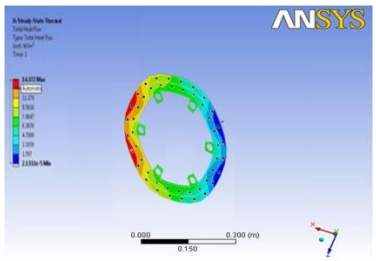

Fig.19 Total Deformation

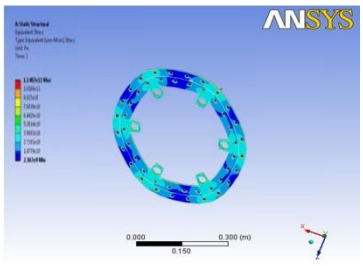

Fig.20 Strain Energy

- **Structural Analysis- Cast Iron**

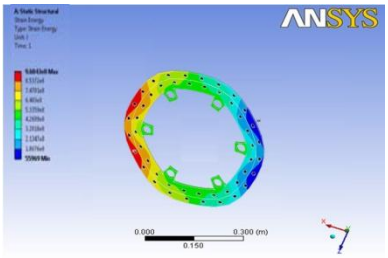

Fig.21 Equivalent Stress

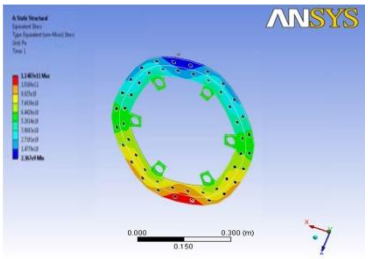

Fig.22 Total Deformation

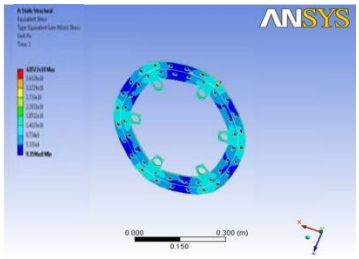

Fig.23 Strain Energy

- **Structural Analysis- Carbon Reinforced Polymer**

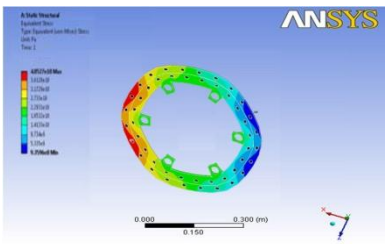

Fig.24 Equivalent Stress

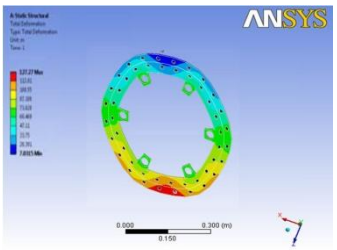

Fig.25 Total Deformation

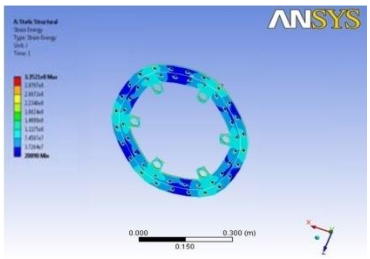

Fig.26 Strain Energy

IV. CONCLUSION

The model was modeled by using Pro-E and in the format of IGES which is a readable format of analysis software. By observing the Structural analysis and Thermal analysis results using Aluminum alloy and Carbon Reinforced Polymer the stress values are within the permissible stress value. So using Aluminum Alloy and Carbon Reinforced Polymer is safe for Disc Brake. By observing the frequency analysis, the vibrations are less for Aluminum Alloy than other two materials since its natural frequency is less. And also weight of the Aluminum alloy reduces almost 3 times when compared with Alloy Steel and Cast Iron since its density is very less. Thereby mechanical efficiency will be increased. But the strength of Carbon Reinforced material is more than Aluminum Alloy. Since the Thermal Analysis also Carbon Reinforced is also permissible. By observing analysis results, Carbon Reinforced Polymer is best material for Disc Brake.

Future scope:

1. By changing the model dimensions new results can be obtained.
2. By changing the model also better results may obtained.

REFERENCES

[1]. Darle W.Dudley, 1954, Hand book of practical gear design Alec strokes, 1970, High performance of gear design.
[2]. Maitra, G.M, 2004, Hand Book of Gear Design, TataMcGrawHill, New Delhi.
[3]. S.Md.Jalaluddin., 2006, "Machine Design, "Anuradha publications, Chennai.
[4]. Thirupathi Chandrupatla, Ashok D.Belegundu, "Introduction to finite element in Engineering" ,2003.
[5]. Gao C. H., Lin X. Z. (2002), Transient temperature field analysis of a brake in a non-axisymmetric three-dimensional model, J. Mater. Proc. Technol., Vol. 129, No 1, 513–517.
[6]. Nowacki W. (1962), Thermoelasticity, Pergamon Press, Oxford.
[7]. Ramachandra Rao V. T. V. S., Ramasubramanian H. and Seetharamu K. N. (1989), Analysis of temperature field in brake disc for fade assessment, Wärme- und Stoffübertragung, Vol. 24, No 1, 9-17.
[8]. Darle W.Dudley, 1954, Hand book of practical gear design Alec strokes, 1970, High performance of gear design.

ISSN (e): 2250 – 3005 || Vol, 04 || Issue, 10 || October– 2014 ||
International Journal of Computational Engineering Research (IJCER)

Industrial Spherical pressure vessel design & analysis using FEA

[1]K.S.J.Prakash, [2]T.Mastanaiah

[1] PG student, Department of Mechanical Engineering, Vikas College of Engineering & Technology, Nunna
[2] Guide (Assoc.prof), Department of Mechanical Engineering, Vikas College of Engineering & Technology, Nunna

ABSTRACT:

A pressure vessel is a type of container which is used to store liquids or gases under a pressure different from the ambient pressure. Different shapes of pressure vessels exist but most generally cylindrical and spherical shapes are used. Spherical vessels are theoretically 2 times stronger than cylindrical ones but due to the manufacturing difficulties, cylindrical ones are generally preferred in the industry. Mostly the pressure vessels are thin walled but here we are generating multi layered wall.

In this project we are designing spherical pressure vessel by using pro-e and the analysis is done by using ansys. Here two models are generated one is solid walled which is regularly used and another one is multi layered pressure vessel. And the analysis is done on the two models by changing the actual material with the composite material. The results are compared actual solid model with the multi layered pressure vessel and the comparison further extended to find the better material for that the actual material results of the model is compared with the composite material results. By the comparison we may find better design and the design proposed to the company.

I. INTRODUCTION

- **Pressure Vessels**

The term pressure vessel referred to those reservoirs or containers, which are subjected to internal or external pressures. The pressure vessels are used to store fluids under pressure. The fluid being stored may undergo a change of state inside the pressure vessels as in case of steam boilers or it may combine with other reagents as in chemical plants. Pressure vessels find wide applications in thermal and nuclear power plants, process and chemical industries, in space and ocean depths, and in water, steam, gas and air supply system in industries. The material of a pressure vessel may be brittle such as cast iron, or ductile such as mild steel.

- **High Pressure Vessels**

High Pressure vessels are used as reactors, separators and heat exchangers. They are vessel with an integral bottom and a removable top head, and are generally provided with an inlet, heating and cooling system and also an agitator system. High Pressure vessels are used for a pressure range of 15 N/mm^2 to a maximum of 300 N/mm^2. These are essentially thick walled cylindrical vessels, ranging in size from small tubes to several meters diameter. Both the size of the vessel and the pressure involved will dictate the type of construction used.

II. STRUCTURAL ANALYSIS BY ANSYS

2.1 Structural Analysis of spherical pressure vessel with hydrostatic pressure.

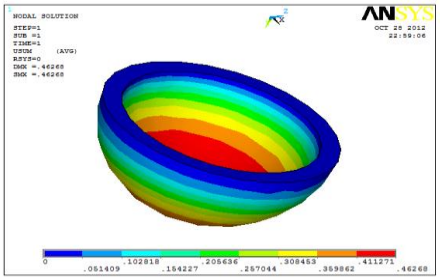

Fig 1.Vector sum displacement

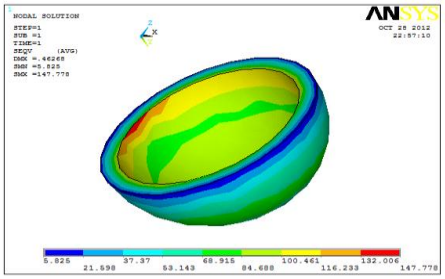

Fig 2. Von-misses stresses

2.2 Structural Analysis of spherical pressure vessel with burst pressure

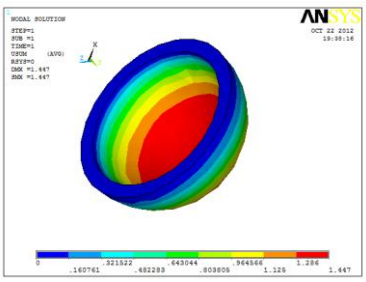

Fig 3.Vector sum displacement

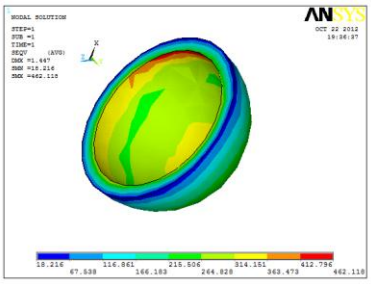

Fig 4. Von-misses stresses

2.3 Structural Analysis of dished end of the multi layer pressure vessel with hydrostatic pressure 27.3 N/mm^2

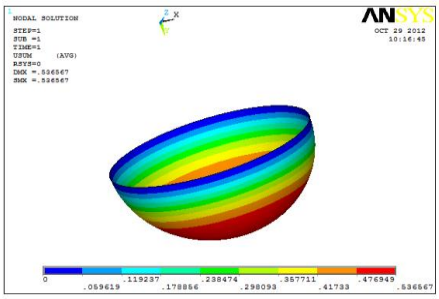

Fig 5.Vector sum displacement

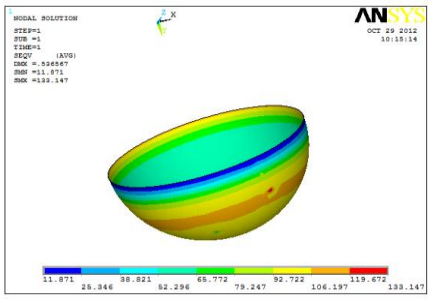

Fig 6. Von-misses stresses

2.4 Structural Analysis of dished end of the multi layer pressure vessel with burst pressure 64.52 N/mm^2

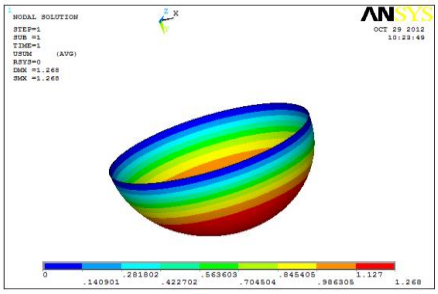

Fig 7.Vector sum displacement

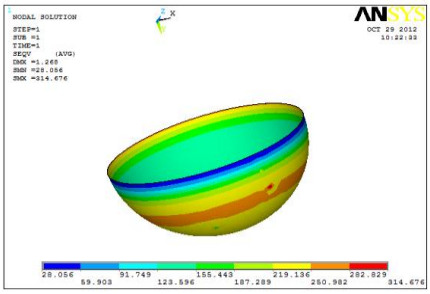

Fig 8.Von-misses stresses

2.5 Structural Analysis of dished end of the multi layer pressure vessel with hydrostatic pressure 27.3 N/mm^2

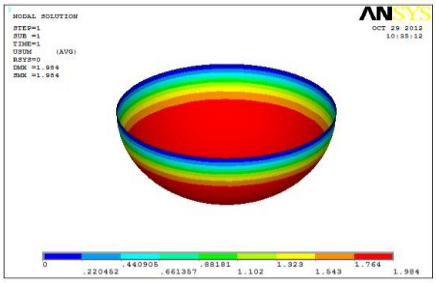

Fig9.Vector sum displacement

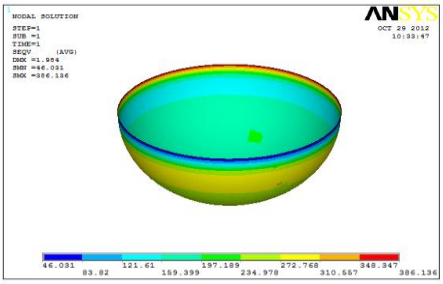

Fig 10.Von-misses stresses

2.6 Structural Analysis of dished end of the multi layer pressure vessel with burst pressure 64.52 N/mm^2

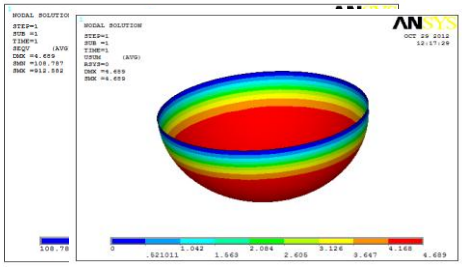

Fig 11.Vector sum displacement **Fig 12.Von-misses stresses**

III. RESULTS & DISCUSSION

3.1 Structural Analysis of dished end of the mono layer pressure vessel with hydrostatic pressure 27.3 N/mm^2

Stresses & Deformation	Minimum (N/mm^2)	Maximum (N/mm^2)
Von Mises Stresses	5.825	147.778
Vector sum deformation	0.0000	0.46268

Table 1.Results at pressure of 27.3 N/mm^2

3.2 Structural Analysis of burst pressure in dished end of the mono layer pressure vessel with burst pressure 85.37 N/mm^2

Stresses & Deformation	Minimum (mm)	Maximum (mm)
Vector sum deformation	0.0000	1.447
Von Mises Stresses	18.216	462.118

Table 2.Results at pressure of 85.37 N/mm^2

3.3 Structural Analysis of dished end of the multi - layer pressure vessel with hydrostatic pressure 27.3 N/mm^2

Stresses & Deformation	Minimum (mm)	Maximum (mm)
Vector sum deformation	0.0000	0.536567
Von Mises Stresses	11.871	133.147

Table 3.Results at pressure of 27.3 N/mm^2

3.4 Structural Analysis of burst pressure in dished end of the multi - layer pressure vessel with burst pressure 64.52 N/mm^2

Stresses & Deformation	Minimum (mm)	Maximum (mm)
Vector sum deformation	0.0000	1.268
Von Mises Stresses	28.056	314.676

Table 4.Results at pressure of 64.52 N/mm^2

3.5 Structural Analysis of dished end of the multi - layer pressure vessel with hydrostatic pressure 27.3 N/mm^2

Deformation	Minimum (mm)	Maximum (mm)
Vector sum deformation	0.0000	1.984
Von Mises Stresses	46.031	386.136

Table 5.Results at pressure of 27.3 N/mm^2

3.6 Structural Analysis of burst pressure in dished end of the multi - layer pressure vessel with burst pressure 64.52 N/mm^2

Deformation	Minimum (mm)	Maximum (mm)
Vector sum deformation	0.0000	4.689
Von Mises Stresses	108.787	912.582

Table 6.Results at pressure of 64.52 N/mm^2

IV. CONCLUSIONS AND FUTURE SCOPE

4.1 Conclusions

1. At present multilayered vessels are being used extensively in many industries when compare to solid wall pressure vessels. Because, there is a huge difference in weight of the vessel and uniform stress distribution among the vessel wall thickness.
2. There is a percentage saving in material of **28.48%** by using multilayered vessels in the place of solid walled vessel when both the vessels are manufactured with same material i.e. SA515 Grade 70 steel **.**
3. There is a percentage saving in material of **91.62%** by using multilayered CFRP material vessels when compared to multilayered SA515 Grade 70 steel material vessels.
4. This decreases not only the overall weight of the component but also the cost of the material required to manufacture the pressure vessel. This is one of the main aspects of designer to keep the weight and cost as low as possible.
5. The Stress variation from inner side to outer side of the multilayered pressure vessel is around **11.76%,** where as to that of solid wall vessel is **17.32%.** This means that the stress distribution is uniform when compared to that of solid wall vessel.
6. Minimization of stress concentration is another most important aspect of the designer. It also shows that the material is utilized most effectively in the fabrication of shell.
7. Owing to the advantages of the multi layered pressure vessels over the conventional single walls pressure vessels, it is concluded that multi layered pressure vessels are superior for high pressures and high temperature operating conditions.
8. The burst pressures for various fiber orientations are predicted using the Tsai-Wu failure criteria. The **± 25°** fiber orientation angle is obtained as the optimum fiber orientation angle for the composite pressure vessel subjected to high internal pressure loading.

4.2 Future Scope

1. Analysis on different layer materials to reduce cost of production
2. Optimization of shell thickness for the given conditions.

REFERENCES

[1]. BHPV manual on Multilayer Pressure Vessels.
[2]. ASME Code Book Section VIII & Division I.
[3]. International Journal of Engineering Trends and Technology- Volume3 Issue5- 2012, ISSN: 2231-5381.
[4]. R.S.Khurmi and J.K.Gupta., "A Test Book of Machine Design" S.Chand publications.
[5]. Brownell and Young, "Process Equipment Design" Seely, F.B., and Smith,
[6]. John F.Henvey " Pressure Vessel Design -Nuclear and Chemical Applications" An East-west Edition, Newyork
[7]. Henry H.Bednar " Pressure Vessel Code Book"
[8]. Fratcher, G.E : New alloys for Multilayer Vessels" Vol. 33
[9]. Harold.H.Wait e, "Pressure Vessel and Piping Design Analysis"
[10]. Mc Cabe, J.S and Rothrock, E.W., "Multilayer Vessels for High Pressure," ASME Mechanical Engineering PP 34-39.
[11]. Mc Cabe, J.S and Rothrock, E.W., " Recent Developments in Multilayer Vessels," British chemical engineering Vol.16, No6,1971
[12]. Noel, M.R., "Multiwall Pressure Vessels," British chemical Engineering Vol.15, No7, 1970.
[13]. O.C.Zienkeewz."The Finite Element Method in Structural and Continuum Mechanics.
[14]. Ansys User's Manual, Swanson Anlysis Systems, Inc.1995.
[15]. E.N. Buarque, J.R.M.Almeida, "The effect of cylindrical defects on the tensile strength of glass fiber/vinyl-ester matrix reinforced composite pipes", *Composite Structures*, Vol. 79, pp. 270–279, 2007.
[16]. J.M. Duell, J.M. Wilson, M.R. Kessler, "Analysis of a carbon composite overwrap pipeline repair system", *International Journal of Pressure Vessels and Piping*, Vol. 85, pp. 782–788, 2008.
[17]. R.R. Chang, "Experimental and theoretical analyses of first-ply failure of laminated composite pressure vessels", *Composite Structures*, Vol. 49, pp. 237-243, 2000
[18]. L. Parnas, N. Katırcı, "Design of fiber-reinforced composite pressure vessels under various loading conditions", *Composite Structures*, Vol. 58, pp. 83-95, 2002.
[19]. M.A. Wahab, M.S. Alam, S.S. Pang, J.A. Peck, R.A. Jones, "Stress analysis of non-conventional composite pipes", *Composite Structures*,Vol. 79, pp. 125–132, 2007.
[20]. R.M. Guedes, "Stress–strain analysis of a cylindrical pipe subjected to a transverse load and large deflections", *Composite Structures*, Vol.88, pp. 188–194, 2009.
[21]. H. Bakaiyan, H. Hosseini, E. Ameri, "Analysis of multi-layered filament-wound composite pipes under combined internal pressure and thermo mechanical loading with thermal variations", *Composite Structures*, Vol. 88, pp. 532–541, 2008.
[22]. F. Ratter, D. Lueddeke, S.C. Huang, "Finite Element Analysis of the Lateral Crushing Behaviour of Segmented Composite Tubes", *Journal of Engineering Technology and Education*, Vol. 6, No.1, , pp. 1-16, 2009.
[23]. DOT CCFC standards.
[24]. Nagesh, "Finite-element Analysis of Composite Pressure Vessels with Progressive Degradation", *Defence Science Journal*, Vol. 53, No. 1, pp. 75-86, 2003.

ISSN (e): 2250 – 3005 || Vol, 04 || Issue, 10 || October– 2014 ||
International Journal of Computational Engineering Research (IJCER)

Effect of Tyre Overload and Inflation Pressure on Rolling Loss (resistance) and Fuel Consumption of Automobile Cars

Sadda. Mahendra[1] , N. Amara Nageswara Rao[2]
[1]PG student, Department of mechanical engineering, Nimra institute of science & technology, Ibrahimpattanam.
[2]Guide(Assoc.Prof), Department of mechanical engineering, Nimra institute of science & technology, Ibrahimpattanam

ABSTRACT:

Rolling loss or rolling resistance is an ever important property for the tyre and automotive industries because of its practical implication. The tyre rolls under a load, it deforms. The load presses down on the tyre and squashes it against the road. As the tyre turns, the squashed part comes off the road and returns to its original shape while another part of the tyre gets squashed. The sidewalls of the tyre flex over and over again, close to 500 times per minute at highway speeds. And, the tread goes from a circular to a flat shape and back to circular again there are some practical things that can reduce deformation and heat. Inflation pressure has an effect. Underinflated tyres deform much more, get much hotter, and cut fuel economy. So properly inflated tyres save fuel by reducing rolling resistance.

Fuel consumption and tyre rolling loss in all types of automobiles have become increasingly important because of adverse environmental effects and economic costs. If rolling resistance is reduced because of better tyre maintenance, consumers may end up spending less on tyres, because properly inflated tyres will have longer wear in addition to providing better fuel economy. In this thesis, the effect of rolling resistance on fuel consumption of radial passenger and truck tyres is discussed. A possible method of optimizing fuel use by adjusting the tyre load/pressure Conditions will be suggested. All these estimates will be obtained for radial tyres. Finite element analysis is done on the tyre by applying tyre load and inflation pressure. The investigations are made on two tyre models of automobile cars Skoda Rapid and Ford Classic. Modeling is done in Pro/Engineer and analysis is done in Ansys.

KEYWORDS: *Ansys, Rolling loss or rolling resistance, Pro/Engineer, Tyre.*

I. INTRODUCTION

The pneumatic tyre plays an increasingly important role in the vehicle performance of road. However, this status is achieved because of more than one hundred years' tyre evolution since the initial invention of the pneumatic tyre by John Boyd Dunlop around 1888. Tyres are required to produce the forces necessary to control the vehicle. As we know that the tyre is the only means of contact between the road and the vehicle but they are at the heart of vehicle handling and performance (Nicholas, 2004). The inflated rubber structure provides comfortable ride for transportation. With the growing demand for the pneumatic tyre, many improvements have been made based on the initial conception, such as the reinforcement cords, the beads, the vulcanization, the materials and the introduction of the tubeless tyre. The relationship between human and tyre and environmental surrounding play an important role for developing of tyre technology. These concerns include traffic accidents caused by tyre failure, the waste of energy due to bad tyre conditions, the pollution through the emission of harmful compounds by tyres, and the degradation of road surfaces related to tyre performance, etc.Tyre as one of the most important components of vehicles requires to fulfill a fundamental set of functions are to provide load-carrying capacity, to provide cushioning and dampening against the road surface, to transmit driving and braking torque, to provide cornering force, to provide dimensional stability, to resist abrasion (Mir Hamid, 2008). Tyres have ability to resist the longitudinal, lateral, and vertical reaction forces from the road surface without severe deformation or failure. Tyre performance is depends on the tyre rolling resistance, cornering properties, tyre traction, tyre wear, tyre temperature, tyre noise, tyre handling and characteristics, etc. There are various losses associated with the vehicle that affect its fuel economy as it is being operated. These losses include engine, driveline, aerodynamic and rolling losses, while the rolling loss is associated with the vehicle tyres.

1.1 . Tyre axis terminology

It is need to understand some of the basic terminology for tyre, especially regarding the systems of coordinates, orientations, velocities, forces, moments. Nomenclature and definitions based on the SAE standard as shown in Figure 1 X-axis is the intersection of the wheel plane and the road plane with positive direction forward. The Z-axis perpendicular to the road plane with positive direction downward. The Y-axis in the road plane, its direction being chosen to make the axis system orthogonal and right hand. There are several forces, moments and angles that prove to be very important in tyre behavior. All these forces can be seen as the forces and moments acting on the tyre from the road. First, there are two main angles to consider, the camber angle and the slip angle. The camber angle is the inclination angle from its vertical position while the slip angle is the difference in wheel heading and direction.

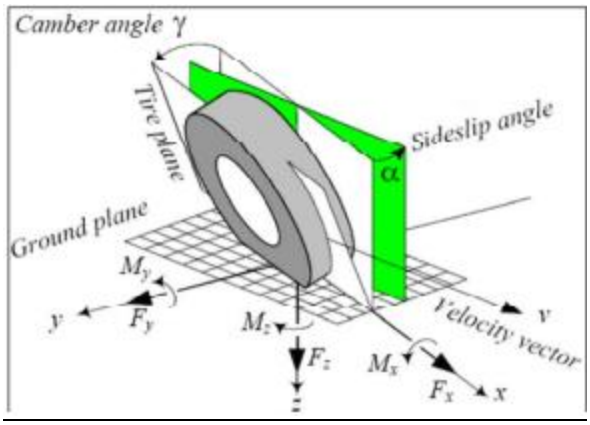

Figure 1.Tyre Axis Terminology

II. INTRODUCTION TO PRO/ENGINEER

Pro/ENGINEER Wildfire is the standard in 3D product design, featuring industry-leading productivity tools that promote best practices in design while ensuring compliance with your industry and company standards. Integrated Pro/ENGINEER CAD/CAM/CAE solutions allow you to design faster than ever, while maximizing innovation and quality to ultimately create exceptional products.

Customer requirements may change and time pressures may continue to mount, but your product design needs remain the same - regardless of your project's scope, you need the powerful, easy-to-use, affordable solution that Pro/ENGINEER provides.

3. 3D models of tyre and rim assembly

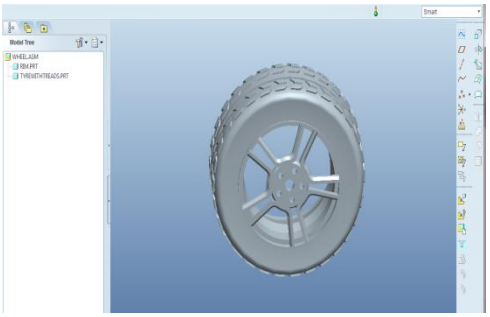

Figure 2.Assembly of Skoda

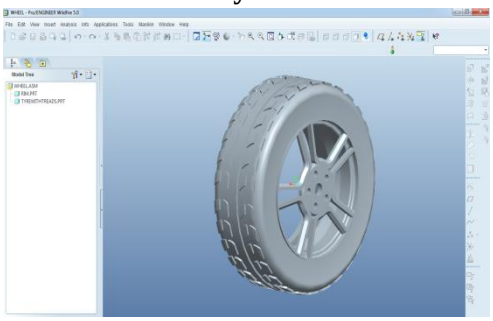

Figure 3.Assembly of Ford

4. Analysis by using ansys

4.1 Structural analysis of Skoda tyre

4.1.1 Car weight + 5 persons weight (at pressure 1.116)

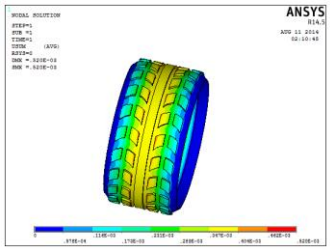

Figure 4. Displacement

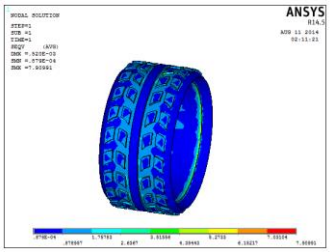

Figure 5. Stress

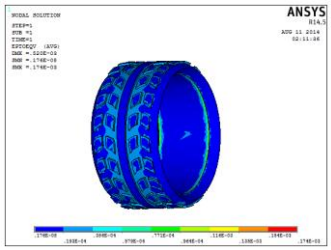

Figure 6.Strain

4.1.2 Car weight + 6 persons weight (pressure - 1.118n/mm^2)

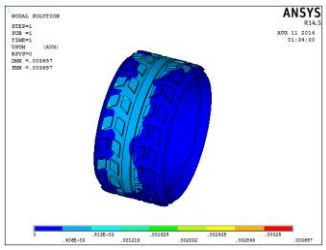

Figure 7. Displacement

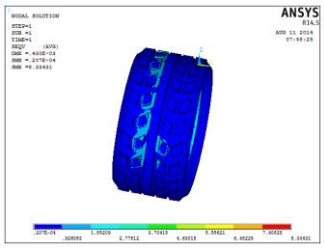

Figure 8. Stress

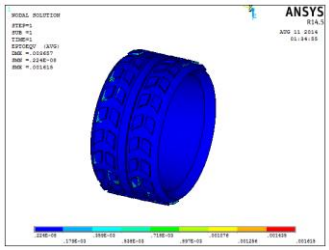

Figure 9. Strain

4.1.3 Car weight + 7 persons weight (at 1.214 pressure)

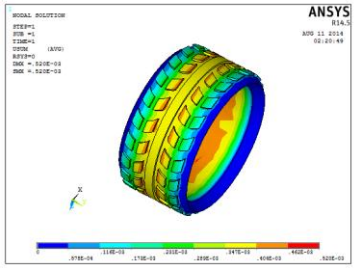

Figure 10. Displacement

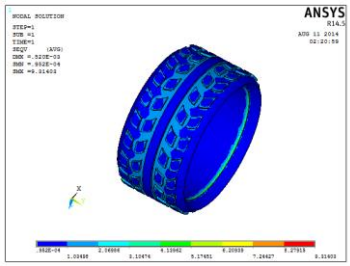

Figure 11. Stress

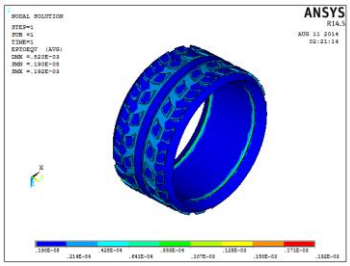

Figure 12. Strain

4.2 Structural analysis of ford tyre

4.2.1 Car weight + 5 persons weight (pressure at 0.6211)

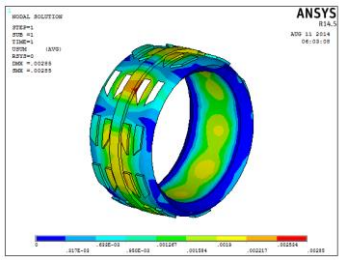

Figure 13. Displacement

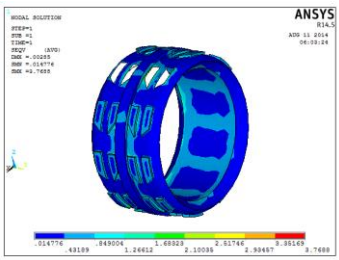

Figure 14. Stress

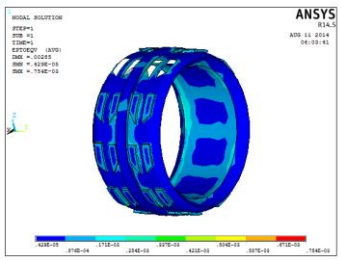

Figure 15. Strain

4.2.2 Car weight + 6 persons weight(at pressure 0.65 n/mm^2)

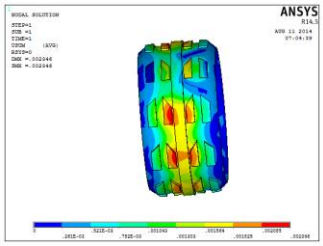

Figure 16. Displacement

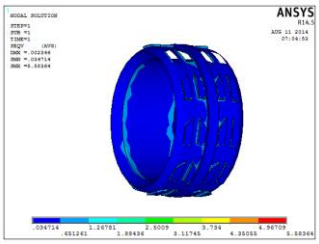

Figure 17. Stress

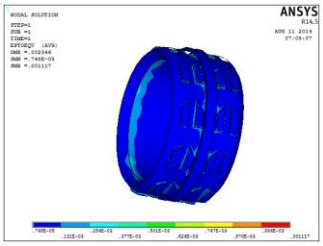

Figure 18. Strain

4.2.3 Car weight + 7 persons weight (at pressure 0.6790 n/mm^2)

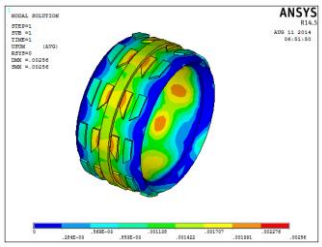

Figure 19. Displacement

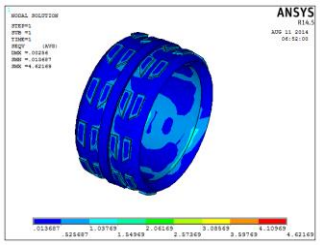

Figure 20. Stress

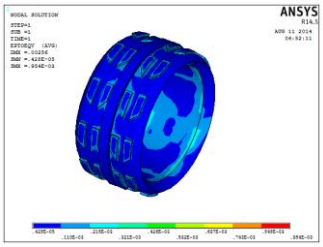

Figure 21. Strain

III. RESULTS TABLE

5.1 Skoda tyre

Pressure (N/mm^2)	Displacement (mm)	Stress(N/mm^2)	Strain
At 1.116	0.520e-03	7.90991	174e-02
At 1.181	0.003657	8.33431	0.001615
At 1.214	0.520e-03	9.31402	0.192e-03
Inflation pressure(0.036)	0.130e-04	0.160046	0.325e-05

Table 1.Results of skoda tyre

5.2 Ford tyre

Pressure (N/mm^2)	Displacement (mm)	Stress(N/mm^2)	Strain
At 0.6211	0.00285	3.7688	0.754e-03
At 0.650	0.002346	5.58364	0.001117
At 0.6790	0.00256	4.62169	0.954e-03
Inflation pressure(0.036)	0.739e-03	0.510433	0.112e-03

Table 2.Results of ford tyre

IV. CONCLUSION

In this thesis, the effect of tyre over load and inflation pressure on the rolling loss and fuel consumption is analyzed. The investigations are made on two models of tyre Skoda Rapid and Ford Classic. The analysis is done by applying the loads of car weight and persons weight. When the car is overloaded, also analysis is done. Analysis is done by applying inflation pressure. The material used for tyre is rubber.
Modeling is done in Pro/Engineer and analysis is done in Ansys.

The analysis is done by applying the car weight + 5 persons weight, overloading the tyre, that is, car weight + 6 persons weight and car weight + 7 persons weight. The analysis is also done by applying the inflation pressure.

By observing the analysis results, the stresses produced are less than the yield strength value of rubber even the tyre is overloaded. The rolling loss will be more for overloading than the specified load and the fuel consumption will also be more. A possible method of optimizing fuel consumption by adjusting tyre operating load/pressure conditions is suggested. Increasing tyre pressure is a convenient and inexpensive method of partially or fully compensating for rolling resistance increase. Some fuel saving might be accomplished by this method.

By comparing the results ford classic tyre is best which is getting less stress values compared to Skoda tyre in the case of overloaded condition and the fuel consumption also more for Skoda compared to ford classic.

6.1 By the results the following Observations are made:

1. The more stress is developed when the vehicle is over loaded.
2. The rolling loss also increased by over loading.
3. The stresses are produced more than the material yield strength in the case of over loaded condition.
4. If the rolling loss increased the stress on the tyre also increased simultaneously the load on the engine will be more with this effect the fuel consumption will be more.
5. From the above observations we are concluding that by the over load of the tyre the fuel consumption is more and inflation of rolling loss also increases.
6. In the case of overloading condition also ford stress values are less compared to Skoda so we are concluding that ford tyres are better than Skoda in the fuel consumption of over loading condition.

6.2 Suggestions:

1. To optimize the fuel consumption the over loading must be decreased.
2. And the pressure of air in tyres must be monitored and by increasing the pressure we may optimize the fuel consumption.
3. By the above two conditions the fuel consumption in automobiles are optimized.
4. By reducing the weight of the car also the consumption may optimized.
5. Usage of composite material parts, which will reduces the weight of the cars and the fuel consumption reduced accordingly.

REFERENCES

[1]. Parametric study and experimental evaluation of vehicle tyre performance by Virkar D S1 and Thombare D G
[2]. Tyre inflation pressure influence on a vehicle stopping distances by Vladimír Rievaj, Ján Vrábel, Anton Hudák
[3]. Design of automatic tyre inflation system by Hemant Soni, Pratik Golar, AshwinKherde
[4]. Walter J D & Conant F S, Tyre Sci Technol, 2 (1974) 238.
[5]. Lou A Y C, Tyre Sci Technol, 6 (1978) 176.
[6]. Keefe R L & Koralek A S, in Tyre rolling resistance, edited by Schuring D J Rubber (Division AC S, Akron, Ohio), 1983, 78.
[7]. Bezbatchenko W, Title: The Effect of Tyre Construction on Fuel Economy" SAE paper #740067 Society of Automotive Engineers (1974) New York.
[8]. Schuring D J, Tyre Sci Technol (1976) 3.
[9]. Williams A R, The Influence of Tyre and Road Surface Design on Tyre Rolling Resistance, Inst Petroleum Report, IPSI-003 (1981), London, UK.
[10]. Luchini J R, Peters I M & Arthur R H, Tyre Sci Technol, (1994) 206.
[11]. Warholic, Tyre Rolling Loss Prediction from Finite Element Analysis of a Statically Loaded Tyre, M. S. E. Thesis, University of Akron, Akron, Ohio, 1987.

ISSN (e): 2250 – 3005 || Vol, 04 || Issue, 10 || October– 2014 ||
International Journal of Computational Engineering Research (IJCER)

Computer Modeling Air Drawing in Melt Blowing Nonwovens Process Produced by Dual Slot Annular Die

Bo ZHAO

[1]College of Textiles, Zhongyuan University of Technology, Henan, Zhengzhou, 450007, P.R.China

ABSTRACT:

An air-drawing model of polymer melt blowing process is established and solved by introduced the numerical computation results of the air jet flow field of dual slot annular die. Meanwhile, the model is also verified by the experimental results obtained with our university's equipment. The influence of the density and the specific heat capacity of polymer melt at constant pressure changing with polymer temperature on the fiber diameter are also studied. The predicted fiber diameters tally with the experimental data well. The effects of the processing parameters on the fiber diameter are further investigated in this paper. We find that a lower polymer throughput rate, a higher polymer melt initial temperature，a higher air initial temperature, and a higher air initial velocity can all produce finer fibers. The results show the great perspective of this research in the field of computer-assisted design (CAD) of melt blowing process and technology.

KEYWORDS: *melt blowing, dual slot annular die, nonwovens, air drawing model, computer modeling, processing parameters, fiber diameter.*

I. INTRODUCTION

Melt blowing technology is a single step process to make melt blowing nonwovens directly from thermoplastic polymers with the aid of high velocity and hot air to attenuate the polymer melt fiber, which dates back to the 1950's [1]. The melt blowing web is ideally suited for medical materials, roof materials, hygienic materials, and so on. The dual slot annular die is shown in Figure 1. The annular die is often used to produce polymers fibers in this process. Researchers have been studying air drawing models of polymers, especially shambaugh and his colleagues [2-5].

In this paper, an air drawing model of polymer will be established based on numerical computational method and verify the numerical results with the experimental data obtained with our university's equipment, at the same time, we also consider the effects of the variation of polymer processing parameters and further study the effects of melt blowing process parameters on the fiber diameter. Based on the new air drawing model in melt blowing process, one improvement will be further made on the model in this work**:** considering the influences on fiber diameter of the variation of the density and the specific heat capacity of polymer melt at constant pressure changing with polymer temperature. The final fiber diameter can then be predicted with the aid of this air drawing model. It is found that the model can be applied to predicting the drawing effects successfully. Effects of the processing parameters on the fiber diameter will also be investigated by utilizing the

air drawing model. The results also reveal the great potential for this research in the computer-assisted design (CAD) of melt blowing process, technology and equipment.

II. AIR DRAWING MODEL OF POLYMERS IN MELT BLOWING PROCESS

The polymer air drawing model consists of a continuity equation, a momentum equation, an energy equation, and a constitutive equation [1, 6]. The surrounding air conditions (velocity and temperature) are considered as given functions of axial position, are obtained by numerical simulation. In the literatures [1-5], the density ρ_f and specific heat capacity of polymer melt at constant pressure C_{Pf} are considered to be constant. In fact, they vary with polymer temperature T. In this research, we establish an air drawing model that differs from others in citations as indicated above, and consider the effects of the variation of polymer density and polymer specific heat capacity with polymer temperature at constant temperature. Because the air velocity and temperature obtained by the numerical solution of the air jet flow field of dual slot annular die, we can predict the drawing effects with the aid of this air drawing model.

2.1 Continuity equation

$$W = \frac{\pi}{4} D^2 \mathrm{V} \rho_f \qquad (1)$$

Where W =polymer mass flow rate, D =fiber diameter, V =fiber velocity, and ρ_f =polymer density. As the polymer density varies with polymer temperature, the following correlation [7] is also introduced**:**

$$\rho_f = \frac{1}{1.145 + 0.000903 \times T} \qquad (2)$$

Where T is the polymer temperature.

2.2 Momentum equation

$$\frac{dF_{rheo}}{dz} = \frac{\pi}{2} j \rho_a C_f (V_a - V)^2 D + W \frac{dV}{dz} - \rho_f \frac{\pi}{4} D^2 g \qquad (3)$$

Where F_{rheo} =rheological force, z =axial direction, ρ_a =air density, ρ_f =polymer density, V =fiber velocity, V_a =air velocity, g =gravitational acceleration, and C_f =air drawing coefficient.

The rheological force is as following.

$$F_{rheo} = \frac{\pi}{4} D^2 (\tau_{xx} - \tau_{yy}) \qquad (4)$$

Where τ_{xx} = the axial tensile stress of polymer, and τ_{yy} =the transversal tensile stress of polymer.

C_f is given by the following correlation:

$$C_f = \beta \mathrm{Re}^{-n} \qquad (5)$$

β and n are the constants of Matsui's correlation and Re is the Reynolds number. Re is defined by the following relation:

$$\mathrm{Re} = \frac{D\left|u_a - u\right|}{\upsilon_a} \qquad (6)$$

Where υ_a =the air kinematic viscosity.

2.3 Energy equation

$$\rho_f C_{pf} \frac{dT}{dz} V = -\frac{4h(T - T_a)}{D} \qquad (7)$$

Where T =polymer temperature, T_a =air temperature, h =heat transfer coefficient, C_{pf} =specific heat capacity of the polymer at constant pressure, and C_{pf} =specific heat capacity of the polymer at constant pressure.

Like polymer density, the correlation of the specific heat capacity at a constant pressure of the polymer melt changing with the polymer temperature [7] is as following**:**

$$C_{pf} = 0.3669 + 0.00242 \times T \qquad (8)$$

2.4 Constitutive equation

As is commonly known, polypropylene polymer is a kind of non-Newtonian fluid, the constitutive equation of a power-law fluid is introduced in our model.

$$\tau_{xx} = 2\eta\left(\frac{dV}{dz}\right)^m$$

$$\tau_{yy} = -\eta\left(\frac{dV}{dz}\right)^m \qquad (9)$$

Where τ_{zz} =axial extra stress of polymer, τ_{xx} =transversal extra stress of polymer, η =shear viscosity, and m is power-law exponent.

2.5 Boundary conditions

$$V(0)=V_0,\ F(0)=F_0,\ D(0)=D_0,\ T(0)=T_0,\ F_{rheo}(0)=0 \qquad (10)$$

Here F_0=he initial rheological force of the polymer melt, V_0 =the initial velocity of the polymer melt, D_0 =initial diameter of the polymer melt, and T_0 =the initial temperature of the polymer melt .

The "freezing-point" is defined as the boundary condition. The method used for determining the initial rheological force F_0 is the searching "freezing-point" method, which requires checking whether the fiber diameters before and beyond some "point" along the filament are equal to each other when F_0 is considered to be the sum of the cumulative gravitational and air drawing force acting upon the frozen part of the filament fiber. If the fiber diameters are found to be the same, the "point" is the so-called "freezing-point" and used in this iteration is the appropriate initial rheological force

III. EXPERIMENTAL

3.1 Material characterization

The polymer used is Y-3500 polypropylene with a melt flow rate of 34.2g/10min.

3.2 Process parameters

The melt blowing processing parameters concerned are the polymer throughput rate, polymer melt initial temperature, air initial temperature, and air initial velocity and die-to-collector distance, the ranges of the parameters are 0.30-0.98g/min/hole, 275-330℃, 275-340℃, 30-145m/s and 0-25cm, respectively. To condense the discussions and comparison, a group of fundamental parameters was assumed during the computations: a polymer throughput rate 0.64 g/min/hole, a polymer melt primary temperature 300℃, a air initial velocity 85m/s, a air initial temperature 300℃and die-to-collector distance 18cm, When one of the processing parameters was varied, the fundamental values of the other process parameters were held constant.

3. 3 The parameters of dual-slot annular die of melt blowing process

The dual slot annular die parameters are as following: The outside diameter h=2.40mm, the slot wide e=0.56mm, and the inside diameter b=1.28mm.

3. 4 Test conditions

All the samples tested are conditioned for 24 hours at 65% RH and 20℃ before evaluation.

3. 5Test methods

The image analysis method was employed to measure the fiber diameter. The images of nonwoven samples were acquired with a Questar three-dimensional video frequency microscope (Questar Corp., New Hope, PA) with an enlargement factor of 600 and a depth of focus of 1mm and then processed with Image-Pro Plus image analysis software(Media Cybernetics, Inc., Silver Spring, MD) to measure the fiber diameter. The image processing includes enhancement, smoothing, binarization, and filtering. The fibers of the melt blowing nonwoven are regarded as cylinders because their cross sections are nearly round. Twenty fibers are chosen to measure their diameters in each grid, so altogether there are 200 fibers to be measured in 10 grids. The mean value of the diameters of 200 fibers was considered as the fiber diameter of the polypropylene (PP) nonwoven sample.

The melt flow index (MFI) experiments of polypropylene (PP) were measured (performed) with a temperature 230℃, a load capacity 2.160kg, a aperture of capillary tube 2.095mm and a length of capillary tube 8mm on RL--11B type melt flow indexer at ambient room temperature conditions.

3.6 Numerical methods for solving the air jet flow field model of melt blowing

The air jet flow field model is solved by using the finite difference method. The SIMPLE algorithm is utilized to solve the problem of velocity pressure couple and the staggered grid is presented to avoid tooth-like distributions of velocity and pressure. The preferred difference scheme for space independent variables is the second-order upwind difference scheme and the TDMA method is used to solve the difference equations.

With the help of numerical simulations of the air jet flow field, we can determine the distributions of the x-component of air velocity V_a and air temperature T_a along the axial position x. Then we can solve the air drawing model of the polymer using a fourth-order Runge-Kutta method.

IV. EFFECTS OF VARIATIONS OF THE PROCESSING PARAMETERS ON THE FIBER DIAMETER

4.1 Effect of the polymer throughput rate on the fiber diameter

Figure 2 shows the effect of the polymer throughput rate on fiber diameter. The polymer throughput rate is 0.88, 0.64 and 0.48 g/min/hole in turn from top to bottom. As expected, lower polymer throughput rates give finer fibers and more rapid attenuation. When the polymer throughput rate is 0.48g/min/hole, the final fiber diameter is 19.1% finer than that when the polymer throughput rate is 0.88g/min/hole.

4.2 Effect of the polymer melt initial temperature on the fiber diameter

Figure 3 illustrates how changes in polymer melt initial temperature cause changes in the rate of fiber attenuation. The polymer melt initial temperature is 280, 300 and 320℃are considered. As expected, the higher polymers melt initial temperature, the finer the fibers will be. The fiber diameter corresponding to the polymer melt initial temperature of 320℃is 19.9% finer than that corresponding to the temperature of 280℃.

4.3 Effect of the air initial velocity on the fiber diameter

Figure 4 reveals the effect of the air initial velocity on fiber diameter. The air initial velocity is 50, 85, and 115m/s in turn from top to bottom. Note that the higher the air initial speed is, the finer the fibers will be. The higher air initial velocity will cause the fibers to be attenuated much higher. When the air initial speed increases to 115m/s, the final fiber diameter is 20.5% finer than that when the air initial speed is 50m/s.

4.4 Effect of the air initial temperature on the fiber diameter

Figure 5 shows the effect of the higher polymer melt initial temperature on fiber diameter. The air initial temperature is 280, 300, and 320℃ in turn from top to bottom As expected, higher polymer melt initial temperature will cause the fibers to be more finely attenuated. The fiber diameter corresponding to the polymer melt initial temperature of 320℃is 18.6% finer than that corresponding to the temperature of 280℃.

V. COMPARISON OF IMPROVED MODEL WITH PRIMARY MODEL

Model predictions considering the influences of the polymer temperature on the density and specific heat capacity of polymer melt at constant pressure. The melt blowing process parameters here are the polymer throughput rate, the polymer melt initial temperature, the air initial temperature, and the air initial velocity, and the variation ranges of the parameters are 0.30--0.98 g/min/hole, 275--330℃, 275--340℃,and 30-145m/s, respectively.

Table 1 shows the fiber diameter changing by considering the polymer density and the specific heat capacity of polymer melt at constant pressure varying with the polymer temperature. As can be seen, the predictions given by the two models are not same, two models have much difference from each other. It can be concluded that the variations in density and the specific heat capacity of polymer melt at constant pressure with the polymer temperature have very important effects on fiber diameter.

The model predictions can be improved remarkably by considering the influences of polymer temperature on the density and specific heat capacity of polymer melt at constant pressure. Therefore, the variation in density and specific heat capacity of polymer melt at constant pressure with the polymer temperature has important effects on fiber diameter. It has been concluded that the predicted fiber diameters are much closer to the experimental results, which further confirms the effectiveness of the polymer air drawing model established in this paper. From the above analyses, it can be seen that the fiber diameter is directly related to the polymer throughput rate, polymer melt initial temperature, air initial temperature, and air initial velocity.

VI. CONCLUSIONS

In this paper, an air drawing model of polymer will be established based on numerical computational method and verify the numerical results with the experimental data obtained with our university's equipment, at the same time, we also consider the effects of the variation of polymer processing parameters and further study the effects of melt blowing process parameters on the fiber diameter. The final fiber diameter can then be predicted with the aid of this air drawing model. It is found that the model can be applied to predicting the drawing effects successfully. Effects of the processing parameters on the fiber diameter will also be investigated by utilizing the air drawing model. The results also reveal the great potential for this research in the computer-assisted design (CAD) of melt blowing process, technology and equipment.

REFERENCES

[1]. M. A. J. Uyttendaele, , *AIChE J.*, 36, 175（1990）
[2]. V. Bansal, and R. L. Shambaugh, Ind. Eng. Chem. Res., 37, 1799（1998）
[3]. A. S. Harpham, and R. L. Shambaugh, Ind. Eng. Chem. Res., 36, 3937（1997）
[4]. B. Majumdar, and R. L Shambaugh, J. Rheol., 34, 591(1990).
[5]. A. S. Harpham, and R. L. Shambaugh, Ind. Eng. Chem. Res., 35, 1099（1996）
[6]. T. Chen, Textile Res. J., 73, 651(2003).
[7]. K. F. Zieiminski, and J. E. Spruiell, Synthetic Fibers, 25, 31(1986).

ACKNOWLEDGEMENTS

The permission by Phoenics Inc. to use their software with an educational license is gratefully acknowledged.

NOMENCLATURE

W= polymer mass flow rate, kg/s.
D= filament fiber diameter, mm.
V= filament fiber velocity, m/s.
V_a = air velocity, m/s.
g= gravitational acceleration, g/s^2
C_{pf} =specific heat capacity of melt, J/(kg.K).
h =convective heat transfer coefficient, W/（m^2.K）
T= polymer temperature, ℃
T_a = the air temperature, ℃
j = sign carrier of the air drag force, when j is-1 for $v_{a>}$v and 1 for $v_{a<}$ v.

Greek Symbols

ρ_f=polymer density, kg/m^3.

ρ_a = air density, kg/m^3.

η = the shear viscosity of air, Pa.s

τ_{zz} =axial extra stress, Pa.

τ_{xx} =transversal extra stress, Pa.

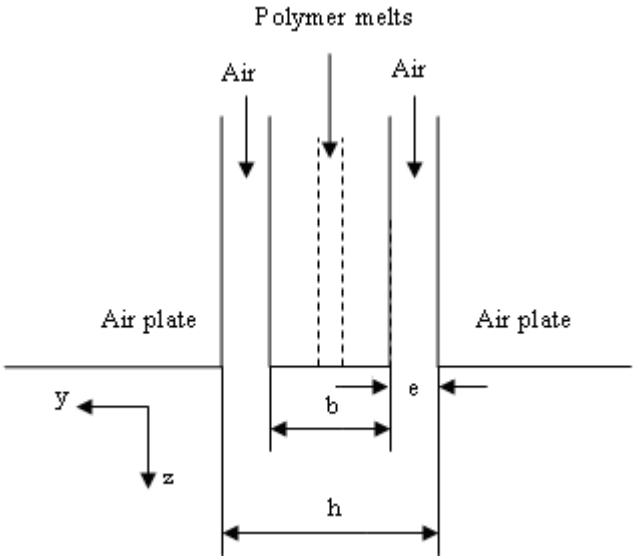

Fig.1. Dual-slot annular die of melt blowing process

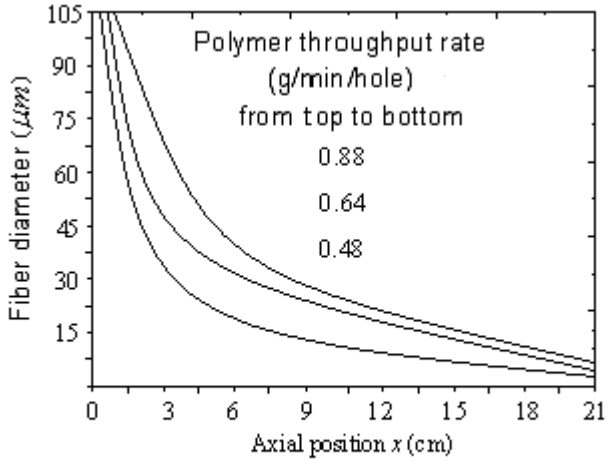

Fig. 2 Showing relationship between fiber diameter and axial position with polymer throughput rate (g/min/hole)

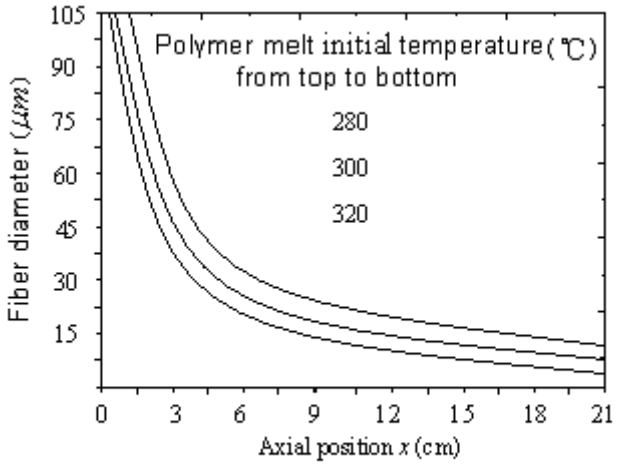

Fig. 3 Showing relationship between fiber diameter and axial position with polymer melt initial temperature (℃)

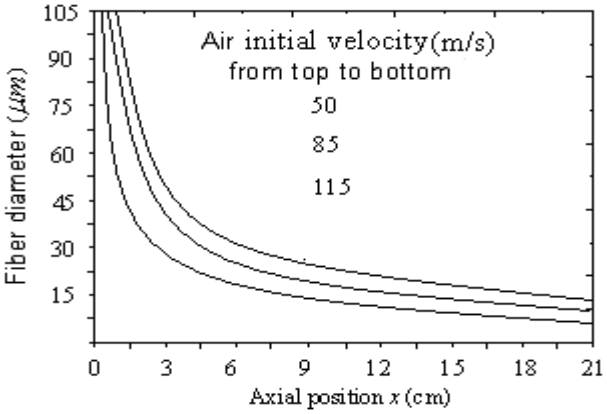

Fig. 4 Showing relationship between fiber diameter and axial position with air initial velocity(m/s)

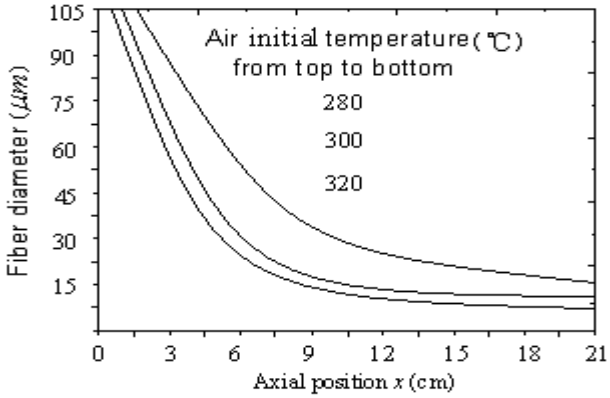

Fig. 5 Showing relationship between fiber diameter and axial position with air initial temperature(℃)

Table 1. Comparison of model predictions between improved model and primary model

Improved Model			Primary Model		
Measured diameter (μm)	Predicted diameter (μm)	Prediction error (%)	Measured diameter (μm)	Predicted diameter (μm)	Prediction error (%)
12.569	12.022	4.35	12.569	11.420	9.14
11.234	10.754	4.27	11.234	10.324	8.10
13.416	12.978	3.26	13.416	12.512	6.74
14.112	13.502	4.32	14.112	13.232	6.24
13.239	12.664	4.34	13.239	12.224	7.67

Corresponding author: Dr. Bo Zhao
Mailing Addresss: College of Textiles, Zhongyuan University of Technology, No.41 Zhongyuan Road, Zhengzhou, Henan 450007, People's Republic of China

ISSN (e): 2250 – 3005 || Vol, 04 || Issue, 10 || October– 2014 ||
International Journal of Computational Engineering Research (IJCER)

Design and Analysis of a Hybrid Suspension System

Valaparla. Sarojini[1], N.Amaranageswara Rao[2]
[1]PG Student, Department of Mechanical Engineering, Nimra Institute of Science & Technology, Ibrahimpattanam, Vijayawada.
[2]Guide (Assoc.Prof), Department of Mechanical Engineering, Nimra Institute of Science & Technology, Ibrahimpattanam, Vijayawada.

ABSTRACT:
Leaf springs are one of the oldest suspension components they are still frequently used, especially in commercial vehicles. The commonly used leaf springs in the vehicle suspension system are subjected to millions of varying stress cycles leading to fatigue failure. A lot of research has been done for improving the performance of leaf spring. Here in this project also we did an attempt of designing hybrid suspension system which was used in autos by using that concept of designing we designed a hybrid leaf spring. For this thesis we took Tata ace auto leaf spring as a reference and designed it by using modeling software. In the analysis we used ansys package and the results are compared with the hybrid suspension system for the same load. The main objective of the project is that to increase the load capacity of the leaf spring from this project we are trying to achieve this and further suggestions are made by observing the results.The model was designed by using Pro-E and analyzed using Ansys.

KEYWORDS : *Ansys, Fatigue , Hybrid Leaf Spring , Pro-e, Suspension system.*

I. INTRODUCTION

A spring is defined as an elastic body, whose function is to distort when loaded and to recovers its original shape when the load is removed.Semi- elliptic leaf springs are almost universally used for suspension in light and heavy commercial vehicles. For cars also, these are widely used in rear suspension. The spring consists of a number of leaves called blades. The blades are varying in length. The blades are us usually given an initial curvature or cambered so that they will tend to straighten under the load. The leaf spring is based upon the theory of a beam of uniform strength. The lengthiest blade has eyes on its ends. This blade is called main or master leaf, the remaining blades are called graduated leaves. All the blades are bound together by means of steel straps.

- **Objective of Suspension**

✓ To prevent the road shocks from being transmitted to the vehicle components.
✓ To safeguard the occupants from road shocks
✓ To preserve the stability of the vehicle in pitting or rolling, while in motion
✓ Basic Considerations for vertical loading

II. INTRODUCTION TO ANSYS

ANSYS is general-purpose finite element analysis (FEA) software package. Finite Element Analysis is a numerical method of deconstructing a complex system into very small pieces (of user-designated size) called elements. The software implements equations that govern the behaviour of these elements and solves them all; creating a comprehensive explanation of how the system acts as a whole. These results then can be presented in tabulated, or graphical forms. This type of analysis is typically used for the design and optimization of a system far too complex to analyze by hand. Systems that may fit into this category are too complex due to their geometry, scale, or governing equations. ANSYS is the standard FEA teaching tool within the Mechanical Engineering Department at many colleges. ANSYS is also used in Civil and Electrical Engineering, as well as the Physics and Chemistry departments. ANSYS provides a cost-effective way to explore the performance of products or processes in a virtual environment. This type of product development is termed virtual prototyping

III. MODELING BY USING PRO-E

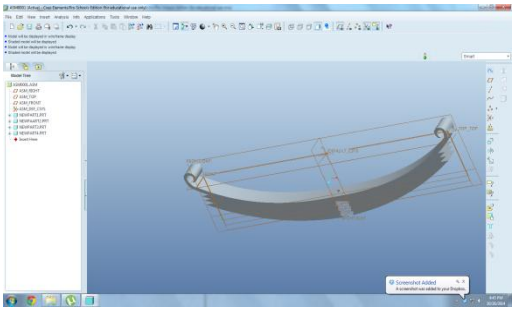

Fig 1. Actual model of Leaf spring suspension system

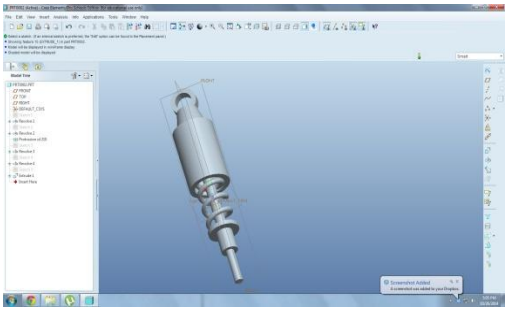

Fig 2.Helical Spring suspension system

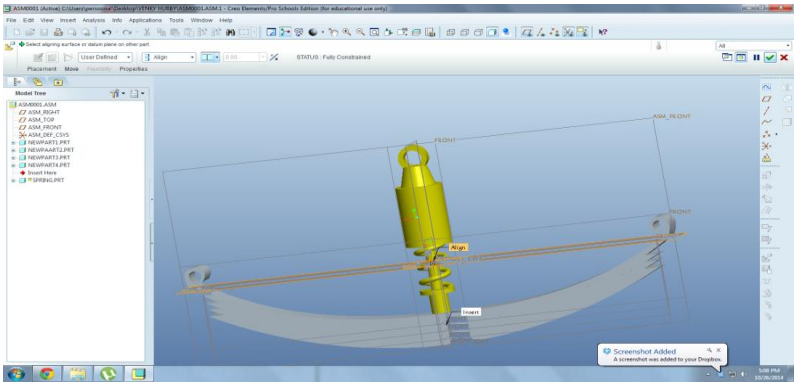

Fig 3. Assembly of the Hybrid suspension system

IV. RESULTS & DISCUSSION

i. **Leaf spring for steel 65Si7 material (**2tons load)

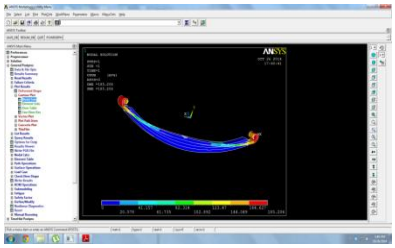

Fig 4. Total deformation

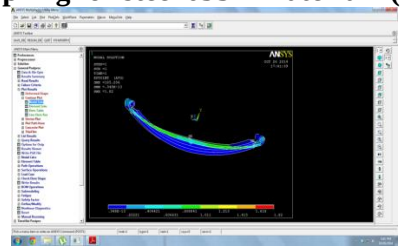

Fig 5.Stress intensity

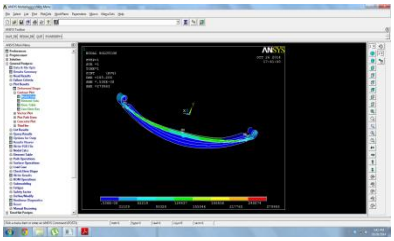

Fig 6.Strain intensity

ii. **Leaf spring for steel 65Si7 material (**3tons load)

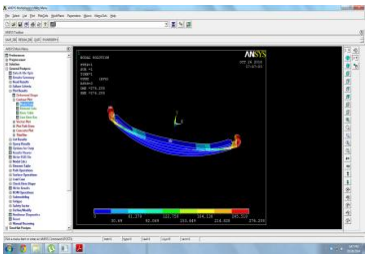

Fig 7.Total deformation

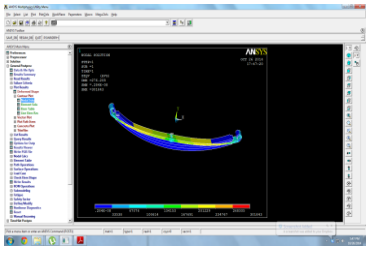

Fig 8.Stress intensity

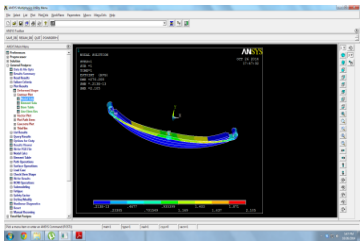

Fig 9.Strain intensity

iii. **Leaf spring for steel 65Si7 material (**1tons load)

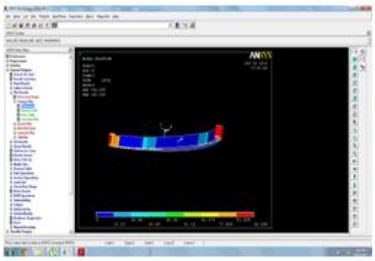

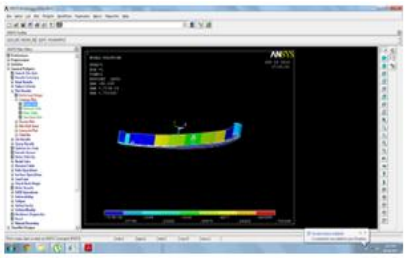

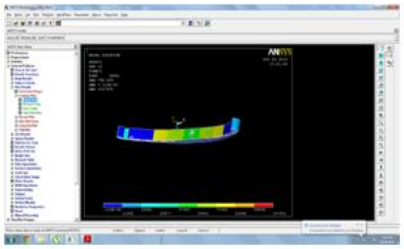

Fig 10. Total deformation

Fig 11.Stress intensity **Fig 12.Strain intensity**

4.2.1. Composite Leaf spring (2tons load)

\

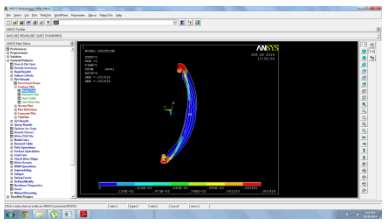

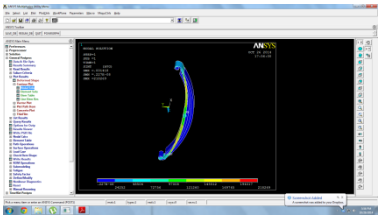

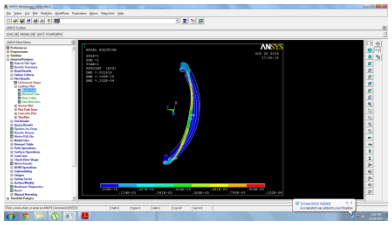

Fig 13. Total deformation **Fig 14.Stress intensity** **Fig 15.Strain intensity**

4.2.2. Composite Leaf spring (3tons load)

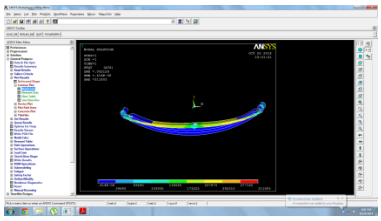

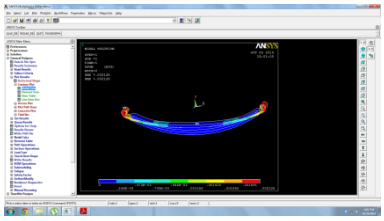

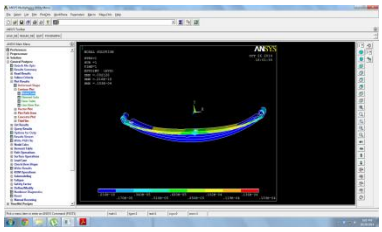

Fig 16. Total deformation **Fig 17.Stress intensity** **Fig 18.Strain intensity**

4 .2.3. Composite Leaf spring (1tons load)

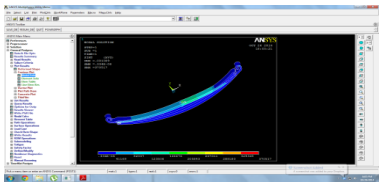

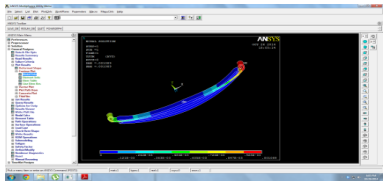

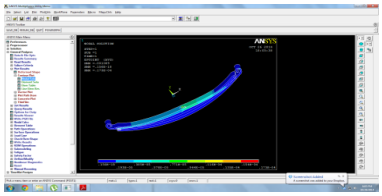

Fig 19.Total deformation **Fig 20.Stress intensity** **Fig 21.Strain intensity**

4.3.1. Hybrid helical suspension system for 65Si7 material (For 2 tons)

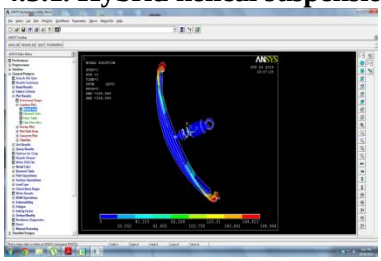

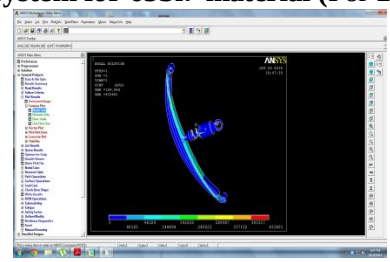

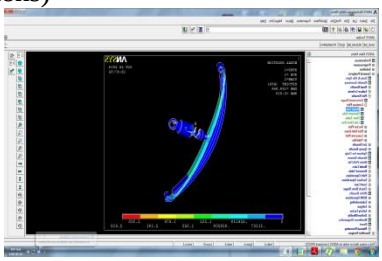

Fig 22.Total deformation **Fig 23.Stress intensity** **Fig 24.Strain intensity**

4.3.2. Hybrid helical suspension system for 65Si7 material (For 3 tons)

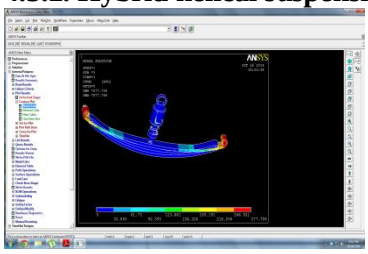

Fig 25.Total deformation

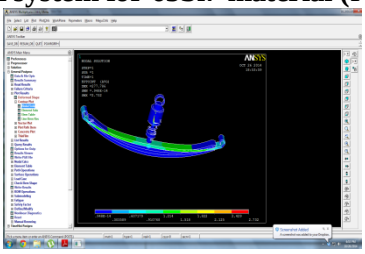

Fig 26.Stress intensity

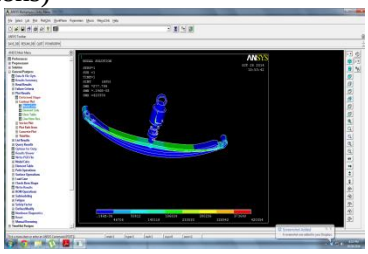

Fig 27.Strain intensity

4.3.3. Hybrid helical suspension system for 65Si7 material (For 1 tons)

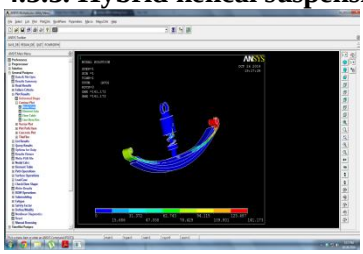

Fig 28.Total deformation

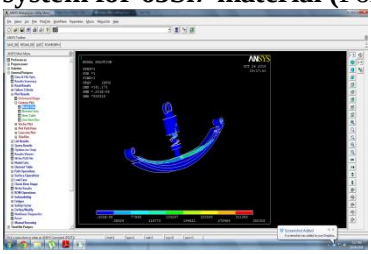

Fig 29.Stress intensity

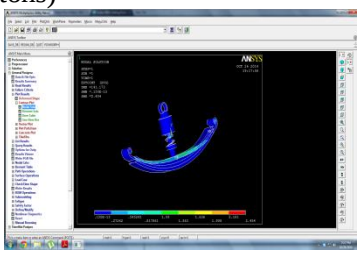

Fig 30.Strain intensity

4.4.1. Composite Hybrid helical suspension system (For 2 tons)

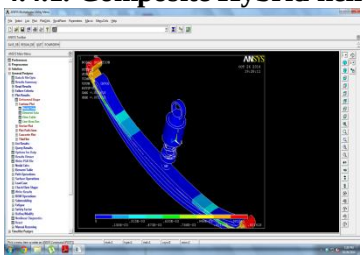

Fig 31.Total deformation

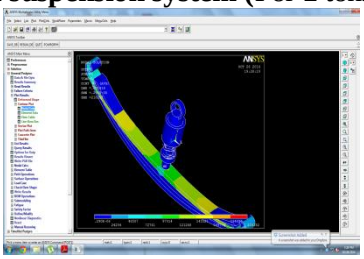

Fig 32.Stress intensity

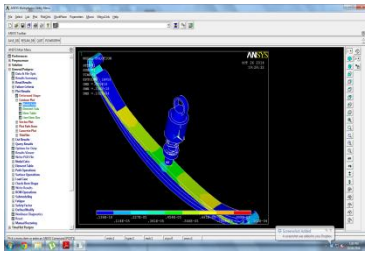

Fig 33.Strain intensity

4.4.2. Composite Hybrid helical suspension system (For 3 tons)

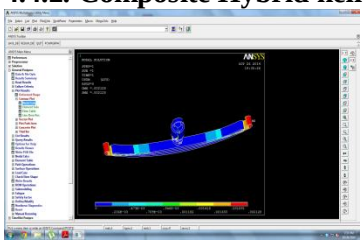

Fig 34.Total deformation

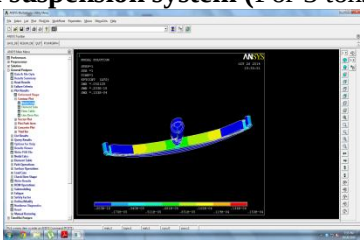

Fig 35.Stress intensity

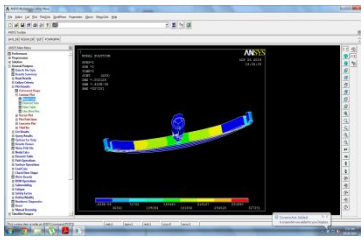

Fig 36.Strain intensity

4.4.3. Composite Hybrid helical suspension system (For 1 tons)

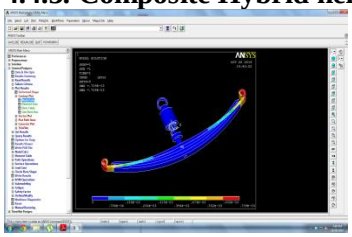

Fig 37.Total deformation

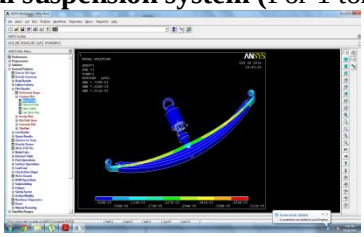

Fig 38.Stress intensity

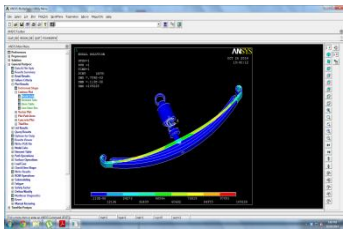

Fig 39.Strain intensity

V. STRESS RESULTS SUMMARY

Stress values						
Used material	Steel			Composite		
Applied weight	1 ton	2 tons	3 tons	1 ton	2 tons	3 tons
Actual leaf suspension	92	185	276	.00108	.00212	.00414
Hybrid suspension	90.2	184	277	.0079	.00212	.00418

VI. CONCLUSION

In this thesis we designed actual leaf suspension and hybrid suspension system with 3d modeling software and analyzed the stress values using Fea package.Here the actual leaf model was designed and analyzed for different stresses at different loads by changing the materials.As the same the hybrid suspension system was designed and analyzed for different stresses at different loads by changing the materials.After the analysis the stress values of the actual suspension system with two materials are compared the stress values are less for composite material compared to actual so composite material can be used for designing the actual suspension system.The stress values of the hybrid suspension system are also compared with two different materials then we came to know that the stress values are less for composite material compared to actual so composite material can be used for designing the hybrid suspension system.Finally the results of the actual suspension with the hybrid suspension are compared so we observed that for composite there is little difference and for actual there is more difference in stress values from this we conclude that by using hybrid suspension system we can add more weight that the actual suspension.The actual truck capacity is 2 tons for actual suspension by using hybrid suspension system we can add more than 2 tons. And the design best under load of 3 tons.

REFERENCES

[1]. Machine design by R.S. Khurmi

[2]. Psg, 2008."design data," Kalaikathir achchagam publishers, coimbatore, India Intelligent Systems": A Comparative Study Hindawi Publishing Corporation Applied

[3]. Computational Intelligence and Soft Computing Volume 2011, Article ID 183764, 18 pages.

[4]. Abbas Fadhel Ibraheem, Saad Kareem Shather & Kasim A. Khalaf, "Prediction of Cutting Forces by using Machine Parameters in end Milling Process", Eng. & Tech. Vol.26.No.11, 2008.

[5]. S. Abainia, M. Bey, N. Moussaoui and S. Gouasmia." Prediction of Milling Forces by Integrating a Geometric and a Mechanistic Model", Proceedings of the World Congress on Engineering 2012 Vol III WCE 2012, July 4 - 6, 2012, London, U.K.

[6]. Md. Anayet u patwari, a.k.m. nurul amin, waleed f. Farris, „prediction of tangential cutting force in end milling of Medium carbon steel by coupling design of experiment and Response surface methodology". Journal of mechanical engineering, vol. Me 40, no. 2, December 2009 Transaction of the mech. Eng. Div., the institution of engineers, Bangladesh.

[7]. Smaoui, M.; Bouaziz,z. &Zghal,A., „Simulation of cutting forces for complex surfaces in Ball-End milling", Int j simul model 7(2008) 2,93-105.

[8]. **Rajendran, I., Vijayarangan, S. "**Optimal Design of a Composite Leaf Spring using Genetic Algorithms" *Int. Jr. of Computer and Structures* 79 2001: pp. 1121 – 1129.

[9]. **Rajendran, I., Vijayarangan, S. "**Design and Analysis of a Composite Leaf Spring" *Journal of Institute of Engineers* India 82 2002: pp. 180 – 187.

[10]. **Daugherty, R. L. "**Composite Leaf Springs in Heavy Truck Applications". K. Kawata, T.Akasaka (Eds). Composite Materials *Proceedings of Japan-US Conference* Tokyo,1981: pp. 529 – 538.

[11]. **Dharam, C. K. "**Composite Materials Design and Processes for Automotive Applications". The ASME Winter Annual Meeting, San Francisco, December 10-15, 1978: pp. 19 – 30.

[12]. **Vijayarangan, S., Ganesan, N. "**Static Stress Analysis of a Composite Bevel Gear using a Three-dimensional Finite Element Method" Computer Structures 51 (6 1994: pp. 771 – 783.

[13]. **Tanabe, K., Seino, T., Kajio, Y. "**Characteristics of Carbon/Glass Fiber Reinforced Plastic Leaf Spring", SAE 820403 1982: pp. 1628 – 1634.

[14]. **Yu, W. J., Kim, H. C. "**Double Tapered FRP Beam for Automobile Suspension Leaf Spring" Comp. Structure 1998: pp. 279 – 300.

[15]. **Jones, R. M. "**Mechanics of Composite Materials". 2e, Mc Graw-Hill Book Company, 1990.

[16]. **ANSYS Inc**: "ANSYS Users Manual", Rev. 1995, 5.2-Vol. I – IV, Houston, PA.

[17]. P. Beardmore, "Composite structure for automobiles," 1986.

[18]. R.S. Khurmi, J.K. Kupta. "A text book of Machine Design," 2000.

[19]. Shiva Shankar, Sambagam Vijayarangan. "Mono Composite Leaf Spring for Light Weight Vehicle – Design,End Joint Analysis and Testing," Gulur Siddaramanna – 2006